AD-A102 279 ARMY MISSILE COMMAND REDSTONE ARSENAL AL DIRECTED E--ETC F/G 20/5
COMPILATION OF ATOMIC AND MOLECULAR DATA RELEVANT TO GAS LASERS--ETC(U)
DEC 80 E W MCDANIEL, M R FLANNERY, E W THOMAS
UNCLASSIFIED DRSMI-RH-81-4-VOL-7 NL

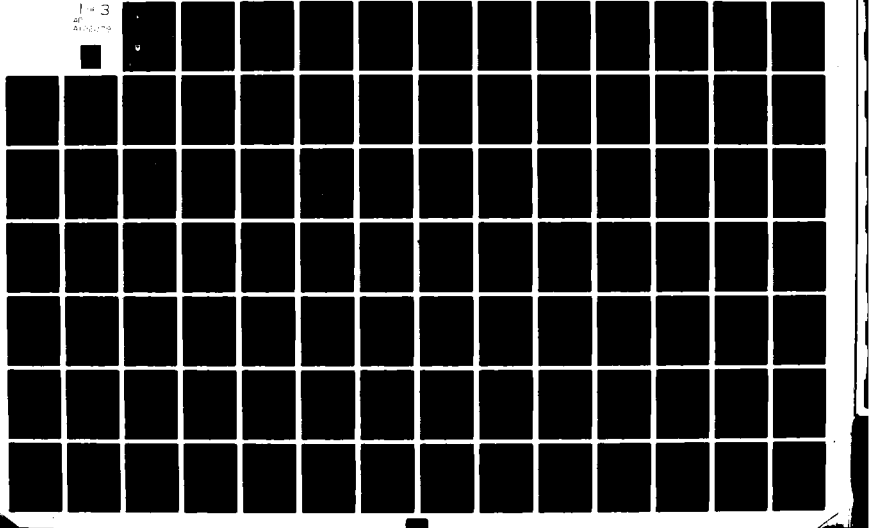

AD A102279

A101037

(2)

TECHNICAL REPORT RH-81-4

LEVEL III

COMPILATION OF ATOMIC AND MOLECULAR DATA RELEVANT TO GAS LASERS

VOLUME VII

E. W. McDaniel, M. R. Flannery, and E. W. Thomas
School of Physics, Georgia Institute of Technology
Atlanta, Georgia 30332

S. T. Manson
Physics Department, Georgia State University
Atlanta, Georgia 30303

J. W. Gallagher
Joint Institute for Laboratory Astrophysics
University of Colorado
Boulder, Colorado 80302

T. A. Barr, Jr. and T. G. Roberts
Directed Energy Directorate
US Army Missile Laboratory

DTIC
ELECTE
JUL 20 1981

December 1980

U.S. ARMY MISSILE COMMAND
Redstone Arsenal, Alabama 35809

APPROVED FOR PUBLIC RELEASE; DISTRIBUTION UNLIMITED.

DTIC FILE COPY

DD FORM 1021, 1 JUL 79 PREVIOUS EDITION IS OBSOLETE

81 7 20 079

DISPOSITION INSTRUCTIONS

DESTROY THIS REPORT WHEN IT IS NO LONGER NEEDED. DO NOT RETURN IT TO THE ORIGINATOR.

DISCLAIMER

THE FINDINGS IN THIS REPORT ARE NOT TO BE CONSTRUED AS AN OFFICIAL DEPARTMENT OF THE ARMY POSITION UNLESS SO DESIGNATED BY OTHER AUTHORIZED DOCUMENTS.

TRADE NAMES

USE OF TRADE NAMES OR MANUFACTURERS IN THIS REPORT DOES NOT CONSTITUTE AN OFFICIAL INDORSEMENT OR APPROVAL OF THE USE OF SUCH COMMERCIAL HARDWARE OR SOFTWARE.

Unclassified

SECURITY CLASSIFICATION OF THIS PAGE *(When Data Entered)*

REPORT DOCUMENTATION PAGE		READ INSTRUCTIONS BEFORE COMPLETING FORM
1. REPORT NUMBER TR-RH-81-4	2. GOVT ACCESSION NO. AD-A102279	3. RECIPIENT'S CATALOG NUMBER
4. TITLE *(and Subtitle)* COMPILATION OF ATOMIC AND MOLECULAR DATA RELEVANT TO GAS LASERS, VOLUME VII.		5. TYPE OF REPORT & PERIOD COVERED Technical Data 6. PERFORMING ORG. REPORT NUMBER
7. AUTHOR(s) E.W. McDaniel, M.R. Flannery, E.W. Thomas, S.T. Manson, J.W. Gallagher, T.A. Barr, Jr. and T.G. Roberts		8. CONTRACT OR GRANT NUMBER(s)
9. PERFORMING ORGANIZATION NAME AND ADDRESS Commander, US Army MissileCommand, ATTN: DRSMI-R, Redstone Arsenal, AL 35898		10. PROGRAM ELEMENT, PROJECT, TASK AREA & WORK UNIT NUMBERS
11. CONTROLLING OFFICE NAME AND ADDRESS Commander, US Army Missile Command, ATTN: DRSMI-RP, Redstone Arsenal, AL 35898		12. REPORT DATE December 1980 13. NUMBER OF PAGES
14. MONITORING AGENCY NAME & ADDRESS*(If different from Controlling Office)*		15. SECURITY CLASS. *(of this report)* Unclassified 15a. DECLASSIFICATION/DOWNGRADING SCHEDULE

16. DISTRIBUTION STATEMENT *(of this Report)*

Approved for public release; distribution unlimited.

17. DISTRIBUTION STATEMENT *(of the abstract entered in Block 20, if different from Report)*

18. SUPPLEMENTARY NOTES

See Volume VI

19. KEY WORDS *(Continue on reverse side if necessary and identify by block number)*

Excitation
Ionization
Laser pumping mechanisms
Heavy Nuclides
Light nuclides
High energy electron beams
High energy ion beams

20. ABSTRACT *(Continue on reverse side if necessary and identify by block number)*

This volume and the succeeding volume are the seventh and the eighth in a series that presents data relevant to research and development in the field of gas lasers. Volumes I and II are entitled, "Compilation of Data Relevant to Rate Gas-Rare Gas and Rare Gas-Monohalide Excimer Lasers," December 1977. Volumes III, IV, and V comprise a "Compilation of Data Relevant to Nuclear Pumped Lasers," December 1978. Volume VI provides a "Cumulative Reactant

(Abstract continued on back)

DD FORM 1 JAN 73 1473 EDITION OF 1 NOV 65 IS OBSOLETE

Unclassified

SECURITY CLASSIFICATION OF THIS PAGE *(When Data Entered)*

ABSTRACT (Continued)

Species Index for Volumes I-V of the Compilation of Data Relevant to Gas Lasers," September 1979. These six volumes, authored by E.W. McDaniel and other personnel at Georgia Tech, Georgia State University, the Joint Institute of Laboratory Astrophysics (JILA), and the Army Missile Command (MICOM), were published as MICOM Technical Report H-78-1 at Redstone Arsenal, Alabama.

Volumes I and II were prepared in the context of the two most-used techniques for gas laser pumping: electrical discharges and high intensity, high energy electron and ion beams. Heavy emphasis was placed on the rare gases and halogens (atoms, molecules, and ions), and the rare gas-halides, although a significant amount of material on other species was included. Volumes III, IV, and V contain much information relevant to electrical discharges and high intensity, high energy electron and ion beams, but are oriented toward a third pumping technique: nuclear pumping. Since nuclear reactions may also become interesting in some form of hybrid laser where the excitation and ionization produced by the reaction products might be used to supply electrons for an electrical discharge laser or an initiator for a pulsed chamical laser, or as an initiator and sustainer for a continuous wave (CW) chemical laser; data relevant to these systems was also included.

The present volumes serve to update most of the areas covered in the previous documents. Those areas not treated here are considered to have been adequately dealt with earlier, as far as immediate data needs are concerned. However, even in those areas where new data are not presented here, references are given to past volumes in order to facilitate access to the previous data. Another function of the present work is to expand somewhat the scope of our data coverage, both with respect to atomic and molecular structural properties and with respect to atomic collisions. New species and sets of collision partners that have recently assumed importance are treated here, and other systems that may become important in the gas laser contex are given attention. A significant amount of new material is also added to the chapter on surface impact phenomena, partly because of current interest in hollow-cathode lasers.

PREFACE

This volume and the succeeding volume are the seventh and the eighth in a series that presents data relevant to research and development in the field of gas lasers. Volumes I and II are entitled, "Compilation of Data Relevant to Rare Gas-Rare Gas and Rare Gas-Monohalide Excimer Lasers," December 1977. Volumes III, IV, and V comprise a "Compilation of Data Relevant to Nuclear-Pumped Lasers," December 1978. Volume VI provides a "Cumulative Reactant Species Index for Volumes I-V of the Compilation of Data Relevant to Gas Lasers," September 1979. These six volumes, authored by E.W. McDaniel and other personnel at Georgia Tech, Georgia State University, the Joint Institute of Laboratory Astrophysics (JILA), and the Army Missile Command (MICOM), were published as MICOM Technical Report H-78-1 at Redstone Arsenal, Alabama.

Volumes I and II were prepared in the context of the two most-used techniques for gas laser pumping: electrical discharges and high intensity, high energy electron and ion beams. Heavy emphasis was placed on the rare gases and halogens (atoms, molecules, and ions), and on the rare gas-halides, although a significant amount of material on other species was included. Volumes III, IV, and V contain much information relevant to electrical discharges and high intensity, high energy electron and ion beams, but are oriented toward a third pumping technique: nuclear pumping. Since nuclear reactions may also become interesting in some form of hybrid laser where the excitation and ionization produced by the reaction products might be used to supply electrons for an electrical discharge laser or an initiator for a pulsed chemical laser, or as an initiator and sustainer for a continuous wave (CW) chemical laser; data relevant to these systems was also included.

The present volumes serve to update most of the areas covered in the previous documents. Those areas not treated here are considered to have been adequately dealt with earlier, as far as immediate data needs are concerned. Such areas include all nuclear processes, and atomic collisions occurring at "high" energies, i.e., above about 100 eV impact energy. However, even in those areas where new data are not presented here, references are given to past volumes in order to facilitate access to the previous data. Attention should also be called to another document that may prove useful to those requiring data--"Bibliography: Sources of Information on Phenomena of Interest in Gas Laser Research and Development," Technical Report RH-77-1, by E.W. McDaniel, H.W. Ellis, F.L. Eisele, and M.G. Thackston, January 1977, US Army Missile Command, Redstone Arsenal, Alabama. A second, updated edition of this bibliography will be published early in 1981.

Another function of the present volume is to expand somewhat the scope of our data coverage. both with respect to atomic and molecular structural properties and with respect to atomic collisions (by the

latter term, we mean two- and three-body collisions between electrons, ions, atoms, molecules, and photons at impact energies sufficiently low that nuclear forces are unimportant). New species and sets of collision partners that have recently assumed importance are treated here, and other systems that may become important in the gas laser context are given attention. A significant amount of new material is also added to the chapter on surface impact phenomena, partly because of current interest in hollow-cathode lasers.

In conclusion, we wish to thank C.F. Barnett, former Director of the Controlled Fusion Atomic Data Center at the Oak Ridge National Laboratory, and E.C. Beaty, Chief of the Information Center at JILA, for their cooperation and the use of their facilities. In certain areas, our work would have been immensely more difficult without their assistance. Chapter D on photon collision processes in gases was put together with the aid of several scientists. Particularly significant were the contributions of Dr. Joseph Berkowitz, of Argonne National Laboratory, whose book Photoabsorption, Photoionization, and Photoelectron Spectroscopy (Academic Press, New York, 1979) provided us with a wealth of references and critically evaluated data on atoms and molecules. We gratefully acknowledge being allowed access to the manuscript prior to publication, as well as Dr. Berkowitz providing us with a number of large-size versions of figures from his book. In addition, we acknowledge the contributions of Professor C.E. Brion, of the University of British Columbia, for providing us with a complete set of reprints, spanning a decade, of his very extensive work on partial and total cross sections of atoms and molecules. Also, the expert help of Professor H.W. Ellis, of Eckerd College, St Petersburg, Florida, on the transport properties of electrons, ions, and neutrals in gases is gratefully acknowledged.

Compilation of Atomic and Molecular Data Relevant to Gas Lasers - Vol. VII.

Table of Contents

Chapter		Page
A.	Structural Properties of Atoms, Molecules, and Ions	2543
B.	Heavy Particle - Heavy Particle Collisions	2672
	(No new entries on high-energy collisions here.)	
C.	Electron - Heavy Particle Collisions	2897
D.	Photon Collision Processes in Gases	3006
E.	Transport Properties of Electrons, Ions, and Neutrals in Gases	3134
	(No new entries on neutrals here.)	
F.	Interactions with Static Electric and Magnetic Fields	3157
	(No new entries here.)	
G.	Particle Penetration in Gases (Ions, Neutrals, and Electrons)	3157
	(No new entries here.)	
H.	Particle and Photon Interactions with Solids	3158
	(No new entries on photons here.)	
I.	Secondary Electron Spectra	3204
J.	Nuclear Data	3218
	(No new entries here.)	

(Chapters C through J appear in Vol. VIII.)

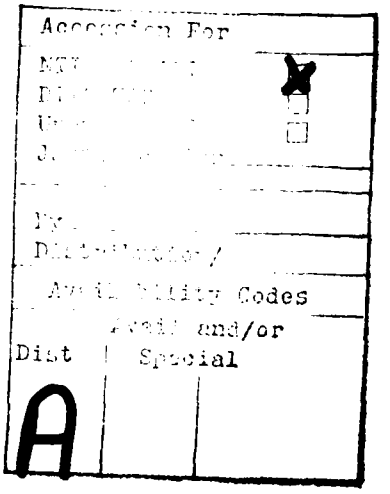

A. STRUCTURAL PROPERTIES OF ATOMS, MOLECULES, AND IONS.

CONTENTS

		Page
A-1.	General References on Potential Energy Curves, Electronic Energies, Spectroscopic Constants and Absorption and Emission Spectra of Excimer Systems.	2544
A-2.	Potential Energy Curves, Electronic Energies, Transition Moments and Spectroscopic Constants of Valence Electronic States of F_2, I_2 and I_2^+.	2548
A-3.	Transition Moments and Absorption Profiles for Electronic States of Ne_2^+, Ar_2^+, Kr_2^+, Xe_2^+, Potential Energy Curves, Spectroscopic Constants and Absorption Cross Sections for Hg_2^+ and Ar_3^+	2574
A-4.	Franck-Condon Factors for XeCl, Electronic Structure of $HgCl_2$, $HgBr_2$ and ArBr, Potential Energy Curves for Zn_2, Cd_2 and LiCa . .	2632
A-5.	Electronic Structure and Spectra for Li_2 and Na_2. Van der Waals Coefficients for Neutral (H, He, Ne, Ar, Kr, Xe, Li, Na, K, Rb - Neutral Interactions.	2660

GLOSSARY

CI:	Configuration Interaction	OVC:	Optimized Valence Configuration
VB:	Valence Bond	MBS:	Minimal Bases Set
POL:	Polarization	STO:	Slater-Type-Orbitals
GVB:	Generalized Valence Bond	1 Hartree	≡ 1 a.u. = 27.21 eV
SCF:	Self Consistent Field	1 Rydberg	≡ 13.6 eV
		1 Bohr	≡ 0.529 Å

A-1. GENERAL REFERENCES ON POTENTIAL ENERGY CURVES, ELECTRONIC ENERGIES, SPECTROSCOPIC CONSTANTS AND ABSORPTION AND EMISSION SPECTRA OF EXCIMER SYSTEMS.*

GENERAL REFERENCES

1. J. S. Wright and S. K. Gray, "Rotated Morse Curve-Spline Potential Function for A + BC Reaction Dynamics: Application to (Cℓ, HBr), (F, H_2) and (H^+, H_2)", J. Chem. Phys. 69, 67 (1978).

2. P. M. Dehmer and J. L. Dehmer, "Photoelectron Spectra of Ar_2 and Kr_2 and Dissociation Energies of the Rare Gas Dimer Ions", J. Chem. Phys. 69, 125 (1978).

3. G. Brual, Jr. and S. M. Rothstein, "Rare Gas Interactions Using an Improved Statistical Model", J. Chem. Phys. 69, 1177 (1978).

4. R. A. Aziz, V. P. S. Nain, J. S. Carley, W. L. Taylor and G. T. McConville, "An Accurate Intermolecular Potential for Helium", J. Chem. Phys. 70, 4330 (1979).

5. R. A. Aziz, J. Presley, U. Buck and J. Schleusener, "An Accurate Intermolecular Potential for Ar - Kr", J. Chem. Phys. 70, 4737 (1979).

6. J. H. Goble and J. S. Winn, "Analytic Potential Functions for Weakly Bound Molecules: The X and A States of NaAr and the A State of NaNe", J. Chem. Phys. 70, 2051 (1979).

7. Y. S. Kim, "Study of the Ar - N_2 Interaction. I. Electron Gas Model (Gordon-Kim Model) Potential Calculation", J. Chem. Phys. 68, 5001 (1978).

8. S. Lee and Y. S. Kim, "Study of the Ar - N_2 Interaction. II. Modification of the Electron Gas Model at Intermediate and Large Distances", J. Chem. Phys. 70, 4856 (1979).

9. D. D. Konowalow and M. L. Olson, "The Electronic Structure and Spectra of the X $^1\Sigma_g^+$ and A $^1\Sigma_u^+$ States of Li_2", J. Chem. Phys. 71, 450 (1979).

10. K. D. Sen, "Slater Transition-State Calculations of Shake-Up Energies in Ne, Ar and Kr", J. Chem. Phys. 71, 1035 (1979).

11. P. J. Hay, W. R. Wadt, L. R. Kahn, R. C. Raffenetti and D. H. Phillips, "Ab initio Studies of the Electronic Structure of UF_6, UF_6^+ and UF_6^- Using Relativistic Effective Core Potentials", J. Chem. Phys. 71, 1767 (1979).

12. D. E. Freeman, K. Yoshino and Y. Tanaka, "Emission Spectrum of Rare Gas Dimers in the Vacuum UV Region. II. Rotational Analysis of Band System I of Ar_2", J. Chem. Phys. 71, 1780 (1979).

---

*These references are in addition to those previously given in Vol. I, Chapter A, pages 8-14 and in Vol. III, Chapter A, pages 1163-1166.

13. S. Huginaga, "GTO Basis Sets for In, Sn, Sb, Te, I and Xe", J. Chem. Phys. 71, 1980 (1979).

14. P. A. Christiansen, Y. S. Lee and K. S. Pitzer, "Improved Ab initio Effective Core Potentials for Molecular Calculations", J. Chem. Phys. 71, 4445 (1979).

15. L. M. Brescansin, J. R. Leite and L. G. Ferreira, "A Study of the Ground States and Ionization Energies of H_2, C_2, N_2, F_2 and CO Molecules by the Variational Cellular Method", J. Chem. Phys. 71, 4923 (1979).

16. P. E. Siska, "One-Electron Model Potential Calculations of van der Waals Forces. I. $He^*(2^1S, 2^3S)$ + Ne, Ar, Kr, Xe", J. Chem. Phys. 71, 3942 (1979).

17. G. D. Purvis and R. J. Bartlett, "The Potential Energy Curve for the $X\ ^1\Sigma_g^+$ State of Mg_2 Calculated with Coupled Pair Many Electron Theory", J. Chem. Phys. 71, 548 (1979).

18. C. F. Bender, T. N. Rescigno, H. F. Schaefer and A. E. Orel, "Potential Energy Curves for Diatomic Zinc and Codmium", J. Chem. Phys. 71, 1122 (1979).

19. M. F. Golde and A. Kuaran, "Chemiluminescence of Argon Bromide. I. The Emission Spectrum of ArBr", J. Chem. Phys. 72, 434 (1980).

20. M. F. Golde and K. Kuaran, "Chemiluminescence of Argon Bromide. II. Potential Curves of ArBr and Population Distributions in the B(1/2) and C(3/2) Electronic States", J. Chem. Phys. 72, 442 (1980).

21. T. Bergeman and P. F. Liao, "Photoassociation, Photoluminescence and Collisional Dissociation of the Sr_2 Dimer", J. Chem. Phys. 72, 886 (1980).

22. W. R. Wadt, "The Electronic Structure of Hg $C\ell_2$ and Hg Br_2 and its Relationship to Photodissociation", J. Chem. Phys. 72, 2469 (1980).

23 D. D. Konowalow, M. E. Rosenkrantz and M. L. Olson, "The Molecular Electronic Structure of the Lowest $^1\Sigma_g^+$, $^3\Sigma_u^+$, $^1\Sigma_u^+$, $^3\Sigma_g^+$, $^1\Pi_u$, $^1\Pi_g$, $^3\Pi_u$ and $^3\Pi_g$ States of Na_2", J. Chem. Phys. 72, 2612 (1980).

24. H. Inouye and K. Noda, "Repulsive Potentials Derived from the Integral Elastic Scattering of Ar^+ and Ne^+ Ions in Collision with He Atoms", J. Chem. Phys. 72, 3695 (1980).

25. D. G. Hopper, "MCSCF/CI Ground State Potential Energy Surface, Dipole Moment Function and Gas Phase Vibrational Frequencies for the Nitrogen Dioxide Positive Ion", J. Chem. Phys. 72, 4676 (1980).

26. M. D. Peña, C. Pando and J. A. R. Renuncio, "Combination Rules for Two-Body van der Waals Coefficients", J. Chem. Phys. 72, 5269 (1980).

27. P. J. Bruna, S. D. Pejerimhoff and R. J. Buenker, "Theoretical Prediction of the Potential Curves for the Lowest-Lying States of the Isovalent Distances CN^+, Si_2, SiC, CP^+ and SiN^+ Using the Ab initio MRD-CI Method", J. Chem. Phys. 72, 5437 (1980).

28. D. D. Konowalow and P. S. Julienne, "Li_2 and Na_2 $^3\Sigma_g^+ - {}^3\Sigma_u^+$ Excimer Emission", J. Chem. Phys. 72, 5815 (1980).

29. R. M. Berns and A van der Avoira, "$N_2 - N_2$ Interaction Potential From Ab initio Calculations, with Application to the Structure of $(N_2)_2$", J. Chem. Phys. 72, 6107 (1980).

30. R. Luypaert, G. de Vlieger and J. van Craen, "Lifetimes and Collisional Quenching Cross Sections of Single Rotational States in Bromine", J. Chem. Phys. 72, 6283 (1980).

31. W. J. Stevens, "Molecular Anions: The Ground and Excited States of LiF", J. Chem. Phys. 72, 1536 (1980).

32. M. Cobb, T. F. Moran, R. F. Borkman and R. Childs, "Ab initio Potential Energy Curves for the Low Lying Electronic States of N_2^{2+}", J. Chem. Phys. 72, 4463 (1980).

33. L. S. Bartell, M. J. Rothman, C. S. Ewig and J. R. Van Wager, "Pseudopotential SCF-MO Studies of Hypervalent Compounds. I. XeF_2 and XeF_4", J. Chem. Phys. 73, 367 (1980).

34. M. J. Rothman, L. S. Bartell, C. S. Ewig and J. R. Van Wager, "Pseudopotential SCF-MO Studies of Hypervalent Compounds. II. XeF_2^+ and XeF_6", J. Chem. Phys. 73, 375 (1980).

35. A. D. McLean, O. Gropen and S. Huzinaga, "Near Hartree-Fock Calculations on I_2 and its Positive and Negative Ions", J. Chem. Phys. 73, 396 (1980).

36. O. Gropen, S. Huzinaga and A. D. McLean, "Model Potential SCF Calculations on $C\ell_2$, Br_2, I_2", J. Chem. Phys. 73, 402 (1980).

37. R. P. Saxon and B. Liu, "Ab initio Configuration Interaction Study of the Rydberg States of O_2. I. A General Computational Procedure for Diabatic Molecular Rydberg States and Test Calculations on the $^3\Pi_g$ States of O_2", J. Chem. Phys. 73, 870 (1980).

38. R. P. Saxon and B. Liu, "Ab initio Configuration Interaction Study of the Rydberg States of O_2. II. Calculations on the $^3\Sigma_g^-$, $^3\Sigma_u^-$, $^3\Pi_g$, $^1\Pi_g$ and $^1\Sigma_g^+$ Symmetries", J. Chem. Phys. 73, 876 (1980).

39. J. W. Moskowitz, S. Topiol and L. C. Snyder, "The Application of an Atomic Effective Potential to the Electronic Structure and Bonding of Si_2", J. Chem. Phys. 73, 881 (1980).

40. A. Sur, A. K. Hui and J. Tellinghuisen, "Noble Gas Halides: The B → X and D → X Systems of XeCℓ", J. Molec. Spectros. 74, 465 (1979).

41. W. R. Wadt, "The Electronic States of Ne_2^+, Ar_2^+, Kr_2^+, Xe_2^+. II. Absorption Cross Sections for the $1(1/2)_u \rightarrow 1(3/2)_g$, $1(1/2)_g$, $2(1/2)_g$ Transitions", J. Chem. Phys. (in press).

42. D. C. Cartwright and P. J. Hay, "Theoretical Studies of the Valence Electronic States and the $^1\Pi_u \leftarrow X\ ^1\Sigma_g^+$ Absorption Spectrum of the F_2 Molecule", J. Chem. Phys. 70, (1979) 3191.

43. H. H. Michels, R. H. Hobbs and L. A. Wright, "Electronic Structure of the Noble Gas Dimer Ions. II. Theoretical Absorption Spectrum for the $A\ ^2\Sigma^+_{1/2u} \rightarrow D\ ^2\Sigma^+_{1/2g}$ System", J. Chem. Phys. (in press).

44. H. H. Michels, R. H. Hobbs and J. W. D. Connolly, "Electronic Structure and Photoabsorption of the Hg_2^+ Dimer Ion", Chem. Phys. Letts. (in press).

45. H. H. Michels, R. H. Hobbs and L. A. Wright, "Visible Photoabsorption by Noble Gas Trimer Ions", Appl. Phys. Letts. (in press).

A-2. POTENTIAL ENERGY CURVES, ELECTRONIC ENERGIES, TRANSITION MOMENTS AND SPECTROSCOPIC CONSTANTS OF VALENCE ELECTRONIC STATES OF F_2, I_2 and I_2^+.

CONTENTS

		Page
A-2.1.	References	2550
A-2.2.	Energies of the singlet states of F_2	2551
A-2.3.	Energies of the triplet states of F_2	2552
A-2.4.	Vertical excitation energies for the states of F_2	2553
A-2.5.	Spectroscopic Constants for F_2	2554
A-2.6.	Dissociation energies of the ground state of F_2	2555
A-2.7.	Spectroscopic constants for the lowest $^3\Pi_u$ state in F_2 and $C\ell_2$	2556
A-2.8.	Repulsive curves of F_2	2557
A-2.9.	Quadrupole moment and electric field gradient (a.u.) for the F_2 ground state	2558
A-2.10.	Transition moment (a.u.) for the $1^1\Sigma_g^+ \rightarrow {}^1\Pi_u$ excitation in F_2	2559
A-2.11.	Potential energy curves for the ground electronic state and lowest $^1\Pi_u$ state of F_2	2560
A-2.12.	Potential energy curves for the singlet valence states of F_2 dissociating into ground state F atoms.	2561
A-2.13.	Potential energy curves for the ground electronic states and those triplet electronic states dissociating into ground state F atoms.	2562
A-2.14.	Orbital diagrams for F_2	2563
A-2.15.	Potential energy curves for the ground state and the valence $^3\Pi_u$ and $^1\Pi_u$ electronic states of F_2	2564
A-2.16.	Comparison between the measured and theoretical $G_{v''}$ values for the ground state of F_2	2565
A-2.17.	Comparison between the measured and theoretical $B_{v''}$ values for the ground state of F_2	2566

Page

A-2.18. Quadrupole moment as a function of internuclear distance for ground state of F_2. 2567

A-2.19. Electronic transition moment, as a function of internuclear distance, for the $^1\Pi_u \leftarrow X^1\Sigma_g^+$ excitation in F_2 . . . 2568

A-2.20. Molar absorbancy, as a function of incident radiation wavelength, for F_2 in its lowest vibrational level and for F_2 initially in v"=1 and 2 2569

A-2.21. Comparison of bound-continuum Franck-Condon factors for F_2. 2570

A-2.22. SCF potential curves for $I_2^+(^2\Pi)$. 2571

A-2.23. Spectroscopic analysis of potential curves for I_2, I_2^+, I_2^- 2572

A-2.24. Molecular quadrupole moments for I_2, I_2^+ and I_2^-. 2572

A-2.25. SCF potential curves for I_2, I_2^- and I_2^+. 2573

A-2.26. SCF electron affinities and ionization potentials for I, I^+, I_2, I_2^+. 2573

A-2. General References

1. D. C. Cartwright and P. J. Hay, "Theoretical Studies of the Valence Electron States and the $^1\Pi_u \leftarrow X\ ^1\Sigma_g^+$ Absorption Spectrum of the F_2 Molecule", J. Chem. Phys. 70, 3191 (1979). (A-2.1) - (A-2.21).

2. A. D. McClean, O. Gropen and S. Huzinaga, "Near Hartree-Fock Calculations on I_2 and its Positive and Negative Ions", J. Chem. Phys. 73, 396 (1980). (A-2.22) - (A-2.26).

3. O. Gropen, S. Huzinaga and A. D. McClean, "Model Potential SCF Calculations on Cl_2, Br_2 and I_2", J. Chem. Phys. 73, 402 (1980).

A-2.1. References in Tables (A-2.5 - A-2.7) and Figures (A-2.15 - A-2.20).

1. a) K. Hijikata, Rev. Mod. Phys. 32, 445 (1960); b) J. Chem. Phys. 34, 221 (1961); c) ibid, 231 (1961).

2. S. Fraga and B. J. Ransil, J. Chem. Phys. 36, 1127 (1962).

3. A. C. Wahl, J. Chem. Phys. 41, 2600 (1964).

4. G. Das and A. C. Wahl, J. Chem. Phys. 44, 87 (1966).

5. F. E. Harris and H. H. Michels, Int. J. Quant. Chem. 1, 329 (1967).

6. H. F. Schaefer III, J. Chem. Phys. 52, 6241 (1970).

7. G. Das and A. C. Wahl, Phys. Rev. Letts. 24, 440 (1970).

8. G. Das and A. C. Wahl, J. Chem. Phys. 56, 3532 (1972).

9. D. J. Ellis, K. E. Banyard, A. D. Tait and M. Dixon, J. Phys. B 6, L233 (1973).

10. E. Kasseckert, Z. Naturforsch. 28a, 704 (1973).

11. J. C. Ellenbogen, O. W. Day and D. W. Smith, J. Chem. Phys. 66, 4795 (1977).

12. E. A. Colbourn, M. Dagenais, A. E. Douglas and J. W. Raymonda, Can. J. Phys. 54, 1343 (1976).

13. B. Rosen, Spectroscopic Data, (Pergamon Press, Oxford, 1970).

14. A. L. G. Rees, J. Chem. Phys. 26, 1567 (1957).

15. M. Karplus and H. J. Kolker, J. Chem. Phys. 38, 1263 (1963).

16. R. S. Mulliken and C. A. Rieke, Rep. Prog. Phys. 8, 231 (1941).

17. S. R. LaPaglia, J. Chem. Phys. 48, 537 (1968).

18. R. K. Steunenberg and R. C. Vogel, J. Am. Chem. Soc. 78, 901 (1956).

19. D. C. Cartwright and P. J. Hay, J. Chem. Phys. 70, 3191 (1979).

Tabular Data A-2.2. Calculated energies of the singlet states of F_2 from POL-CI calculations. All energies are relative to -190.0 a.u. (Hartree)

R(Å)	$1^1\Sigma_g^+$	$^1\Pi_u$	$^1\Pi_g$	$^1\Delta_g$	$2^1\Sigma_g^+$	$^1\Sigma_u^-$
1.10	-8.754712	-8.296229	-7.987712	-7.840293	-7.818810	-7.664117
1.20	-8.843093	-8.508040	-8.282038	-8.178496	-8.157384	-8.048394
1.30	-8.882522	-8.636871	-8.473672	-8.396737	-8.378698	-8.312610
1.42	-8.895255	-8.724705	-8.617294	-8.561208	-8.547890	-8.513651
1.50	-8.892769	-8.758819	8.679156	-8.633343	-8.622984	-8.601669
1.60	-8.883990	-8.785234	-8.731788	-8.696307	-8.688990	-8.677718
1.80	-8.862161	-8.810314	-8.788170	-8.767440	-8.763920	-8.761464
2.00	-8.845432	-8.819910	-8.811807	-8.799980	-8.798222	-8.798262
2.40	-8.831066	-8.825783	-8.825366	-8.821283	-8.820711	-8.821314
4.00	-8.827312	-8.826839	-8.826944	-8.826224	-8.826194	-8.826251

Tabular Data A-2.3. Calculated energies of the triplet states of F_2 from POL-CI calculations. All energies are relative to -190. a.u. (Hartrees)

R(Å)	$^3\Pi_u$	$^3\Pi_g$	$1\,^3\Sigma_u^+$	$^3\Sigma_g^-$	$^3\Delta_u$	$2\,^3\Sigma_u^+$
1.10	-8.366177	-8.038903	-8.039467	-8.879596	-8.744634	-8.692755
1.20	-8.572280	-8.323135	-8.313049	-8.214061	-8.042750	-8.038217
1.30	-8.694252	-8.505171	-8.491359	-8.427151	-8.307796	-8.303968
1.42	-8.773297	-8.639096	-8.625381	-8.584322	-8.509816	-8.506790
1.50	-8.801398	-8.695759	-8.683344	-8.651606	-8.598417	-8.595843
1.60	-8.820398	-8.743251	-8.732906	-8.709239	-8.675098	-8.672995
1.80	-8.831998	-8.793066	-8.786641	-8.773265	-8.759797	-8.758373
1.90	-8.832494	—	—	—	—	—
2.00	-8.831974	-8.813475	-8.809801	-8.802501	-8.797214	-8.796215
2.10	-8.831174	—	—	—	—	—
2.40	-8.829163	-8.825088	-8.824089	-8.821839	-8.820896	-8.820354
4.00	-8.826946	-8.826840	-8.827307	-8.826251	-8.826224	-8.826193

Tabular Data A-2.4. Vertical excitation energies for the states of F_2 from POL-CI calculations at R = 1.42 A.

State	Excitation	Energy (eV) GVB-CI	POL-CI
		Singlet States	
$1^1\Sigma_g^+$	—	0.00[a]	0.00[b]
$^1\Pi_u$	$1\pi_u \rightarrow 3\sigma_u$	5.24	4.64
$^1\Pi_g$	$1\pi_g \rightarrow 3\sigma_g$	7.78	7.56
$^1\Delta_g$	$1\pi_u^2 \rightarrow 3\sigma_g^2$	10.25	9.09
$2^1\Sigma_g^+$	"	10.44	9.45
$^1\Sigma_u^-$	$1\pi_u\, 1\pi_g \rightarrow 3\sigma_g^2$	11.18	10.38
		Triplet States	
$^3\Pi_u$	$1\pi_u \rightarrow 3\sigma_u$	4.26	3.32
$^3\Pi_g$	$1\pi_g \rightarrow 3\sigma_g$	7.46	6.97
$1^3\Sigma_u^+$	$3\sigma_g \rightarrow 3\sigma_u$	7.01	7.34
$^3\Sigma_g^-$	$1\pi_u^2 \rightarrow 3\sigma_g^2$	9.94	8.46
$3\Delta_u$	$1\pi_u\, 1\pi_g \rightarrow 3\sigma_g^2$	11.25	10.49
$2^3\Sigma_u^+$	"	11.31	10.57

[a] E_T = - 198.81355 a.u.

[b] E_T = - 198.895255 a.u.

Tabular Data A-2.5. Spectroscopic Constants for F_2.

Ref.	Author	Total Energy	D_e(eV)	R_e(Å)	ω_e	$\omega_e X_e$	B_e	α_e	Type of calculation
(1)	Hijikata	-197.9428	2.02	1.437					MB-STO, CI
(2)	Fraga & Ransil	-197.9558	2.05						MB-STO, CI
(3)	Wahl	-198.7683	-1.63	1.418	1257	9.85	1.003	.0108	STO, SCF
(4)	Das & Wahl	-198.8377	.54	1.450	678				STO, OC
(5)	Harris & Michels	-197.9583	2.04	1.381					MBS, valence CI
(6)	Schaefer	-198.8303	0.32	1.656	516				VB
		-198.9619	0.69	1.588					CI
(7,8)	Das & Wahl	-198.9809	1.67	1.413	942		. 88	.0160	STO, OVC
(9)	Ellis et al.	-197.96	—	1.397	1158	12.4	. 91	.0111	MBS-CI
(10)	Kasseckert	-198.8641	1.56	1.508	874				STO, SCF-CI
(11)	Ellenborgen et al.	-198.8777	1.619						Extended Koopman
(19)	Cartwright and Hay	-198.8953	1.85	1.418	946.3	10.62	.87	.0116	POL-CI
	Experiment	-199.67[b]	1.602±.006	1.4118	916.6[a)]	11.24[a)]	.8902[a)]	.0137[a)]	$v'' \leq 8$
					924.3	22.23	.89	.0145	$v'' \leq 22$

[a] reference 12

[b] reference 6

Tabular Data A-2.6. Comparison of calculated dissociation energies of the ground state of F_2

	No. of Configs.	Total energy[a] $R = R_e$	$R = \infty$	D_e (eV)
Das, Wahl (1972)[b]				
OVC	2	-0.84325	-0.81820	0.68
OVC	6	-0.88526	-0.81820	1.82
OVC + pert. theory		-0.98092	-0.91934	1.67
Cartwright and Hay (1979)[d]				
GVB-PP	2	-0.80933	-0.78855	0.56
GVB-CI	6	-0.81355	-0.79955	0.68
POL-CI	268	-0.89525	-0.82731	1.91
Experiment[c]				1.602 ± 0.006

[a] Relative to -198. hartree

[b] Reference 8

[c] Reference 12

[d] Reference 19

Tabular Data A-2.7. Comparison of Spectroscopic constants for the lowest $^3\Pi_u$ state in F_2 and $C\ell_2$.

	Ref.	R_e(Å)	D_e(eV)	ω_e (cm^{-1})	$\omega_e x_e$ (cm^{-1})	B_e (cm^{-1})	α_e (cm^{-1})
$F_2(^3\Pi_u)$	18	1.881	0.15	303			
$F_2(X^1\Sigma_g^+)$	12	1.4118	1.602	917	11.2	0.89	0.0137
$\alpha_2(^3\Pi_{o^+u})$	13	2.396	0.30	362	5.45	0.1680	0.0037
$C\ell_2(X^1\Sigma_g^+)$	13	1.988	2.51	560	2.70	0.2441	0.00153

Tabular Data A-2.8. Exponential fits of the repulsive curves of F_2 from the POL-CI calculations. The parameters a and b refer to a potential of the form $V(R) = ae^{-bR}$

State	a(eV)	b($\mathring{A}^{-1}$)
$^1\Pi_u$	2.801	5.131
$^1\Pi_g$	5.688	4.359
$^1\Delta_g$	7.236	4.037
$2^1\Sigma_g^+$	7.585	3.972
$^1\Sigma_u^-$	11.273	3.126
$^3\Pi_u$	1.452	7.146
$^3\Pi_g$	5.104	4.490
$1^3\Sigma_u^+$	5.500	4.243
$^3\Sigma_g^-$	6.633	4.171
$^3\Delta_u$	8.614	4.118
$2^3\Sigma_u^+$	8.699	4.099

Tabular Data A-2.9. Quadrupole moment and electric field gradient (a.u.)[†] for the F_2 ground state using the POL-CI wavefunction.

R(Å)	θ_{zz}	q_{zz}
1.0	-0.38444	-5.69727
1.1	-0.07072	-5.77319
1.2	+0.22671	-5.87022
1.3	0.49823	-5.95351
1.4	0.73759	-6.00917
1.42	0.78124	-6.01652
1.5	0.94105	-6.03278
1.6	1.10636	-6.02391
1.7	1.23263	-5.98520
1.8	1.32133	-5.92258
2.0	1.40674	-5.76052
2.4	1.39292	-5.46749
3.0	1.32984	-5.20782
4.0	1.32425	-5.43992

[†]1 a.u. for θ_{zz} is ea_o^2 = 1.3450×10^{-26} cgsesu. (quadrupole moment)

1 a.u. for q_{zz} is e/a_o^3 = $3.2414 \times 10^{+15}$ cgsesu. (electric field gradient at nucleus)

Tabular Data A-2.10. Transition moment (a.u.) for the $1^1\Sigma_g^+ \rightarrow {}^1\pi_u$ excitation in F_2 (1 a.u. = 2.542 D)

R(Å)	GVB-CI [3s2pld]basis	POL-CI [3s2pld]basis	POL-CI [4s3pld]basis
1.10	-0.1567	0.0007	0.0944
1.20	-0.1291	.0000	.0234
1.30	-0.0989	.0076	.0199
1.42	-0.0652	.0164	.0255
1.50	-0.0467	.0204	.0289
1.60	-0.0287	.0231	.0313
1.70	-0.0160	.0235	.0315
1.80	-0.0073	.0222	.0299
2.0	-0.0001	.0170	.0237
2.4	0.0016	.0071	.0112
3.0	0.0006	.0020	.0034
4.0	0.0002	.0007	.0053

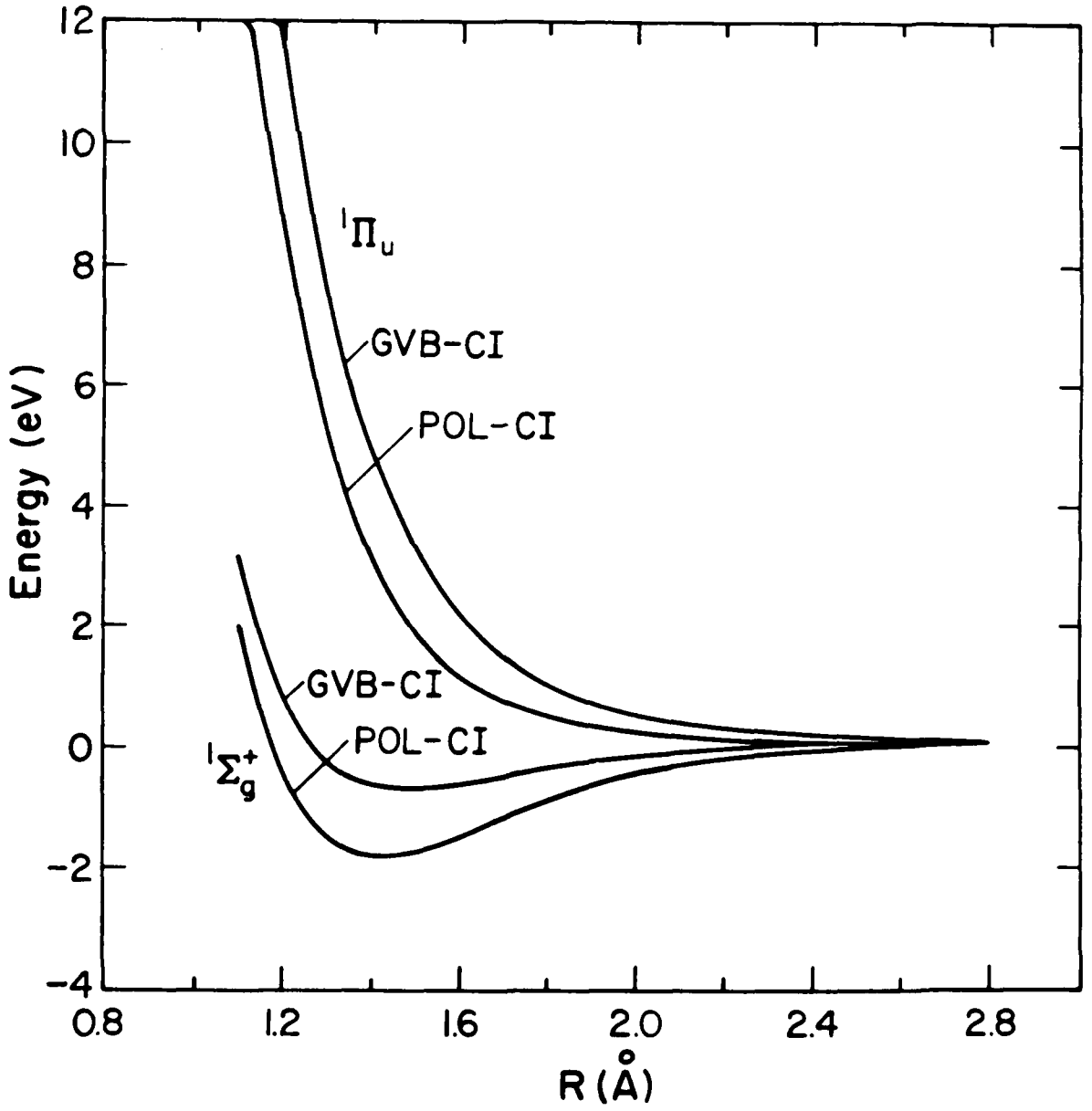

Graphical Data A-2.11. Potential energy curves for the ground electronic state and lowest $^1\Pi_u$ state of F_2 as calculated using the GVB-CI and POL-CI descriptions.

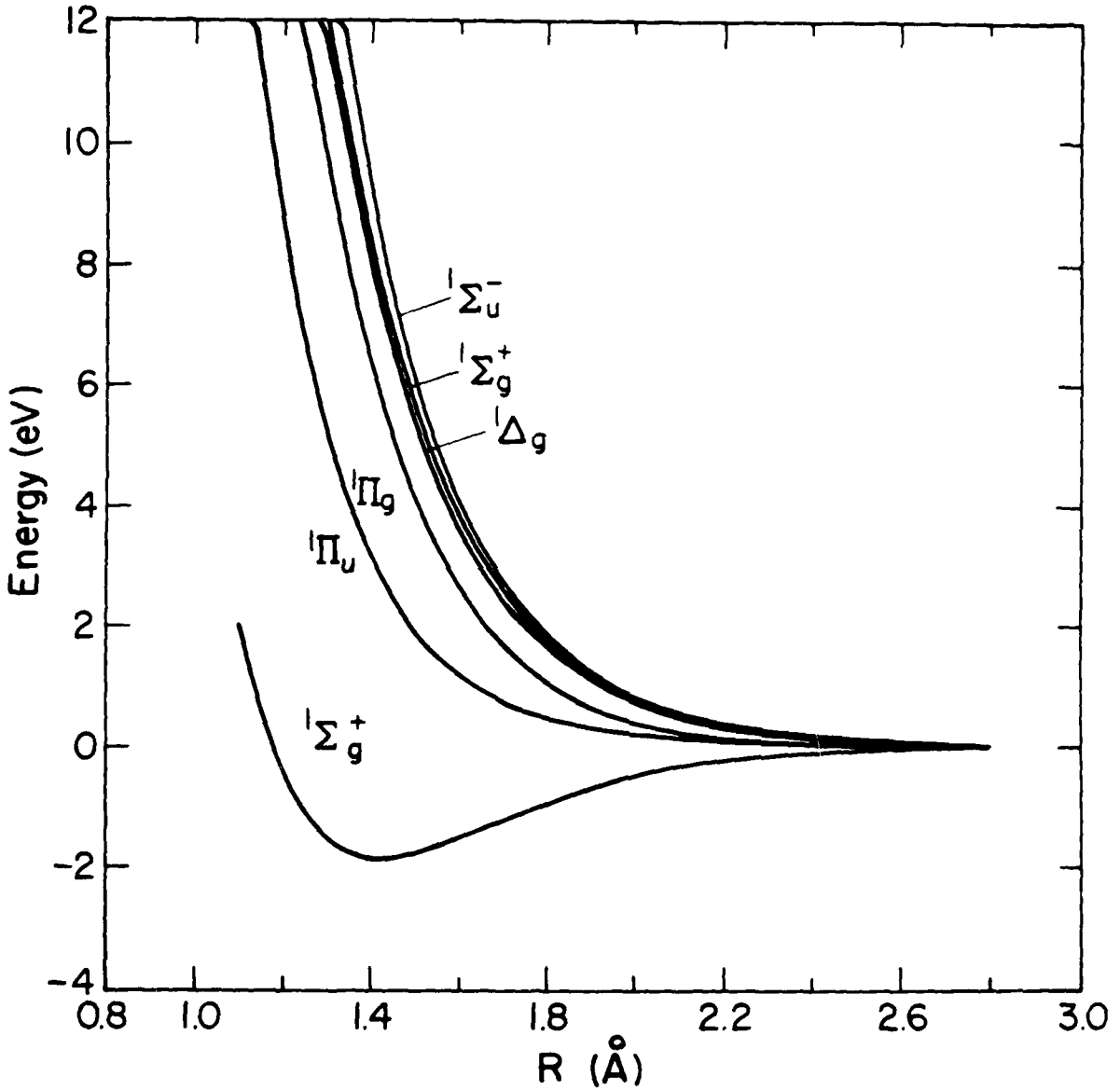

Graphical Data A-2.12. Potential energy curves, obtained using the POL-CI description, for the singlet valence states of F_2 dissociating into ground state F atoms.

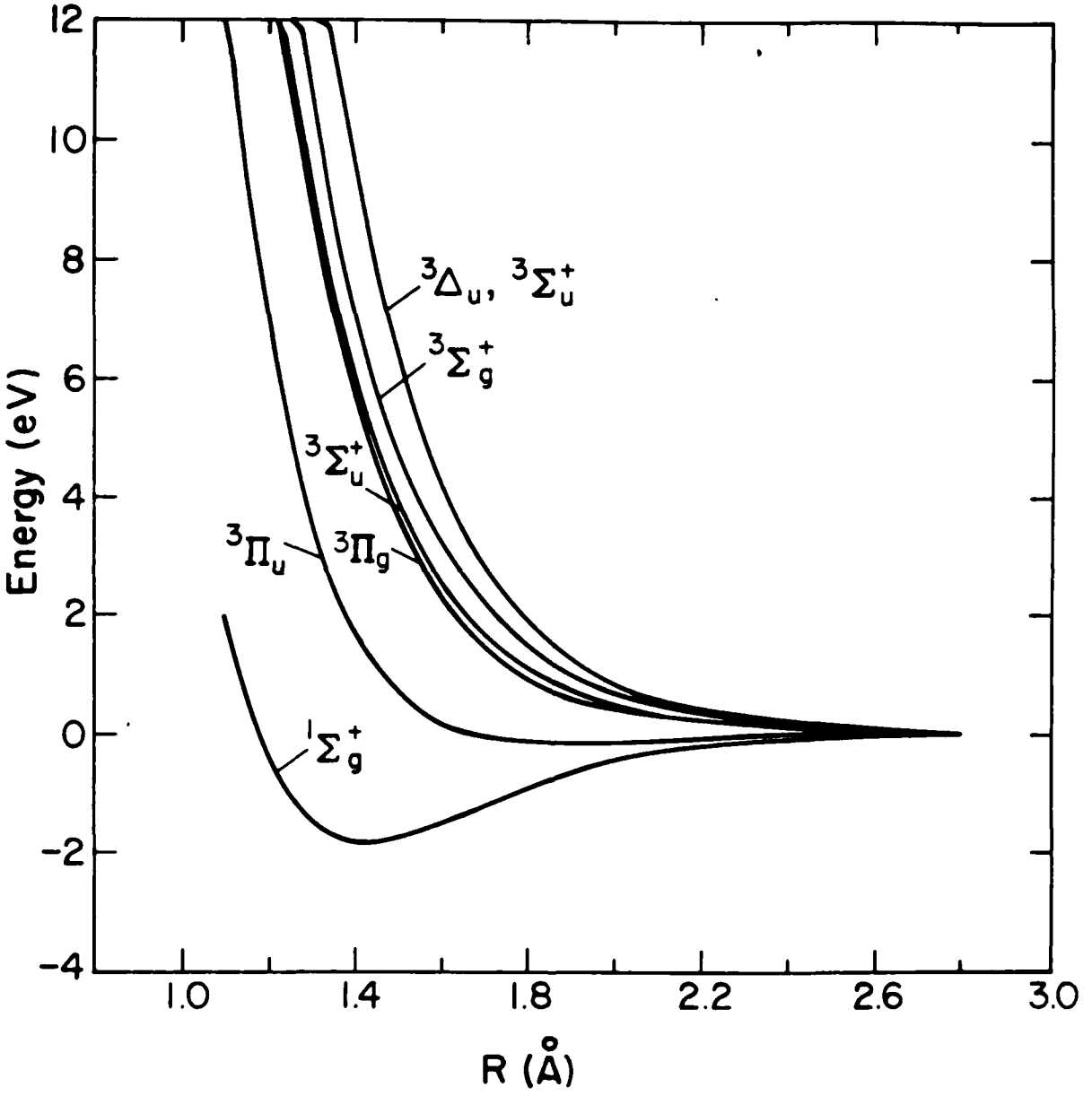

Graphical Data A-2.13. Potential energy curves, obtained using the POL-CI description for the ground electronic states and those triplet electronic states dissociating into ground state F atoms.

F_2 VALENCE STATES

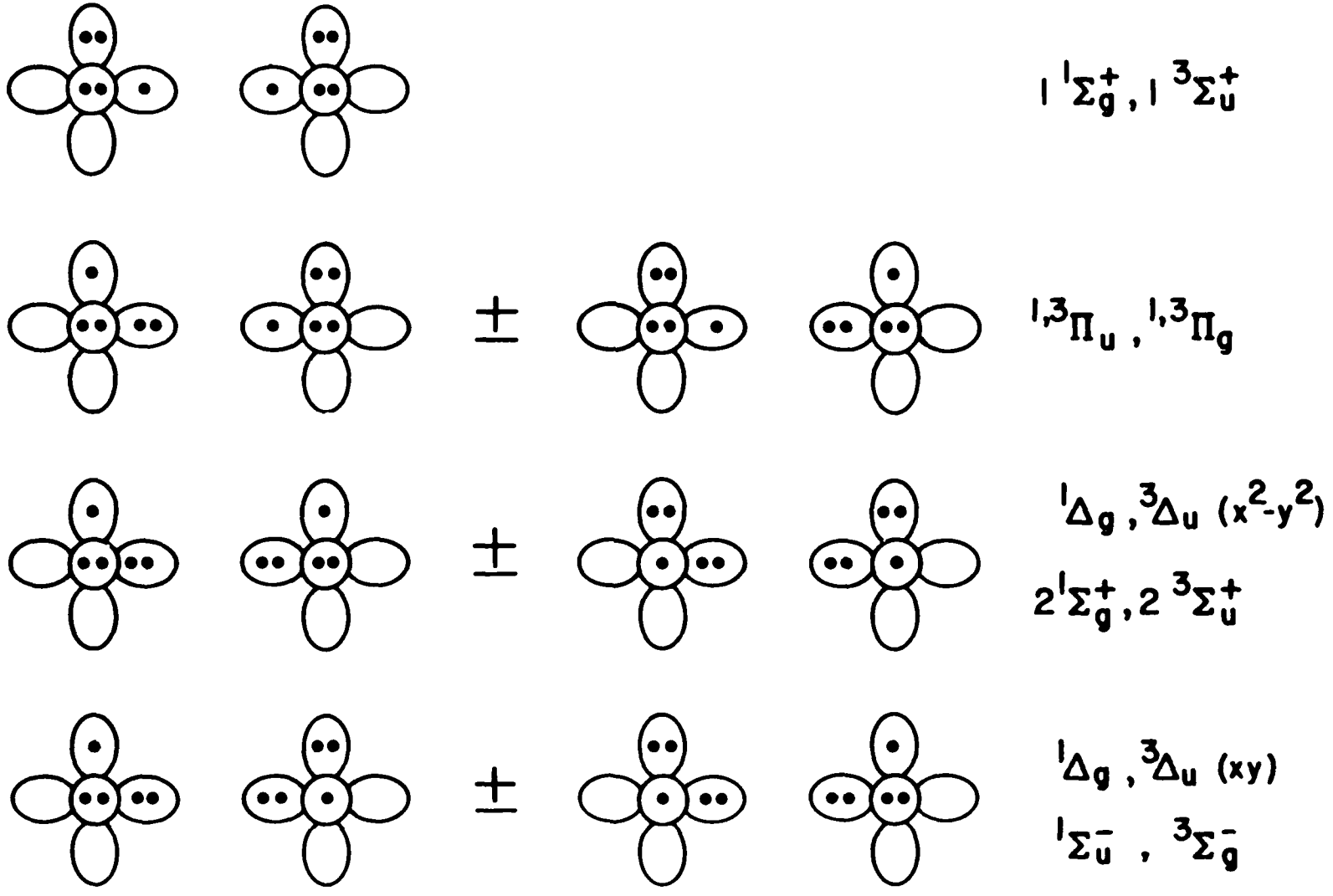

Graphical Data A-2.14. Orbital diagrams indicating how two ground state (^2P) F atoms are combined to give the various valence electronic states. Only the atomic p-orbitals are shown and the electron occupancy is indicated by dots.

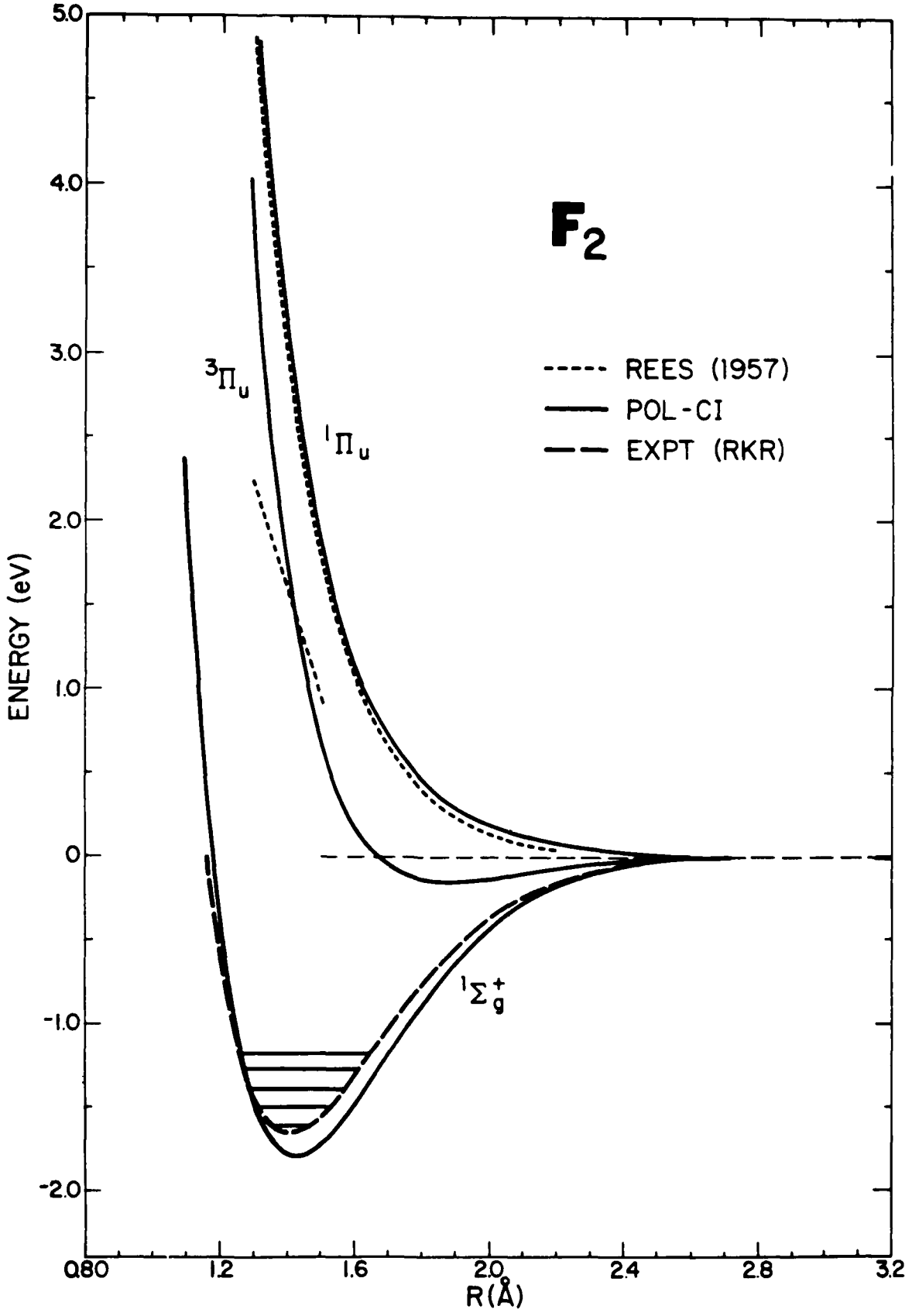

Graphical Data A-2.15. Potential energy curves for the ground state and the valence $^3\Pi_u$ and $^1\Pi_u$ electronic states of F_2 as calculated using the POL-CI description. Experimental ground state curve (Reference 12) and Rees (Reference 14) of A-2.1.

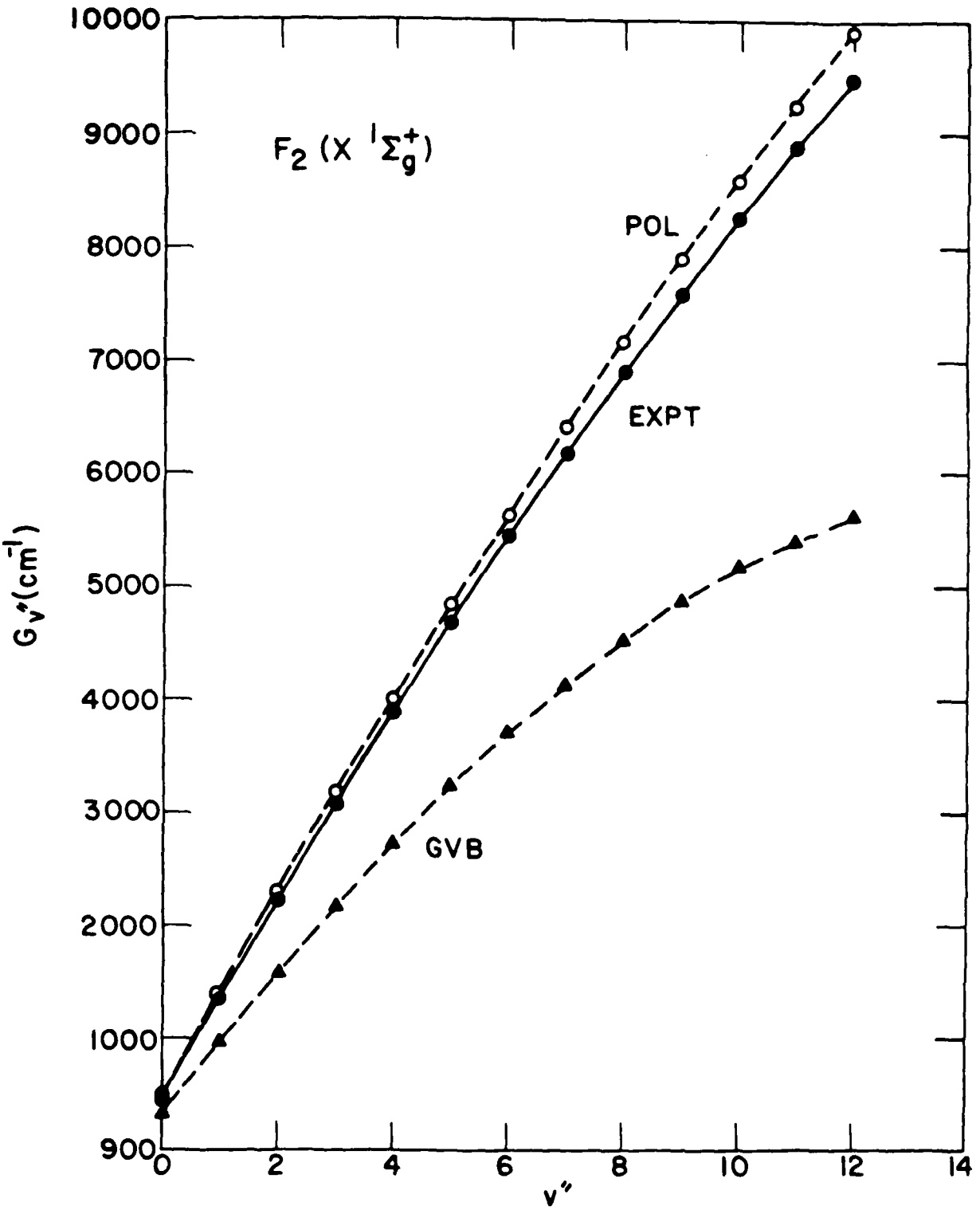

Graphical Data A-2.16. Comparison between the measured (Reference 14) and theoretical $G_{v''}$ values for the ground state of F_2, as a function of the vibrational quantum number. Results obtained using both the POL-CI and GVB wavefunctions are shown for comparison.

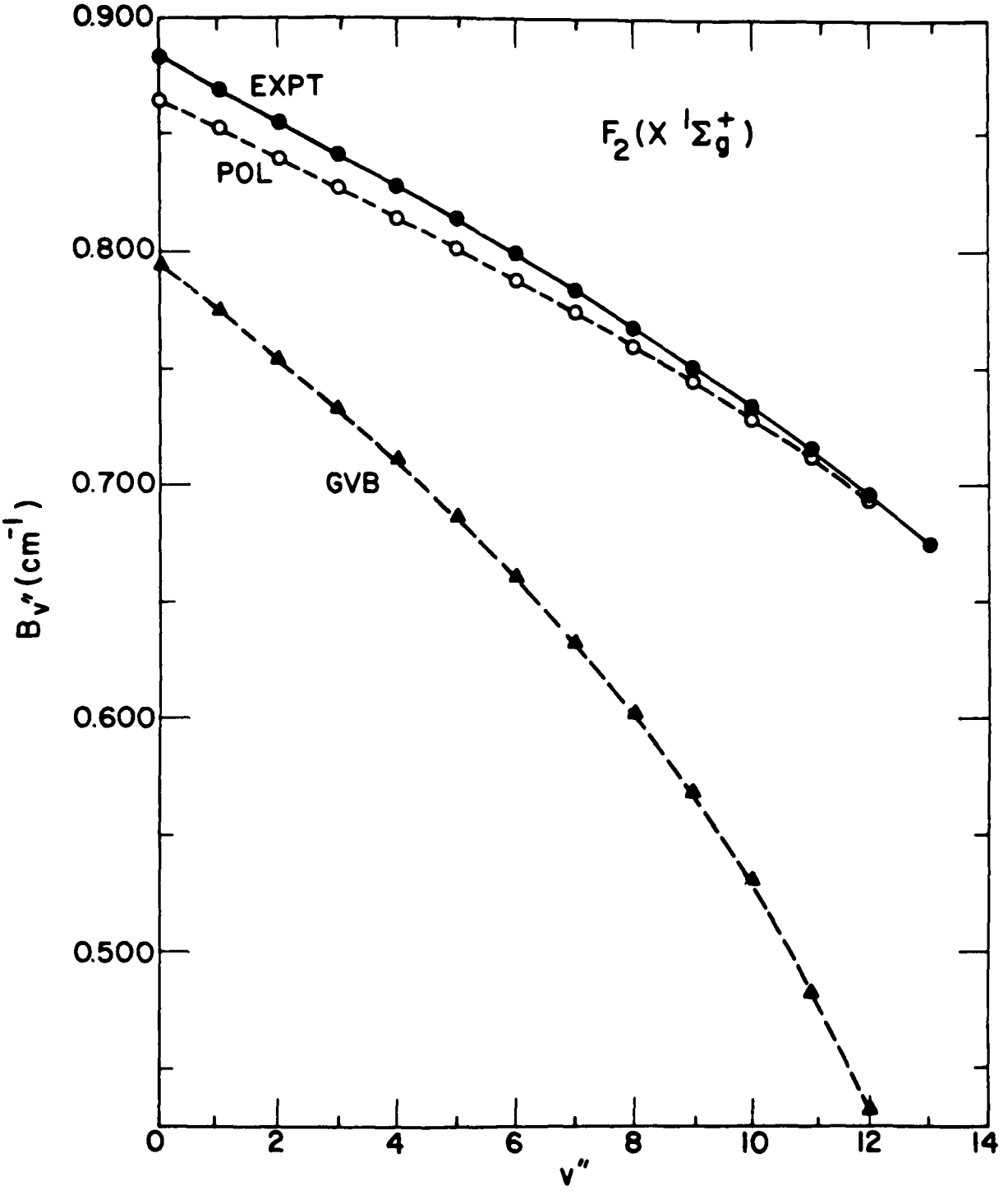

Graphical Data A-2.17. Comparison between the measured and theoretical $B_{v''}$ values for the ground state of F_2, as a function of the vibrational quantum number. Results obtained using both the POL-CI and GVB wavefunctions descriptions for the ground state are shown for comparison.

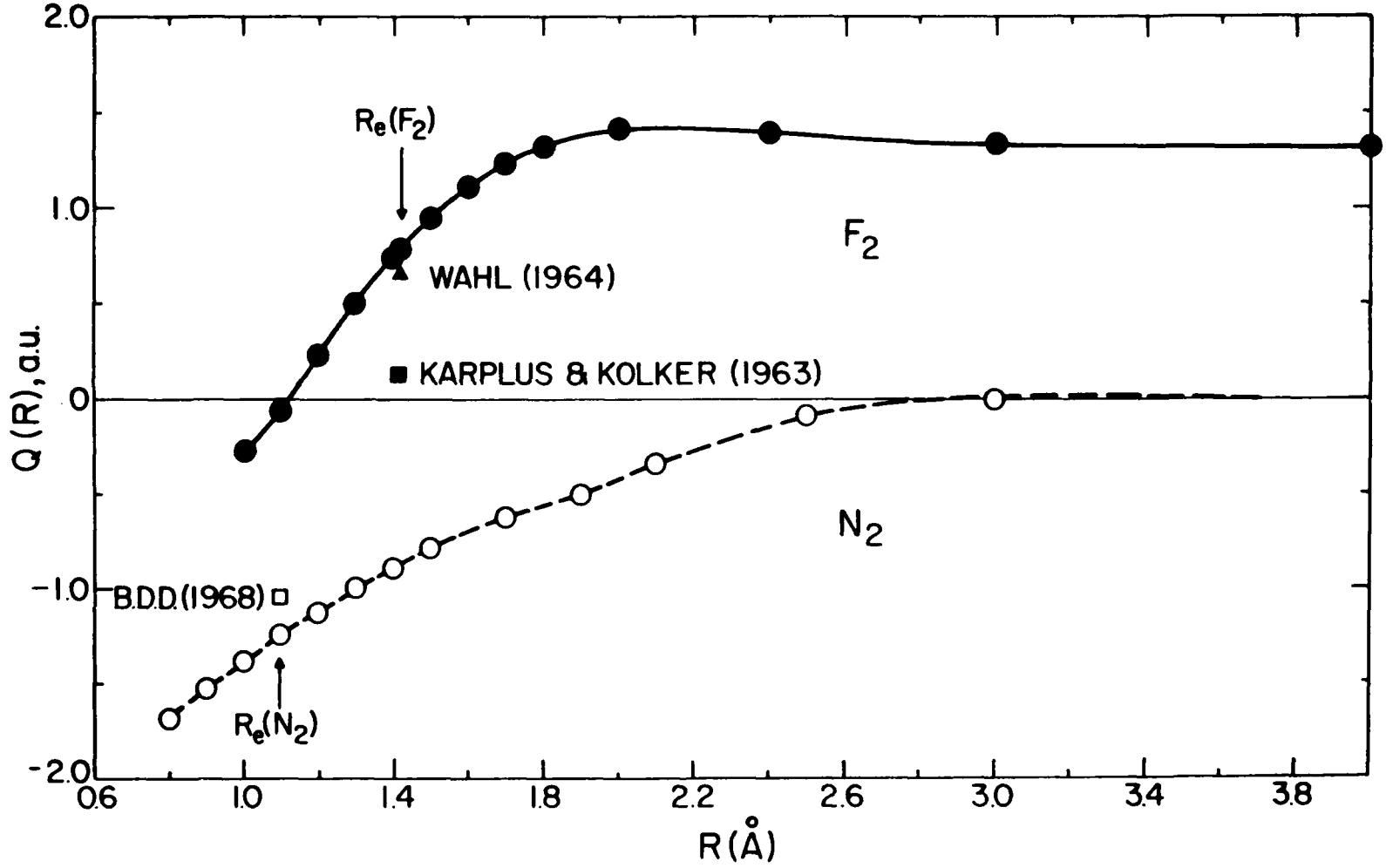

Graphical Data A-2.18. Quadrupole moment, as a function of internuclear distance, for ground state of F_2, as obtained using the POL-C I description. Wahl (Reference 3), Karplus and Kolker (Reference 15).

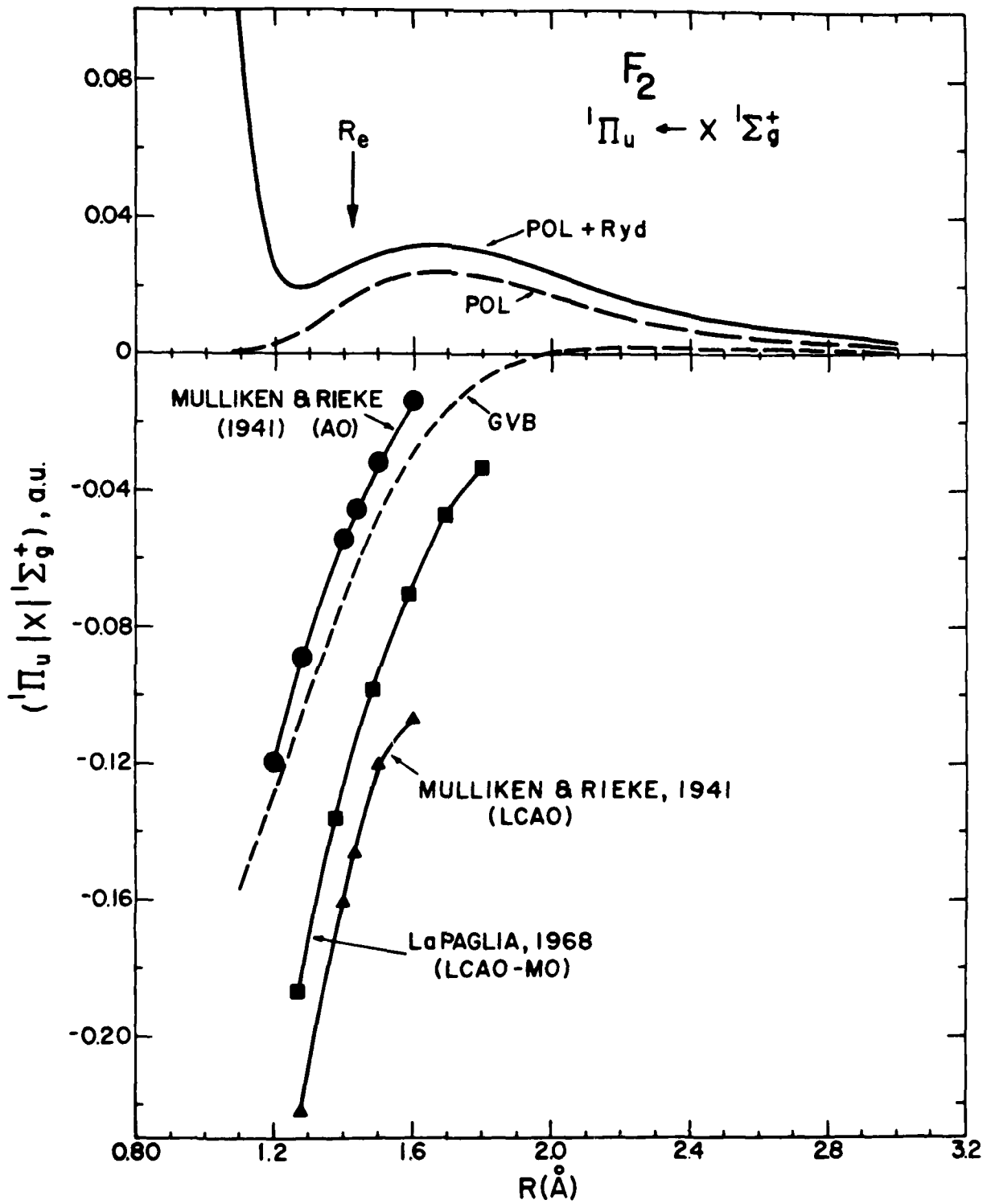

Graphical Data A-2.19. Electronic transition moment, as a function of internuclear distance, for the $^1\Pi_u \leftarrow X^1\Sigma_g^+$ excitation in F_2. Results obtained using the GVB-CI, POL-CI and POL-CI with Rydberg functions are compared to values in References 16 and 17.

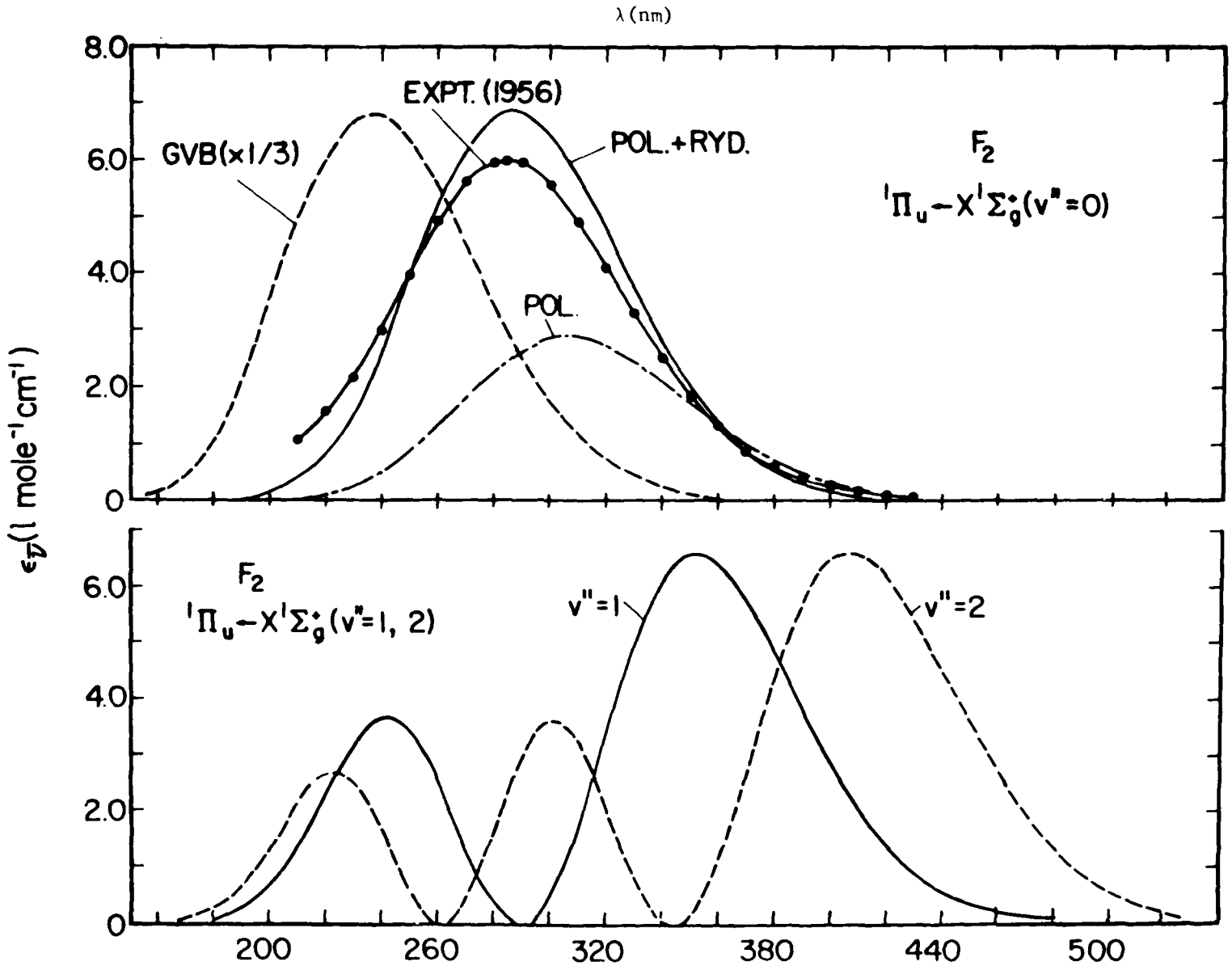

Graphical Data A-2.20. Molar absorbancy, as a function of incident radiation wavelength λ, for F_2 in its lowest vibrational level (upper portion) and for F_2 initially in v"=1 and 2 (lower portion). Except (Reference 18).

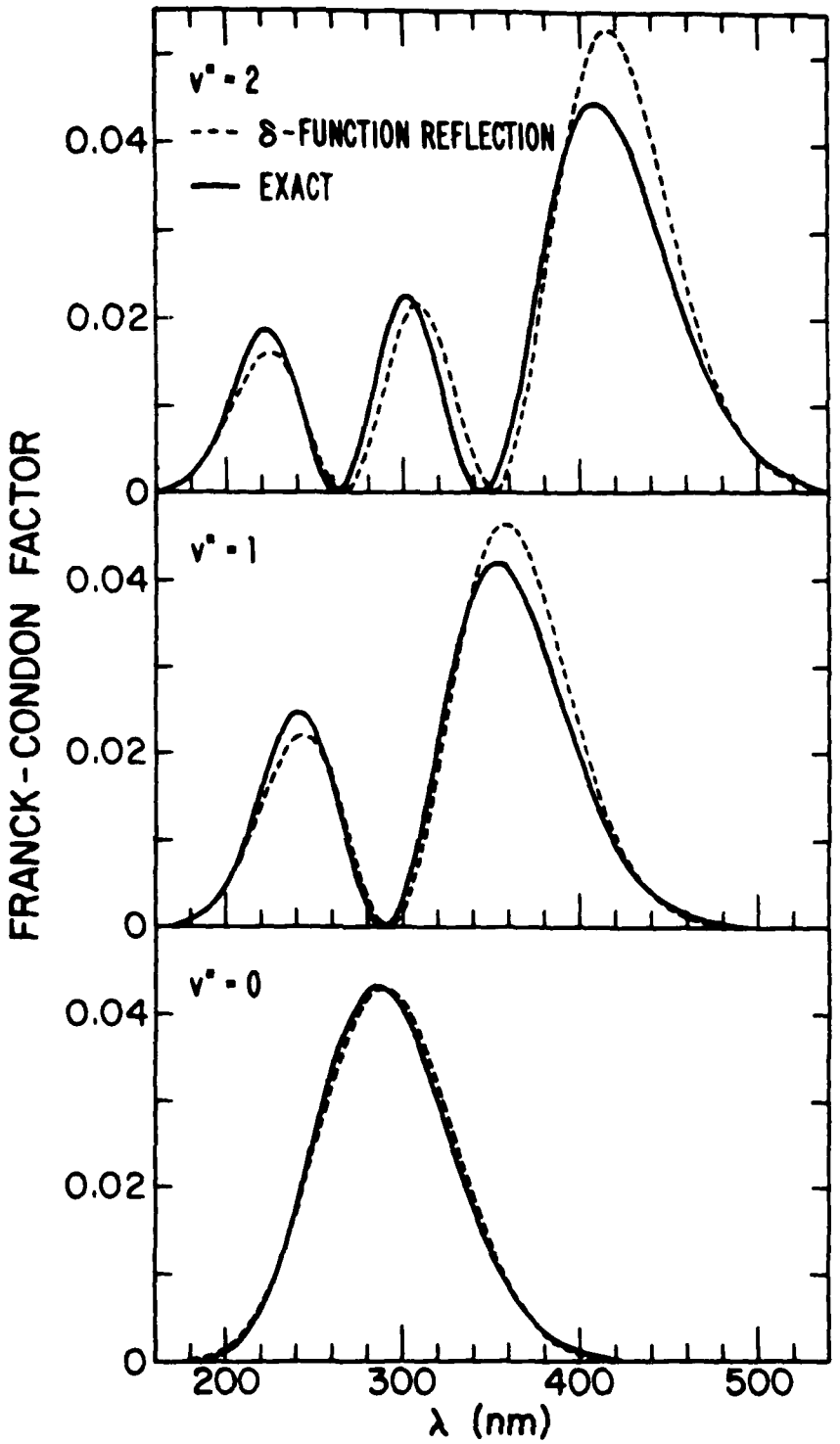

Graphical Data A-2.21. Comparison of bound-continuum Franck-Condon factors for F_2 calculated using the complete vibrational wavefunction and using the delta-function-reflection method.

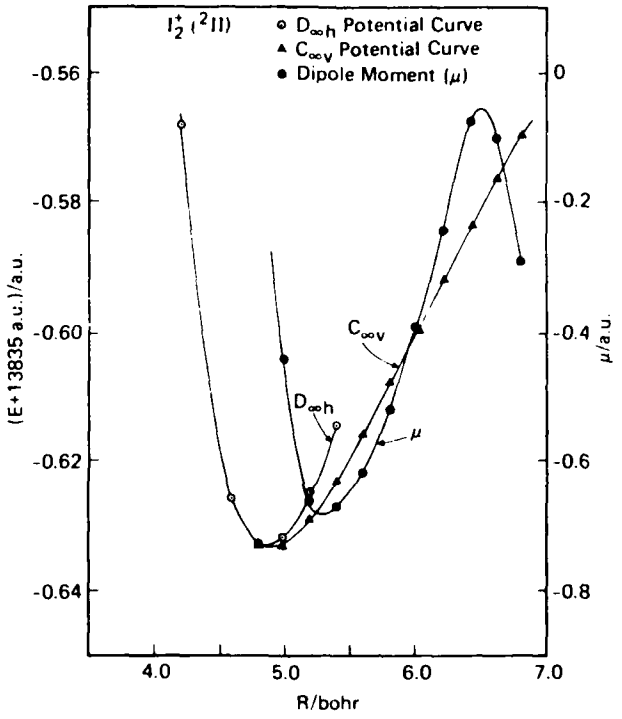

Graphical Data A-2.22. SCF potential curves for $I_2^+(^2\Pi)$ showing, in the range 4.8–5.4 bohr, two stable solutions of the SCF equations, the higher with $D_{\infty h}$ symmetry, the lower with $C_{\infty v}$ symmetry. Also shown is the dipole moment curve (computed relative to the nuclear midpoint) of the $C_{\infty v}$ solution.

Tabular Data A-2.23. Spectroscopic analysis of potential curves.[a]

Molecule	Total energy (hartree)	Property R_e (bohr)	R_e (Å)	ω_e (cm^{-1})	$\omega_e x_e$ (cm^{-1})	B_e (cm^{-1})	α_e (cm^{-1})
I_2 ($^1\Sigma$) SCF	−13835.97608	5.061	2.678	230.2	0.34	0.03706	0.00008
expt.[b]			2.667	214.52	0.61	0.03738	0.00012
I_2^- ($^2\Sigma$) SCF	−13836.05591	6.258	3.311	106.8	0.35	0.0242	0.00009
expt.[c]			3.28	109	0.3		
I_2^+ ($^2\Pi$) SCF[d]	−13835.63323	4.861	2.572	275	0.47	0.04016	0.00008
SCF[e]	−13835.63351	4.896	2.591	227	9.0	0.03961	0.00020
I_2^+ ($^2\Sigma$) SCF	−13835.54514	5.770	3.053	120.7	0.26	0.02850	0.00010

[a] All values are for I^{127}.
[b] *Selected Constants. Spectroscopic Data Relative to Diatomic Molecules*, edited by B. Rosen (Pergamon, New York, 1970).
[c] Empirical estimate of W. B. Person, J. Chem. Phys. 38, 109 (1963).
[d] Potential curve with delocalized wave functions (A-2.22)
[e] Potential curve with localized wave functions (A-2.22)

Tabular Data A-2.24. Molecular quadrupole moments from SCF wave functions (all entries in atomic units).

	I_2 ($^1\Sigma$)		I_2^- ($^2\Sigma$)		I_2^+ ($^2\Pi$)		I_2^+ ($^2\Sigma$)	
R (bohr)	$\langle z^2-\frac{1}{2}\rho^2\rangle_1$	$\theta_{c.m.}$	$\langle z^2-\frac{1}{2}\rho^2\rangle_1$	$\theta_{c.m.}$	$\langle z^2-\frac{1}{2}\rho^2\rangle_1$	$\theta_{c.m.}$	$\langle z^2-\frac{1}{2}\rho^2\rangle_1$	$\theta_{c.m.}$
4.6					1105.8442	10.346		
4.8	1217.1694	3.951			1203.9366	11.423		
5.0	1320.5035	4.497			1306.2923	12.458		
5.2	1428.1307	4.989			1412.9000	13.460		
5.4	1540.0478	5.432					1520.4378	17.752
5.6							1635.6618	18.578
5.8							1755.1269	19.383
6.0			1927.6029	−10.603			1878.8273	20.173
6.2			2057.7465	−10.817				
6.4			2192.2352	−11.115				
6.6			2331.0592	−11.489				

$$\theta_{c.m.} = \theta_1 - \mu_1 R + qR^2/4; \quad \theta_1 = 53R^2 - \langle z_1^2 - \frac{1}{2}\rho_1^2 \rangle$$

where μ_1 is the dipole moment relative to the left-hand nucleus as the coordinate origin, and q is the net charge on the system, θ_1 and θ_{cm} are the molecular quadrupole moments relative to the nucleus, and to the center of mass (internuclear midpoint) respectively. (See A. D. McLean and M. Yoshimine, J. Chem. Phys. 47, 1927 (1967)).

Tabular Data A-2.25. SCF potential curves for I_2, I_2^-, and I_2^+.[a,b]

	Total energy + 13835.0 (hartree)			
R (bohr)	$I_2(^1\Sigma_g^+)$	$I_2^-(^2\Sigma_u^+)$	$I_2^+(^2\Pi_u)$	$I_2^+(^2\Sigma_g^+)$
3.8	−0.69759		−0.40080	−0.21333
4.2	−0.88306		−0.56839	−0.40357
4.4	−0.92923			−0.45544
4.6	−0.95649	−0.94863	−0.62580	−0.49010
4.8	−0.97066	−0.98274	−0.63289	−0.51297
5.0	−0.97582	−1.00807	−0.63161 −0.63288*	−0.52772
5.2	−0.97488	−1.02618	−0.62486 −0.62921*	−0.53687
5.4	−0.96985	−1.03871	−0.61464 −0.62327*	−0.54209
5.6	−0.96219	−1.04699	−0.61603*	−0.54457
5.8	−0.95290	−1.05209	−0.60811*	−0.54512
6.0	−0.94273	−1.05483	−0.59995*	−0.54433
6.2	−0.93217	−1.05586	−0.59185*	−0.54262
6.4	−0.92160	−1.05566	−0.58404*	−0.54031
6.6	−0.91124	−1.05461	−0.57664*	−0.53762
6.8		−1.05299	−0.56974	−0.53475
7.0	−0.89179	−1.05100	−0.56339*	−0.53180
10.0	−0.81064	−1.03867*	−0.52035*	
20.0		−1.03457*	−0.51292*	−0.51358*

[a]All energies reported in this table are directly computed with the ALCHEMY programs written at the IBM San Jose Research Laboratory.

[b]Energies marked with an asterisk are from wave functions with a nonzero dipole moment relative to the nuclear midpoint. Those without an asterisk are from wave functions with the symmetry of the nuclear frame.

Tabular Data A-2.26. SCF electron affinities and ionization potentials.

Energy levels	Property	SCF (eV)	Expt. (eV)
$I(^2P_u)$, $I^-(^1S_g)$	E.A. (I)	2.48	3.063 ± 0.003[a]
$I^+(^3P_1)$, $I(^2P_u)$	I.P. (I)	9.62	10.451[b]
$I_2(^1\Sigma_g^+)$, $I_2^-(^2\Sigma_u^+)$	E.A. (I_2) (adiab.) E.A. (I_2) (vert.)	2.17 1.04	2.58 ± 0.1[c] 1.7 ± 0.07[d]
$I_2^+(^2\Pi_u)$, $I_2(^1\Sigma_g^+)$	I.P. (I_2)	9.33	9.28 ± 0.02[e]
$I_2^+(^2\Sigma_g^+)$, $I_2(^1\Sigma_g^+)$	I.P. (I_2)	11.73	

[a]R. S. Berry and C. W. Reimann, J. Chem. Phys. 38, 1540 (1963). If the spin–orbit effect is taken out, this value would increase to 3.37 eV to better compare with the SCF value, see the text.

[b]C. E. Moore, "Analysis of Optical Spectra," Natl. Stand. Ref. Data Ser. Natl. Bur. Stand. (1969).

[c]W. A. Chupka, J. Berkowitz, and David Gutman, J. Chem. Phys. 55, 2724 (1971).

[d]J. Jortner and W. Sokolov, Nature (London) 190, 1004 (1961).

[e]K. Watanabe, J. Chem. Phys. 26, 542 (1957) gives 74 850 ± 160 cm^{-1}, from which the table entry is computed.

A-3. TRANSITION MOMENTS AND ABSORPTION PROFILES FOR ELECTRONIC STATES OF Ne_2^+, Ar_2^+, Kr_2^+, Xe_2^+, POTENTIAL ENERGY CURVES, SPECTROSCOPIC CONSTANTS AND ABSORPTION CROSS SECTIONS FOR Hg_2^+ AND Ar_3^+.

CONTENTS

		Page
A-3.1.	Transition moments (in a.u.) calculated for the $1(1/2)_u \rightarrow 1(3/2)_g$, $1(1/2)_u \rightarrow 1(1/2)_g$ and $1(1/2)_u \rightarrow 2(1/2)_g$ excitations in Ne_2^+	2578
A-3.2.	Transition moments (in a.u.) calculated for the $1(1/2)_u \rightarrow 1(3/2)_g$, $1(1/2)_u \rightarrow 1(1/2)_g$ and $1(1/2)_u \rightarrow 2(1/2)_g$ excitations in Ar_2^+	2579
A-3.3.	Transition moments (in a.u.) calculated for the $1(1/2)_u \rightarrow 1(3/2)_g$, $1(1/2)_u \rightarrow 1(1/2)_g$ and $1(1/2)_u \rightarrow 1(3/2)_g$ excitations in Kr_2^+	2580
A-3.4.	Transition moments (in a.u.) calculated for the $1(1/2)_u \rightarrow 1(3/2)_g$, $1(1/2)_u \rightarrow 1(1/2)_g$ and $1(1/2)_u \rightarrow 2(1/2)_g$ excitations in Xe_2^+	2581
A-3.5.	Calculated cross-sections (in cm^2) for $1(1/2)_u \rightarrow 2(1/2)_g$ in Ne_2^+ at 100K, 300K, 600K.	2582
A-3.6.	Calculated cross-sections (in cm^2) for $1(1/2)_u \rightarrow 2(1/2)_g$ in Ar_2^+ at 100K, 300K, 600K.	2583
A-3.7.	Calculated cross-sections (in cm^2) for $1(1/2)_u \rightarrow 2(1/2)_g$ in Kr_2^+ at 100K, 300K, 600K.	2585
A-3.8.	Calculated cross-sections (in cm^2) for $1(1/2)_u \rightarrow 2(1/2)_g$ in Xe_2^+ at 100K, 300K, 600K.	2587
A-3.9.	Comparison of theoretical and experimental cross-sections (in 10^{-18} cm^2) for Ne_2^+ at (350.7 and 356.7)nm and Ar_2^+ at 4.13.1nm.	2589
A-3.10.	Experimental and theoretical values for the wave-length (in nm) and magnitude (in 10^{-18} cm^2) of the maximal absorption cross-section for the $1(1/2)_u \rightarrow 2(1/2)_g$ transition in Ne_2^+, Ar_2^+, Kr_2^+ and Xe_2^+ at 300K	2590
A-3.11.	Transition moment functions for the $1(1/2)_u \rightarrow 1(3/2)_g$ transition	2591
A-3.12.	Transition moment functions for the $1(1/2)_u \rightarrow 1(3/2)_g$ transition	2592
A-3.13.	Transition moment functions for the $1(1/2)_u \rightarrow 2(1/2)_g$ transition	2593

Page

A-3.14. Absorption profiles for Ne_2^+ $1(1/2)_u \rightarrow 2(1/2)_g$ 2594

A-3.15. Absorption profiles for Ar_2^+ $1(1/2)_u \rightarrow 2(1/2)_g$ 2595

A-3.16. Absorption profiles for Kr_2^+ $1(1/2)_u \rightarrow 2(1/2)_g$ 2596

A-3.17. Absorption profiles for Xe_2^+ $1(1/2)_u \rightarrow 2(1/2)_g$ 2597

A-3.18. Absorption profiles for Ne_2^+ $1(1/2)_u \rightarrow 1(1/2)_g$ 2598

A-3.19. Absorption profiles for Ar_2^+ $1(1/2)_u \rightarrow 1(1/2)_g$ 2599

A-3.20. Absorption profiles for Kr_2^+ $1(1/2)_u \rightarrow 1(1/2)_g$ 2600

A-3.21. Absorption profiles for Xe_2^+ $1(1/2)_u \rightarrow 1(1/2)_g$ 2601

A-3.22. Absorption profiles for Ne_2^+ $1(1/2)_u \rightarrow 1(3/2)_g$ 2602

A-3.23. Absorption profiles for Ar_2^+ $1(1/2)_u \rightarrow 1(3/2)_g$ 2603

A-3.24. Absorption profiles for Kr_2^+ $1(1/2)_u \rightarrow 1(3/2)_g$ 2604

A-3.25. Absorption profiles for Xe_2^+ $1(1/2)_u \rightarrow 1(3/2)_g$ 2605

A-3.26. Absorption cross-sections for $1(1/2)_u \rightarrow 1(1/2)_g$ in Ar_2^+ 2606

A-3.27. Absorption cross-sections for $1(1/2)_u \rightarrow 1(1/2)_g$ in Kr_2^+ 2607

A-3.28. Absorption cross-sections for $1(1/2)_u \rightarrow 1(1/2)_g$ in Xe_2^+ 2608

A-3.29. Total photoabsorption cross-sections for the $A\ ^2\Sigma_{1/2u}^+ \rightarrow D\ ^2\Sigma_{1/2g}^+$ transition of Ne_2^+ 2609

A-3.30. Total photoabsorption cross-sections for the $A\ ^2\Sigma_{1/2u}^+ \rightarrow D\ ^2\Sigma_{1/2g}^+$ transition of Ar_2^+ 2610

A-3.31. Total photoabsorption cross-sections for the $A\ ^2\Sigma_{1/2u}^+ \rightarrow D\ ^2\Sigma_{1/2g}^+$ transition of Kr_2^+ 2611

A-3.32. Total photoabsorption cross-sections for the $A\ ^2\Sigma_{1/2u}^+ \rightarrow D\ ^2\Sigma_{1/2g}^+$ transition of Xe_2^+ 2612

A-3.33. Photoabsorption cross-sections for the $A\ ^2\Sigma_{1/2u}^+ \rightarrow D\ ^2\Sigma_{1/2g}^+$ transition of Ar_2^+ as a function of vibrational level 2613

A-3.34. Photoabsorption cross-sections for the $A\ ^2\Sigma_{1/2u}^+ \rightarrow D\ ^2\Sigma_{1/2g}^+$ transition of Kr_2^+ as a function of vibrational level 2614

A-3.35. Photoabsorption cross-sections for the $A\ ^2\Sigma_{1/2u}^+ \rightarrow D\ ^2\Sigma_{1/2g}^+$ transition of Xe_2^+ as a function of vibrational level 2615

A-3.36. Total photoabsorption cross-sections for the $A\ ^2\Sigma_{1/2u}^+ \rightarrow D\ ^2\Sigma_{1/2g}^+$ transition of Ne_2^+ 2616

Page

A-3.37. Total photoabsorption cross-sections for the A $^2\Sigma^+_{1/2u}$ → D $^2\Sigma^+_{1/2g}$ transition of Ar_2^+. 2617

A-3.38. Total photoabsorption cross-sections for the A $^2\Sigma^+_{1/2u}$ → D $^2\Sigma^+_{1/2g}$ transition of Kr_2^+. 2618

A-3.39. Total photoabsorption cross-sections for the A $^2\Sigma^+_{1/2u}$ → D $^2\Sigma^+_{1/2g}$ transition of Xe_2^+. 2619

A-3.40. Photoabsorption cross-sections for the A $^2\Sigma^+_{1/2u}$ → D $^2\Sigma^+_{1/2g}$ transition of Kr_2^+ as a function of several vibrational levels. . . . 2620

A-3.41. Cross-sections for the A $^2\Sigma^+_{1/2u}$ → D $^2\Sigma^+_{1/2g}$ transition of Ne_2^+ at 300K 2621

A-3.42. Cross-sections for the A $^2\Sigma^+_{1/2u}$ → D $^2\Sigma^+_{1/2g}$ transition of Ar_2^+ at 300K 2622

A-3.43. Cross-sections for the A $^2\Sigma^+_{1/2u}$ → D $^2\Sigma^+_{1/2g}$ transition of Kr_2^+ at 300K 2623

A-3.44. Cross-sections for the A $^2\Sigma^+_{1/2u}$ → D $^2\Sigma^+_{1/2g}$ transition of Xe_2^+ at 300K 2624

A-3.45. Density functional potential energy curves for Hg_2^+ 2625

A-3.46. Spectroscopic constants for Hg_2^+. 2625

A-3.47. Low-lying potential energy curves for Hg_2^+. 2626

A-3.48. Total photoabsorption cross-sections for the A $^1\Sigma^+_{1/2u}$ → B $^1\Sigma^+_{1/2g}$ transition of Hg_2^+. 2627

A-3.49. Spectroscopic constants and total electronic energies for Ar_3^+. 2628

A-3.50. Jahn-Teller energies for the ground state of Ar_3^+ 2629

A-3.51. Potential energy curves for Ar_3^+. 2630

A-3.52. Noble gas dimer and trimer ion absorption cross-sections . . . 2631

A-3. References

1. W. R. Wadt, "The Electronic States of Ne_2^+, Ar_2^+, Kr_2^+, Xe_2^+. II. Absorption Cross Sections for the $1(1/2)_u \rightarrow 1(3/2)_g$, $1(1/2)_g$, $2(1/2)_g$ Transitions", J. Chem. Phys. (in press). Tabular and Graphical Data (A-3.1) - (A-3.28).

2. H. H. Michels, R. H. Hobbs and L. A. Wright, "Electronic Structure of the Noble Gas Dimer Ions. II. Theoretical Absorption Spectrum for the $A^2\Sigma_{1/2,u}^+ \rightarrow D^2\Sigma_{1/2,g}^+$ System", J. Chem. Phys. (in press). Tabular and Graphical Data (A-3.29.) - (A-3.44).

3. L. C. Lee and G. P. Smith, "Photodissociation Cross Sections of Ne_2^+, Ar_2^+, Kr_2^+ and Xe_2^+", from 3500 to 5400 Å", Phys. Rev. A 19, 2329 (1979).

4. J. A. Vanderhoff, "Photodissociation Cross Sections for Ar_2^+, Kr_2^+ and Xe_2^+ at 3.0 and 3.5 eV", J. Chem. Phys. 68, 3311 (1978).

5. R. O. Hunter, J. Oldenettel, C. Howton and M. V. McCusker, SRI Technical Report No. 1, Project PYU-6158, May 1978.

6. W. J. Stevens, M. Gardner and A. Karo, "Theoretical Determination of Bound-Free Absorption Cross Sections in Ar_2^+", J. Chem. Phys. 67, 2860 (1977).

7. W. R. Wadt, D. C. Cartwright and J. S. Cohen, "Theoretical Absorption Spectra for Ne_2^+, Ar_2^+, Kr_2^+ and Xe_2^+ in the Near Ultraviolet", Appl. Phys. Letts 31, 672 (1977).

8. H. H. Michels, R. H. Hobbs and J. W. D. Connolly, "Electronic Structure and Photoabsorption of the Hg_2^+ Dimer Ion", Chem. Phys. Letts. (in press). (A-3.45 - A-3.48).

9. H. H. Michels, R. H. Hobbs and L. A. Wright, "Visible Photoabsorption by Noble Gas Trimer Ions", Appl. Phys. Letts. (in press). (A-3.49 - A-3.53).

Note that absorption spectra and cross sections are intimately related to dipole properties, transition moments, and potential energy curves for electronic states of the various systems.

Tabular Data A-3.1. Transition moments (in a.u.) calculated for the $1(1/2)_u \rightarrow 1(3/2)_g$, $1(1/2)_u \rightarrow 1(1/2)_g$ and $1(1/2)_u \rightarrow 2(1/2)_g$ excitations in Ne_2^+.

R(a.u.)	$1(1/2)_u \rightarrow 1(3/2)_g$	$1(1/2)_u \rightarrow 1(1/2)_g$	$1(1/2)_u \rightarrow 2(1/2)_g$
2.5	0.0162	0.0220	1.25
3.0	0.0229	0.0403	1.47
3.5	0.0210	0.0752	1.70
4.0	0.0164	0.154	1.94
5.0	0.00775	0.646	2.37
6.0	0.00296	2.07	2.11
7.0	0.000977	3.33	0.921
8.0	0.0000083	3.95	0.301

Tabular Data A-3.2. Transition moments (in a.u.) calculated for the $1(1/2)_u \rightarrow 1(3/2)_g$, $1(1/2)_u \rightarrow 1(1/2)_g$ and $1(1/2)_u \rightarrow 2(1/2)_g$ excitations in Ar_2^+.

R(a.u.)	$1(1/2)_u \rightarrow 1(3/2)_g$	$1(1/2)_u \rightarrow 1(1/2)_g$	$1(1/2)_u \rightarrow 2(1/2)_g$
3.0	0.032	0.0148	0.134
4.0	0.0272	0.0687	1.63
4.25	0.0272	0.0899	1.79
4.5	0.0261	0.118	1.94
4.75	0.0244	0.156	2.09
5.0	0.0222	0.207	2.23
5.25	0.0198	0.275	2.37
5.5	0.0175	0.365	2.50
5.75	0.0152	0.484	2.63
6.0	0.0131	0.641	2.74
6.25	0.0112	0.845	2.84
6.5	0.00954	1.11	2.90
6.75	0.00801	1.44	2.90
7.0	0.00666	1.84	2.83
8.0	0.00299	3.54	1.67

Tabular Data A-3.3. Transition moments (in a.u.) calculated for the $1(1/2)_u \rightarrow 1(3/2)_g$, $1(1/2)_u \rightarrow 1(1/2)_g$ and $1(1/2)_u \rightarrow 1(3/2)_g$ excitations in Kr_2^+.

R(a.u)	$1(1/2)_u \rightarrow 1(3/2)_g$	$1(1/2)_u \rightarrow 1(1/2)_g$	$1(1/2)_u \rightarrow 2(1/2)_g$
3.5	0.0445	0.0568	0.202
4.25	0.0506	0.201	1.42
4.75	0.0479	0.353	1.77
5.0	0.0449	0.462	1.91
5.25	0.0412	0.602	2.04
5.5	0.0372	0.778	2.15
5.75	0.0331	0.997	2.23
6.0	0.0291	1.26	2.28
6.25	0.0253	1.57	2.27
6.5	0.0218	1.91	2.21
6.75	0.0186	2.27	2.08
7.0	0.0158	2.62	1.89
8.0	0.00785	3.68	0.994

Tabular Data A-3.4. Transition moments (in a.u.) calculated for the $1(1/2)_u \rightarrow 1(3/2)_g$, $1(1/2)_u \rightarrow 1(1/2)_g$ and $1(1/2)_u \rightarrow 2(1/2)_g$ excitations in Xe_2^+.

R(a.u.)	$1(1/2)_u \rightarrow 1(3/2)_g$	$1(1/2)_u \rightarrow 1(1/2)_g$	$1(1/2)_u \rightarrow 2(1/2)_g$
4.5	0.0536	0.258	0.881
5.0	0.0569	0.497	1.42
5.5	0.0551	0.826	1.74
5.75	0.0527	1.04	1.85
6.0	0.0494	1.28	1.90
6.25	0.0456	1.55	1.92
6.50	0.0416	1.84	1.89
7.0	0.0336	2.44	1.70
7.25	0.0298	2.72	1.55
7.5	0.0263	2.99	1.40
7.75	0.0231	3.23	1.24
8.0	0.0202	3.46	1.08
9.0	0.0116	4.19	0.558
10.0	0.00680	4.78	0.248

Tabular Data A-3.5. Calculated cross-sections (in cm^2) for $1(1/2)_u \rightarrow 2(1/2)_g$ in Ne_2^+ at 100K, 300K, 600K. [5.381(-20) = 5.38×10^{-20}]

λ(nm)	100K	300K	600K
180	5.38(-20)	6.32(-20)	1.35(-19)
190	2.65(-19)	3.00(-19)	5.33(-19)
200	9.45(-19)	1.04(-18)	1.57(-18)
210	2.65(-18)	2.82(-18)	3.66(-18)
220	5.85(-18)	6.06(-18)	6.94(-18)
230	1.06(-17)	1.07(-18)	1.10(-17)
240	1.60(-17)	1.59(-17)	1.51(-17)
250	2.09(-17)	2.05(-17)	1.83(-17)
260	2.37(-17)	2.30(-17)	1.98(-17)
270	2.38(-17)	2.30(-17)	1.97(-17)
280	2.15(-17)	2.09(-17)	1.81(-17)
290	1.77(-17)	1.74(-17)	1.57(-17)
300	1.34(-17)	1.33(-17)	1.30(-17)
310	9.42(-18)	9.68(-18)	1.04(-17)
320	6.16(-18)	6.60(-18)	8.06(-18)
330	3.80(-18)	4.30(-18)	6.12(-18)
340	2.24(-18)	2.71(-18)	4.60(-18)
350	1.25(-18)	1.65(-18)	3.44(-18)
360	6.72(-19)	9.87(-19)	2.56(-18)
370	3.50(-19)	5.81(-19)	1.91(-18)
380	1.76(-19)	3.39(-19)	1.43(-18)
390	8.59(-20)	1.97(-19)	1.08(-18)
400	4.08(-20)	1.14(-19)	8.16(-19)
410	1.89(-20)	6.61(-20)	6.21(-19)
420	8.57(-21)	3.86(-20)	4.75(-19)
430	3.78(-21)	2.27(-20)	3.67(-19)
440	1.64(-21)	1.34(-20)	2.86(-19)
450	6.98(-22)	8.02(-21)	2.25(-19)
460	2.91(-22)	4.84(-21)	1.77(-19)
470	1.20(-22)	2.95(-21)	1.40(-19)
480	4.83(-23)	1.82(-21)	1.10(-19)

Tabular Data A-3.6. Calculated cross-sections (in cm^2) for $1(1/2)_u \rightarrow 2(1/2)_g$ in Ar_2^+ at 100K, 300K, 600K normalized to experimental cross-sections of Lee and Smith[a] and Vanderhoff[b] at (350.7 and 356.9)nm and 413.1 nm [2.68(-21) = 2.68×10^{-21}]

λ(nm)	100K	300K	600K
200	2.68(-21)	2.73(-20)	2.84(-19)
210	2.57(-20)	1.60(-19)	9.44(-19)
220	1.69(-19)	6.73(-19)	2.34(-18)
230	8.20(-19)	2.17(-18)	4.91(-18)
240	2.84(-18)	5.38(-18)	8.57(-18)
250	7.80(-18)	1.11(-17)	1.34(-17)
260	1.66(-17)	1.89(-17)	1.85(-17)
270	2.79(-17)	2.67(-17)	2.27(-17)
280	3.97(-17)	3.38(-17)	2.61(-17)
290	4.62(-17)	3.68(-17)	2.74(-17)
300	4.80(-17)	3.77(-17)	2.80(-17)
310	4.23(-17)	3.47(-17)	2.68(-17)
320	3.34(-17)	3.01(-17)	2.49(-17)
330	2.37(-17)	2.48(-17)	2.27(-17)
340	1.40(-17)	1.91(-17)	1.97(-17)
350	8.75(-18)	1.43(-17)	1.70(-17)
360	4.68(-18)	1.03(-17)	1.45(-17)
370	2.30(-18)	7.16(-18)	1.20(-17)
380	1.06(-18)	4.90(-18)	9.92(-18)
390	4.55(-19)	3.26(-18)	8.07(-18)
400	1.86(-19)	2.14(-18)	6.54(-18)
410	7.14(-20)	1.39(-18)	5.28(-18)
420	2.63(-20)	8.93(-19)	4.22(-18)
430	9.28(-21)	5.71(-19)	3.38(-18)
440	3.15(-21)	3.64(-19)	2.70(-18)
450	1.03(-21)	2.31(-19)	2.15(-18)
460	3.22(-22)	1.46(-19)	1.71(-18)
470	9.91(-23)	9.20(-20)	1.37(-18)

continued on next page

Tabular Data A-3.6. (continued)

λ(nm)	100K	300K	600K
480	2.99(-23)	5.79(-20)	1.09(-18)
490	8.82(-24)	3.66(-20)	8.63(-19)
500	2.55(-24)	2.32(-20)	6.81(-19)
510	7.32(-25)	1.48(-20)	5.38(-19)
520	2.08(-25)	9.49(-21)	4.29(-19)
530	5.88(-26)	6.10(-21)	3.45(-19)
540	1.66(-26)	3.94(-21)	2.79(-19)
550	4.63(-27)	2.55(-21)	2.24(-19)
560	1.30(-27)	1.66(-21)	1.75(-19)
570	3.73(-28)	1.06(-21)	1.32(-19)

[a]Reference 3

[b]Reference 4

Tabular Data A-3.7. Calculated cross-sections (in cm^2) for $1(1/2)_u \rightarrow 2(1/2)_g$ in Kr_2^+ at 100K, 300K, 600K normalized to experimental cross-sections of Lee and Smith[a] and Vanderhoff[b] at (350.7 and 356.9)nm and 413.1 nm [1.02(-22) = 1.02×10^{-22}].

λ(nm)	100K	300K	600K
220	1.02(-22)	1.58(-20)	3.17(-19)
230	2.24(-21)	1.12(-19)	1.00(-18)
240	2.97(-20)	5.47(-19)	2.51(-18)
250	2.51(-19)	1.97(-18)	5.26(-18)
260	1.38(-18)	5.33(-18)	9.23(-18)
270	5.22(-18)	1.13(-17)	1.41(-17)
280	1.41(-17)	1.93(-17)	1.89(-17)
290	2.89(-17)	2.82(-17)	2.34(-17)
300	4.51(-17)	3.53(-17)	2.66(-17)
310	5.62(-17)	3.92(-17)	2.83(-17)
320	5.83(-17)	4.01(-17)	2.89(-17)
330	4.96(-17)	3.73(-17)	2.81(-17)
340	3.60(-17)	3.24(-17)	2.62(-17)
350	2.29(-17)	2.68(-17)	2.41(-17)
360	1.26(-17)	2.09(-17)	2.13(-17)
370	6.22(-18)	1.56(-17)	1.85(-17)
380	2.75(-18)	1.13(-17)	1.58(-17)
390	1.11(-18)	7.89(-18)	1.33(-17)
400	4.14(-19)	5.40(-18)	1.10(-17)
410	1.43(-19)	3.61(-18)	9.04(-18)
420	4.66(-20)	2.38(-18)	7.37(-18)
430	1.44(-20)	1.55(-18)	5.97(-18)
440	4.20(-21)	9.99(-19)	4.81(-18)
450	1.19(-21)	6.36(-19)	3.86(-18)
460	3.25(-22)	4.05(-19)	3.08(-18)
470	8.65(-23)	2.56(-19)	2.46(-18)
480	2.25(-23)	1.62(-19)	1.97(-18)
490	5.76(-24)	1.02(-19)	1.56(-18)

continued on next page

Tabular Data A-3.7. (continued)

λ(nm)	100K	300K	600K
500	1.46(-24)	6.42(-20)	1.24(-18)
510	3.66(-25)	4.05(-20)	9.92(-19)
520	9.18(-26)	2.56(-20)	7.81(-19)
530	2.29(-26)	1.61(-20)	6.17(-19)
540	5.75(-27)	1.03(-20)	4.97(-19)
550	1.44(-27)	6.54(-21)	3.94(-19)
560	3.64(-28)	4.16(-21)	3.06(-19)
570	9.30(-29)	2.65(-21)	2.38(-19)
580	2.40(-29)	1.71(-21)	1.92(-19)
590	6.26(-30)	1.11(-21)	1.55(-19)
600	1.66(-30)	6.93(-22)	1.14(-19)

[a]Reference 3

[b]Reference 4

Tabular Data A-3.8. Calculated cross-sections (in cm^2) for $1(1/2)_u \rightarrow 2(1/2)_g$ in Xe_2^+ at 100K, 300K, 600K normalized to experimental cross-sections of Lee and Smith[a] and Vanderhoff[b] at (350.7 and 356.9)nm and 413.1 nm [970(-22) = 9.70×10^{-22}]

λ(nm)	100K	300K	600K
250	9.70(-22)	2.23(-19)	1.63(-18)
260	1.61(-20)	8.83(-19)	3.42(-18)
270	1.61(-19)	2.64(-18)	6.18(-18)
280	1.01(-18)	6.20(-18)	9.78(-18)
290	4.23(-18)	1.17(-17)	1.37(-17)
300	1.26(-17)	1.90(-17)	1.78(-17)
310	2.72(-17)	2.63(-17)	2.13(-17)
320	4.47(-17)	3.24(-17)	2.39(-17)
330	5.76(-17)	3.64(-17)	2.57(-17)
340	5.82(-17)	3.66(-17)	2.59(-17)
350	4.86(-17)	3.44(-17)	2.54(-17)
360	3.41(-17)	3.04(-17)	2.41(-17)
370	2.00(-17)	2.50(-17)	2.20(-17)
380	1.02(-17)	1.96(-17)	1.95(-17)
390	4.59(-18)	1.48(-17)	1.71(-17)
400	1.83(-18)	1.08(-17)	1.47(-17)
410	6.60(-19)	7.53(-18)	1.23(-17)
420	2.18(-19)	5.13(-18)	1.02(-17)
430	6.69(-20)	3.44(-18)	8.39(-18)
440	1.89(-20)	2.23(-18)	6.78(-18)
450	5.03(-21)	1.44(-18)	5.47(-18)
460	1.26(-21)	8.97(-19)	4.33(-18)
470	3.00(-22)	5.54(-19)	3.41(-18)
480	6.85(-23)	3.39(-19)	2.67(-18)
490	1.51(-23)	2.06(-19)	2.09(-18)
500	3.21(-24)	1.24(-19)	1.63(-18)
510	6.66(-25)	7.44(-20)	1.26(-18)
520	1.35(-25)	4.44(-20)	9.79(-19)

continued on next page

Tabular Data A-3.8. (continued)

λ(nm)	100K	300K	600K
530	2.72(-26)	2.67(-20)	7.59(-19)
540	5.44(-27)	1.61(-20)	5.89(-19)
550	1.08(-27)	9.66(-21)	4.63(-19)
560	2.10(-28)	5.50(-21)	3.34(-19)
570	4.07(-29)	3.19(-21)	2.47(-19)
580	7.93(-30)	1.86(-21)	1.85(-19)
590	1.41(-30)	9.52(-22)	1.18(-19)

[a]Reference 3

[b]Reference 4

Tabular Data A-3.9. Comparison of theoretical and experimental cross-sections (in 10^{-18} cm^2) for Ne_2^+ at (350.7 and 356.7)nm and Ar_2^+ at 413.1 nm to determine the extent of equilibration between translational and vibrational degrees of freedom.

	T(K)	Lee & Smith[a]	Theory
Ne_2^+	368	1.93±0.20	1.95,1.47
	602	2.96±0.19	3.38,2.81
Ar_2^+	312	1.05±0.10	1.35
	602	2.00±0.23	4.95

[a]Reference 3

Tabular Data A-3.10. Comparison of experimental and theoretical values for the wavelength (in nm) and magnitude (in 10^{-18} cm^2) of the maximal absorption cross-section for the $1(1/2)_u \rightarrow 2(1/2)_g$ transition in Ne_2^+, Ar_2^+, Kr_2^+ and Xe_2^+ at 300K.

		Hunter[a]	Wadt[b]	Michels[c]	Stevens[d]	Moseley[e]	Abouaf[f]
Ne_2^+	λ_{max}	--	264	287	--	--	--
	σ_{max}	--	23.4	20.0	--	--	--
Ar_2^+	λ_{max}	295±5	297	299	300	293	--
	σ_{max}	38±7	37.8	47.6	50	64	--
Kr_2^+	λ_{max}	320±5	318	322	--	--	330
	σ_{max}	36±7	40.2	57.1	--	--	44
Xe_2^+	λ_{max}	--	337	339	--	--	--
	σ_{max}	--	36.8	68.2	--	--	--

[a] R. O. Hunter, J. Oldenettel, C. Howton and M. W. McCusher, Final Technical Report, Feb. - Nov. 1977, Maxwell Laboratories.

[b] W. R. Wadt, J. Chem. Phys. (in press).

[c] H. H. Michels, R. H. Hobbs and L. A. Wright, J. Chem. Phys. 69, 5151 (1978); 71, 5053 (1979).

[d] W. R. Stevens, M. Gardner, A. Karo and P. Julienne, J. Chem. Phys. 67, 2860 (1977).

[e] J. T. Moseley, R. P. Saxon, B. A. Huber, P. C. Cosby, R. Abouaf and M. Tadjeddine, J. Chem. Phys. 67, 1659 (1977).

[f] R. Abouaf, B. A. Huber, P. C. Cosby, R. P. Saxon and J. T. Moseley, J. Chem. Phys. 68, 2406 (1978).

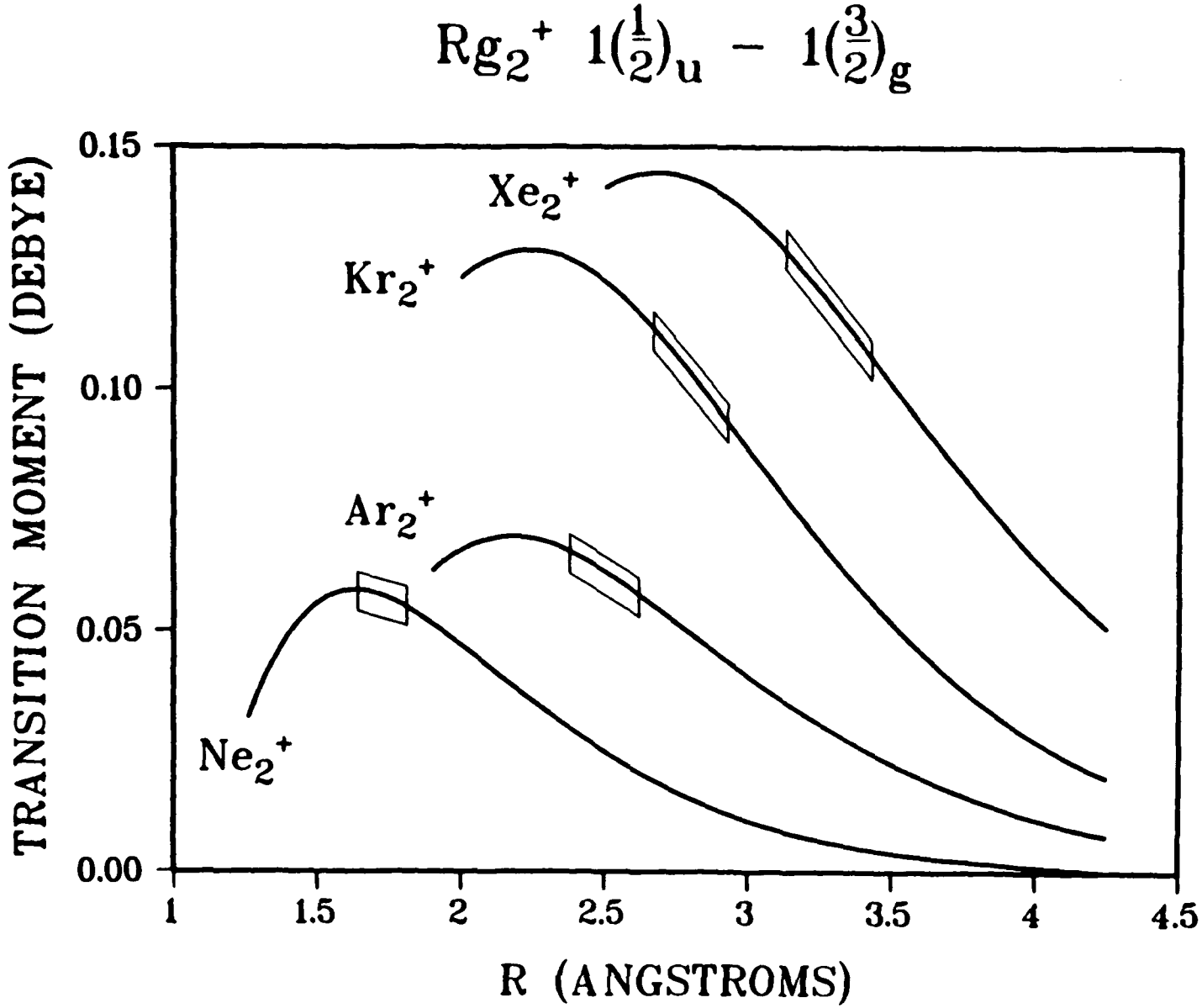

Graphical Data A-3.11. POL CI transition moment functions for the $1(1/2)_u \rightarrow 1(3/2)_g$ transition. The boxes indicate the Franck-Condon regions at 300K.

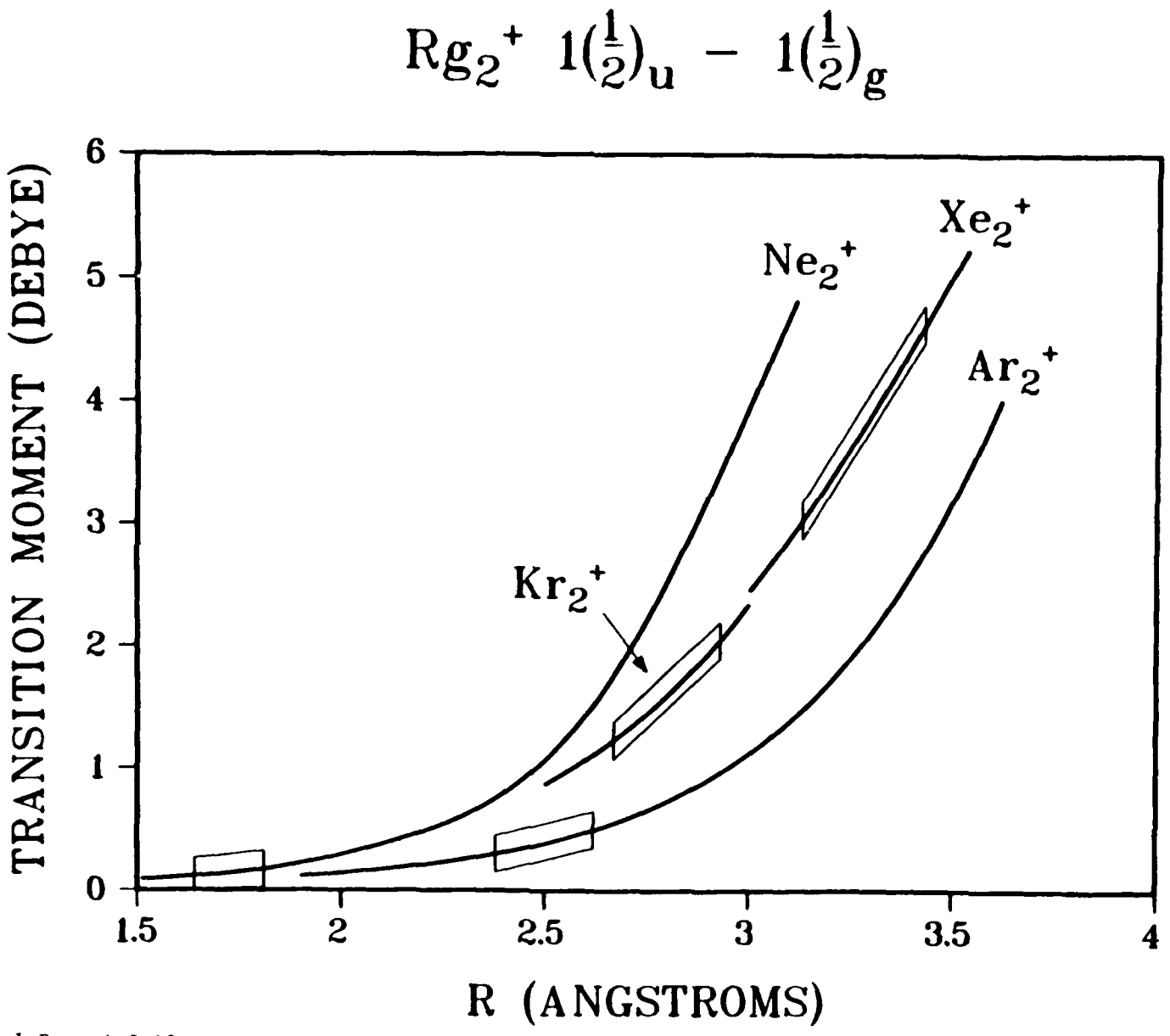

Graphical Data A-3.12. POL CI transition moment functions for the $1(1/2)_u \rightarrow 1(1/2)_g$ transition. The boxes indicate the Franck-Condon regions at 300K.

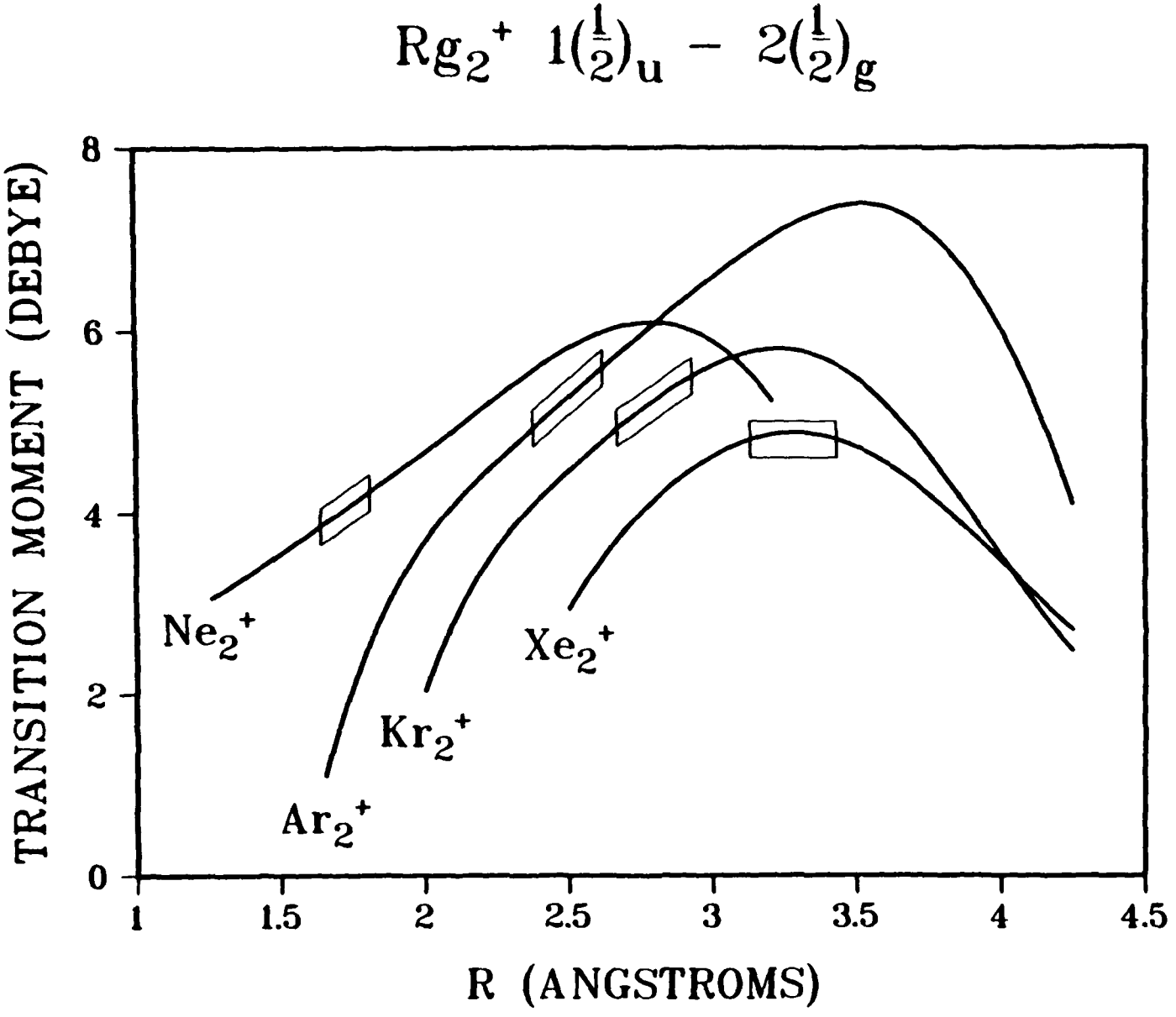

Graphical Data A-3.13. POL CI transition moment functions for the $1(1/2)_u \rightarrow 2(1/2)_g$ transition. The boxes indicate the Franck-Condon regions at 300K.

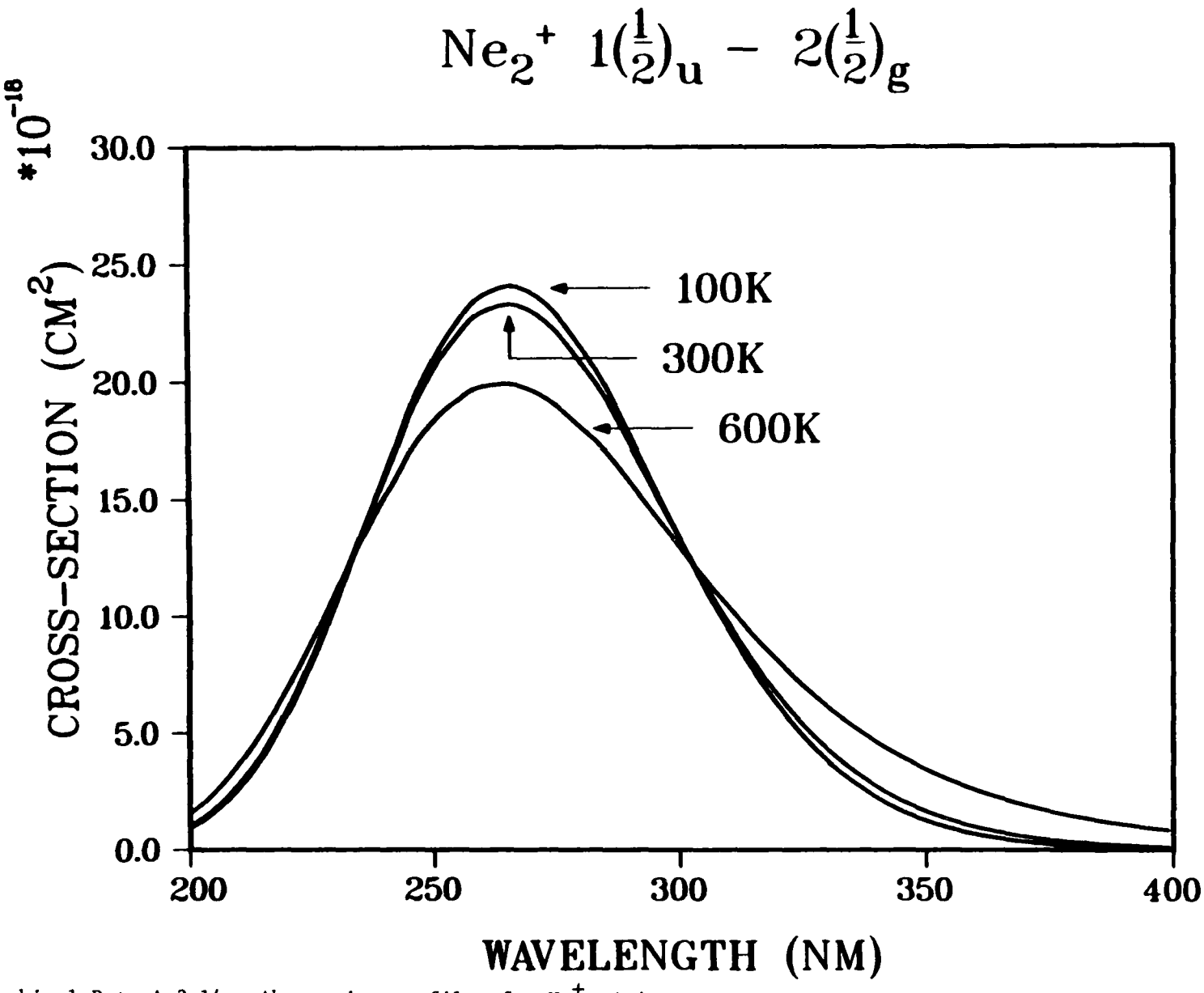

Graphical Data A-3.14. Absorption profiles for Ne_2^+ $1(1/2)_u \rightarrow 2(1/2)_g$.

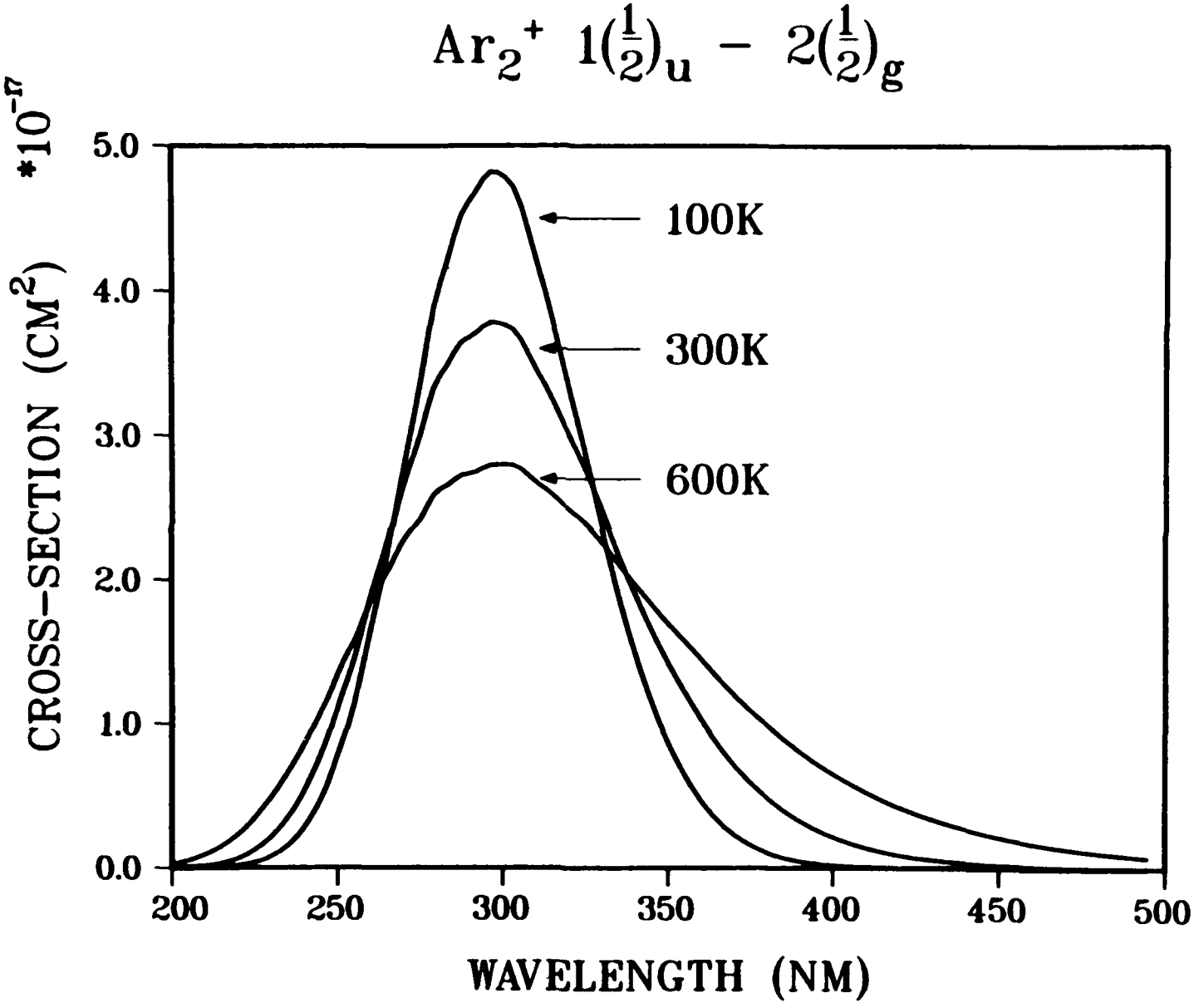

Graphical Data A-3.15. Absorption profiles for Ar_2^+ $1(1/2)_u \rightarrow 2(1/2)_g$.

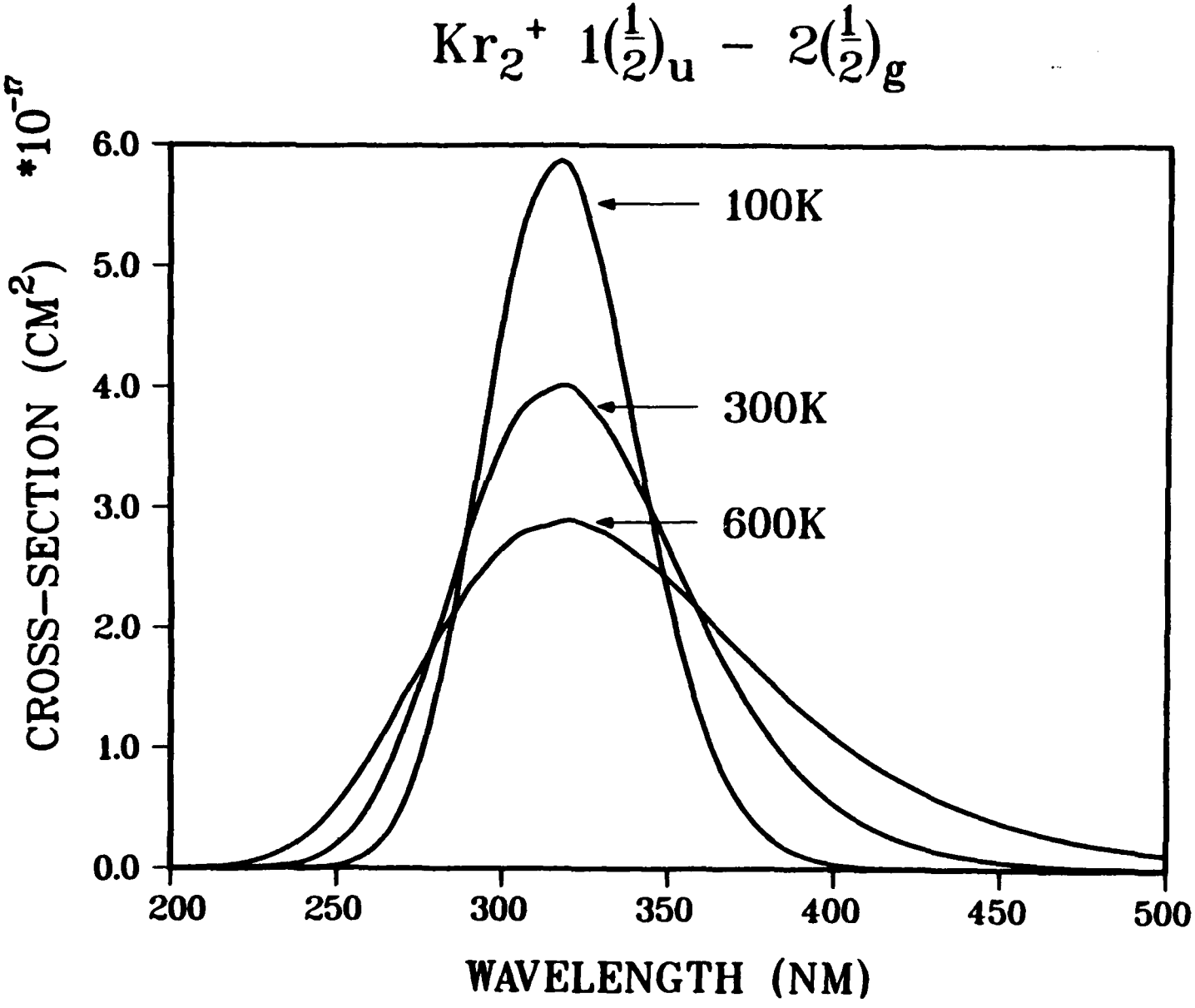

Graphical Data A-3.16. Absorption profiles for Kr_2^+ $1(1/2)_u \rightarrow 2(1/2)_g$.

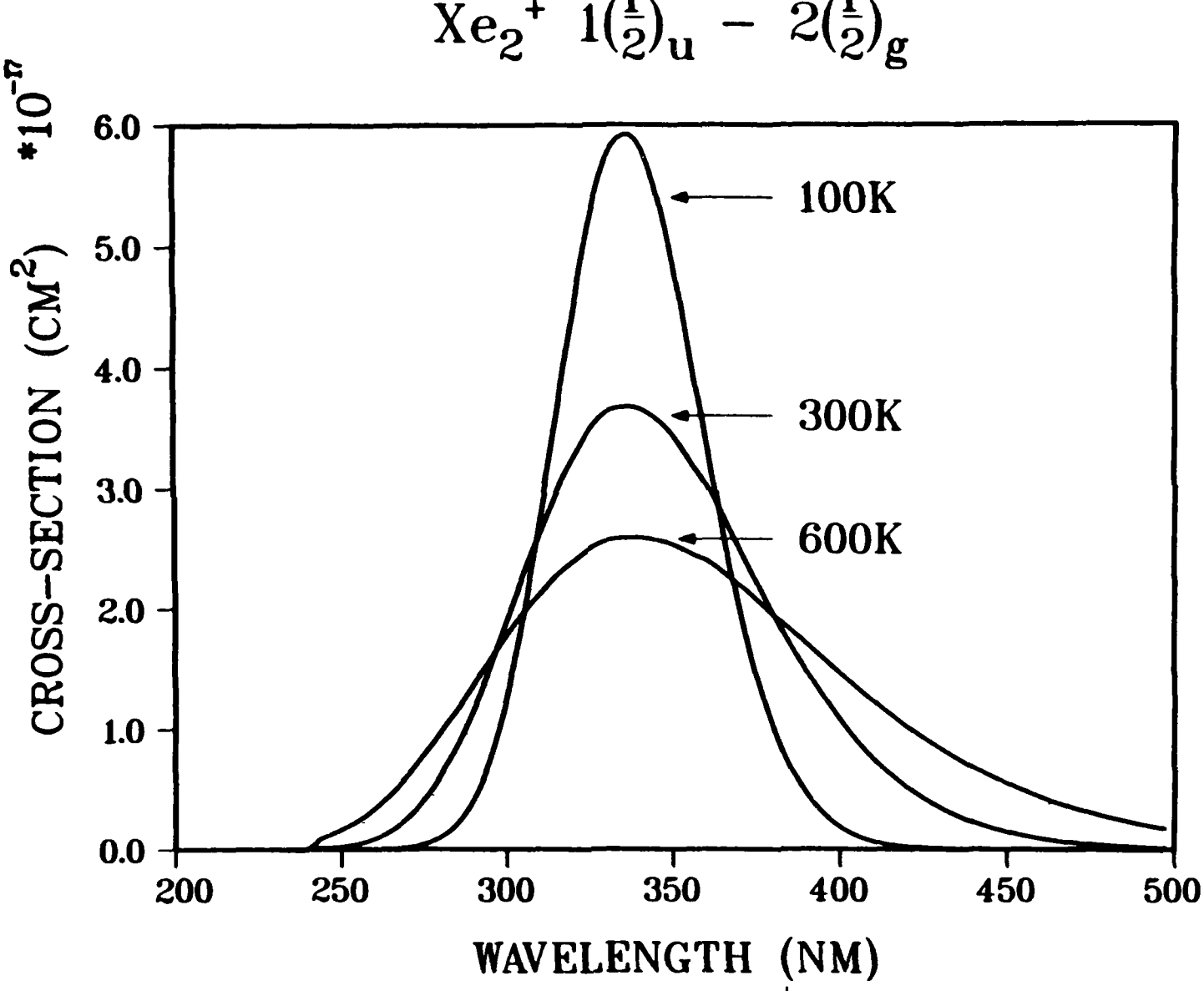

Graphical Data A-3.17. Absorption profiles for Xe_2^+ $1(1/2)_u \rightarrow 2(1/2)_g$.

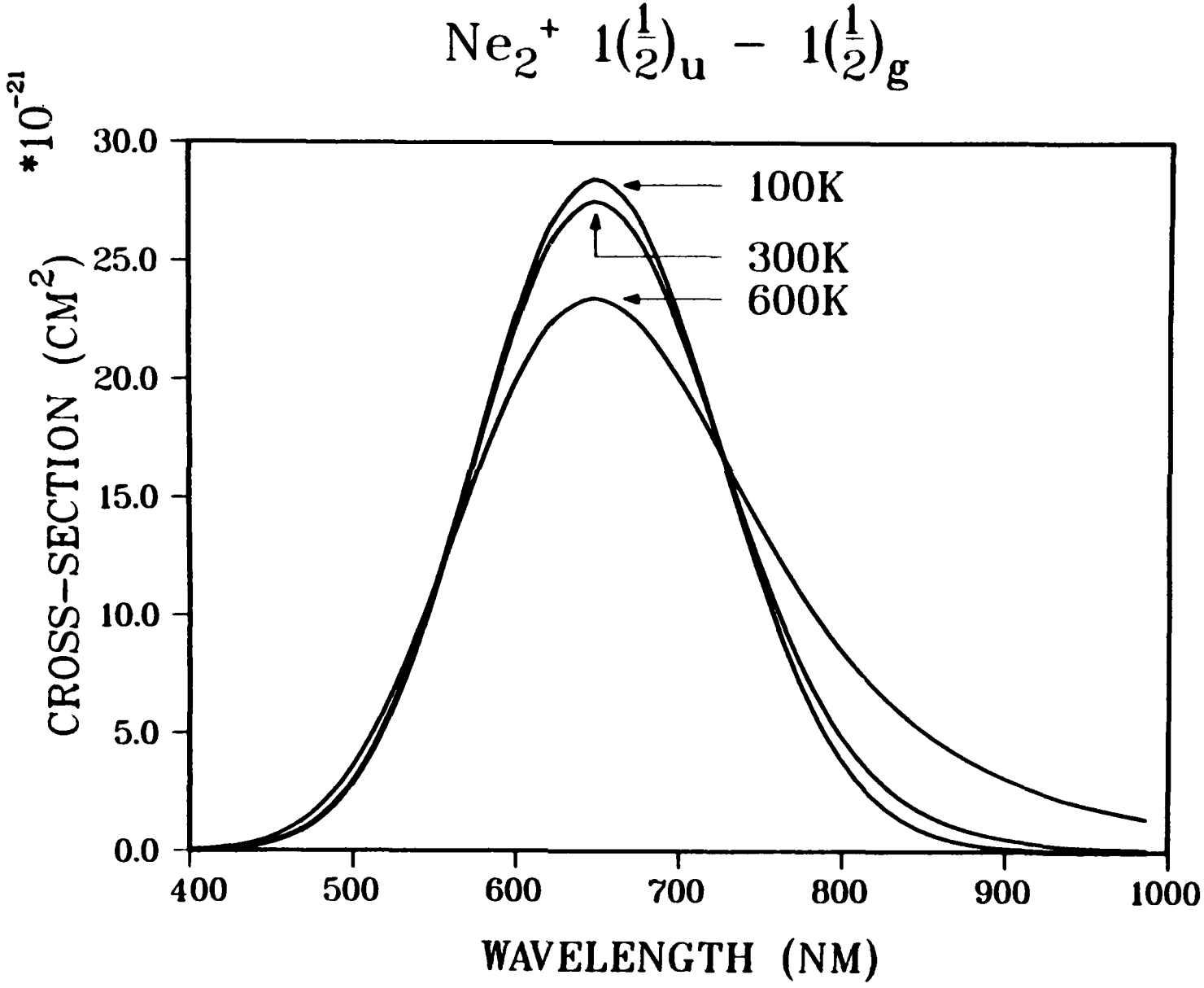

Graphical Data A-3.18. Absorption profiles for Ne_2^+ $1(1/2)_u \rightarrow 1(1/2)_g$.

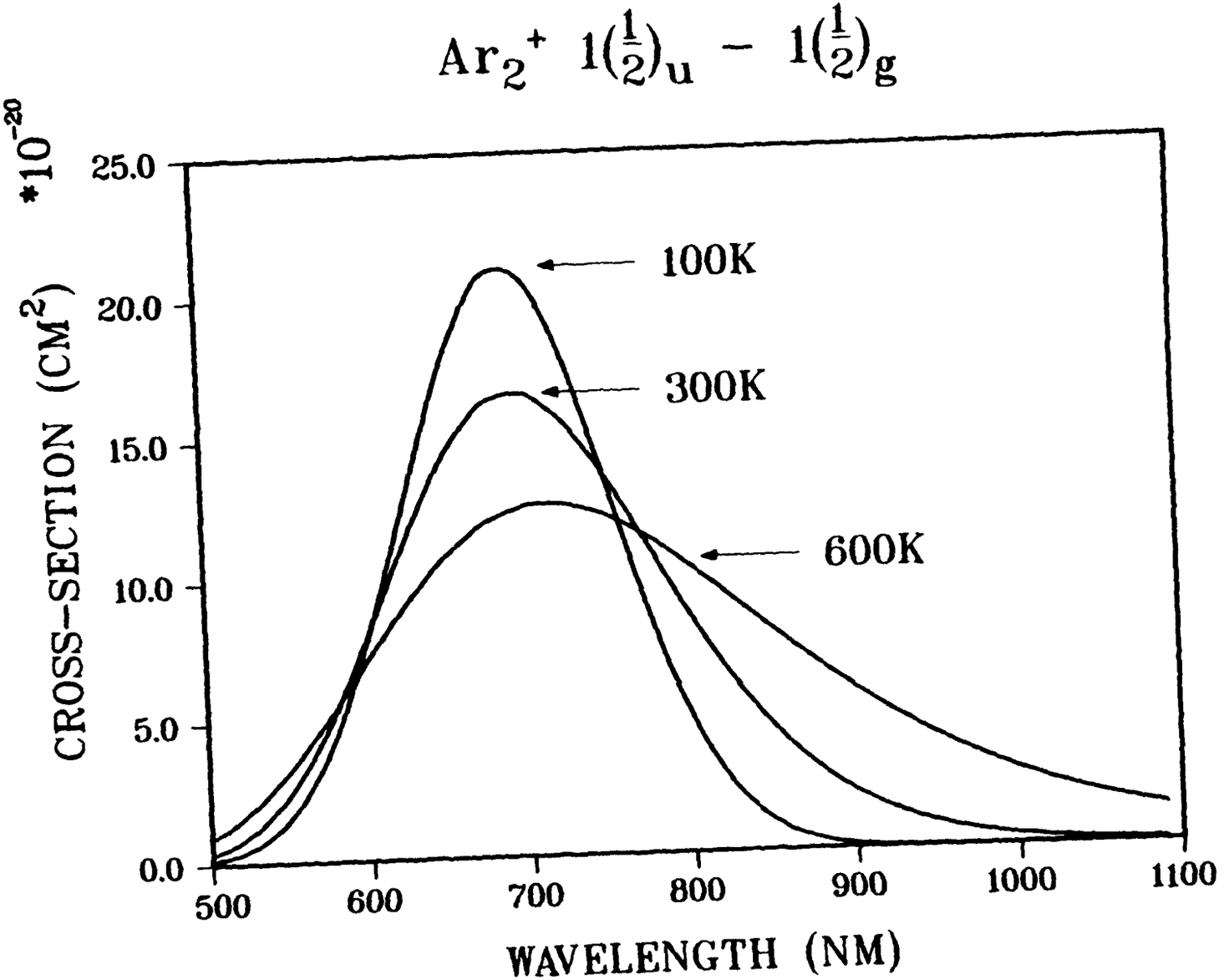

Graphical Data A-3.19. Absorption profiles for Ar_2^+ $1(1/2)_u \rightarrow 1(1/2)_g$.

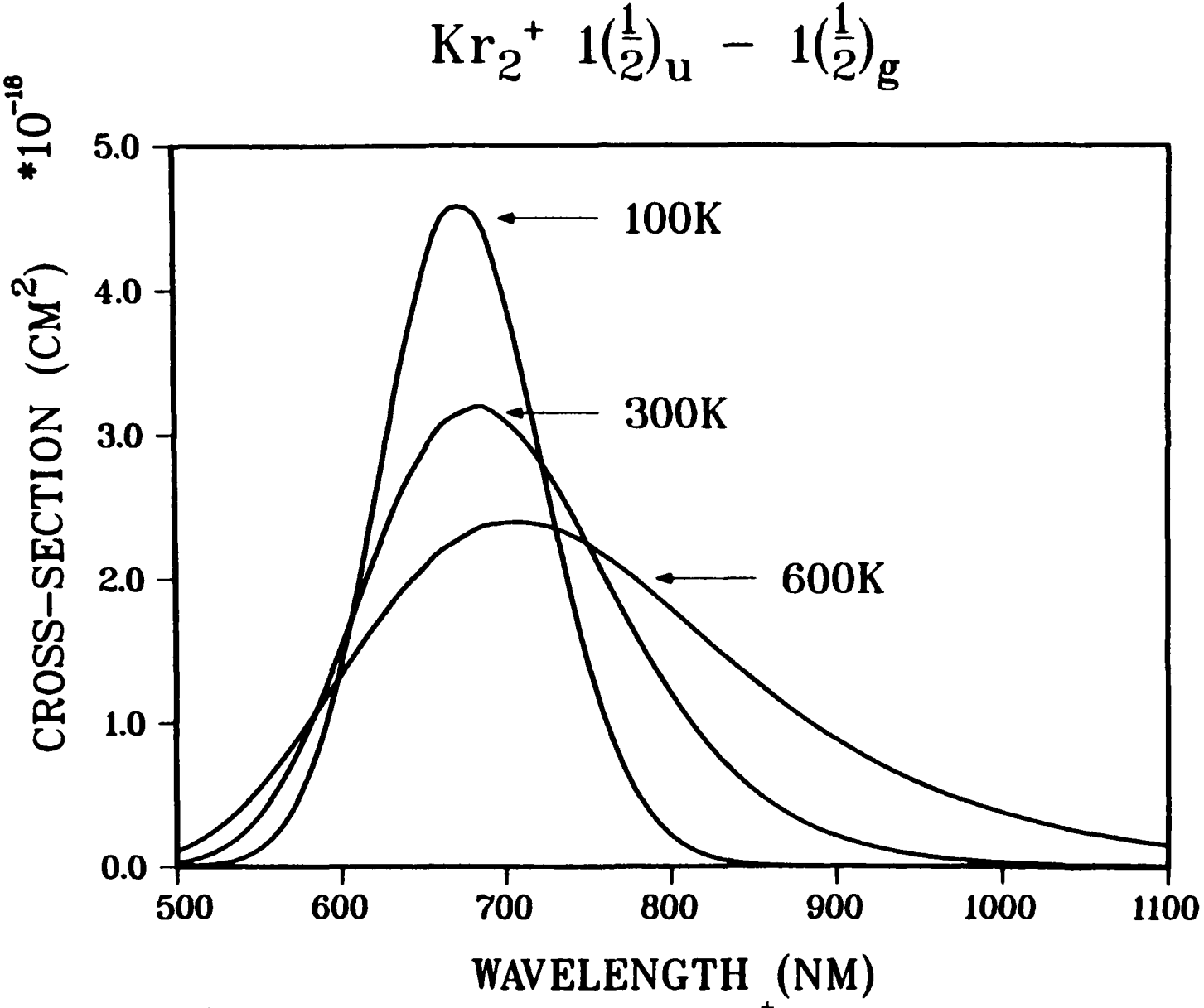

Graphical Data A-3.20. Absorption profiles for Kr_2^+ $1(1/2)_u \rightarrow 1(1/2)_g$.

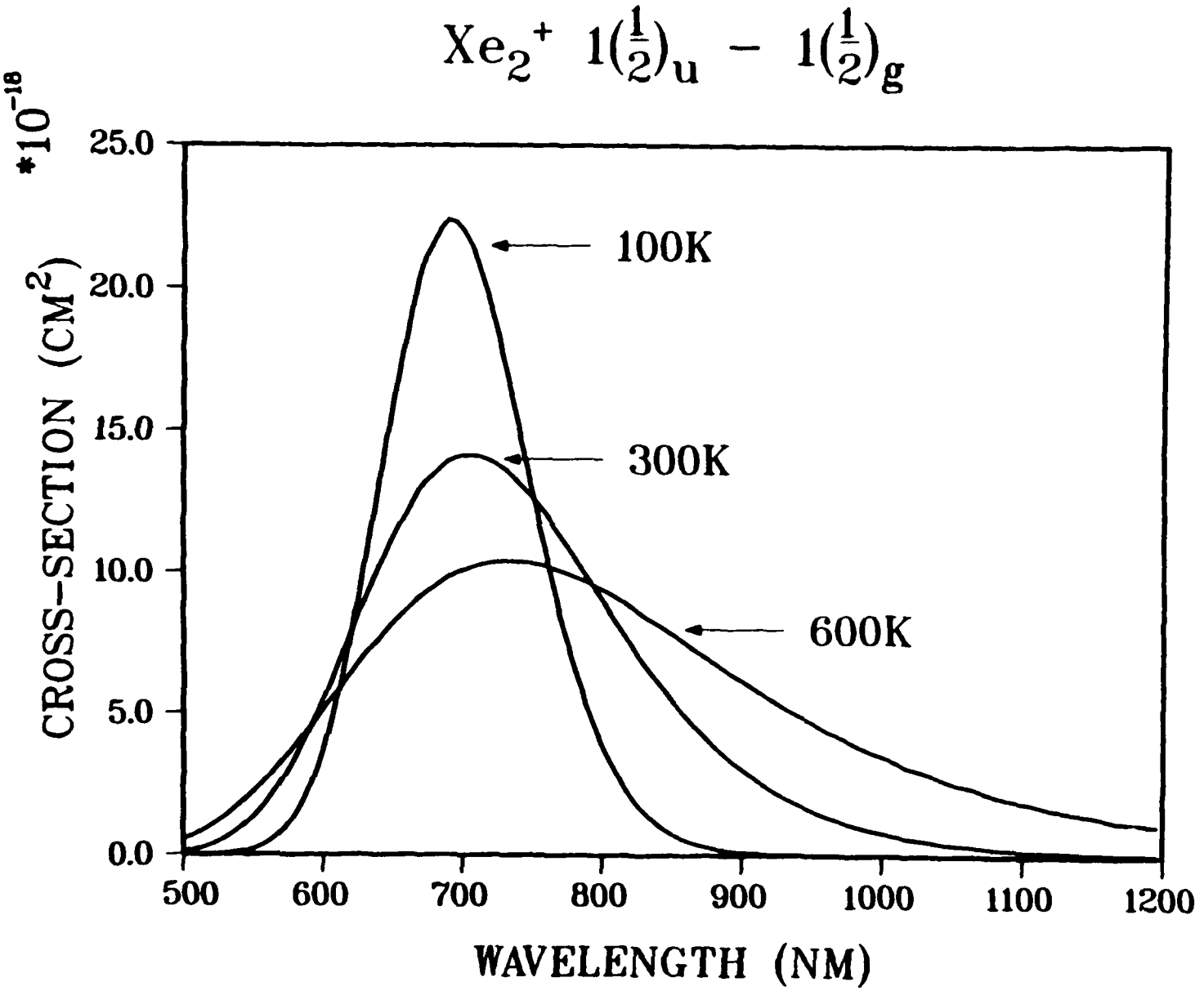

Graphical Data A-3.21. Absorption profiles for $Xe_2^+ \ 1(1/2)_u \rightarrow 1(1/2)_g$.

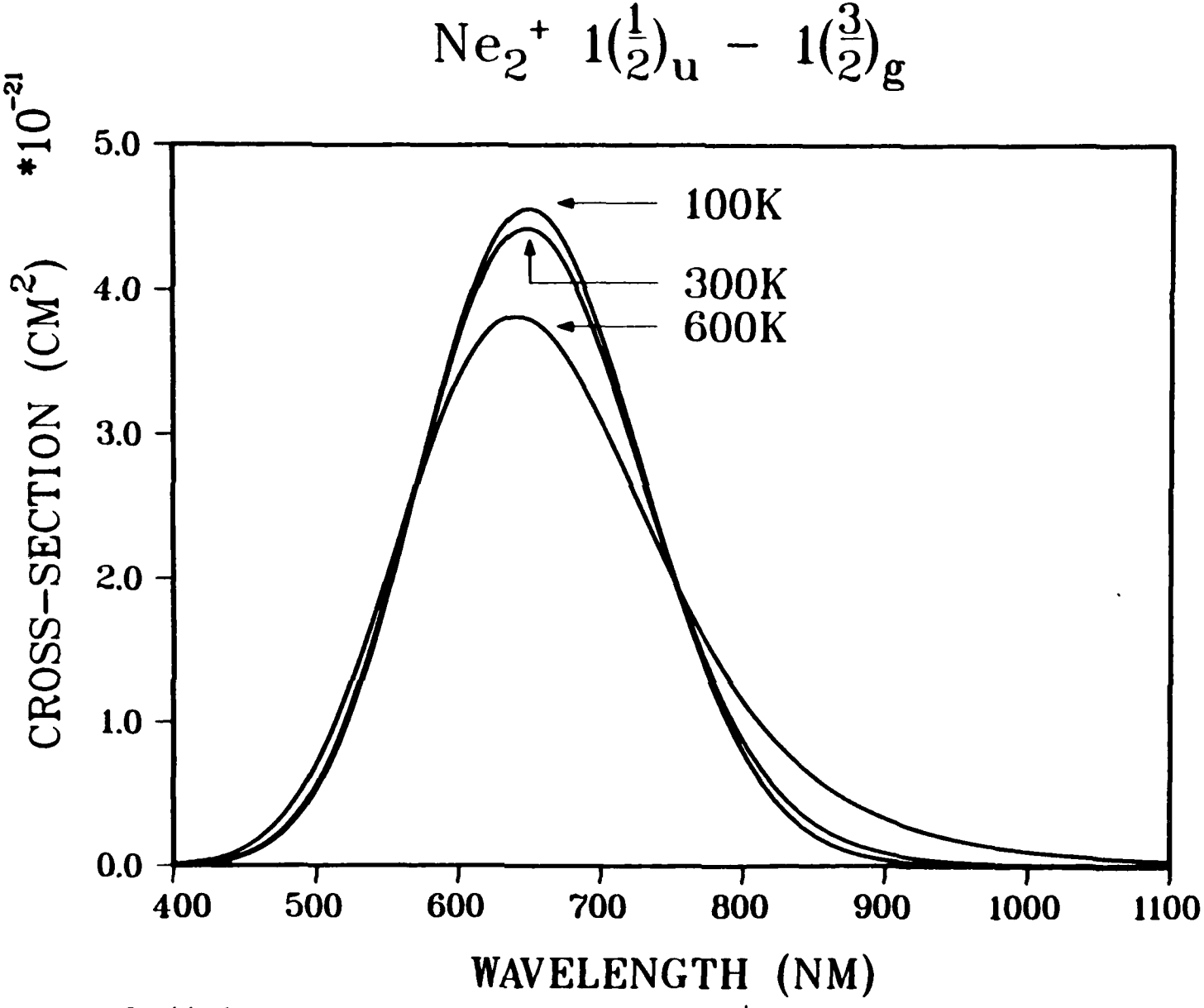

Graphical Data A-3.22. Absorption profiles for Ne_2^+ $1(1/2)_u \rightarrow 1(3/2)_g$.

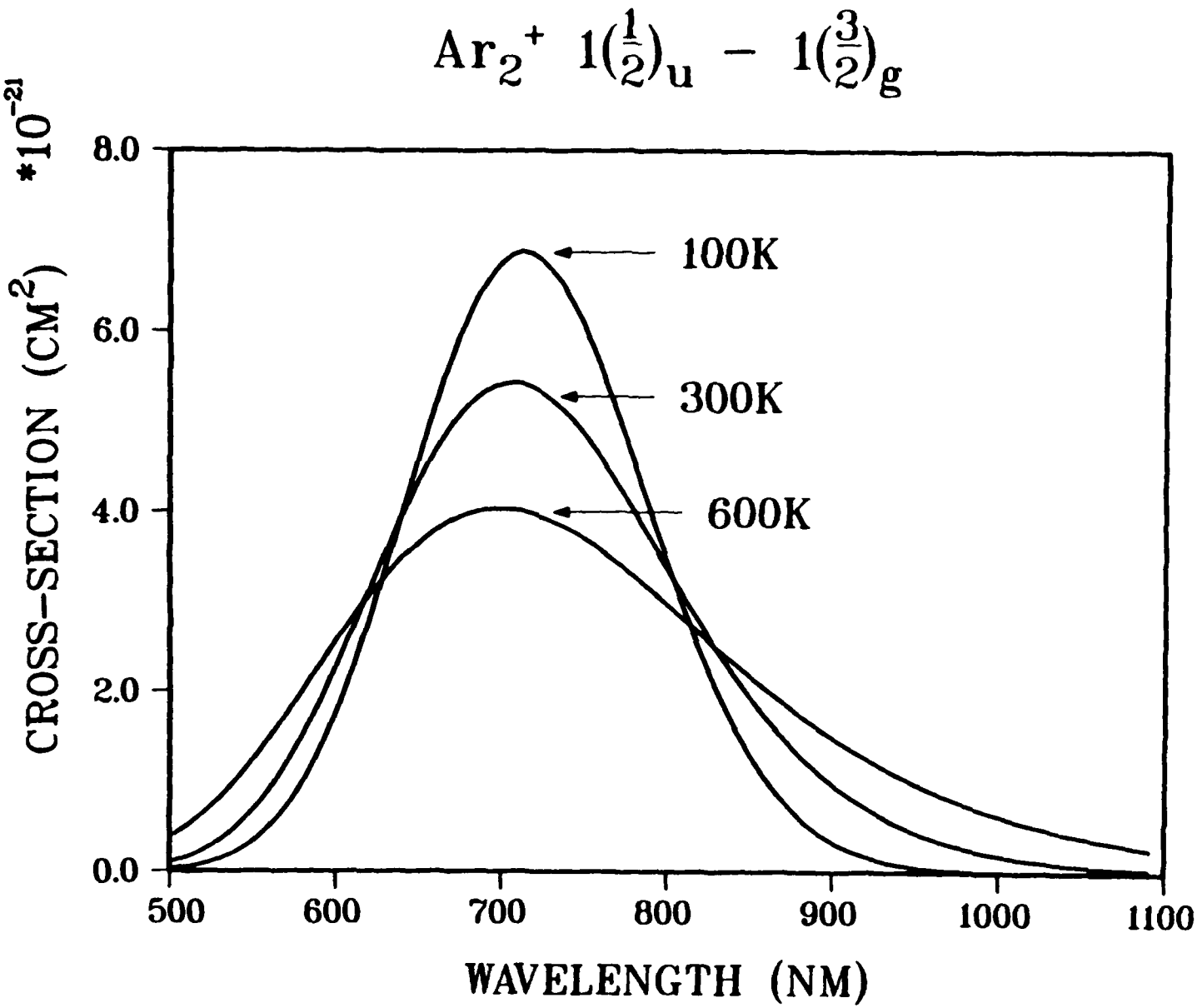

Graphical Data A-3.23. Absorption profiles for Ar_2^+ $1(1/2)_u \rightarrow 1(3/2)_g$.

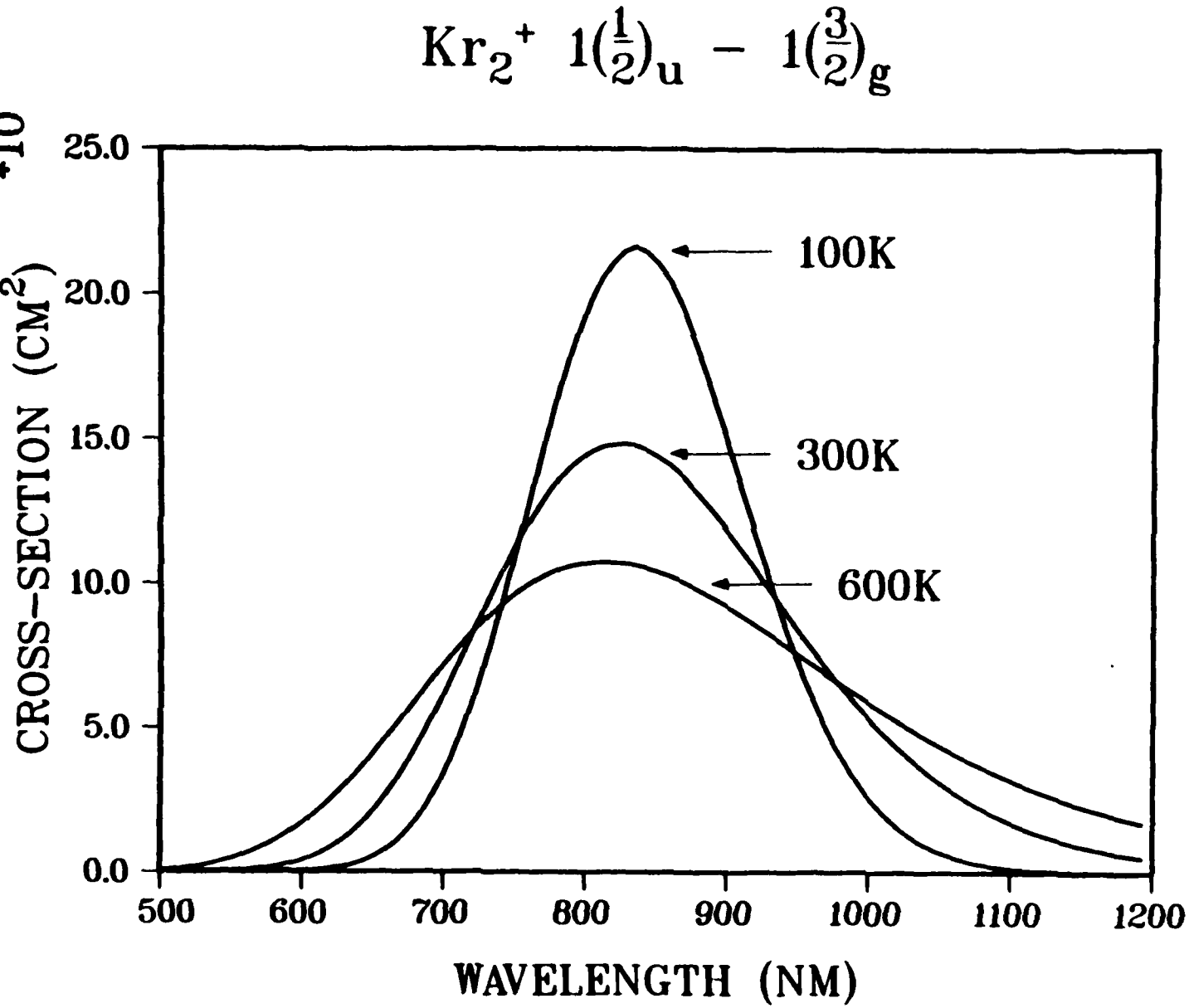

Graphical Data A-3.24. Absorption profiles for Kr_2^+ $1(1/2)_u \rightarrow 1(3/2)_g$.

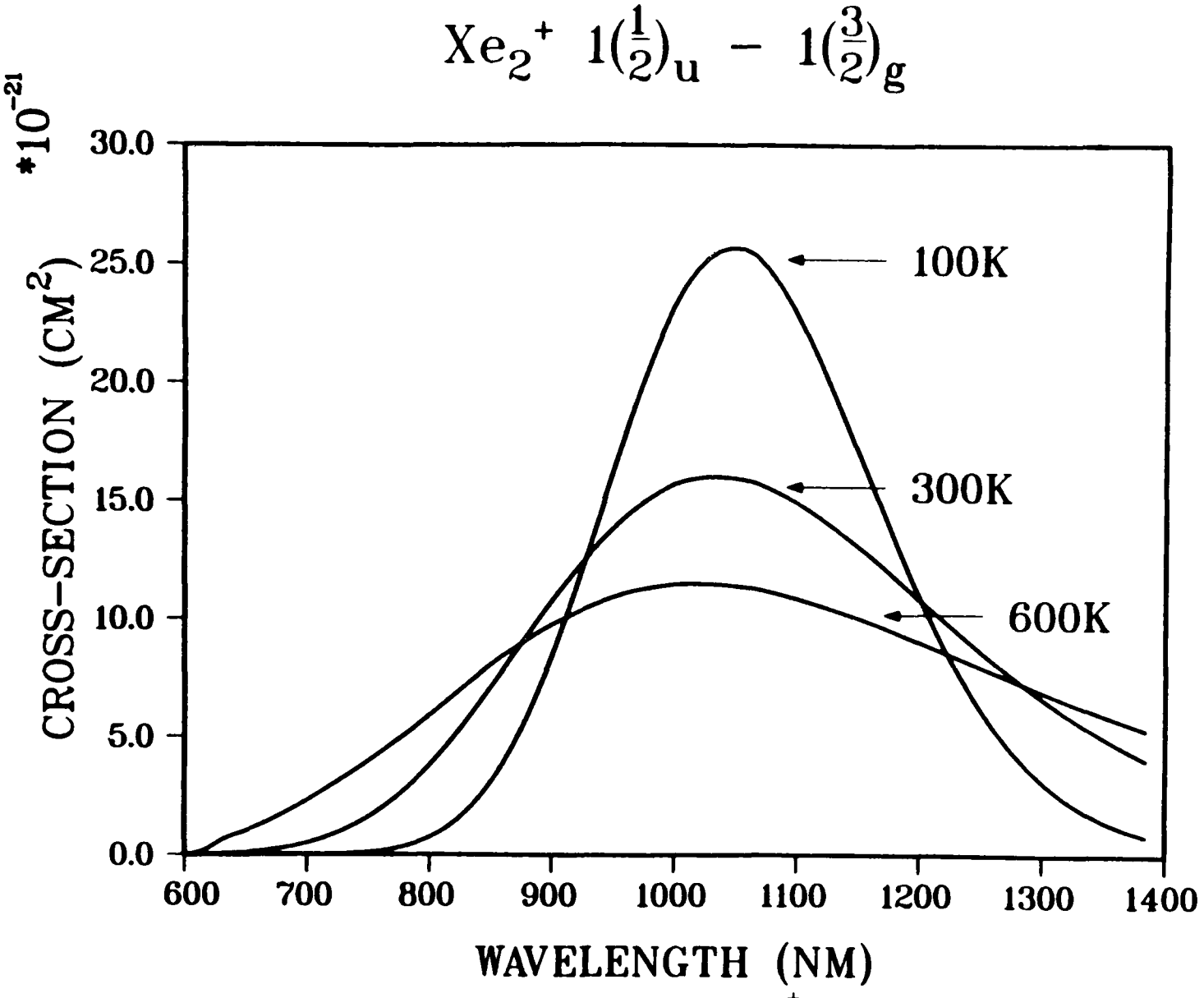

Graphical Data A-3.25. Absorption profiles for Xe_2^+ $1(1/2)_u \rightarrow 1(3/2)_g$.

2605

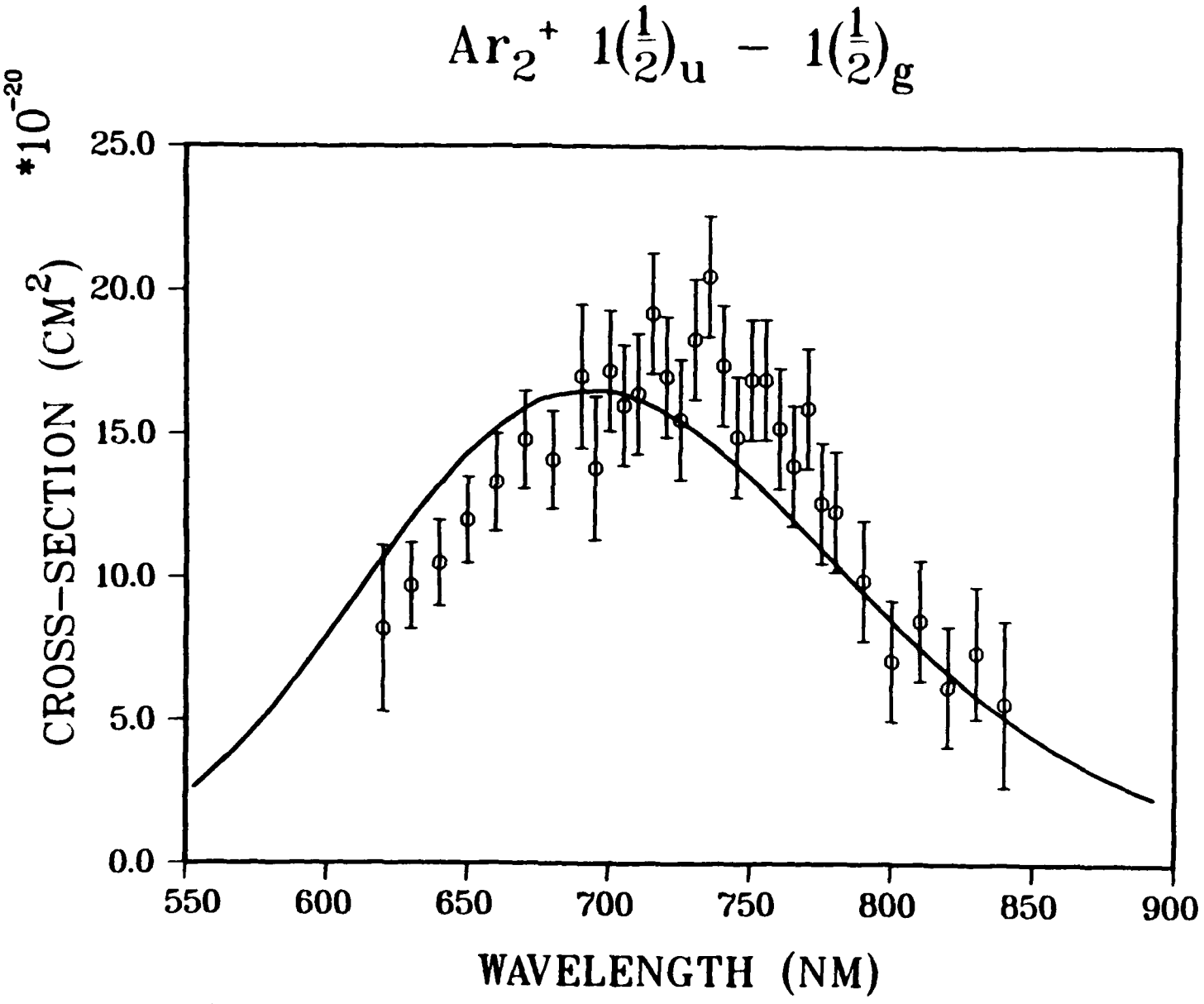

Graphical Data A-3.26. Comparison of theoretical absorption cross-sections (solid line) for $1(1/2)_u \rightarrow 1(1/2)_g$ in Ar_2^+ with those measured by Lee and Smith (Reference 3) at 300K (points with error bars).

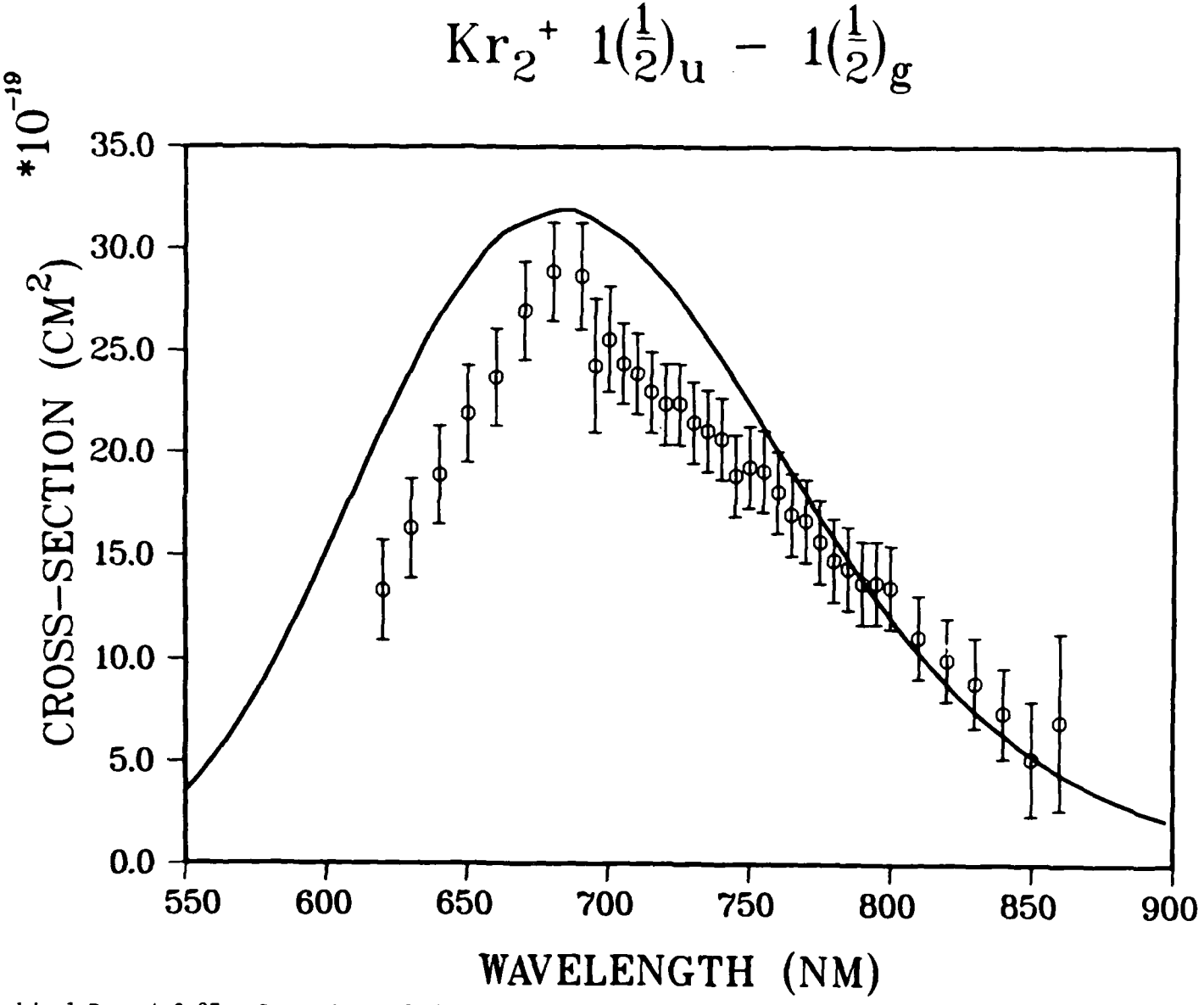

Graphical Data A-3.27. Comparison of theoretical absorption cross-sections (solid line) for $1(1/2)_u \rightarrow 1(1/2)_g$ in Kr_2^+ with those measured by Lee and Smith (Reference 3) (points with error bars).

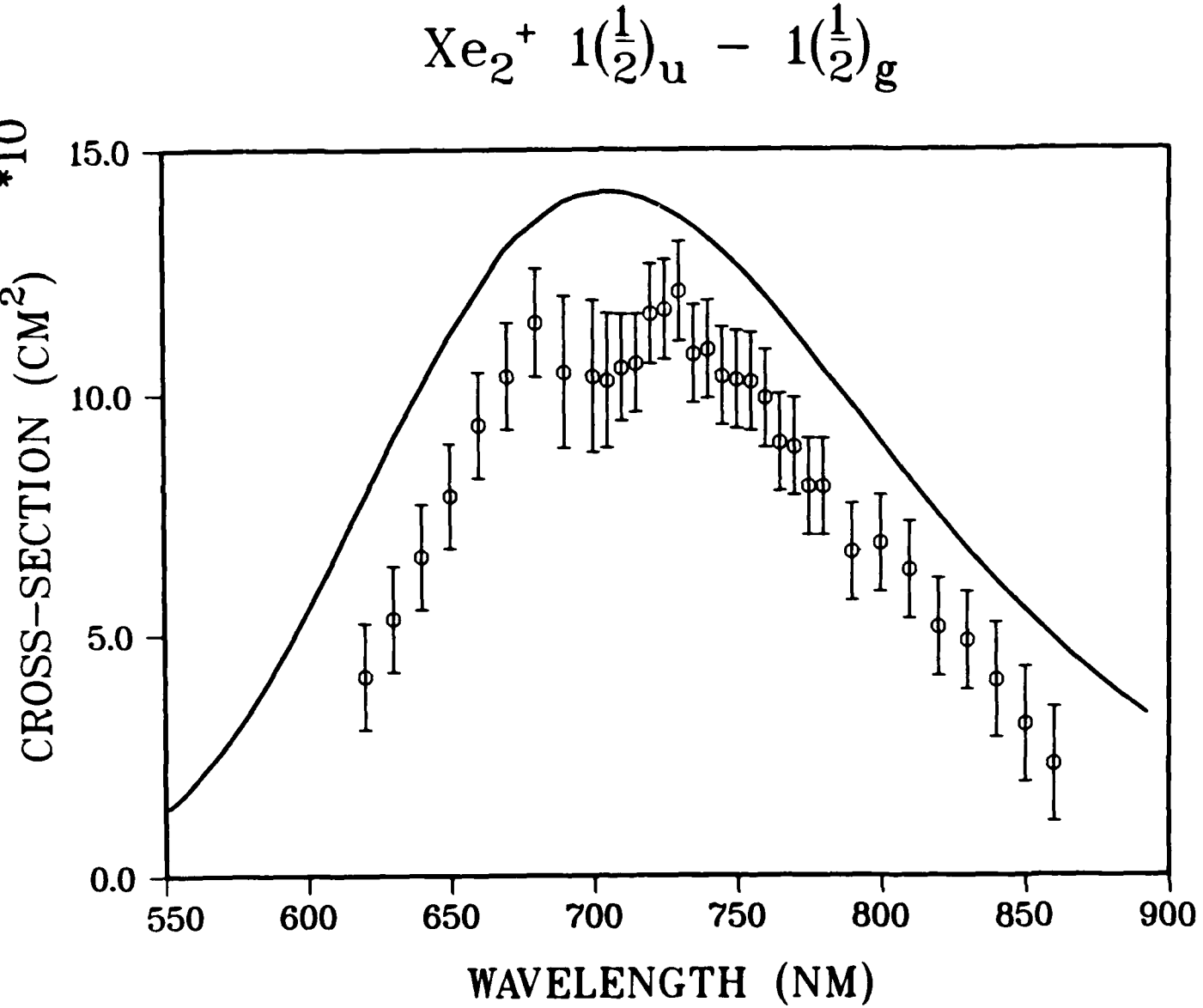

Graphical Data A-3.28. Comparison of theoretical absorption cross-sections (solid line) for $1(1/2)_u \rightarrow 1(1/2)_g$ in Xe_2^+ with those measured by Lee and Smith (Reference 3) (points with error bars).

Tabular Data A-3.29. Total Photoabsorption Cross-Sections for the $A\ ^2\Sigma_{1,u}^+ \rightarrow D\ ^2\Sigma_{1,g}^+$ Transition of Ne_2^+. Boltzmann Averaged Over Vibrational Levels.

Wavelength λ (nm)	Cross-Section, σ (cm^2) T = 150°K	T=300°K	T=600°K
18[illegible]	0.475 -19	0.648 -19	0.181 -18
19[illegible]	0.186 -18	0.231 -18	0.517 -18
20[illegible]	0.546 -18	0.664 -18	0.122 -17
21[illegible]	0.136 -17	0.157 -17	0.243 -17
22[illegible]	0.285 -17	0.318 -17	0.420 -17
23[illegible]	0.527 -17	0.560 -17	0.649 -17
24[illegible]	0.851 -17	0.873 -17	0.907 -17
250	0.123 -16	0.122 -16	0.116 -16
260	0.160 -16	0.156 -16	0.139 -16
270	0.190 -16	0.182 -16	0.155 -16
280	0.208 -16	0.197 -16	0.163 -16
290	0.211 -16	0.200 -16	0.164 -16
300	0.200 -16	0.190 -16	0.158 -16
310	0.178 -16	0.171 -16	0.148 -16
320	0.150 -16	0.147 -16	0.133 -16
330	0.119 -16	0.120 -16	0.177 -16
340	0.904 -17	0.944 -17	0.101 -16
350	0.654 -17	0.718 -17	0.852 -17
360	0.454 -17	0.529 -17	0.709 -17
370	0.303 -17	0.378 -17	0.581 -17
380	0.194 -17	0.264 -17	0.472 -17
390	0.121 -17	0.181 -17	0.380 -17
400	0.725 -18	0.121 -17	0.303 -17
410	0.422 -18	0.800 -18	0.241 -17
420	0.239 -18	0.521 -18	0.190 -17
430	0.131 -18	0.335 -18	0.150 -17
440	0.705 -19	0.214 -18	0.118 -17
450	0.369 -19	0.135 -18	0.928 -18
460	0.188 -19	0.852 -19	0.729 -18
470	0.941 -20	0.533 -19	0.573 -18
480	0.460 -20	0.333 -19	0.450 -18
490	0.221 -20	0.208 -19	0.354 -18
500	0.104 -20	0.129 -19	0.279 -18
510	0.480 -21	0.808 -20	0.220 -18
520	0.218 -21	0.504 -20	0.174 -18

Tabular Data A-3.30. Total Photoabsorption Cross-Sections for the $A\ ^2\Sigma_{1/2u}^+ \rightarrow D\ ^2\Sigma_{1/2g}^+$ Transition of Ar_2^+. Boltzmann Averaged Over Vibrational Levels.

Wavelength λ (nm)	Cross-Section, σ (cm^2) T=150°K	T=300°K	T=600°K
200	0.161 -19	0.845 -19	0.669 -18
210	0.105 -18	0.381 -18	0.178 -17
220	0.495 -18	0.131 -17	0.390 -17
230	0.178 -17	0.355 -17	0.729 -17
240	0.501 -17	0.788 -17	0.119 -16
250	0.114 -16	0.147 -16	0.174 -16
260	0.215 -16	0.235 -16	0.230 -16
270	0.341 -16	0.329 -16	0.281 -16
280	0.465 -16	0.410 -16	0.321 -16
290	0.551 -16	0.462 -16	0.346 -16
300	0.577 -16	0.476 -16	0.353 -16
310	0.537 -16	0.454 -16	0.346 -16
320	0.451 -16	0.403 -16	0.326 -16
330	0.345 -16	0.338 -16	0.298 -16
340	0.242 -16	0.269 -16	0.265 -16
350	0.157 -16	0.205 -16	0.230 -16
360	0.945 -17	0.150 -16	0.196 -16
370	0.536 -17	0.106 -16	0.165 -16
380	0.287 -17	0.733 -17	0.136 -16
390	0.146 -17	0.494 -17	0.112 -16
400	0.709 -18	0.326 -17	0.905 -17
410	0.332 -18	0.212 -17	0.729 -17
420	0.150 -18	0.137 -17	0.584 -17
430	0.660 -19	0.869 -18	0.466 -17
440	0.283 -19	0.549 -18	0.370 -17
450	0.119 -19	0.346 -18	0.294 -17
460	0.491 -20	0.217 -18	0.233 -17
470	0.199 -20	0.135 -18	0.185 -17
480	0.803 -21	0.844 -19	0.146 -17
490	0.322 -21	0.527 -19	0.115 -17
500	0.128 -21	0.330 -19	0.912 -18
510	0.511 -22	0.207 -19	0.726 -18
520	0.203 -22	0.131 -19	0.579 -18
530	0.807 -23	0.826 -20	0.459 -18
540	0.320 -23	0.523 -20	0.362 -18

Tabular Data A-3.31. Total Photoabsorption Cross-Sections for the $A\ ^2\Sigma_{1/2u}^+ \rightarrow D\ ^2\Sigma_{1/2g}^+$ Transition of Kr_2^+. Boltzmann Averaged Over Vibrational Levels.

Wavelength λ (nm)	Cross-Section, σ (cm^2) T = 150°K	T = 300°K	T = 600°K
210	0.887 -21	0.328 -19	0.402 -18
220	0.834 -20	0.159 -18	0.134 -17
230	0.576 -19	0.585 -18	0.307 -17
240	0.304 -18	0.174 -17	0.568 -17
250	0.124 -17	0.434 -17	0.958 -17
260	0.402 -17	0.924 -17	0.148 -16
270	0.105 -16	0.169 -16	0.207 -16
280	0.219 -16	0.268 -16	0.268 -16
290	0.379 -16	0.376 -16	0.322 -16
300	0.553 -16	0.472 -16	0.367 -16
310	0.691 -16	0.541 -16	0.397 -16
320	0.752 -16	0.570 -16	0.411 -16
330	0.721 -16	0.558 -16	0.410 -16
340	0.616 -16	0.512 -16	0.394 -16
350	0.475 -16	0.443 -16	0.369 -16
360	0.333 -16	0.365 -16	0.336 -16
370	0.215 -16	0.288 -16	0.299 -16
380	0.129 -16	0.219 -16	0.261 -16
390	0.721 -17	0.160 -16	0.223 -16
400	0.382 -17	0.114 -16	0.189 -16
410	0.192 -17	0.795 -17	0.158 -16
420	0.922 -18	0.542 -17	0.129 -16
430	0.428 -18	0.362 -17	0.105 -16
440	0.193 -18	0.240 -17	0.857 -17
450	0.852 -19	0.157 -17	0.684 -17
460	0.370 -19	0.102 -17	0.544 -17
470	0.158 -19	0.657 -18	0.438 -17
480	0.675 -20	0.422 -18	0.346 -17
490	0.289 -20	0.270 -18	0.266 -17
500	0.124 -20	0.174 -18	0.207 -17
510	0.537 -21	0.114 -18	0.167 -17
520	0.231 -21	0.749 -19	0.136 -17
530	0.987 -22	0.480 -19	0.104 -17
540	0.411 -22	0.286 -19	0.705 -18
550	0.163 -22	0.153 -19	0.416 -18

Tabular Data A-3.32. Total Photoabsorption Cross-Sections for the A $^2\Sigma_{\frac{1}{2}u}^+ \rightarrow D\ ^2\Sigma_{\frac{1}{2}g}^+$ Transition of Xe_2^+. Boltzmann Averaged Over Vibrational Levels.

Wavelength λ(nm)	Cross-Section, σ (cm^2) T = 150°K	T = 300°K	T = 600°K
220	0.952 -22	0.652 -20	0.430 -19
230	0.141 -21	0.665 -20	0.439 -19
240	0.181 -20	0.606 -19	0.363 -18
250	0.167 -19	0.344 -18	0.176 -17
260	0.111 -18	0.127 -17	0.497 -17
270	0.552 -18	0.340 -17	0.899 -17
280	0.225 -17	0.771 -17	0.140 -16
290	0.700 -17	0.150 -16	0.207 -16
300	0.162 -16	0.239 -16	0.260 -16
310	0.342 -16	0.374 -16	0.344 -16
320	0.605 -16	0.528 -16	0.425 -16
330	0.846 -16	0.645 -16	0.484 -16
340	0.934 -16	0.682 -16	0.499 -16
350	0.828 -16	0.633 -16	0.478 -16
360	0.615 -16	0.533 -16	0.431 -16
370	0.399 -16	0.416 -16	0.372 -16
380	0.234 -16	0.310 -16	0.316 -16
390	0.128 -16	0.224 -16	0.262 -16
400	0.653 -17	0.156 -16	0.217 -16
410	0.321 -17	0.108 -16	0.176 -16
420	0.150 -17	0.735 -17	0.147 -16
430	0.645 -18	0.479 -17	0.116 -16
440	0.259 -18	0.302 -17	0.913 -17
450	0.983 -19	0.182 -17	0.686 -17
460	0.353 -19	0.105 -17	0.482 -17
470	0.121 -19	0.607 -18	0.366 -17
480	0.386 -20	0.299 -18	0.217 -17
490	0.101 -20	0.101 -18	0.796 -18
500	0.161 -21	0.193 -19	0.160 -18

Tabular Data A-3.33. Photoabsorption Cross-Sections for the $A\ ^2\Sigma^+_{1/2u} \rightarrow D\ ^2\Sigma^+_{1/2g}$ Transition of Ar_2^+ as a Function of Vibrational Level.

Continuum State Kinetic Energy ϵ (eV)	Cross-Section, σ (cm^2)				
	v=0	v=1	v=2	v=3	v=4
.9	0.350 -25	0.225 -23	0.665 -22	0.119 -20	0.145 -19
1.0	0.103 -23	0.543 -22	0.130 -20	0.186 -19	0.176 -18
1.1	0.184 -22	0.795 -21	0.153 -19	0.172 -18	0.125 -17
1.2	0.221 -21	0.776 -20	0.119 -18	0.104 -17	0.569 -17
1.3	0.190 -20	0.541 -19	0.655 -18	0.438 -17	0.174 -16
1.4	0.122 -19	0.277 -18	0.262 -17	0.130 -16	0.358 -16
1.5	0.601 -19	0.109 -17	0.784 -17	0.280 -16	0.493 -16
1.6	0.237 -18	0.337 -17	0.181 -16	0.441 -16	0.428 -16
1.7	0.766 -18	0.841 -17	0.326 -16	0.496 -16	0.185 -16
1.8	0.207 -17	0.172 -16	0.459 -16	0.373 -16	0.726 -18
1.9	0.478 -17	0.293 -16	0.501 -16	0.149 -16	0.702 -17
2.0	0.954 -17	0.419 -16	0.407 -16	0.613 -18	0.244 -16
2.1	0.168 -16	0.505 -16	0.221 -16	0.524 -17	0.274 -16
2.2	0.262 -16	0.510 -16	0.532 -17	0.206 -16	0.128 -16
2.3	0.369 -16	0.425 -16	0.132 -18	0.292 -16	0.535 -18
2.4	0.473 -16	0.278 -16	0.786 -17	0.228 -16	0.487 -17
2.5	0.555 -16	0.126 -16	0.211 -16	0.867 -17	0.180 -16
2.6	0.603 -16	0.244 -17	0.299 -16	0.232 -18	0.231 -16
2.7	0.609 -16	0.227 -18	0.289 -16	0.384 -17	0.151 -16
2.8	0.578 -16	0.558 -17	0.197 -16	0.148 -16	0.369 -17
2.9	0.515 -16	0.155 -16	0.833 -17	0.234 -16	0.212 -18
3.0	0.435 -16	0.262 -16	0.104 -17	0.235 -16	0.682 -17
3.1	0.349 -16	0.344 -16	0.788 -18	0.161 -16	0.165 -16
3.2	0.268 -16	0.386 -16	0.678 -17	0.654 -17	0.212 -16
3.3	0.196 -16	0.385 -16	0.159 -16	0.638 -18	0.178 -16
3.4	0.138 -16	0.350 -16	0.245 -16	0.980 -18	0.978 -17
3.5	0.941 -17	0.296 -16	0.302 -16	0.669 -17	0.249 -17
3.6	0.618 -17	0.235 -16	0.321 -16	0.148 -16	0.170 -19
3.7	0.393 -17	0.177 -16	0.306 -16	0.222 -16	0.308 -17
3.8	0.243 -17	0.126 -16	0.267 -16	0.269 -16	0.975 -17
3.9	0.146 -17	0.866 -17	0.217 -16	0.281 -16	0.171 -16
4.0	0.851 -18	0.571 -17	0.166 -16	0.264 -16	0.226 -16
4.1	0.485 -18	0.363 -17	0.121 -16	0.228 -16	0.252 -16
4.2	0.270 -18	0.224 -17	0.837 -17	0.183 -16	0.249 -16
4.3	0.147 -18	0.134 -17	0.557 -17	0.139 -16	0.223 -16
4.4	0.786 -19	0.778 -18	0.357 -17	0.997 -17	0.185 -16
4.5	0.411 -19	0.441 -18	0.221 -17	0.685 -17	0.144 -16
4.6	0.211 -19	0.244 -18	0.132 -17	0.452 -17	0.106 -16
4.7	0.107 -19	0.132 -18	0.777 -18	0.288 -17	0.745 -17
4.8	0.529 -20	0.698 -19	0.441 -18	0.177 -17	0.501 -17

Tabular Data A-3.34. Photoabsorption Cross-Sections for the $A\ ^2\Sigma^+_{1/2u} \rightarrow X\ ^2\Sigma^+_{1/2g}$ Transition of Kr_2^+ as a Function of Vibrational Level

Continuum State Kinetic Energy ϵ (eV)	Cross-Section, σ (cm^2)				
	v=0	v=1	v=2	v=3	v=4
.65	0.719 -25	0.410 -23	0.108 -21	0.175 -20	0.193 -19
.75	0.317 -23	0.144 -21	0.299 -20	0.372 -19	0.316 -18
.85	0.831 -22	0.298 -20	0.478 -19	0.451 -18	0.276 -17
.95	0.142 -20	0.397 -19	0.484 -18	0.335 -17	0.144 -16
1.05	0.191 -19	0.342 -18	0.308 -17	0.159 -16	0.423 -16
1.15	0.179 -18	0.197 -17	0.126 -16	0.419 -16	0.666 -16
1.25	0.668 -18	0.778 -17	0.341 -16	0.663 -16	0.471 -16
1.35	0.138 -17	0.136 -16	0.479 -16	0.678 -16	0.242 -16
1.35	0.266 -17	0.218 -16	0.607 -16	0.582 -16	0.549 -17
1.45	0.804 -17	0.446 -16	0.698 -16	0.190 -16	0.991 -17
1.55	0.191 -16	0.671 -16	0.468 -16	0.296 -18	0.393 -16
1.65	0.365 -16	0.741 -16	0.117 -16	0.233 -16	0.270 -16
1.75	0.578 -16	0.579 -16	0.712 -18	0.424 -16	0.850 -18
1.85	0.774 -16	0.280 -16	0.207 -16	0.252 -16	0.133 -16
1.95	0.892 -16	0.452 -17	0.429 -16	0.180 -17	0.339 -16
2.05	0.913 -16	0.181 -18	0.455 -16	0.566 -18	0.318 -16
2.05	0.899 -16	0.154 -17	0.411 -16	0.729 -17	0.219 -16
2.15	0.854 -16	0.176 -16	0.197 -16	0.296 -16	0.148 -17
2.25	0.645 -16	0.401 -16	0.197 -17	0.365 -16	0.699 -17
2.35	0.470 -16	0.560 -16	0.326 -17	0.212 -16	0.268 -16
2.45	0.388 -16	0.595 -16	0.105 -16	0.111 -16	0.321 -16
2.45	0.313 -16	0.598 -16	0.201 -16	0.348 -17	0.313 -16
2.55	0.193 -16	0.529 -16	0.391 -16	0.151 -17	0.165 -16
2.60	0.147 -16	0.471 -16	0.457 -16	0.706 -17	0.784 -17
2.65	0.110 -16	0.406 -16	0.494 -16	0.153 -16	0.186 -17
2.70	0.813 -17	0.340 -16	0.503 -16	0.244 -16	0.178 -19
2.75	0.589 -17	0.278 -16	0.486 -16	0.328 -16	0.251 -17
2.85	0.296 -17	0.172 -16	0.399 -16	0.432 -16	0.163 -16
2.90	0.205 -17	0.131 -16	0.343 -16	0.445 -16	0.246 -16
2.95	0.140 -17	0.928 -17	0.286 -16	0.433 -16	0.317 -16
3.05	0.636 -18	0.520 -17	0.184 -16	0.361 -16	0.396 -16
3.1	0.422 -18	0.370 -17	0.143 -16	0.312 -16	0.400 -16
3.15	0.278 -18	0.261 -17	0.109 -16	0.263 -16	0.385 -16
3.25	0.118 -18	0.125 -17	0.603 -17	0.173 -16	0.316 -16
3.35	0.482 -19	0.572 -18	0.313 -17	0.104 -16	0.229 -16
3.45	0.191 -19	0.251 -18	0.154 -17	0.583 -17	0.150 -16
3.55	0.238 -20	0.107 -18	0.726 -18	0.308 -17	0.901 -17
3.65	0.280 -20	0.440 -19	0.328 -18	0.154 -17	0.507 -17
3.75	0.104 -20	0.177 -19	0.144 -18	0.740 -18	0.270 -17
3.85	0.383 -21	0.697 -20	0.611 -19	0.342 -18	0.136 -17

Tabular Data A-3.35. Photoabsorption Cross-Sections for the $A\ ^2\Sigma^+_{1/2u} \rightarrow D\ ^2\Sigma^+_{1/2g}$ Transition of Xe_2^+ as a Function of Vibrational Level

Continuum State Kinetic Energy ϵ(eV)	Cross-Section, σ (cm^2)				
	v=0	v=1	v=2	v=3	v=4
.58	0.741 -20	0.175 -18	0.176 -17	0.988 -17	0.330 -16
.62	0.255 -19	0.518 -18	0.440 -17	0.202 -16	0.523 -16
.66	0.763 -19	0.132 -17	0.941 -17	0.346 -16	0.672 -16
.68	0.130 -18	0.209 -17	0.135 -16	0.440 -16	0.727 -16
.72	0.332 -18	0.451 -17	0.239 -16	0.605 -16	0.681 -16
.76	0.780 -18	0.891 -17	0.381 -16	0.720 -16	0.487 -16
.78	0.119 -17	0.124 -16	0.475 -16	0.760 -16	0.367 -16
.82	0.251 -17	0.216 -16	0.643 -16	0.698 -16	0.114 -16
.84	0.358 -17	0.278 -16	0.722 -16	0.619 -16	0.328 -17
.88	0.683 -17	0.429 -16	0.820 -16	0.380 -16	0.224 -17
.92	0.121 -16	0.601 -16	0.797 -16	0.131 -16	0.200 -16
.96	0.200 -16	0.767 -16	0.645 -16	0.315 -18	0.417 -16
1.0	0.315 -16	0.899 -16	0.407 -16	0.656 -17	0.494 -16
1.04	0.467 -16	0.953 -16	0.163 -16	0.277 -16	0.359 -16
1.08	0.649 -16	0.891 -16	0.138 -17	0.494 -16	0.123 -16
1.12	0.843 -16	0.712 -16	0.337 -17	0.558 -16	0.268 -19
1.16	0.103 -15	0.462 -16	0.209 -16	0.419 -16	0.103 -16
1.20	0.118 -15	0.216 -16	0.446 -16	0.182 -16	0.332 -16
1.24	0.128 -15	0.466 -17	0.617 -16	0.161 -17	0.476 -16
1.28	0.131 -15	0.219 -18	0.637 -16	0.371 -17	0.408 -16
1.32	0.128 -15	0.907 -17	0.498 -16	0.224 -16	0.193 -16
1.36	0.117 -15	0.277 -16	0.277 -16	0.441 -16	0.210 -17
1.40	0.102 -15	0.497 -16	0.843 -17	0.547 -16	0.295 -17
1.44	0.845 -16	0.688 -16	0.105 -18	0.487 -16	0.196 -16
1.48	0.673 -16	0.813 -16	0.467 -17	0.315 -16	0.385 -16
1.52	0.517 -16	0.858 -16	0.187 -16	0.130 -16	0.472 -16
1.56	0.387 -16	0.833 -16	0.365 -16	0.166 -17	0.419 -16
1.60	0.281 -16	0.756 -16	0.526 -16	0.105 -17	0.272 -16
1.64	0.199 -16	0.647 -16	0.633 -16	0.962 -17	0.115 -16
1.68	0.138 -16	0.529 -16	0.676 -16	0.231 -16	0.176 -17
1.72	0.941 -17	0.417 -16	0.663 -16	0.368 -16	0.531 -18
1.80	0.429 -17	0.243 -16	0.543 -16	0.551 -16	0.176 -16
1.84	0.288 -17	0.181 -16	0.465 -16	0.584 -16	0.301 -16
1.88	0.192 -17	0.133 -16	0.387 -16	0.579 -16	0.415 -16
1.96	0.807 -18	0.668 -17	0.242 -16	0.484 -16	0.550 -16
1.98	0.643 -18	0.556 -17	0.211 -16	0.451 -16	0.562 -16
2.00	0.500 -18	0.451 -17	0.180 -16	0.410 -16	0.555 -16
2.04	0.299 -18	0.293 -17	0.129 -16	0.329 -16	0.519 -16
2.08	0.173 -18	0.184 -17	0.888 -17	0.252 -16	0.456 -16
2.12	0.977 -19	0.113 -17	0.594 -17	0.186 -16	0.381 -16

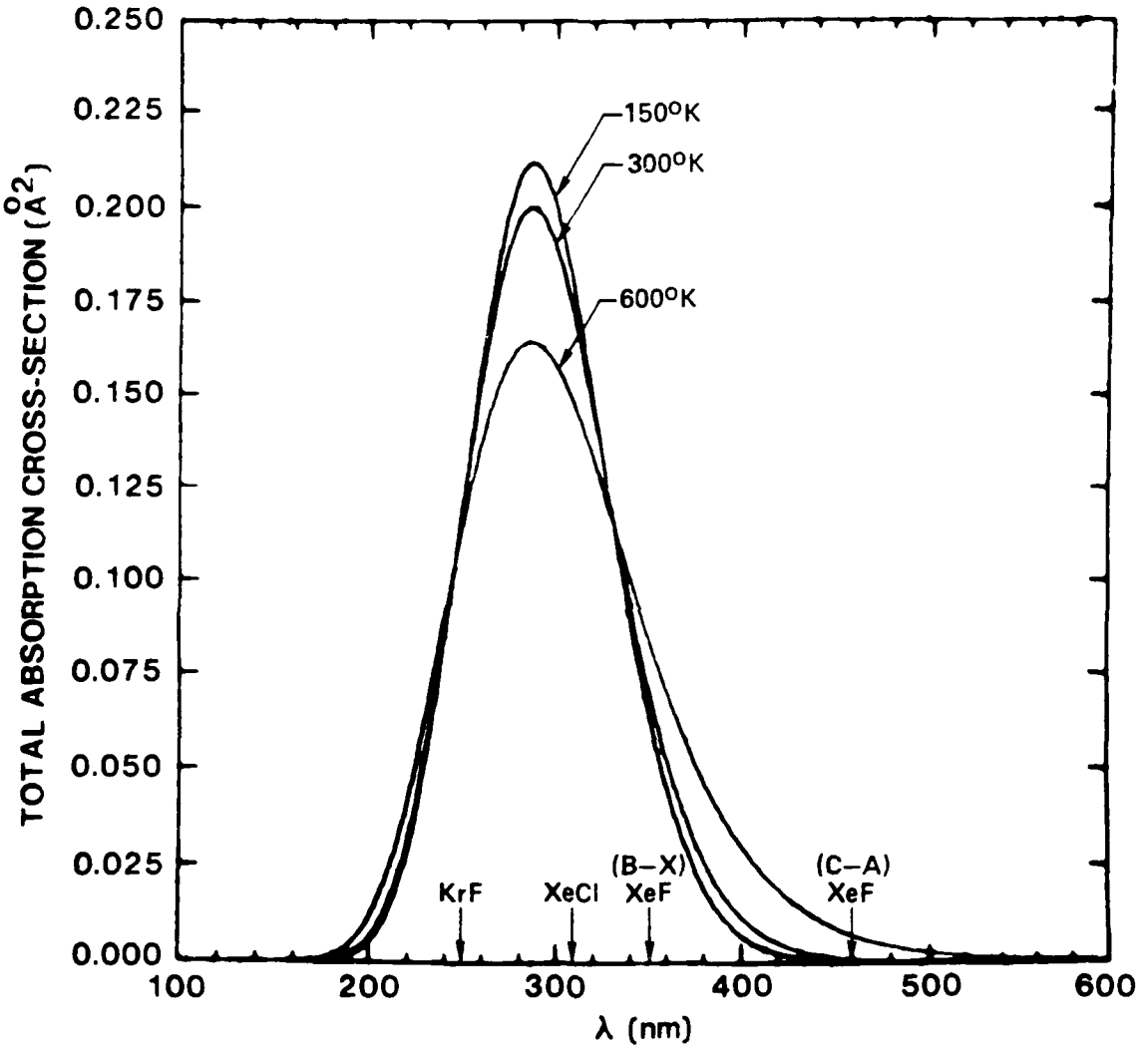

Graphical Data A-3.36. Total Photoabsorption Cross-Sections for the A $^2\Sigma^+_{1/2u}$ → D $^2\Sigma^+_{1/2g}$ Transition of Ne_2^+.

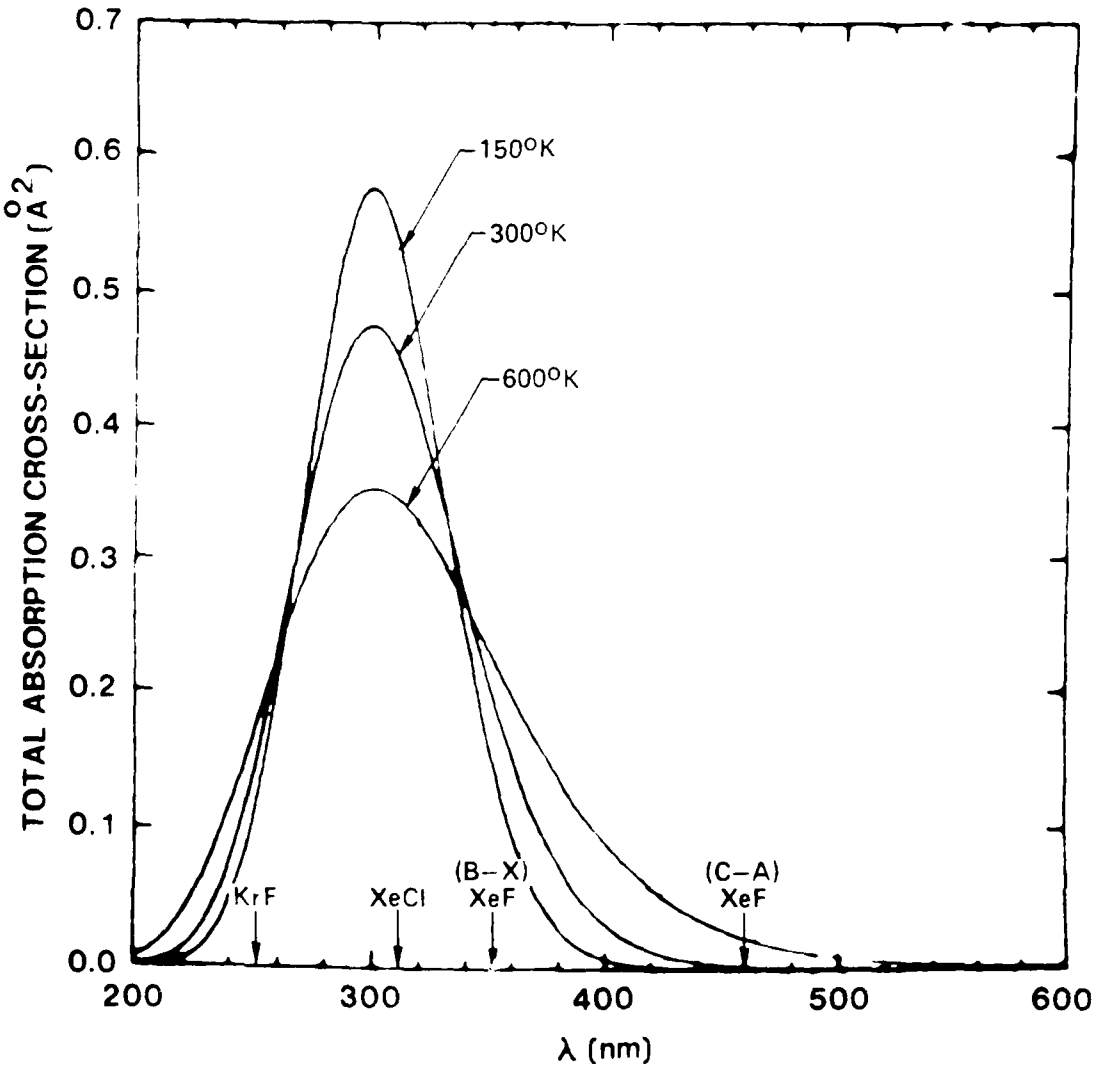

Graphical Data A-3.37. Total Photoabsorption Cross-Sections for the A $^2\Sigma^+_{1/2u}$ → D $^2\Sigma^+_{1/2g}$ Transition of Ar_2^+.

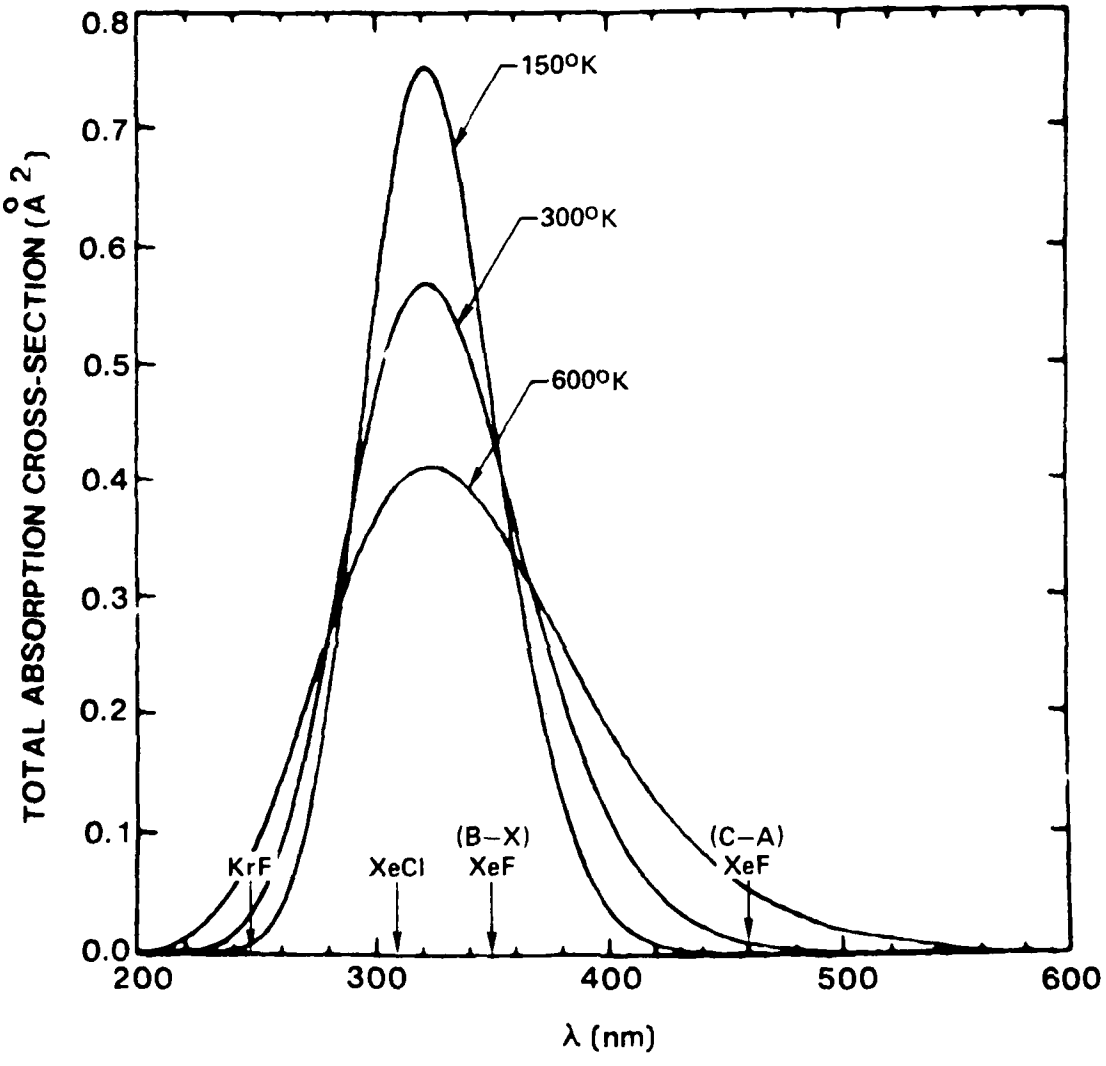

Graphical Data A-3.38. Total Photoabsorption Cross-Sections for the A $^2\Sigma^+_{1/2u}$ → D $^2\Sigma^+_{1/2g}$ Transition of Kr_2^+.

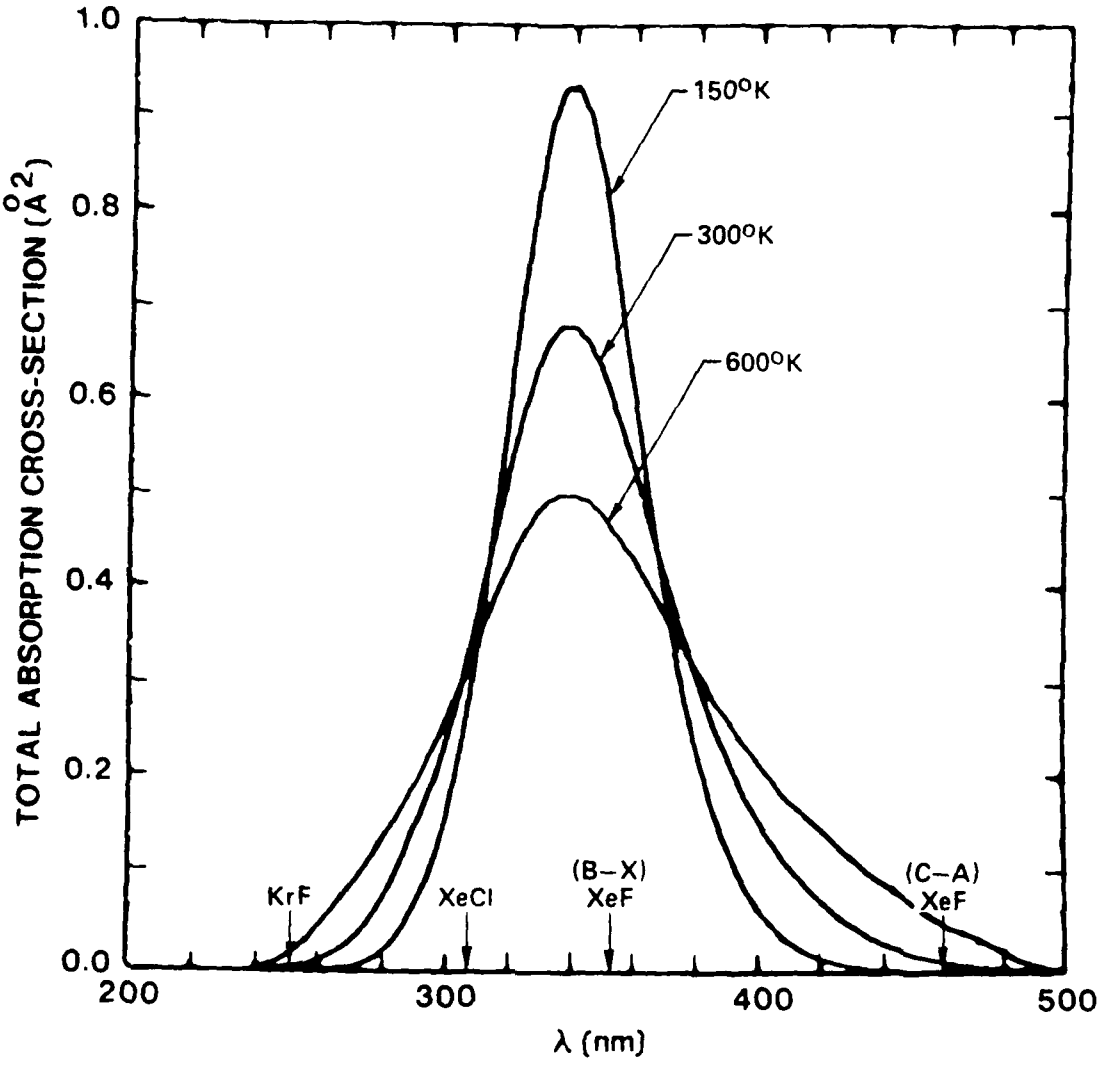

Graphical Data A-3.39. Total Photoabsorption Cross-Sections for the A $^2\Sigma^+_{1/2u}$ D $^2\Sigma^+_{1/2g}$ Transition of Xe_2^+.

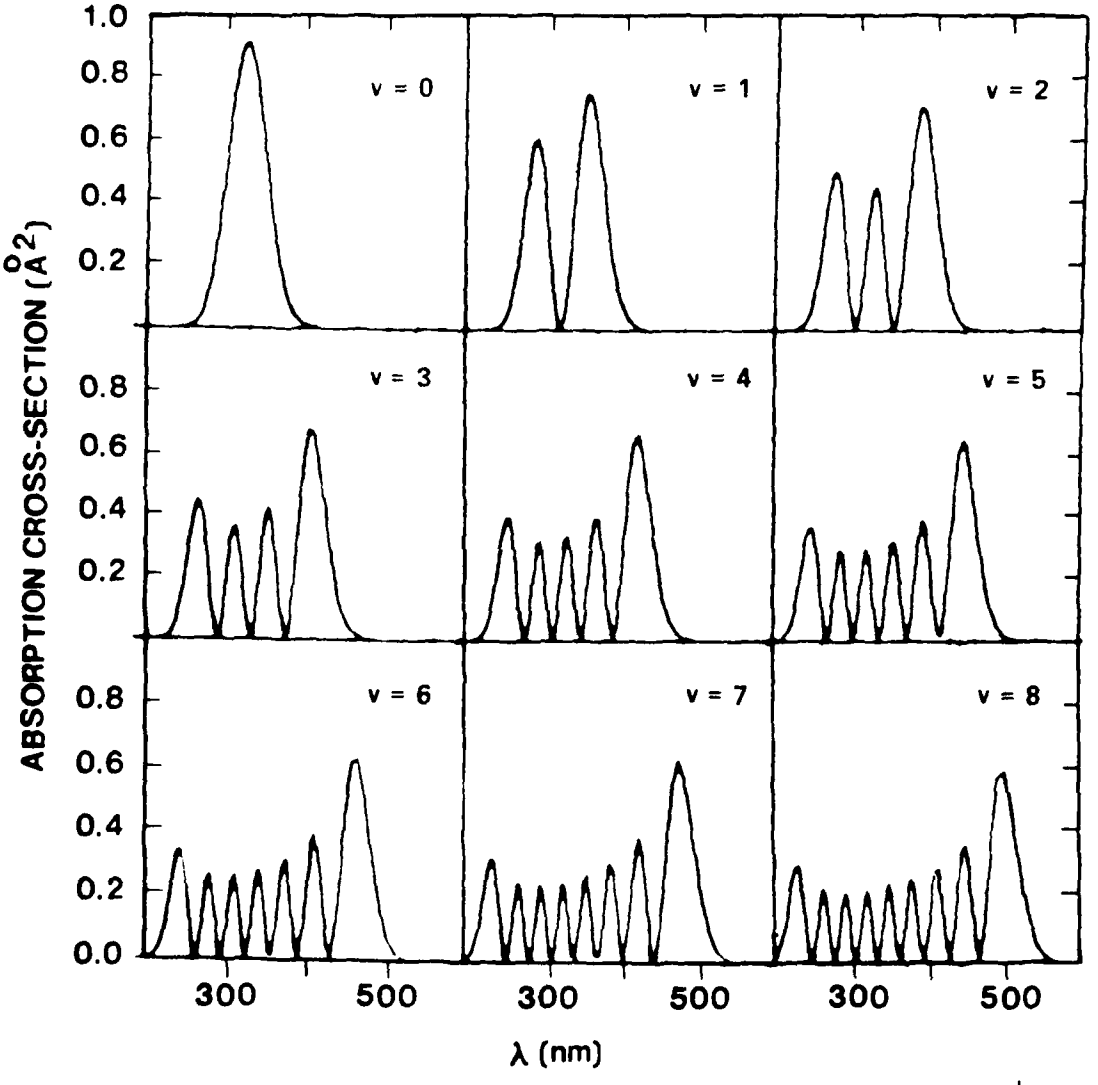

Graphical Data A-3.40. Photoabsorption Cross-Sections for the A $^2\Sigma^+_{1/2u}$ → D $^2\Sigma^+_{1/2g}$ Transition of Kr_2^+ as a Function of Several Vibrational Levels.

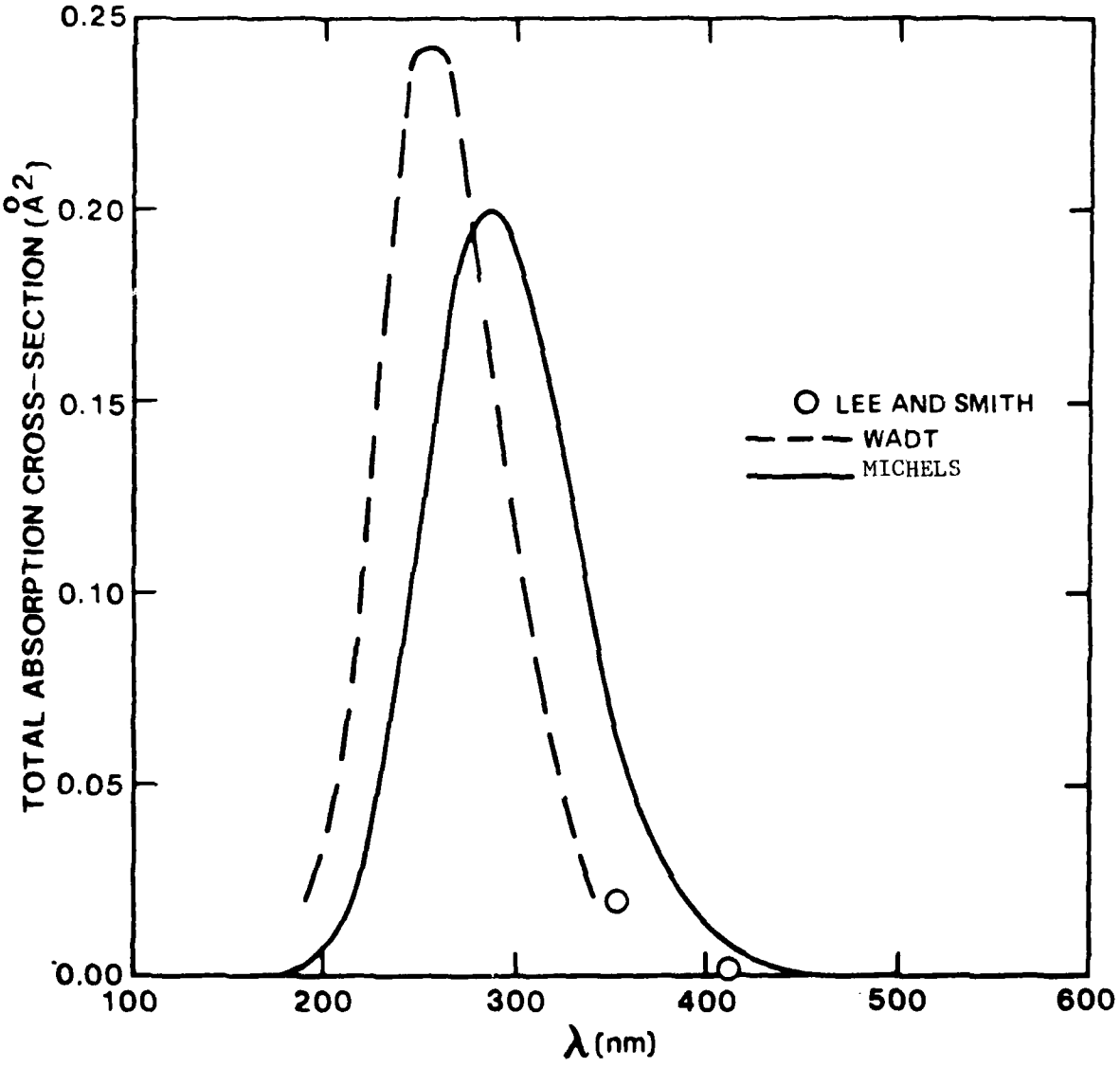

Graphical Data A-3.41. Comparative Cross-Sections for the A $^2\Sigma^+_{1/2u}$ → D $^2\Sigma^+_{1/2g}$ Transition of Ne_2^+ at 300°K. References 3, 7 and 2.

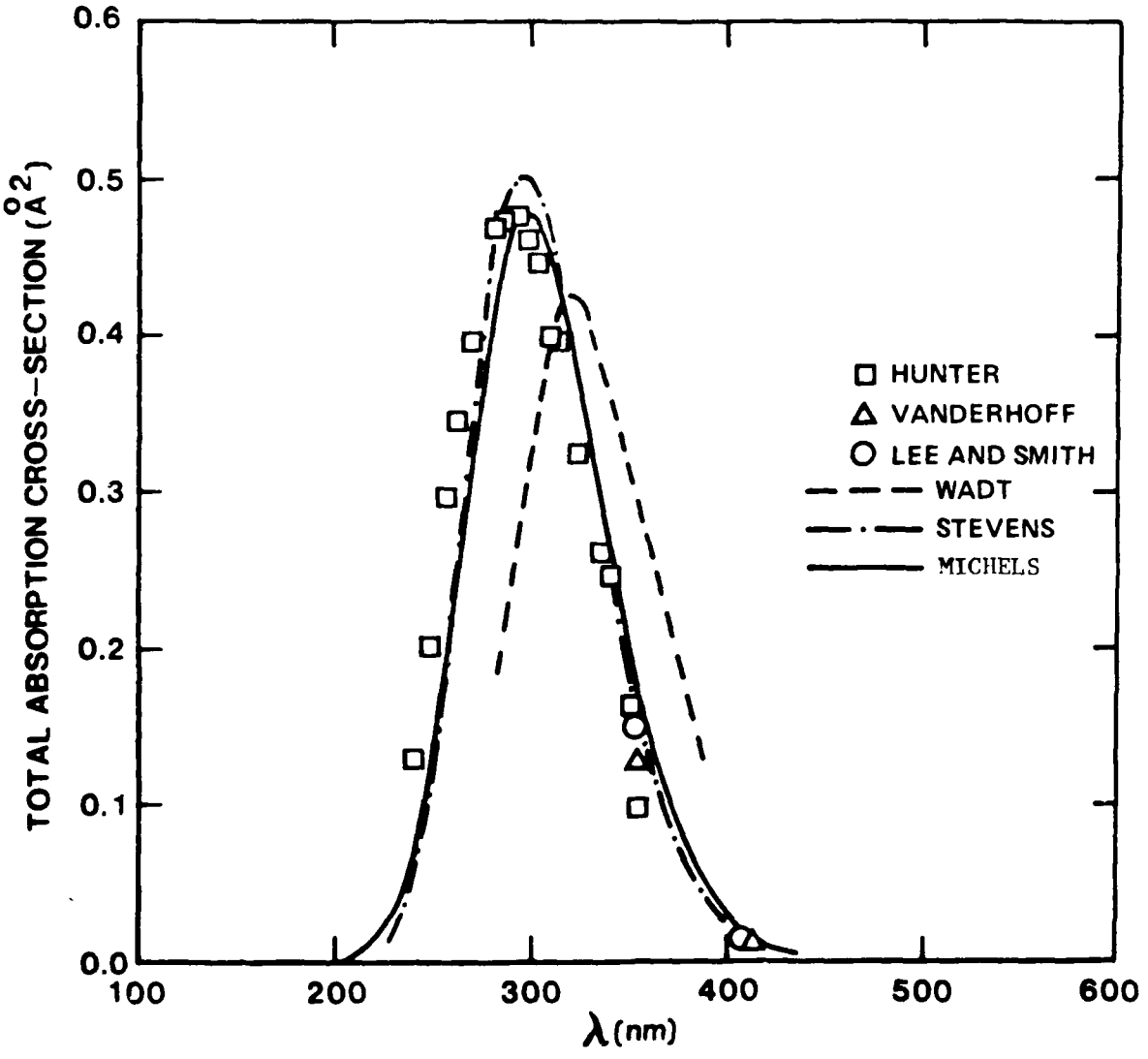

Graphical Data A-3.42. Comparative Cross-Sections for the A $^2\Sigma^+_{1/2u}$ → D $^2\Sigma^+_{1/2g}$ Transition of Ar_2^+ at 300°K References 5, 4, 3, 7, 6 and 2.

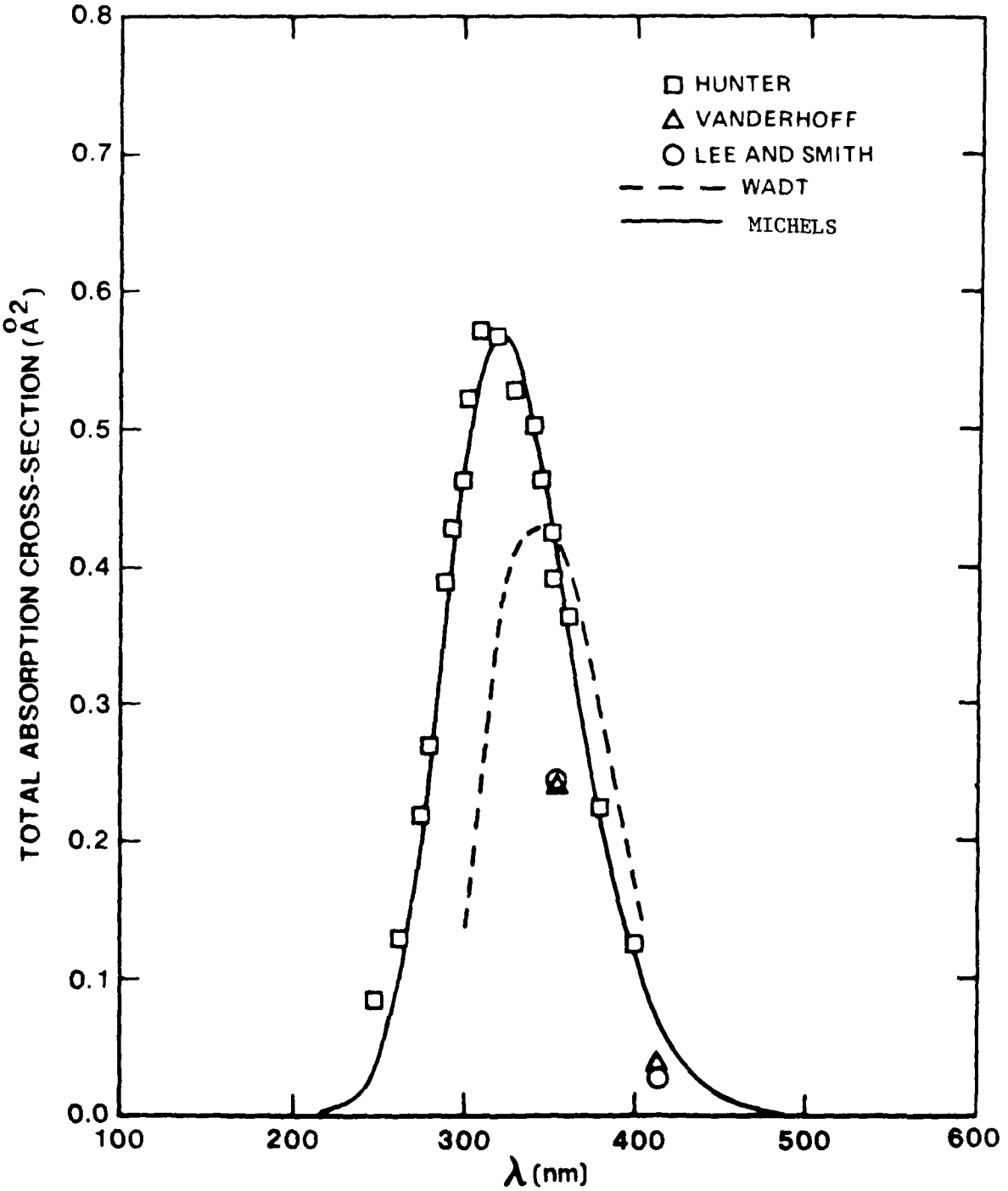

Graphical Data A-3.43. Comparative Cross-Sections for the A $^2\Sigma^+_{1/2u}$ → D $^2\Sigma^+_{1/2g}$ Transition of Kr_2^+ at 300°K. References 5, 4, 3, 7 and 2.

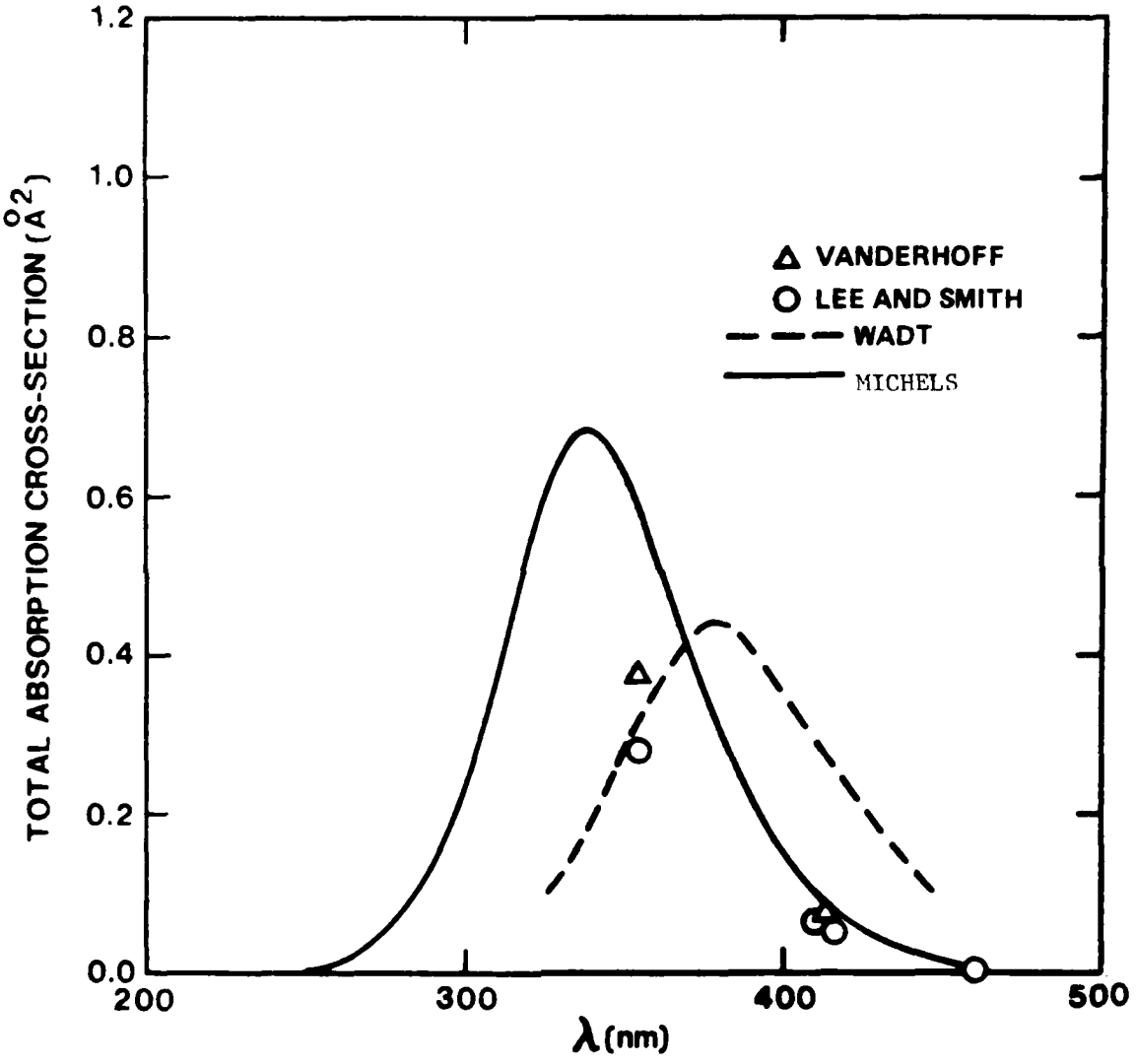

Graphical Data A-3.44. Comparative Cross-Sections for the A $^2\Sigma^+_{1/2u}$ → D $^2\Sigma^+_{1/2g}$ Transition of Xe_2^+ at 300°K. References 4, 3, 7 and 2.

Tabular Data A-3.45. Density Functional Potential Energy Curves for Hg_2^+. Energies in eV relative to V(∞) = 0. E(∞) = -39192.46852 hartrees for the relativistic and E(∞) = -36817.69215 hartrees for the non-relativistic calculations.

	Relativistic		Non-Relativistic	
R(bohrs)	$A\ ^1/_2{}_u^+$	$B\ ^1/_2{}_g^+$	$A\ ^1/_2{}_u^+$	$B\ ^1/_2{}_g^+$
5.0	+0..2993	2.06672	-	-
5.5	-0.56600	1.13473	+0.20436	-
5.75	-0.65036	-	-0.07919	-
6.0	-0.66532	0.68165	-0.30096	1.28249
6.25	-0.63947	-	-0.37634	-
6.5	-0.59049	0.42994	-0.42586	0.85172
7.0	-0.47076	0.27756	-0.43675	0.56600
7.5	-0.35511	-	-0.38477	0.38096
8.0	-0.26042	0.10340	-0.31266	0.26150
8.5	-	-	-0.24817	0.18041
8.75	-	-	-0.21742	-
9.0	-0.13062	0.04599	-0.18994	0.12545
10.0	-0.06259	0.02095	-0.10368	0.07510
∞	0.	0.	0.	0.

Tabular Data A-3.46. Spectroscopic Constants for Hg_2^+ based on Relativistic Density Functional Calculations.

State	T_e(eV)	ω_e(cm^{-1})	$\omega_e X_e$(cm^{-1})	α_e(cm^{-1})	r_e(Å)	B_e(cm^{-1})	D_e(eV)	D_o(eV)
$B\ ^1/_2{}_g^+$	1.347	(vertical excitation energy, repulsive curve)						
$A\ ^1/_2{}_u^+$	0.0	84.66	0.35	0.00007	3.15	0.0170	0.667	0.662

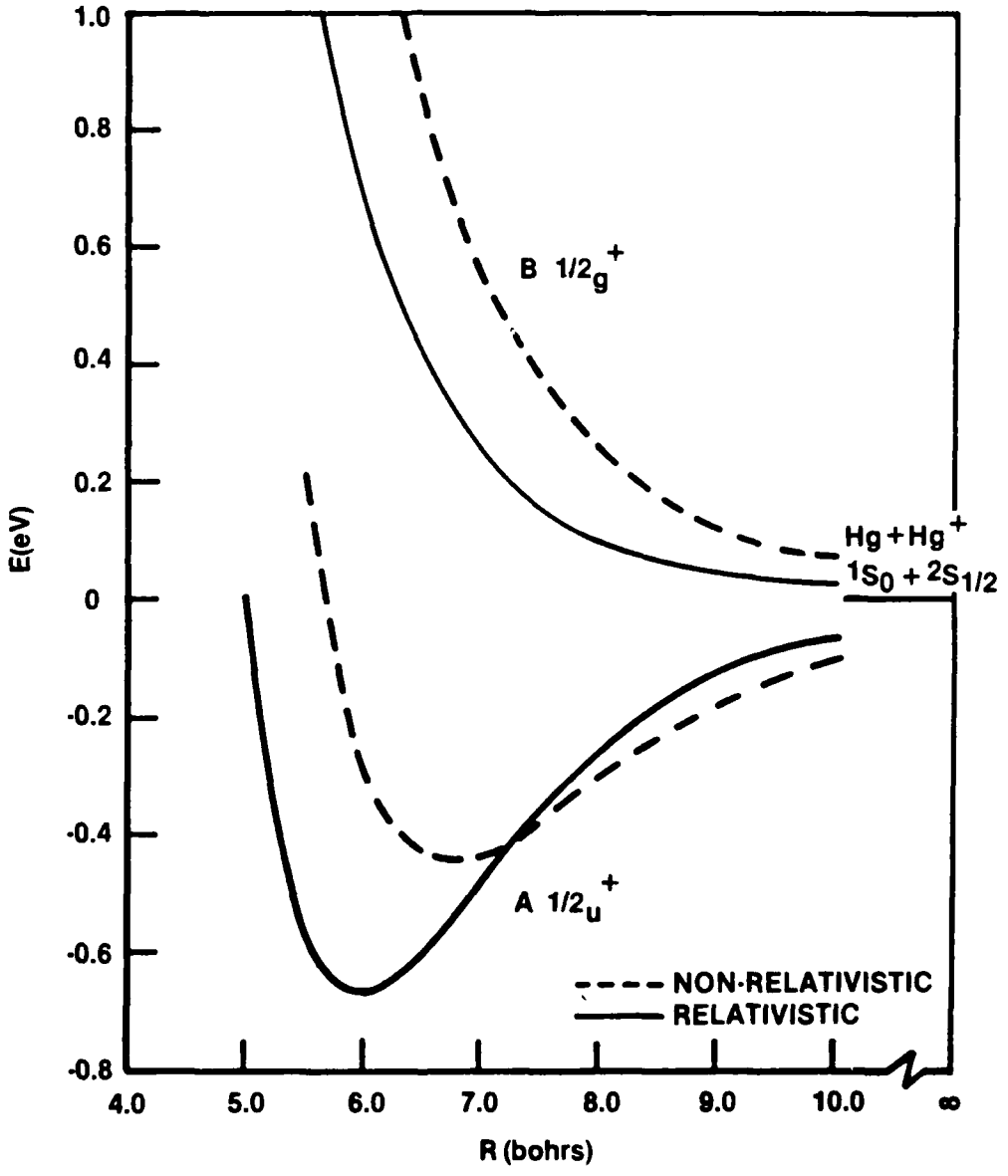

Graphical Data A-3.47. Low-Lying Potential Energy Curves for Hg_2^+ (Density-Functional Method)

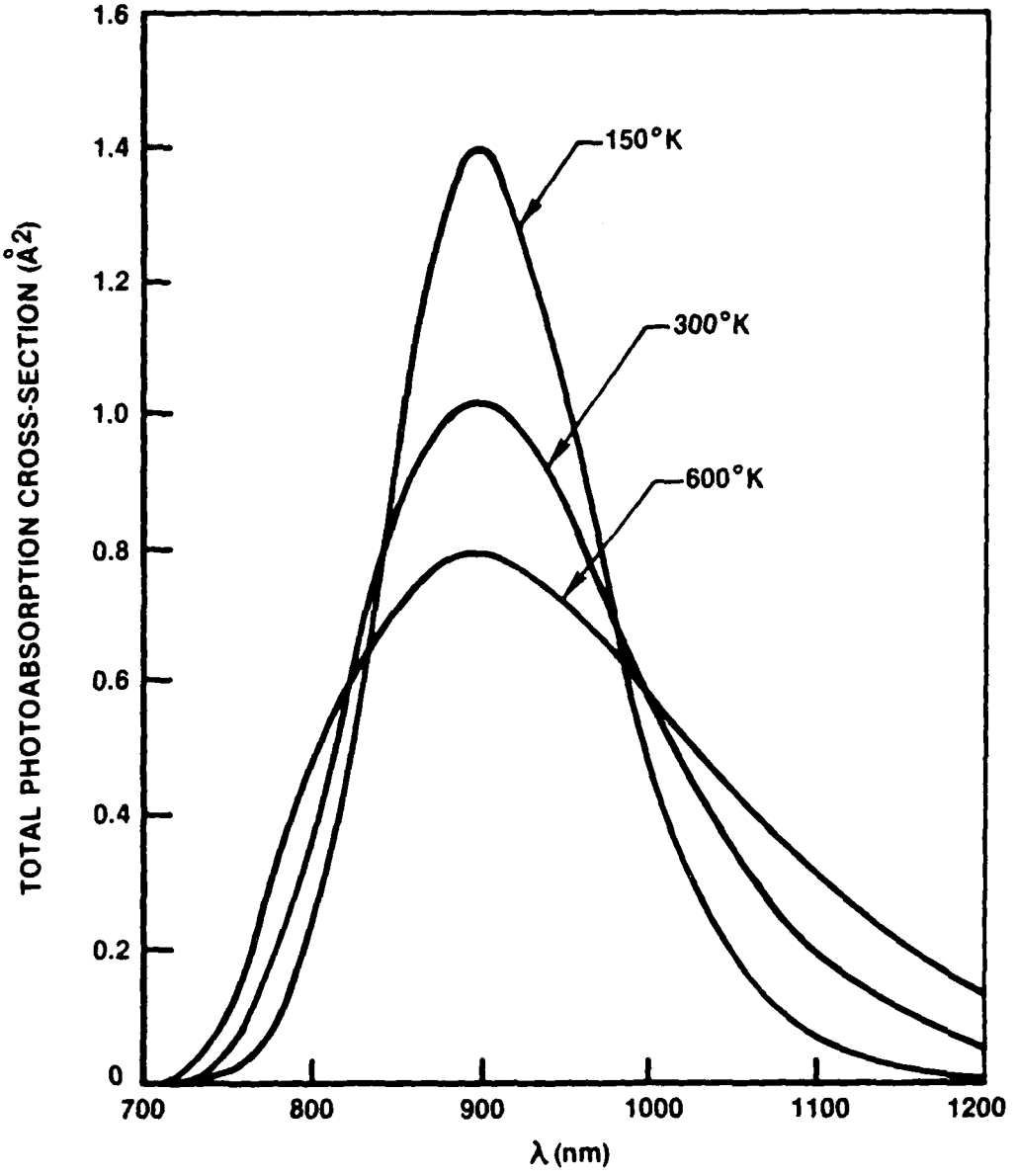

Graphical Data A-3.48. Total Photoabsorption Cross-Sections for the $A\ ^1\Sigma_u^+ \rightarrow B\ ^1\Sigma_g^+$ Transition of Hg_2^+

Tabular Data A-3.49. SPECTROSCOPIC CONSTANTS AND TOTAL ELECTRONIC ENERGIES (in a.u. for a bond length of 5.2 Bohrs) FOR Ar_3^+.

State	D_{3h} (triangular geometry)	T_e(eV)	ω_2(cm^{-1})	R_e(Å)	D_e(eV)[a]	D_o(ev)
$^2A_1'$	-1579.8676	2.19	(Repulsive potential surface)			
$^2E'$ II		1.44				
$^2A_2''$	-1579.9110	1.15				
$^2E''$	-1579.9305	0.70				
$^2A_2'$	-1579.9502	0.25				
$^2E'$	-1579.9609	0.0	174	2.95	1.496	1.472

a) Dissociation energy relative to Ar + Ar + Ar^+ (E(∞) = - 1579.9097)

D_e relative to Ar_2^+ [$A\ ^2\Sigma_{1/2u}^+$] + Ar = 0.17 eV

Absorption Bands

$^2E' \rightarrow {}^2A_1'$	$\lambda_{max} \sim 560$ nm	(Strong)
$^2E' \rightarrow {}^2E''$	$\lambda_{max} \sim 1500$ nm	(Weak)

2628

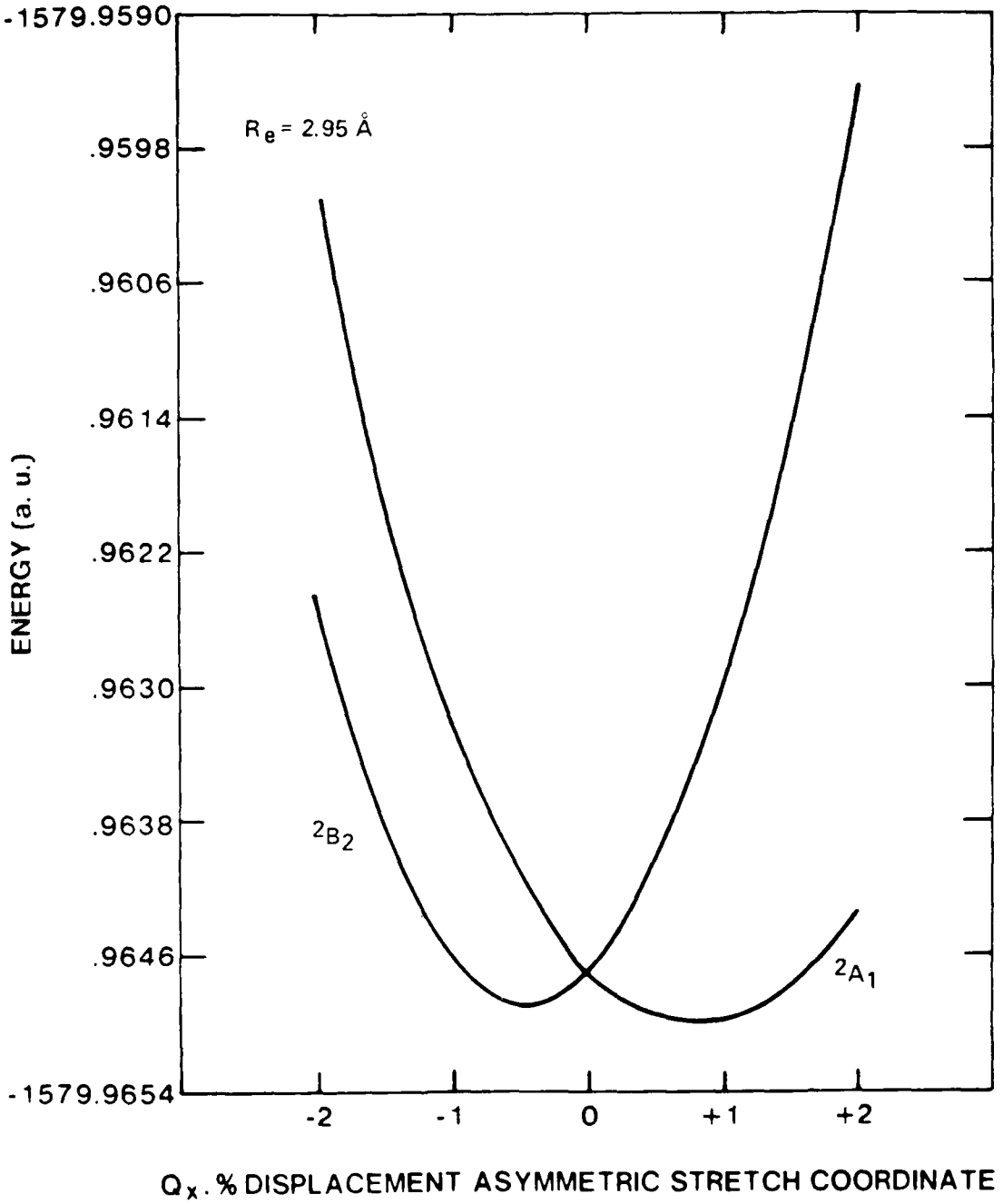

Graphical Data A-3.50. Jahn-Teller Energies for the Ground State of Ar_3^+ in C_{2v} Symmetry.

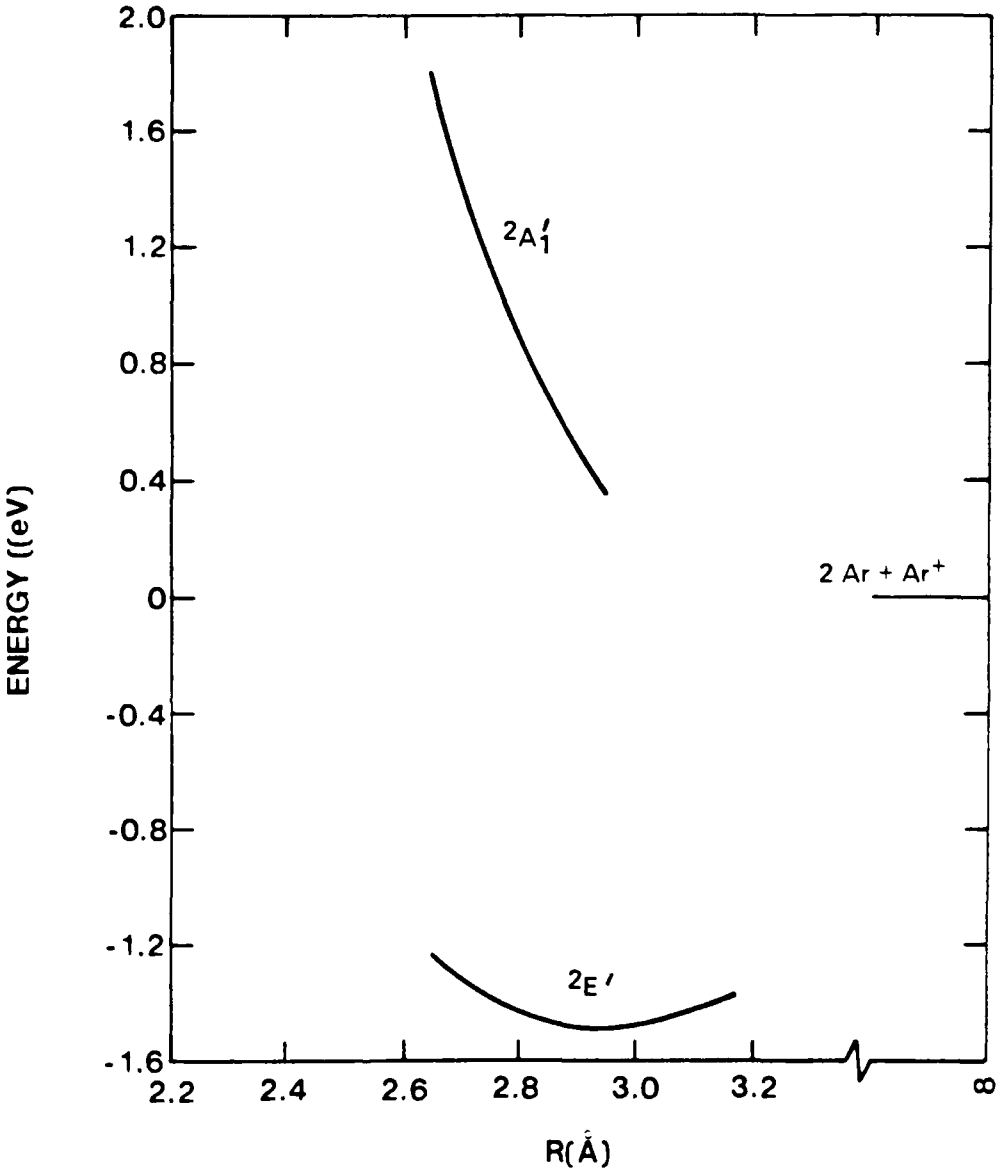

Graphical Data A-3.51. Potential Energy Curves for Ar_3^+.

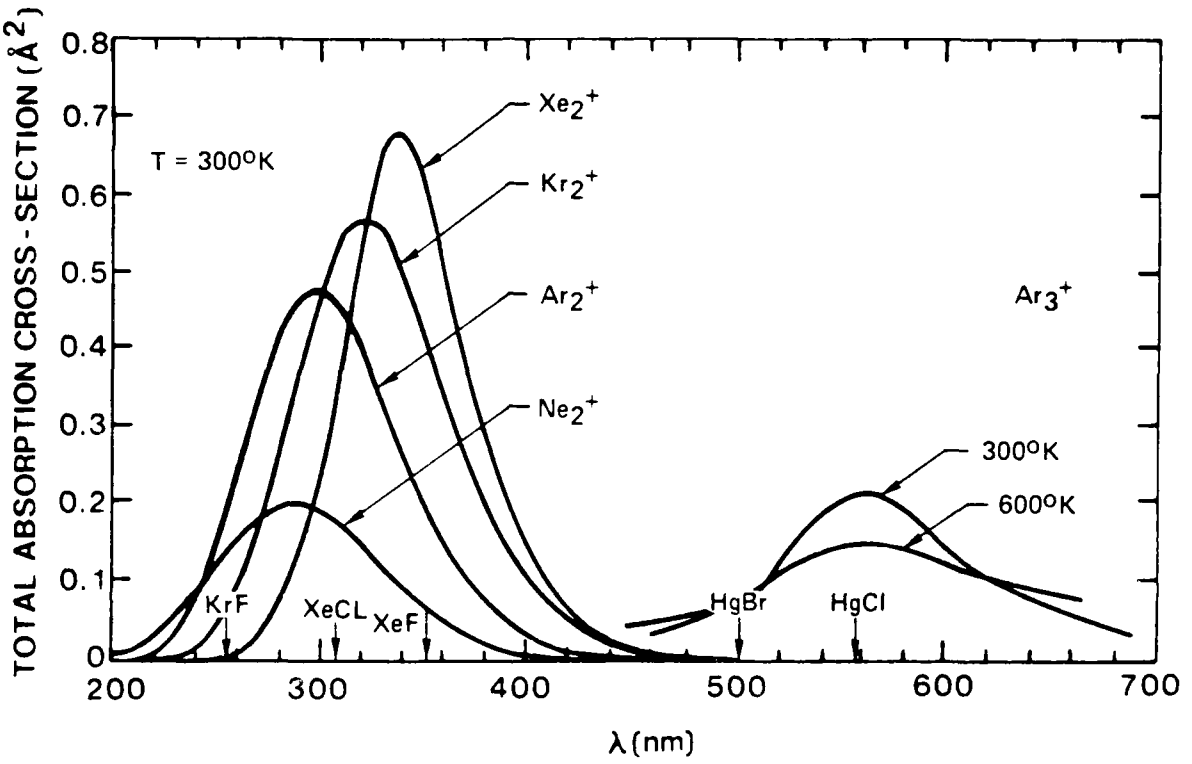

Graphical Data A-3.52. Noble Gas Dimer and Trimer Ion Absorption Cross-Sections.

AD-A102 279 ARMY MISSILE COMMAND REDSTONE ARSENAL AL DIRECTED E--ETC F/G 20/5
COMPILATION OF ATOMIC AND MOLECULAR DATA RELEVANT TO GAS LASERS--ETC(U)
DEC 80 E W MCDANIEL, M R FLANNERY, E W THOMAS
UNCLASSIFIED ORSMI-RH-81-4-VOL-7 NL

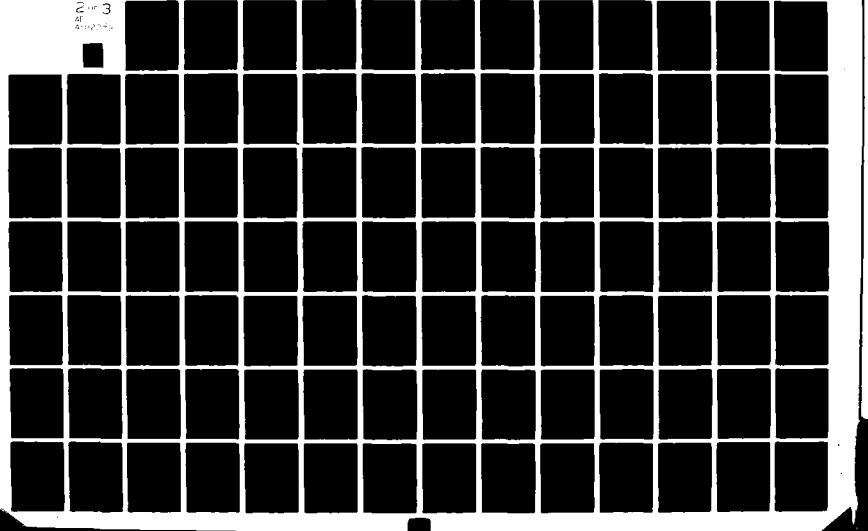

A-4. FRANCK-CONDON FACTORS FOR XeCl, ELECTRONIC STRUCTURE OF $HgCl_2$, $HgBr_2$ AND ArBr, POTENTIAL ENERGY CURVES FOR Zn_2, Cd_2 AND LiCa.

CONTENTS

		Page
A-4.1.	Potential diagram for XeCl	2634
A-4.2.	Assigned bandheads in B → X spectrum of $^{136}Xe^{35}Cl$	2635
A-4.3.	Assigned bandheads in D → X spectrum of $^{136}Xe^{35}Cl$	2635
A-4.4.	Franck-Condon factors (x 10^3) for B-X system of $^{136}Xe^{35}Cl$	2636
A-4.5.	Franck-Condon factors (x 10^3) for D-X system of $^{136}Xe^{35}Cl$	2636
A-4.6.	Spectroscopic studies on $HgBr_2$	2637
A-4.7.	Spectroscopic studies on $HgCl_2$	2637
A-4.8.	Excitation energies for linear $HgCl_2$ and $HgBr_2$	2638
A-4.9.	Hartree-Fock excitation energies (ΔE) and Mulliken populations for linear $HgCl_2$	2639
A-4.10.	Transition moments (M) and oscillator strengths (f) for the vertical dipole-allowed excitations in $HgCl_2$ and $HgBr_2$	2639
A-4.11.	Valence bond orbital diagrams for the ground $1\ ^1\Sigma^+_g$ state of $HgCl_2$	2640
A-4.12.	Contour plots for the highest occupied orbitals of the $1\ ^1\Sigma^+_g$ state of $HgCl_2$	2641
A-4.13.	Contour plots for the lowest virtual orbitals of the $1\ ^1\Sigma^+_g$ state of $HgCl_2$	2642
A-4.14.	Orbital energy level diagram for $HgCl_2$	2643
A-4.15.	Potential curves for the states of $HgCl_2$ as a function of bending angle θ	2644
A-4.16.	Electronic state correlations diagrams for HgCl + Cl → $HgCl_2$	2645
A-4.17.	Experimental energy level diagram for key excited states of $HgCl_2$	2646
A-4.18.	Potential curves of ArBr	2647
A-4.19.	Energy level diagram of ArBr and Br	2647
A-4.20.	ArBr potential curves	2648

Page

A-4.21. Potential energy curves for states of Zn_2. 2649

A-4.22. Potential energy curves for diatomic cadmium 2650

A-4.23. Gerade states of Cd_2 2651

A-4.24. Ungerade states of Cd_2 2652

A-4.25. Computed Cd_2^* $1_u \rightarrow 0_g^+$ fluorescence band at 675°K 2653

A-4.26. Contributions of individual vibrational level to the Cd_2^* fluorescence rate at 675°K 2654

A-4.27. The lowest atomic energy levels (in cm^{-1}) of zinc and cadmium. 2655

A-4.28. Spectroscopic constants for the bound states of Zn_2 and Cd_2. . 2656

A-4.29. Potential energy curves for LiCa 2657

A-4.30. LiCa emission spectrum 2658

A-4.31. Spectroscopic constants for LiCa 2659

A-4.32. Experimental vs. calculated spectra for LiCa 2659

A-4. References

1. A. Sur, A. K. Hui, and J. Tellinghuisen, "Noble Gas Halides", J. Chem. Phys. 74, 465 (1979), and references therein. (A-4.1 - A-4.5).

2. W. R. Wadt, "The Electronic Structure of Hg Cl_2 and Hg Br_2 and its Relationship to Photodissociation", J. Chem. Phys. 72, 2469 (1980). (A-4.6 - A-4.17).

3. M. F. Golde and A. Kvaran, "Chemiluminescence of Argon Bromide. I. The Emission Spectrum of Ar Br", J. Chem. Phys. 72, 434 (1980). (A-4.18 - A-4.19).

4. M. F. Golde and A. Kvaran, "Chemiluminescence of Argon Bromide. II. Potential Curves of Ar Br and Population Distributions in the B(1/2) and C(3/2) Electron States", J. Chem. Phys. 72, 442 (1980). (A-4.20).

5. C. F. Bender, T. N. Rescigno, H. F. Schaefer and A. E. Orel, "Potential Energy Curves for Diatomic Zinc and Cadmium", J. Chem. Phys. 71, 1122 (1979). (A-4.21 - A-4.28).

6. D. K. Neumann, D. J. Benard and H. H. Michels, "Laser Chemiluminescence of Li Ca", Chem. Phys. Letts. 73, 343 (1980). (A-4.29 - A-4.32).

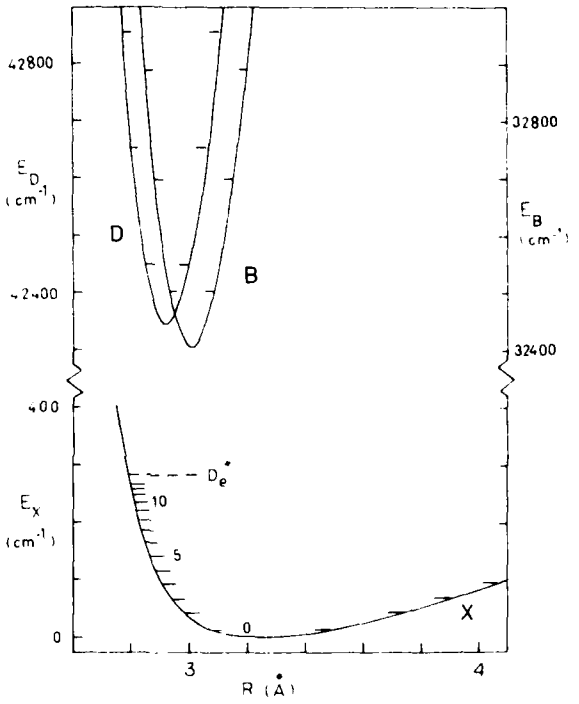

Graphical Data A-4.1. Potential diagram for XeCl, showing the states of relevance to the present study. Note the different energy scales for the three potential curves.

Tabular Data A-4.2. Assigned Bandheads in $B \rightarrow X$ Spectrum of $^{136}Xe^{35}Cl$

v'-v''	Weight	λ(Å)	ν(cm^{-1})	Δν(cm^{-1})[a]
0-6	1	3091.37	32338.7	0.3
0-5	1	89.21	361.3	0.2
0-4	5	86.90	385.6	-0.0
0-3	5	84.50	410.8	-0.1
0-2	5	82.04	436.7	0.1
0-1	5	79.53	463.0	0.3
0-0	5	76.98	490.0	-0.1
1-7	3	74.91	511.8	-0.0
1-6	3	72.97	532.4	0.2
1-5	5	70.83	555.1	0.0
1-4	5	68.55	579.3	-0.2
2-13	0.5	64.46	622.7	0.1
2-12	0.5	63.75	630.2	0.7
2-11	0.5	62.76	640.8	0.4
1-1	5	61.26	656.8	-0.0
1-0	5	58.75	683.6	-0.2
2-1	5	43.35	848.0	0.0
2-0	5	40.80	875.6	0.0
3-5	0.5	35.17	937.5	0.8
3-4	2	32.91	962.1	0.2
3-3	5	30.55	987.7	-0.2
3-1	0.5	25.80	33039.5	0.5
4-9	0.5	24.97	048.5	0.5
3-0	5	23.30	066.8	-0.2
4-7	0.5	21.68	084.5	0.2
4-3	0.5	13.26	177.0	0.2
4-0	5	06.07	256.4	-0.0
5-3	5	2996.21	365.8	-0.1
5-2	3	93.87	391.8	-0.1
5-0	3	89.11	445.0	-0.2
6-0	5	72.48	632.1	-0.1
7-2	5	60.80	764.9	0.1
7-0	3	56.15	817.9	0.2
8-0	5	40.09	34002.7	0.1
9-0	5	24.31	186.1	0.1
10-1	5	11.06	341.7	0.1
10-0	5	08.80	368.4	0.1
11-1	5	2895.78	522.9	-0.1
11-0	5	93.55	549.5	-0.1
12-1	2	80.76	702.9	-0.4
12-0	2	78.60	728.9	0.2

[a] $\nu_{calc} - \nu_{obs}$ from least-squares fit.

Tabular Data A-4.3. Assigned Bandheads in $D \rightarrow X$ Spectrum of $^{136}Xe^{35}Cl$

v'-v''	Weight	λ(Å)	ν(cm^{-1})	Δν(cm^{-1})[a]
0-11	0.5	2368.74	42203.7	-1.4
0-10	1	68.07	215.5	-0.8
0-9	2	67.31	229.2	0.2
0-8	2	66.35	246.3	-0.1
0-7	3	65.30	264.9	0.2
0-6	3	64.13	285.9	0.0
0-5	3	62.87	308.5	-0.1
0-4	3	61.54	332.3	0.0
0-3	2	60.15	357.3	0.2
0-2	3	58.69	383.4	0.2
0-1	1	57.24	409.5	0.6
1-3	1	48.84	561.3	-0.7
1-2	3	47.44	586.6	-0.0
1-1	2	45.99	612.9	0.2
1-0	2	44.52	639.6	0.1
2-2	1	36.40	787.7	0.4
2-1	2	34.92	814.9	-0.2
2-0	3	33.47	841.5	-0.2
3-2	3	25.50	988.3	0.1
3-1	2	24.05	43015.1	-0.1
3-0	2	22.63	041.4	0.2
4-0	3	20.06	089.2	0.4
4-1	3	13.37	213.7	0.1
4-0	3	11.93	240.5	-0.1
5-4	2	06.95	333.9	-0.3
5-1	1	02.86	410.9	0.4
5-0	2	01.41	438.2	-0.3
6-1	1	2292.52	606.7	0.8
6-0	3	91.10	633.8	0.3
7-3	2	85.02	749.8	-0.1
7-0	3	80.90	828.8	0.1
8-0	3	70.88	44022.3	0.0
9-3	2	65.07	135.1	0.1
9-2	1	63.71	161.7	-0.4
9-0	1	61.01	214.4	-0.7

[a] $\nu_{calc} - \nu_{obs}$ from least-squares fit.

Tabular Data A-4.4. Franck-Condon Factors ($\times 10^4$) for B-X System of $^{136}Xe^{35}Cl^a$

v''	v' = 0	1	2	3	4	5
0	121 16	84 20	105 30	93 37	93 44	82 50
1	218 63	65 54	60 66	20 60	8 50	0 45
2	234 119	10 61	6 58	5 31	23 17	32 5
3	186 153	7 37	4 25	13 5	32 0	36 6
4	115 155	58 10	16 3	32 1	14 11	8 23
5	57 133	114 0	32 1	30 13	0 20	1 24
6	21 100	140 6	2 5	8 27	20 16	10 12
7	5 79	131 18	2 8	0 27	28 19	13 5
8	0 44	103 25	14 7	2 17	35 3	7 1
9	0	71	27	2	31	2
10	1	46	41	2	22	0
11	2	26	45	1	14	2
12	2	15	42	0	8	4
13	2	8	35	0	4	5
14	2	5	26	0	2	5

[a]First entry is for N'=N''=0. Second entry, where given, is for N'=N''=50.

Tabular Data A-4.5. Franck-Condon Factors ($\times 10^4$) for D-X System of $^{136}Xe^{35}Cl^a$

v''	v' = 0	1	2	3	4	5
0	29 3	41 6	56 10	66 15	73 20	77 26
1	73 13	70 22	74 33	60 41	45 47	29 49
2	114 31	67 41	48 50	20 50	5 44	0 34
3	139 52	41 51	15 49	0 35	5 21	17 8
4	142 69	13 48	0 35	10 15	22 3	30 0
5	126 78	0 37	4 18	26 2	27 0	20 6
6	105 77	5 23	14 6	31 0	17 5	6 13
7	79 76	19 14	18 2	25 2	6 10	0 15
8	57 55	33 5	17 0	15 5	0 10	2 11
9	39	44	12	7	1	6
10	26	47	7	2	4	9
11	17	45	3	0	6	8
12	11	39	1	0	7	7
13	7	31	0	0	6	5
14	4	23	0	0	5	3

[a]First entry is for N'=N''=0. Second entry, where given, is for N'=N''=50.

Note: N' = N'' = 50 corresponds to the average rotational level in the excited states at temperature 325K. N' = N'' = 0 corresponds to rotationless curves.

Tabular Data A-4.6. Results of spectroscopic studies of Wieland[a] on $HgBr_2$. (All wavelengths in nm)

Absorption Maximum	Excitation Wavelength	Fluorescence Wavelength
224	≥210	none
195	210-190	505-350
183	190-170	none
	170-160	290-270
∿160	160-150	270-250

[a]K. Wieland, Z. Phys. 76, 801 (1932); 77, 157 (1932).

Tabular Data A-4.7. Results of spectroscopic studies of Wieland[a] on $HgCl_2$. (All wavelengths are in nm)

Absorption Maximum	Excitation Wavelength	Fluorescence Wavelength
	≥190	none
181	≤190	560-340
169	≤190	290-270
∿150	≤190	265-240

[a]K. Wieland, Z. Phys. 76, 801 (1932); 77, 157 (1932).

Tabular Data A-4.8. POL CI excitation energies (ΔE) for linear $HgCl_2$ [R(Hg-Cl) = 2.275Å] and $HgBr_2$ [R(Hg-Br) = 2.41Å]. Experimental values are given parenthetically.

State	ΔE (eV) $HgCl_2$	ΔE (eV) $HgBr_2$
$1^1\Sigma_g^+$	0.0[a]	0.0[b]
$1^3\Pi_g$ $(2\pi_g \rightarrow 4\sigma_g)$	4.64	4.00
$1^1\Pi_g$ $(2\pi_g \rightarrow 4\sigma_g)$	4.98	4.29
$1^3\Pi_u$ $(1\pi_u \rightarrow 4\sigma_g)$	5.05	4.35
$1^3\Sigma_u^+$ $(2\sigma_u \rightarrow 4\sigma_g)$	5.29	4.57
$1^1\Pi_u$ $(1\pi_u \rightarrow 4\sigma_g)$	5.46 (6.20)[c]	4.72 (5.64)[c]
$1^1\Sigma_u^+$ $(2\sigma_u \rightarrow 4\sigma_g)$	6.71 (6.85)[d]	5.97 (6.36)[c]
$2^3\Sigma_u^+$ $(2\pi_g \rightarrow 2\pi_u)$	7.18	6.33
$1^3\Delta_u$ $(2\pi_g \rightarrow 2\pi_u)$	7.32	6.47
$1^1\Delta_u$ $(2\pi_g \rightarrow 2\pi_u)$	7.34	6.50
$1^1\Sigma_u^-$ $(2\pi_g \rightarrow 2\pi_u)$	7.48	6.63
$1^3\Sigma_u^-$ $(2\pi_g \rightarrow 2\pi_u)$	7.50	6.65
$2^1\Sigma_u^+$ $(2\pi_g \rightarrow 2\pi_u)$	8.59 (7.32)[e]	7.81 (6.75)[e]

[a] Absolute energy is -74.10161 a.u.

[b] Absolute energy is -70.50335 a.u.

[c] J. Maya, J. Chem. Phys. 67, 4976 (1977).

[d] K. Wieland, Z. Phys. 76, 801 (1932); 77, 157 (1932).

[e] M. Wehrli, Helv. Phys. Acta 13, 153 (1940).

Tabular Data A-4.9. Hartree-Fock excitation energies (ΔE) and Mulliken populations for linear $HgCl_2$ [R(Hg-Cl) = 2.275Å]

State	ΔE(eV)	Mulliken populations	
		Hg	Cl
$1^1\Sigma_g^+$	0.0[a]	11.10	7.45
$1^3\Sigma_u^+$ $(2\sigma_u \rightarrow 4\sigma_g)$	5.26	11.74	7.13
$1^3\Pi_g^+$ $(2\pi_g \rightarrow 4\sigma_g)$	5.35	11.55	7.23
$1^1\Pi_g$ $(2\pi_g \rightarrow 4\sigma_g)$	5.72	11.52	7.24
$1^3\Pi_u$ $(1\pi_u \rightarrow 4\sigma_g)$	5.88	11.54	7.23
$1^1\Pi_u$ $(1\pi_u \rightarrow 4\sigma_g)$	6.22	11.50	7.25
$1^1\Sigma_u^+$ $(2\sigma_u \rightarrow 4\sigma_g)$	7.67	11.44	7.28

[a]Absolute energy is -74.07968 a.u.

Tabular Data A-4.10. Transition moments (M) and oscillator strengths (f) for the vertical dipole-allowed excitations in $HgCl_2$ and $HgBr_2$.

	λ(nm)	M(Debye)	f
A. $HgCl_2$			
$1^1\Sigma_g^+ \rightarrow 1^1\Pi_u$	227	1.08	0.0244
$1^1\Sigma_g^+ \rightarrow 1^1\Sigma_u^+$	185	3.18	0.258
$1^1\Sigma_g^+ \rightarrow 2^1\Sigma_u^+$	144	0.424	0.00586
B. $HgBr_2$			
$1^1\Sigma_g^+ \rightarrow 1^1\Pi_u$	263	1.15	0.0239
$1^1\Sigma_g^+ \rightarrow 1^1\Sigma_u^+$	208	3.20	0.232
$1^1\Sigma_g^+ \rightarrow 2^1\Sigma_u^+$	159	0.471	0.00656

ORBITAL DIAGRAMS FOR $HgCl_2$

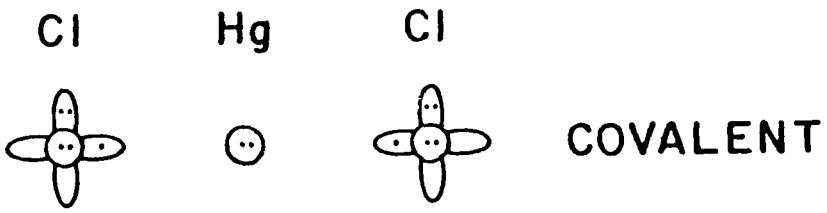

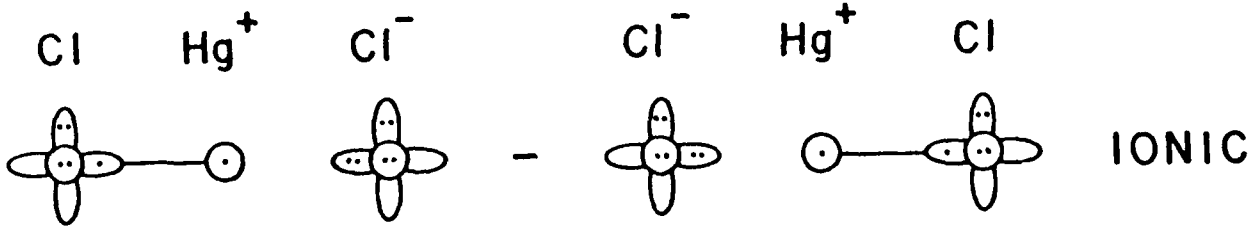

Graphical Data A-4.11. Valence bond orbital diagrams for the ground $1^1\Sigma_g^+$ state of $HgCl_2$.

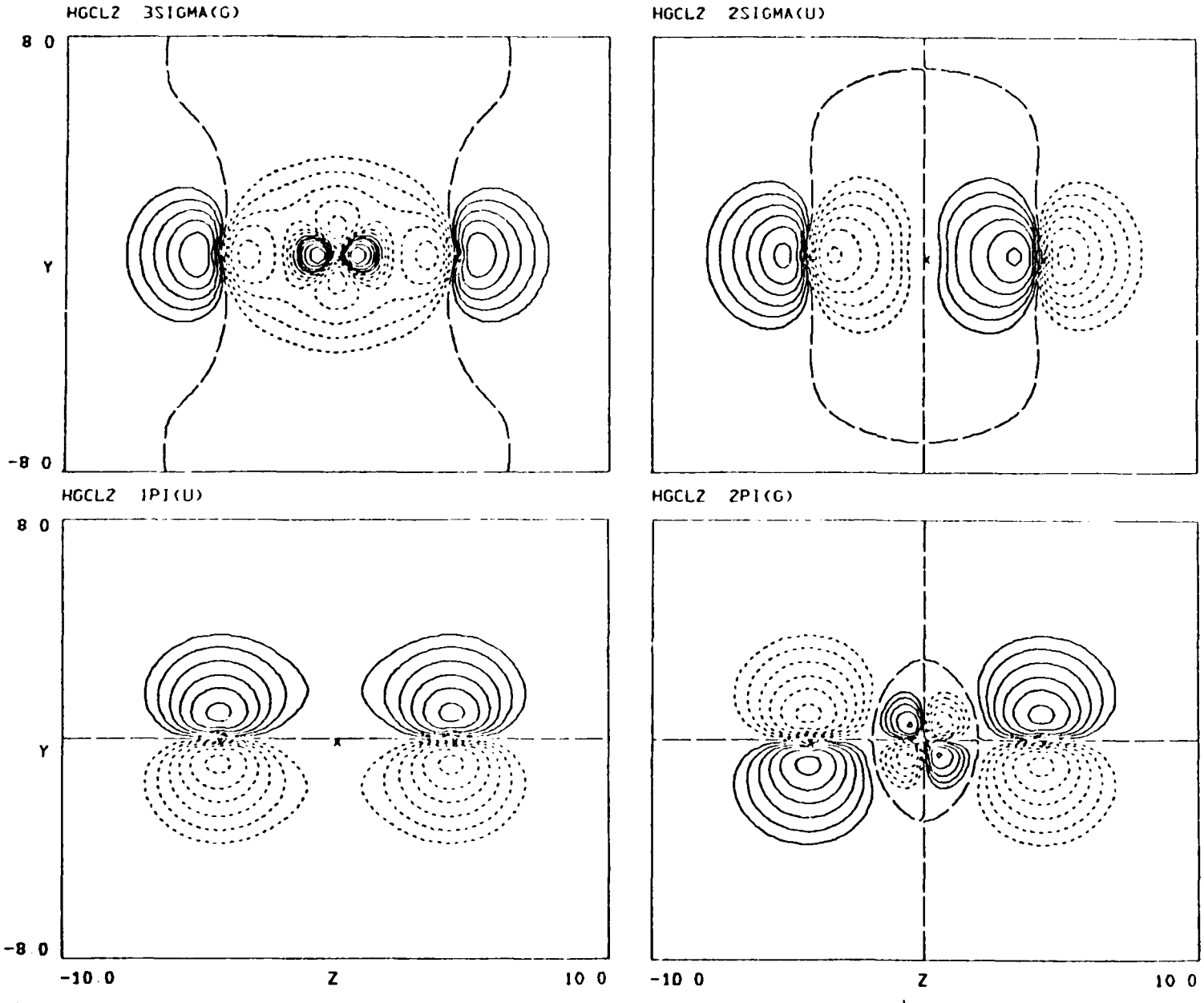

2641

Graphical Data A-4.12. Contour plots for the highest occupied orbitals of the $1^1\Sigma_g^+$ state of $HgCl_2$. Contours are spaced logarithmically starting at 0.02 and increasing by a factor of 1.58489 (= $10^{\cdot 2}$).

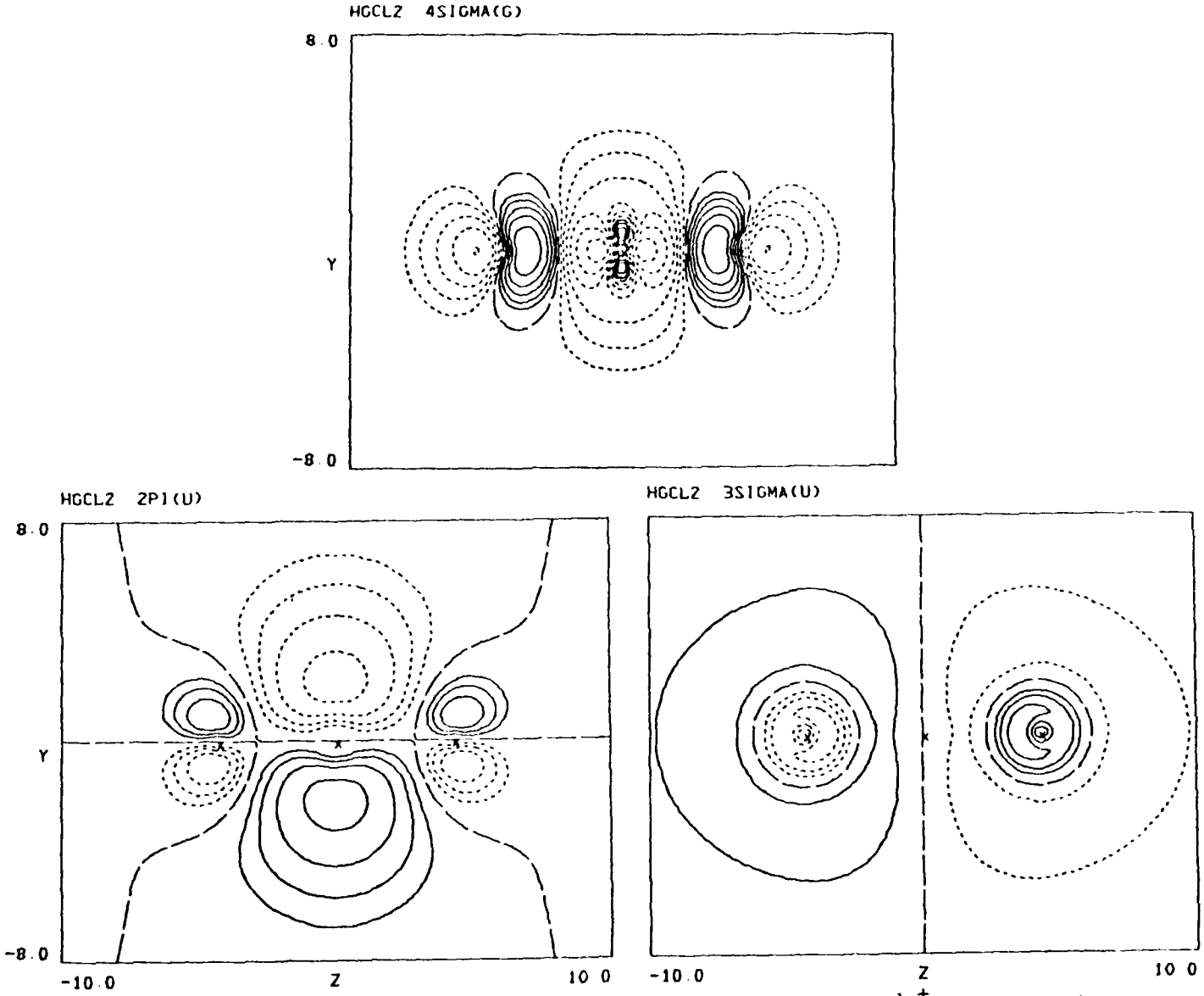

Graphical Data A-4.13. Contour plots for the lowest virtual orbitals of the $1^1\Sigma_g^+$ state of $HgCl_2$.

2642

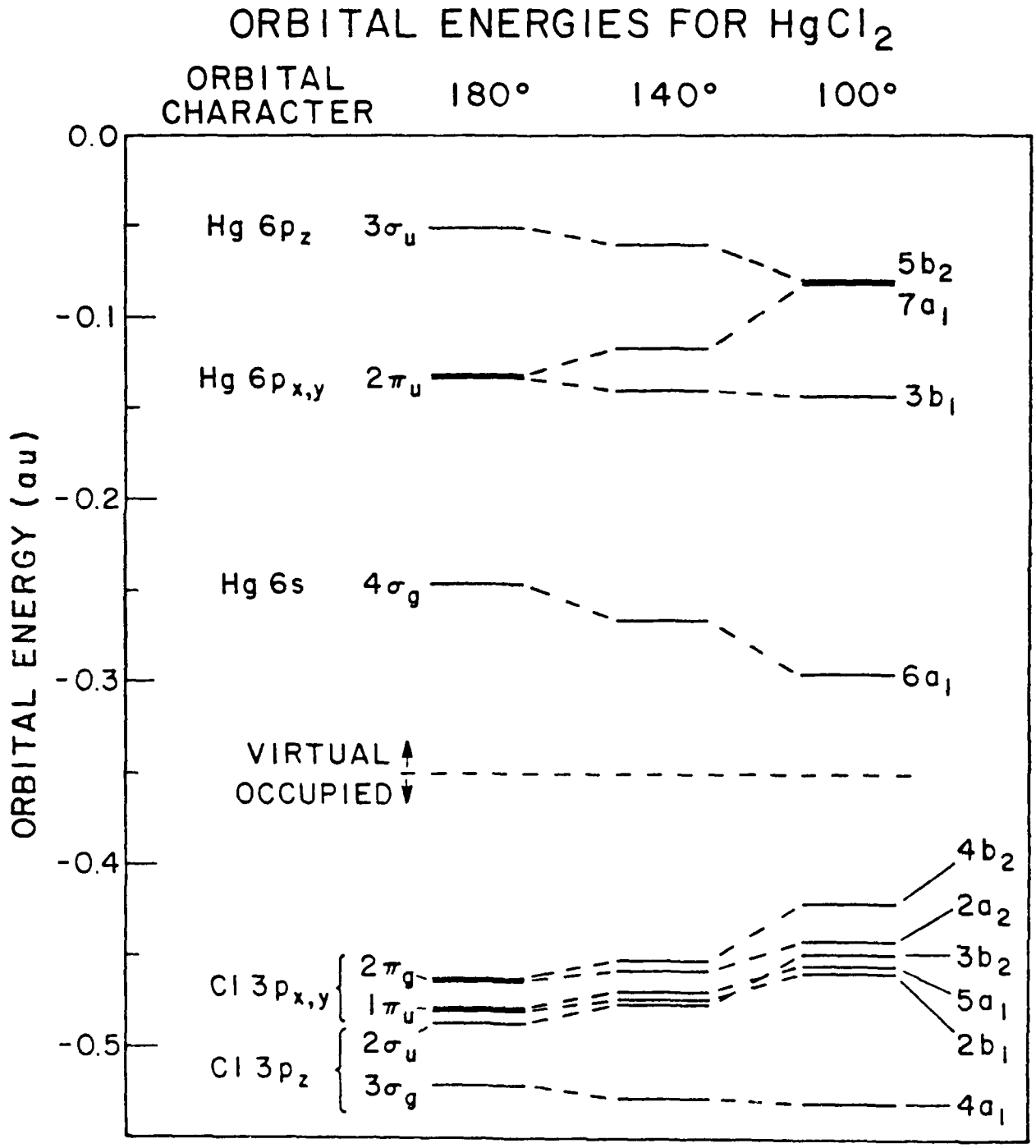

Graphical Data A-4.14. Orbital energy level diagram for $HgCl_2$ (R = 2.275Å) for a bending angle of 180°, 140° and 100°.[2]

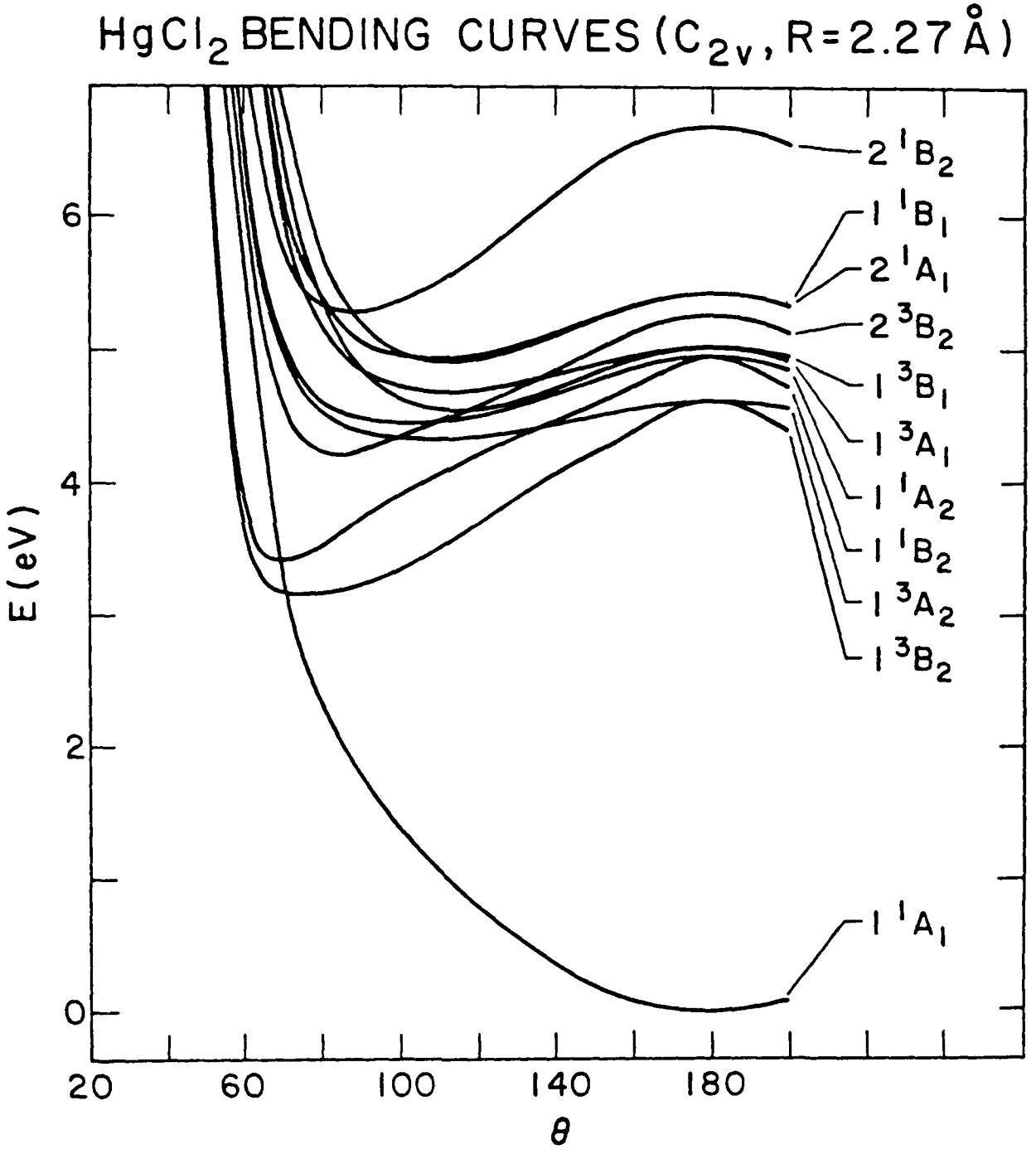

Graphical Data A-4.15. POL(1) CI potential curves for the states of $HgCl_2$ as a function of bending angle, θ.

CORRELATION DIAGRAM FOR $HgCl + Cl \rightarrow HgCl_2$

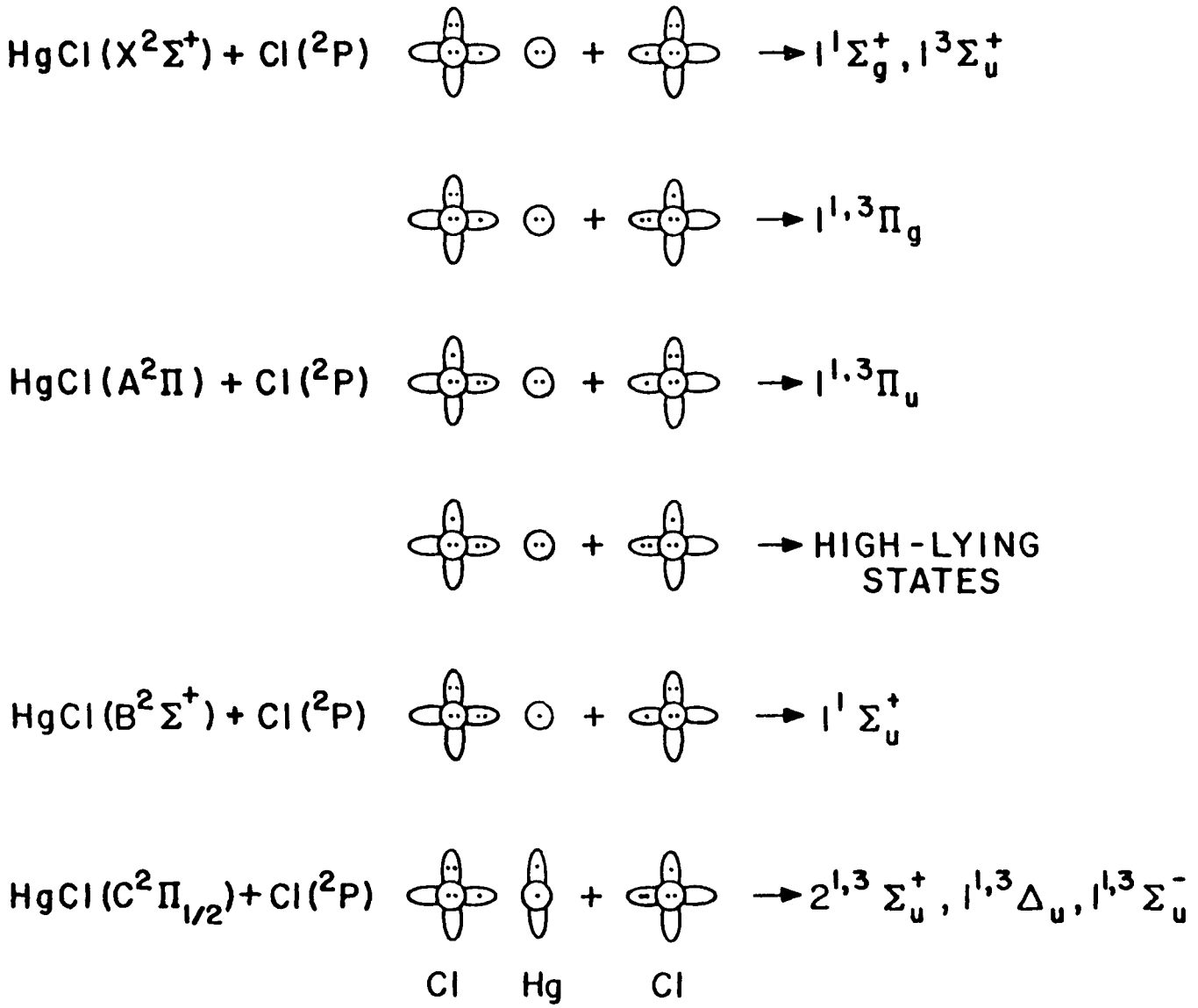

2645

Graphical Data A-4.16. Electronic state correlations diagrams for $HgCl + Cl \rightarrow HgCl_2$.

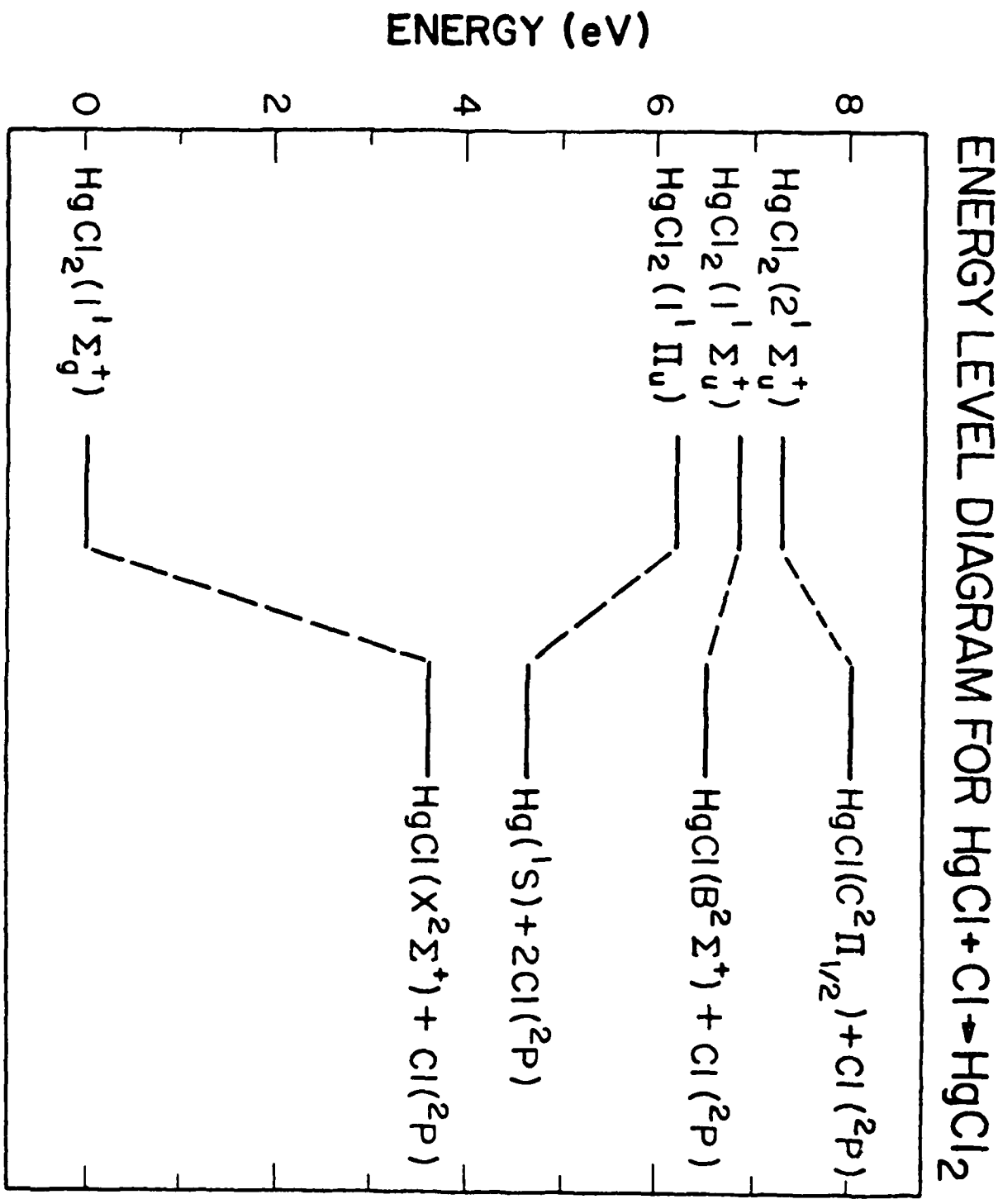

Graphical Data A-4.17. Experimental energy level diagram for key excited states of $HgCl_2$.

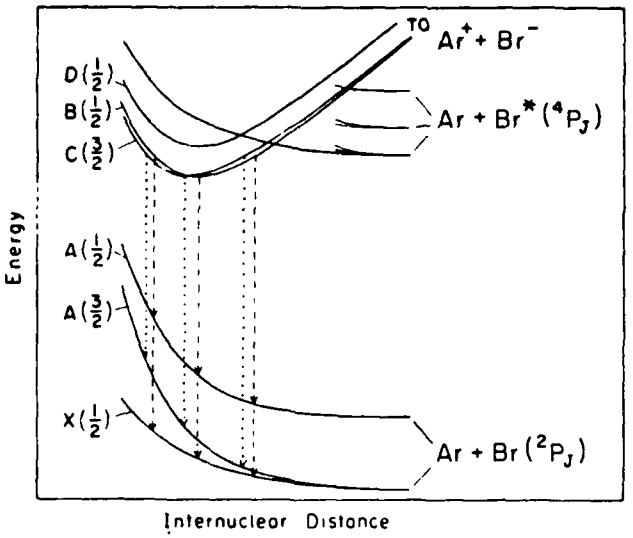

Graphical Data A-4.18. Schematic potential curves of ArBr, with the transitions observed in this study. See Fig. 5 for the ordering of the Br spin-orbit levels.

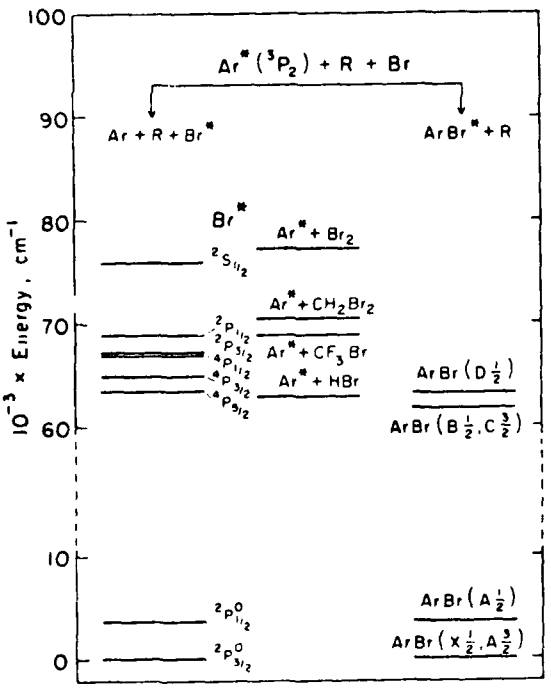

Graphical Data A-4.19. Energy level diagram, illustrating the electronic states of ArBr and Br accessible in the reactions studied.

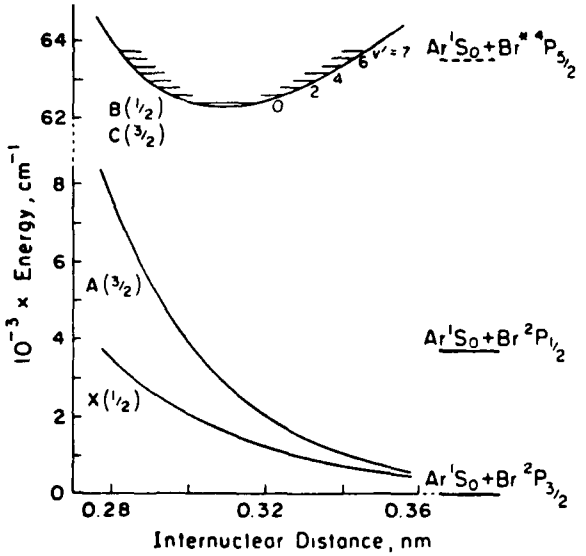

Graphical Data A-4.20. Representative set of ArBr potential curves giving good fits to the experimental ArBr($B-X$) and [$C-A(^3_2)$] continua. Potentials: V'_{B1}, $V''_{X1} = 7.197\times10^6 \exp[-r(\text{nm})/0.03673]$ cm^{-1}; $V''_{A1} = 1.6175\times10^8 \exp(-r/0.02798)$ cm^{-1}.

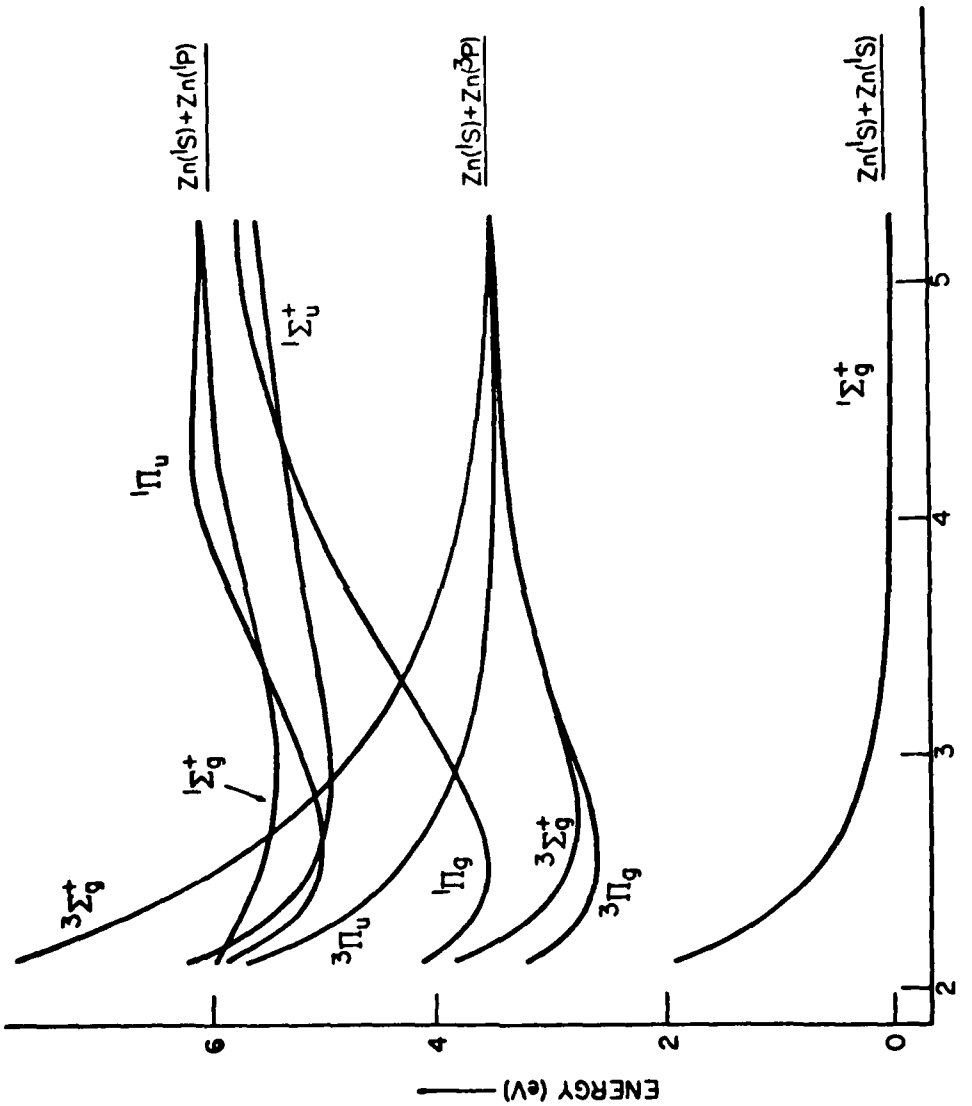

Graphical Data A-4.21. Theoretical potential energy curves for states of Zn_2 arising from $Zn(^1S, ^3P, \text{and } ^1P)$.

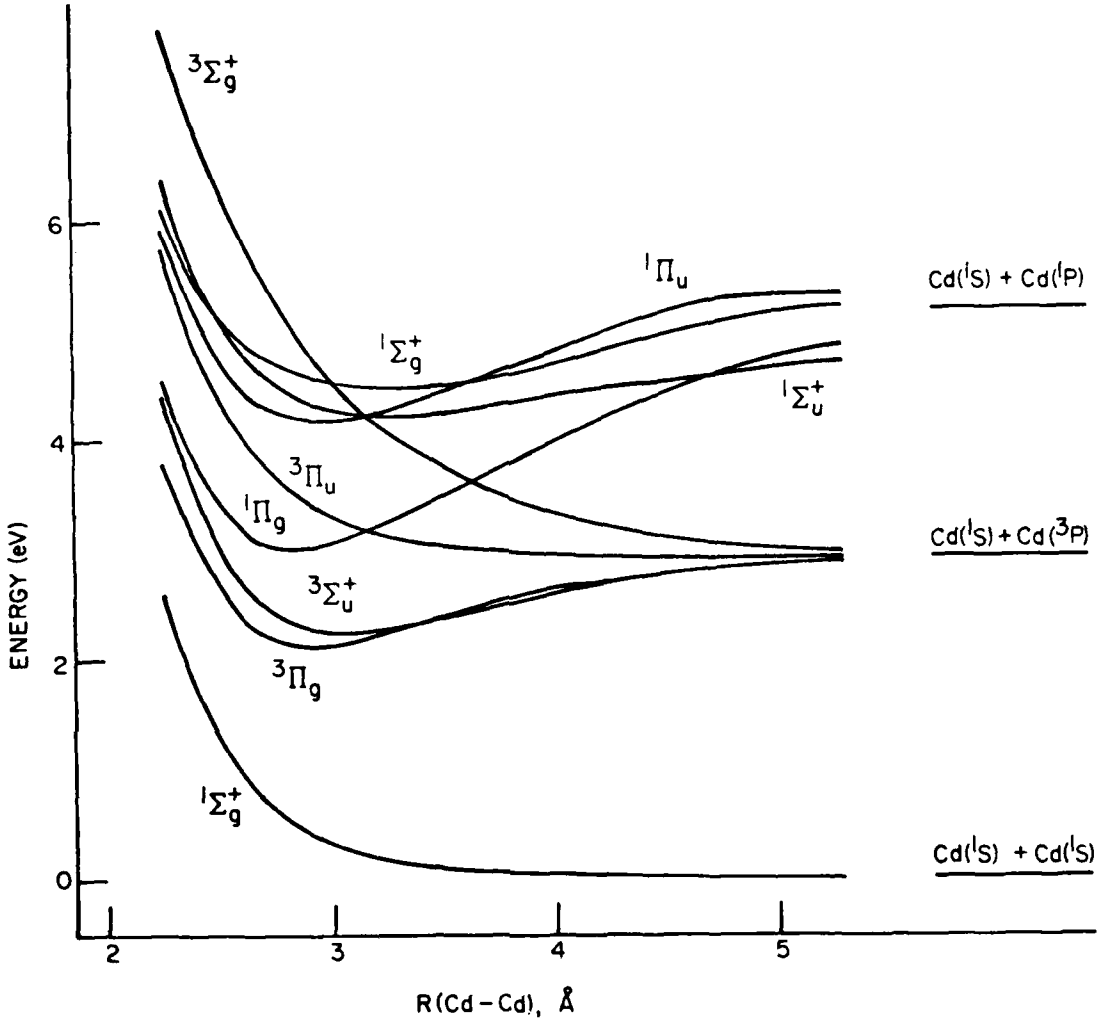

Graphical Data A-4.22. Theoretical potential energy curves for diatomic cadmium. All states of Cd_2 dissociating to Cd(^{1}S) + Cd(^{1}S, ^{3}P, ^{1}P) are included here.

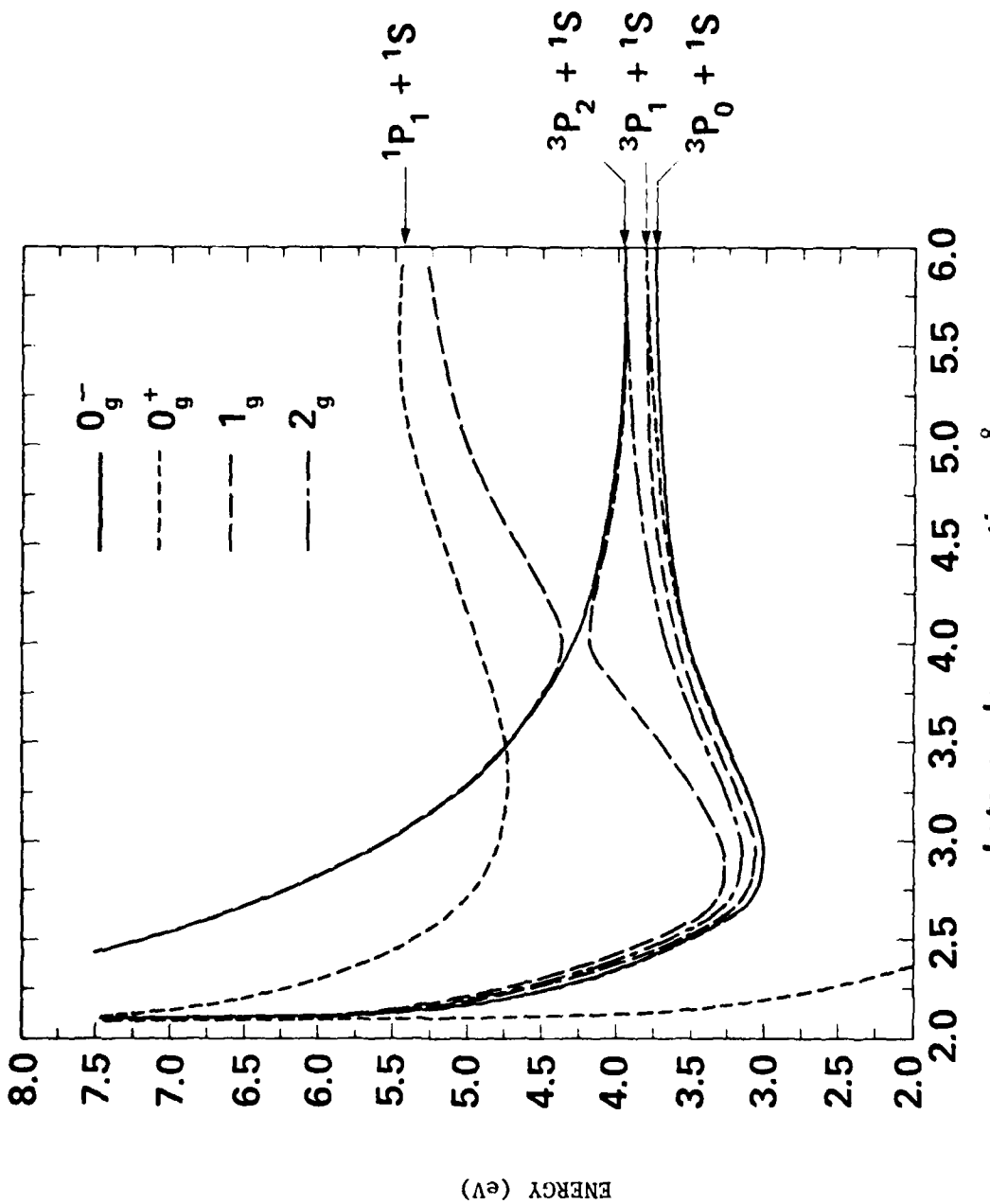

Graphical Data A-4.23. Gerade states of Cd_2 including spin-orbit coupling.

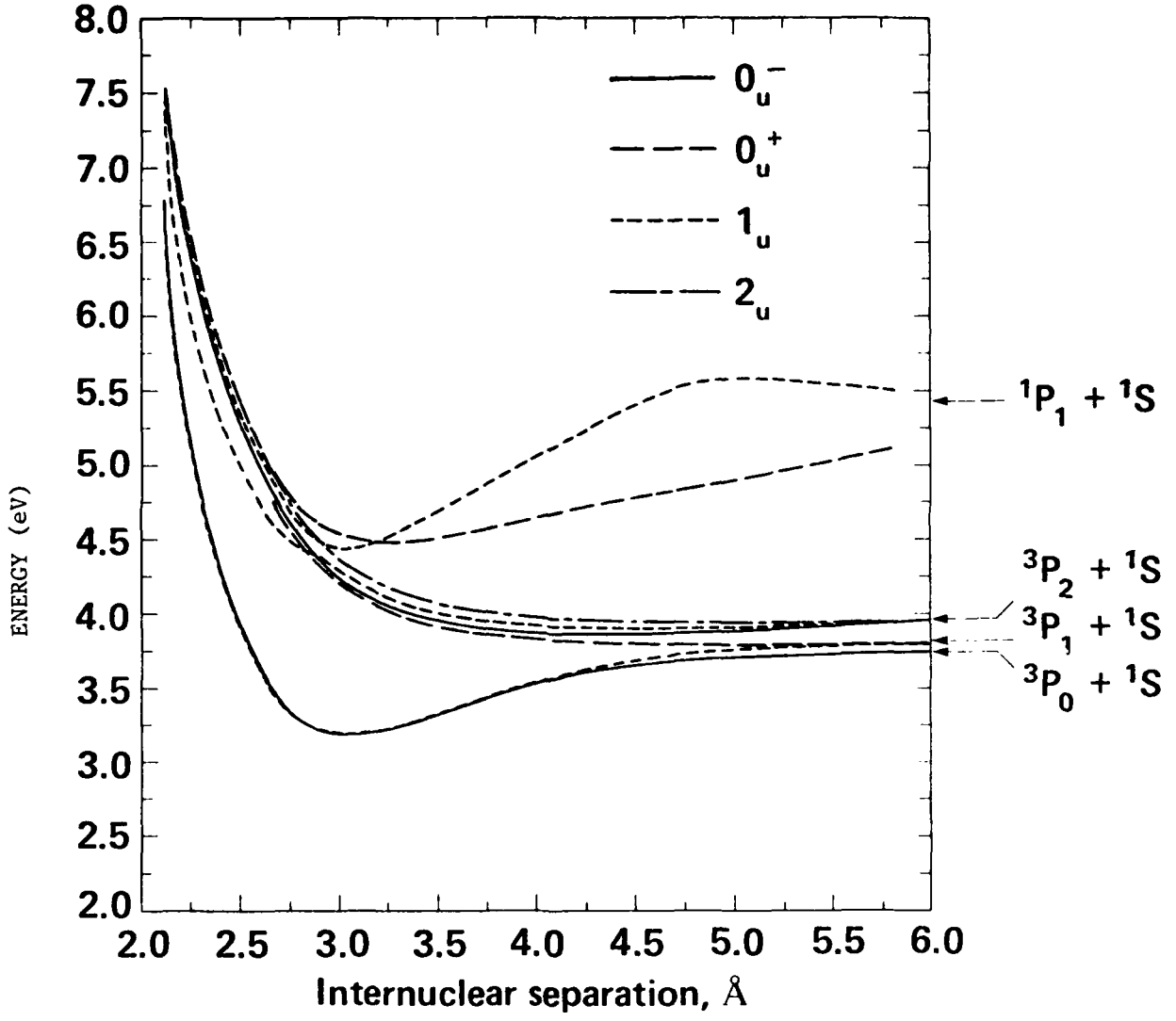

Graphical Data A-4.24. Ungerade states of Cd_2 including spin-orbit coupling.

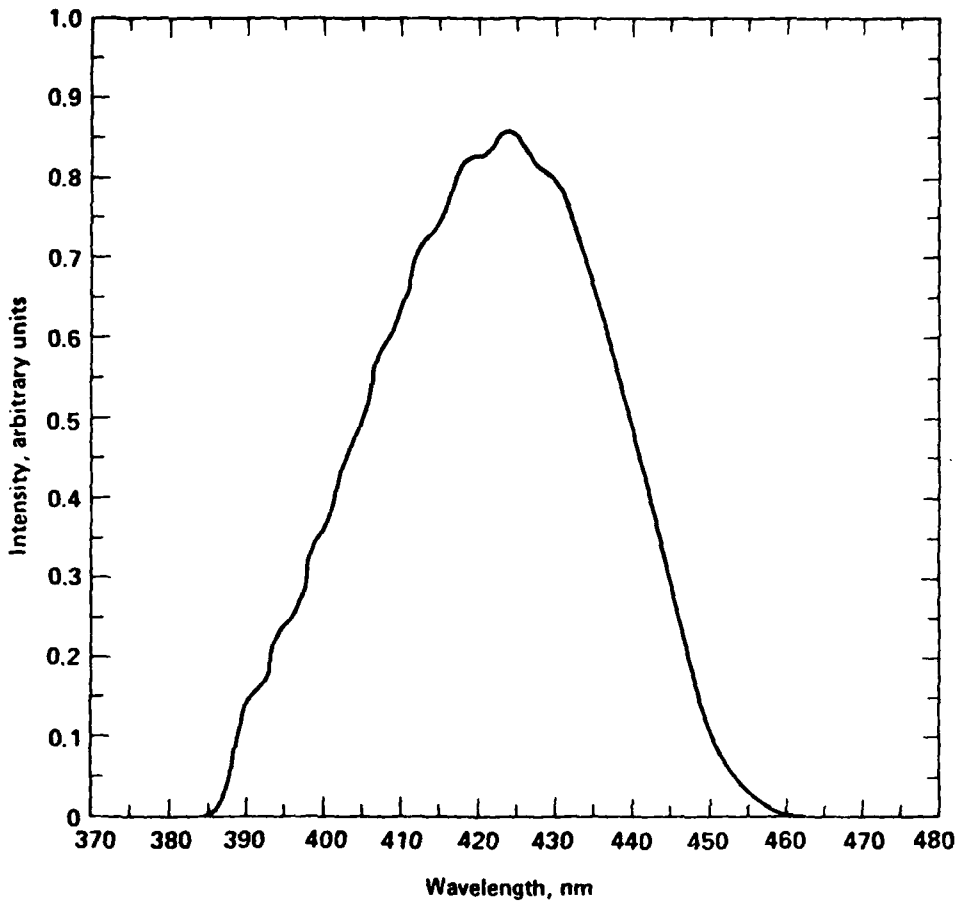

Graphical Data A-4.25. Computed Cd_2^* $1_u \rightarrow 0_g^+$ fluorescence band at 675°K, calibrated in relative units of quanta per unit wavelength per unit time.

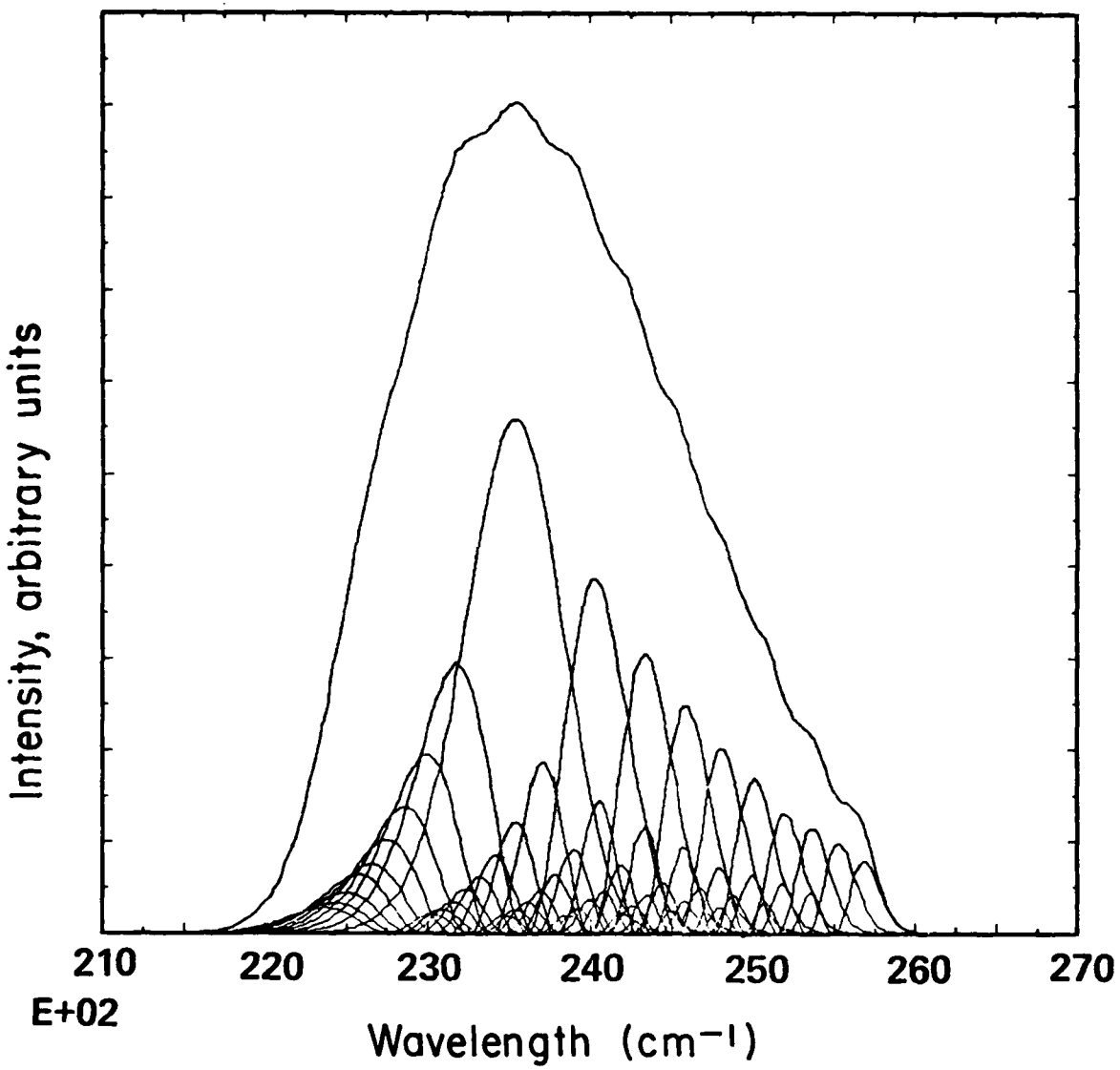

Graphical Data A-4.26. Contributions of individual vibrational level to the Cd_2^* fluorescence rate at 675°K, in relative units of quanta per unit frequency per unit time.

Tabular Data A-4.27. Comparison between theory and experiment for the lowest atomic energy levels (in cm^{-1}) of zinc and cadmium. Note that for the ^3P states the present nonrelativistic treatment does not distinguish fine structure components.

	Zinc		Cadmium	
Electronic State	Theory	Experiment	Theory	Experiment
$^1S_0$ ns^2		0		0
$^3P_0$ ns np		32,310		30,110
$^3P_1$	28,170	32,500	23,570	30,660
$^3P_2$		32,890		31,830
$^1P_1$ ns np	47,960	46,750	41,790	43,690

Tabular Data A-4.28. Predicted spectroscopic constants for the bound states of Zn_2 and Cd_2 dissociating to $^1S + {}^3P$ and to ^1S to ^1P separated atom limits. Excitation energies T_e are given relative to two ground state metal atoms.

	Electronic State	T_e (eV)	Adjusted T_e (eV)	r_e(Å)	D_e(eV)	ω_e(cm^{-1})
Zn_2	$2\,^1\Sigma_g^+$	5.41	5.26	2.96	0.55	108
	$^1\Pi_u$	5.01	4.86	2.62	0.95	175
	$^1\Sigma_u^+$	4.93	4.78	2.90	1.01	115
	$^1\Pi_g$	3.55	3.40	2.51	2.40	204
	$^3\Sigma_u^+$	2.75	3.31	2.73	0.74	154
	$^3\Pi_g$	2.57	3.13	2.57	0.92	175
Cd_2	$2\,^1\Sigma_g^+$	4.47	4.71	3.29	0.72	77
	$^1\Sigma_u^+$	4.22	4.46	3.24	0.96	78
	$^1\Pi_u$	4.17	4.40	2.95	1.02	119
	$^1\Pi_g$	3.01	3.25	2.84	2.17	137
	$^3\Sigma_u^+$	2.23	3.18	3.06	0.70	104
	$^3\Pi_g$	2.12	3.07	2.91	0.80	116

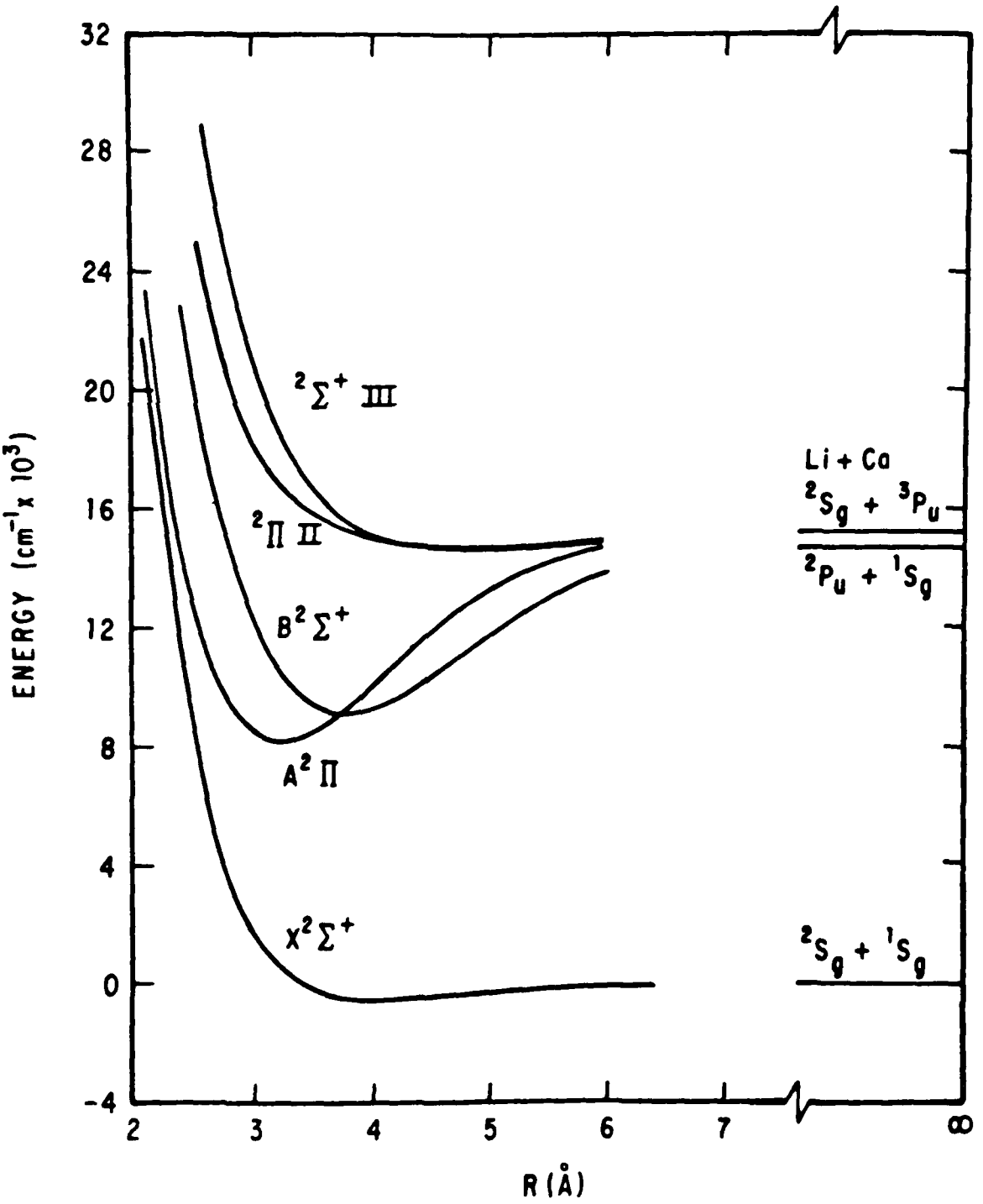

Graphical Data A-4.29. Potential Energy Curves for LiCa

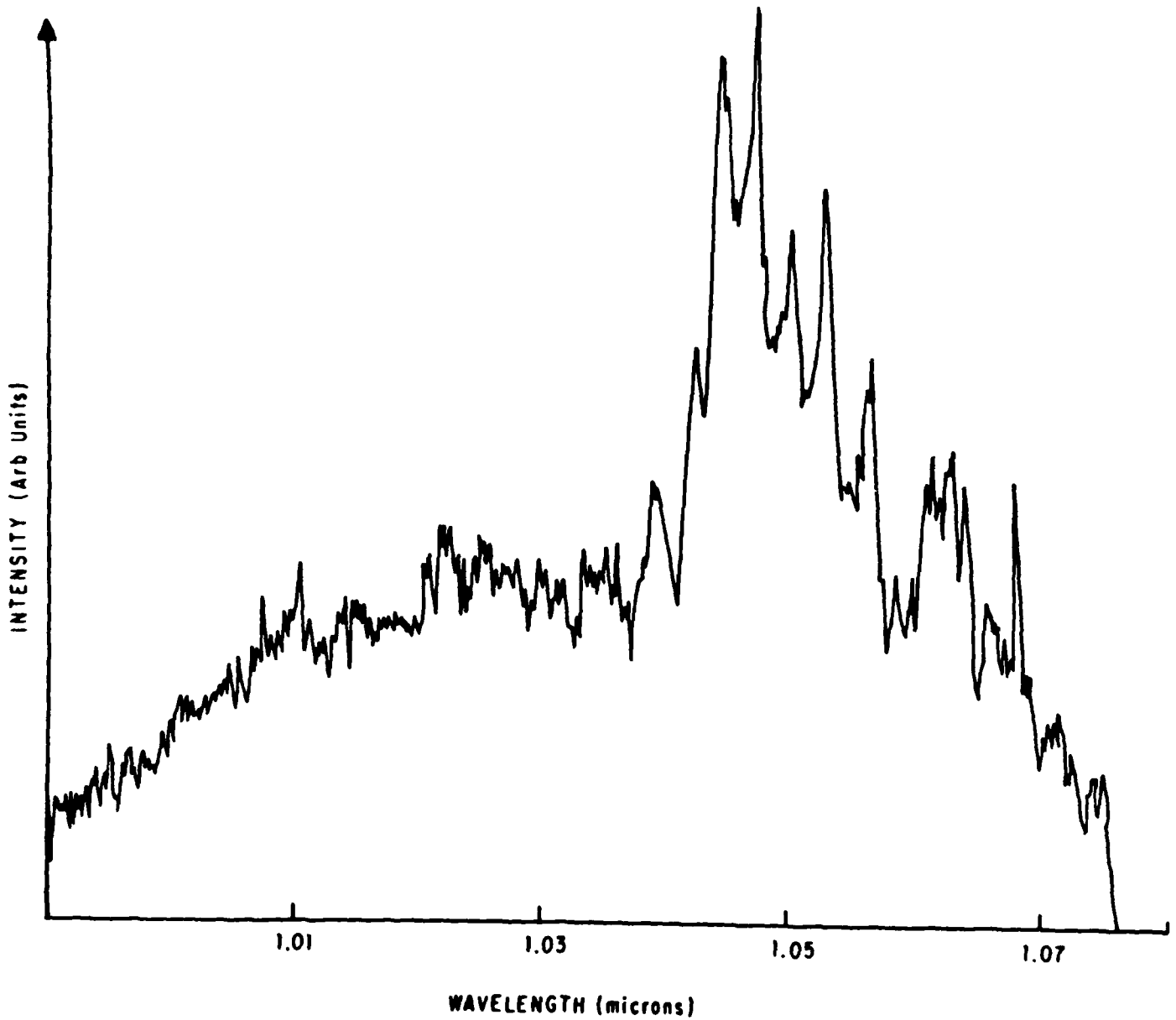

Graphical Data A-4.30. LiCa Emission Spectrum.

Tabular Data A-4.31. Calculated Spectroscopic Constants for LiCa

State	T_e(eV)	ω_e(cm^{-1})	$\omega_e\chi_e$(cm^{-1})	α_e(cm^{-1})	r_e(Å)	B_e(cm^{-1})	D_e(eV)	D_o(eV)
$B^2\Sigma^+$	1.17	197.44	0.96	.0009	.195	3.822	.765	.752
$A^2\Pi$	1.08	252.44	1.29	.0019	.274	3.226	.882	.866
$X^2\Sigma^+$	0.00	93.36	7.32	.0119	.189	3.883	.072	.067

Tabular Data A-4.32. Experimental vs. Calculated Spectra for LiCa

		Wavelength (microns)		Relative Intensity	
v'	v''	λ_{calc}	λ_{obs}	I_{calc}	I_{obs}
$B^2\Sigma^+ \rightarrow X^2\Sigma^+$					
0	0	1.0472	1.0470	1.0	1.0
0	1	1.0531	1.0527	.53	.6
0	2	1.0593	1.0587	.18	.1
0	3	1.0657	—	.03	—
1	0	1.0263	—	.12	—
1	1	1.0320	—	.07	—
1	2	1.0379	1.0380	.34	.4
1	3	1.0441	1.0441	.44	.5
$A^2\Pi \rightarrow X^2\Sigma^+$					
3	0	1.0501	1.0499	.24	.3
3	1	1.0569	1.0563	.28	.4
3	2	1.0625	1.0627	.24	.25
3	3	1.0679	1.0676	.18	.15

A-5. ELECTRONIC STRUCTURE AND SPECTRA FOR Li_2 and Na_2. Van der WAALS COEFFICIENTS FOR NEUTRAL (H, He, Ne, Ar, Kr, Xe, Li, Na, K, Rb - NEUTRAL INTERACTIONS.

CONTENTS

		Page
A-5.1.	Low-lying states of Li_2	2661
A-5.2.	Potential energy curves for the X $^1\Sigma^+_g$ state of Li_2	2662
A-5.3.	Spectroscopic constants for the X $^1\Sigma^+_g$ state of Li_2	2662
A-5.4.	Potential energy curves for the A $^1\Sigma^+_u$ state of Li_2	2663
A-5.5.	Spectroscopic constants for the A $^1\Sigma^+_u$ state of Li_2	2663
A-5.6.	Binding energy curves of Na_2	2664
A-5.7.	Potential curve constants for low-lying electronic states of Na_2	2665
A-5.8.	Li_2 and Na_2 transition operators	2666
A-5.9.	Emission rate per cm^{-1} transition energy interval and gain cross sections (σ_e) for the $1\ ^3\Sigma^+_g \rightarrow 1\ ^3\Sigma^+_u$ emission in Li_2	2667
A-5.10.	Emission rate per cm^{-1} transition energy interval and gain cross sections (σ_e) for the $1\ ^3\Sigma^+_g \rightarrow 1\ ^3\Sigma^+_u$ emission in Na_2	2667
A-5.11.	$Li_2\ ^3\Sigma^+_g$ emission coefficients	2668
A-5.12.	$Na_2\ ^3\Sigma^+_g$ emission coefficients	2668
A-5.13.	Van der Waals formulae using Tabular Data A-5.14 and A-5.15.	2669
A-5.14.	Van der Waals coefficients for dipole-dipole, dipole-quadrupole, and quadrupole-dipole interactions for various neutral-neutral systems	2670
A-5.15.	Van der Waals coefficients for the dipole-octupole, quadrupole-quadrupole, and octupole-dipole interactions for various neutral-neutral systems	2671

A-5 References

1. D. D. Konowalow and P. S. Julienne, "Li_2 and Na_2 $^3\Sigma_g - {}^3\Sigma_u^+$ Excimer Emission", J. Chem. Phys. 72, 5815 (1980). (A-5.1 - A-5.14).

2. D. D. Konowalow and M. L. Olson, "The Electronic Structure and Spectra of the $X\ ^1\Sigma_g^+$ and $A\ ^1\Sigma_u^+$ States of Li_2", J. Chem. Phys. 71, 450 (1979). (A-5.2 - A-5.5).

3. D. D. Konowalow, M. E. Rosenkrantz and M. L. Olson, "The Molecular Electronic Structure and Spectra of the Lowest $^1\Sigma_g^+$, $^3\Sigma_u^+$, $^1\Sigma_u^+$, $^3\Sigma_g^+$, $^1\Pi_u$, $^1\Pi_g$, and $^3\Pi_g$ States of Na_2", J. Chem. Phys. 72, 2612 (1980). (A-5.6 - A-5.7).

4. M. D. Peña, C. Pando and J. A. R. Renuncio, "Combination Rules for Two Body van der Waals Coefficients", J. Chem. Phys. 72, 5269 (1980). (A-5.13 - A-5.15).

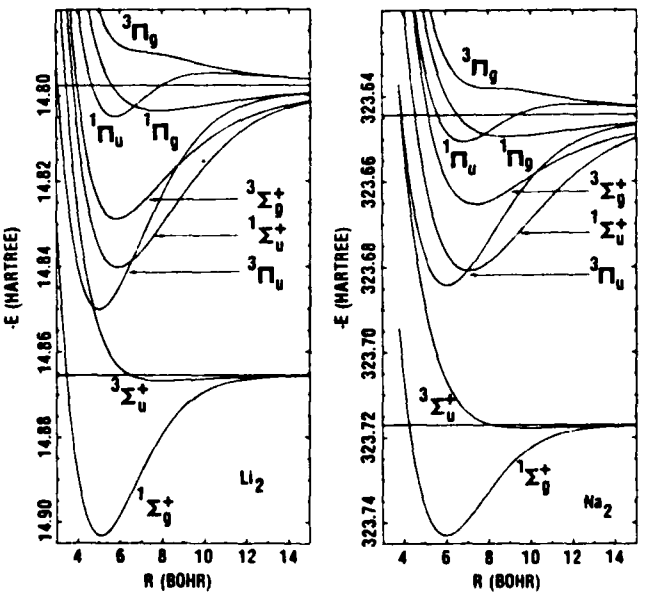

Graphical Data A-5.1. Low-lying states of Li_2 which correspond to the $Li(^2S) + Li(^2S)$ and the $Li(^2S) + Li(^2P)$ asymptotes, and the corresponding states for Na_2. The $2\ ^3\Sigma_u^+$ state for each molecule is not shown. However, it is entirely repulsive and lies just above the $^3\Pi_g$ state.

Tabular Data A-5.2. Comparison of potential energy curves for the $X\,^1\Sigma_g^+$ state of Li_2 obtained from 10-configuration (OVC), two-configuration (BC), and one-configuration (HF) wave functions calculated with the *LC* basis set.[a]

R (bohr)	OVC	BC	HF
2.75	14.803585	14.768744	
3.00	14.829040	14.795172	14.786389
3.50	14.866614	14.835145	
4.00	14.888896	14.860103	14.852994
4.50	14.899780	14.873785	
5.00	14.903191	14.880020	14.871323
5.50	14.902088	14.881733	
6.00	14.898482	14.880910	14.868625
6.50	14.893695	14.878843	
7.00	14.888593	14.876343	14.858576
7.50	14.883728	14.873890	
8.00	14.879429	14.871739	14.846781
8.50	14.875855	14.869987	
9.00	14.873026	14.868637	14.835425
9.50	14.870890	14.867640	
10.00	14.869320	14.866928	14.825286
11.00	14.867401	14.866095	
12.00	14.866454	14.865719	14.809174
15.00	14.865634	14.865467	14.793491[b]
17.00	14.865528	14.865453	14.787012[b]
20.00	14.865478	14.865451	
24.00	14.865460	14.865451	
30.00	14.865453	14.865451	
∞	14.865451	14.865451	

[a]The tabulated values are the *negative* of the total energy in Hartree atomic units. Thus the energy for the OVC function is $-14.803585\ e^2/a_0$ at $R = 2.75\ a_0$.

[b]Calculated with the *L*6 basis set.

Tabular Data A-5.3. Constants describing the $X\,^1\Sigma_g^+$ state of Li_2.

R_e (Å)	D_e (cm^{-1})	ω_e (cm^{-1})	$\omega_e x_e$ (cm^{-1})
2.692	8297	347.1	3.6
2.69	8173	348.5	3.7
2.93	3559	264.3	4.9
2.78	1410	...	...
2.69	7985	...	...
2.70	8000	...	...
...	8450	351.2	2.61
2.673	8640	351.4	2.58
2.673	8541	351.4	2.58
2.673	8600 ± 150	351.4	2.58
...	8385	...	...
2.692	8450 ± 100	...	...

Tabular Data A-5.4. Comparison of potential energy curves for the $A\,^1\Sigma_u^+$ state of Li_2 obtained from five-configuration (OVC), two-configuration (BC), and one configuration (HF) wavefunctions calculated with the *LC* basis set.[a]

R (bohr)	OVC	BC	HF[b]
3.0		14.718149	14.715962
3.5	14.777866	14.768501	14.766149
4.0	14.808064	14.800253	14.797400
4.5	14.825722	14.818776	14.815368
5.0	14.835118	14.828700	14.824702
5.5	14.839270	14.833218	14.828353[c]
6.0	14.840141	14.834385	14.828980
6.5	14.838986	14.833507	14.827303
7.0	14.836612	14.831418	14.824398
7.5	14.833544		14.820826
8.0	14.830134	14.825598	14.816927
8.5	14.826615	14.822499	14.812890
9.0	14.823148	14.819429	14.808820
9.5	14.819863	14.816579	14.804778
10.0	14.816769	14.813992	14.800803
11.0	14.811520	14.809635	14.793169
12.0	14.807556	14.806426	14.786079
15.0	14.801699	14.801534	14.768749
17.0	14.800247	14.800200	14.760392
20.0	14.799243	14.799234	14.751672
24.0	14.798623	14.798621	14.744889
30.0	14.798215	14.798215	14.739492
∞	14.797794	14.797794	

[a]The tabulated values are the *negative* of the total energy in Hartree atomic units. Thus the energy for the OVC function is $-14.777866\ e^2/a_0$ at $R = 3.5\ a_0$.
[b]Calculated with the *L*6 basis set.
[c]This entry corresponds to $R = 5.45$ bohr, not $R = 5.5$ bohr.

Tabular Data A-5.5. Constants describing the $A\,^1\Sigma_u^+$ state of Li_2.

R_e (Å)	D_e (cm^{-1})	ω_e (cm^{-1})	$\omega_e x_e$ (cm^{-1})	
3.13	9299	254	1.7	Our *L*
3.15	9030	246	1.7	Our *L*
3.15	7666	249	2.0	Our *L*
3.08	6879	278	2.8	Our *L*
3.17	7259	255	•••	Pseud
3.02	6104	•••	•••	Calcu
•••	9000	231.5	1.5	Spectr
3.1	9469	255.5	1.6	Absor
3.108	8940	255.4	1.6	Absor Hes
•••	9400 ± 100	•••	•••	*E* sca

Tabular Data A-5.6. Binding energy curves of Na_2.

R (bohr)	$X\,^1\Sigma_g^+$ (XC)[b]	$x\,^3\Sigma_u^+$ $(R4)$[b]	$A\,^1\Sigma_u^+$ $(A4)$[c]	$b\,^3\Sigma_g^+$ $(H4)$[c]	$a\,^3\Pi_u$ $(U3)$[d]	$c\,^3\Pi_g$ $(T3)$[d]	$B\,^1\Pi_u$ $(B3)$[d]	$C\,^1\Pi_g$ $(S3)$[d]
3.8	0.0224100	0.0783293	0.0401706	···	0.0072987	0.0871323	0.0623604	0.0741635
4.0	0.0114145	0.0663480	0.0271564	0.0524699	−0.0032727	···	0.0499107	0.0619211
4.25	0.0004872	0.0539591	0.0135610	0.0373469	−0.0136951	0.0601793	0.0370353	0.0492223
4.5	−0.0079819	0.0437298	0.0023028	0.0246926	−0.0217599	0.0487826	0.0265106	0.0387084
4.75	−0.0144335	0.0352223	−0.0070001	0.0141697	−0.0279448	0.0393364	0.0179421	0.0299463
5.0	−0.0191835	0.0281544	−0.0146076	0.0055356	−0.0325664	0.0315971	0.0110747	0.0226750
5.5	−0.0246140	0.0175203	−0.0255618	−0.0069751	−0.0380776	0.0202861	0.0015394	0.0118087
6.0	−0.0260840	0.0104490	−0.0320663	−0.0145698	−0.0398612	0.0132849	−0.0036661	0.0047240
6.5	−0.0250240	0.0058723	−0.0353761	−0.0187284	−0.0391389	···	−0.0059074	0.0002948
7.0	−0.0225012	0.0029853	−0.0364600	−0.0205817	−0.0368023	0.0072459	−0.0062284	−0.0023576
7.5	−0.0192699	0.0012173	−0.0360270	−0.0209326	−0.0335107	0.0063997	−0.0054135	−0.0038642
8.0	−0.0158636	0.0001758	−0.0345818	−0.0203351	−0.0297304	0.0061666	−0.0040323	−0.0046438
8.5	−0.0126218	−0.0004044	−0.0324850	−0.0191703	−0.0258028	0.0061176	−0.0024960	−0.0049754
9.0	−0.0097541	−0.0006857	−0.0299892	−0.0176825	−0.0219548	0.0060011	0.0010319	−0.0050241
10.0	−0.0054302	−0.0008176	−0.0244925	−0.0144403	−0.0151681	0.0053168	0.0010863	−0.0047213
11.0	−0.0028344	−0.0006963	−0.0190797	−0.0114105	−0.0100529	0.0043927	0.0020914	−0.0041652
12.0	−0.0014496	−0.0005268	−0.0143060	−0.0089138	−0.0066293	0.0035381	0.0023590	−0.0035586
13.0	−0.0007634	−0.0003767	−0.0104512	−0.0069805	−0.0044989	0.0028472	0.0022575	−0.0029807
15.0	−0.0002288	−0.0001799	−0.0055549	−0.0044197	−0.0023883	0.0019075	0.0017638	−0.0020492

[a]Energy in hartrees relative to the asymptotic ($R \to \infty$) energy.
[b]At $R \to \infty$ $E = -323.7169551$ hartree.
[c]At $R \to \infty$ $E = -323.6444029$ hartree.
[d]At $R = \infty$ $E = -323.6444061$ hartree.

Tabular Data A-5.7. Potential curve constants for low-lying electronic states of Na_2.

State	Source[a]	D_e (cm^{-1})	R_e (Å)
$X\,^1\Sigma_g^+$	*N9XC*, 12 config.	5725	3.174
	$B\,^1\Pi_u$–$X\,^1\Sigma_g^+$ spect.	5988 ± 20[b]	3.079
	MCSCF, SHBW	5901	(3.17)[c]
	Valence elect. model	6372	2.95
	Pseudopotential, BJN	5700	3.04
$x\,^3\Sigma_u^+$	*N9R4*, 4 config.	180.2	5.206
	Valence elect. model	85	5.8
	Pseudopotential, BJN	± 44	5.3
$a\,^3\Pi_u$	*N9U3*, 3 config.	8755	3.21
	Valence elect. model	9680	2.77
	Pseudopotential, BJN	9360	3.09
$b\,^3\Sigma_g^+$	*N9H4*, 4 config.	4599	3.91
	Valence elect. model	6210	3.42
$A\,^1\Sigma_u^+$	*N9A4*, 4 config.	8006	3.746
	Spectroscopic[12–15]	7653, 8275	3.638
	MCSCF, SHBW[7]	8930	(3.78)[c]
	Valence elect. model	8066	3.49
	Pseudopotential, BJN	7600	3.60
$B\,^1\Pi_u$		Attractive well	
	N9B3, 3 config.	1380	3.63
	$B\,^1\Pi_u$–$X\,^1\Sigma_g^+$ spect.	2642	3.413
	MCSCF, SHBW[7]	Unbound	(4.0)[c]
	Valence elect. model	4033	3.44
	Pseudopotential, BJN	1940	3.34
$B\,^1\Pi_u$		Long-range hump[d]	
	N9B3, 3 config.	520	6.45 ± 0.10
	$B\,^1\Pi_u$–$X\,^1\Sigma_g^+$ spect.	474	> 5.73
	$B\,^1\Pi_u$–$X\,^1\Sigma_g^+$ spect. A	554 ± 120	?
	MCSCF, SHBW[7]	?	(5.4)[c]
$C\,^1\Pi_g$	*N9S3*, 3 config.	1104	4.69
	Valence elect. model	1450	4.54

[a]The first entry for each state corresponds to our MCSCF wave function described in part in Table II.

[b]Obtained from an extrapolation from $v'' = 45$ which lies at 5428 cm^{-1}.

[c]Values estimated based on SHBW data

[d]The energy listed under the D_e column is the hump height, the value listed in the R_e column is the position of the hump.

Valence Elec. Model: A. C. Roach, J. Mol. Spectrosc. 42, 27 (1972).

Pseudopotential, BJN: J. N. Bardsley, B. R. Junker and D. W. Norcross, Chem. Phys. Letts. 37, 502 (1976).

B $^1\Pi_u$ - X $^1\Sigma_g^+$ spect: P. Kusch and M. M. Hessel, J. Chem. Phys. 68, 2591 (1978).

MCSCF, SHBW: W. J. Stevens, M. M.Hessel, P. J. Bertoncini and A. C. Wahl, J. Chem. Phys. 66, 1477 (1977).

B $^1\Pi_u$ - X $^1\Sigma_g^+$ spect. A: W. Demtröder and M. Stock, J. Mol. Spectrosc. 55, 476 (1975).

Tabular Data A-5.8. Li_2 and Na_2 transition operators.[a]

	$^3\Sigma_g^+ - ^3\Sigma_u^+$		$^3\Sigma_g^+ - ^3\Pi_u$	
R	Li_2	Na_2	Li_2	Na_2
3	3.223		0.593	
4	3.815		1.067	0.857
4.5				0.983
5	4.122	4.163	1.141	1.065
5.5		4.274		1.100
6	4.205	4.345	1.032	1.086
6.5		4.380		1.035
7	4.149	4.385	0.843	0.975
7.5		4.362		0.894
8	4.012	4.327	0.635	0.808
8.5		4.275		0.715
9	3.863	4.224	0.444	0.621
10	3.734		0.303	0.430
11	3.638	4.001	0.199	0.284
12		3.919	0.110	0.174
13		3.857		0.112
15		3.789	0.0573	0.053
17			0.0258	
18		3.735		
20	3.403		0.0137	
21		3.713		
24	3.387		0.0073	
30	3.377		0.0056	

[a]In atomic units, $ea_0 = 1$ electron-bohr.

The transition operator is

$$\mu_o = \sum_k e_k z_k$$

for parallel transitions and

$$\mu_{\pm 1} = \sum_k e_k \frac{\pm x_k - i y_k}{\sqrt{2}}$$

for perpendicular transitions.

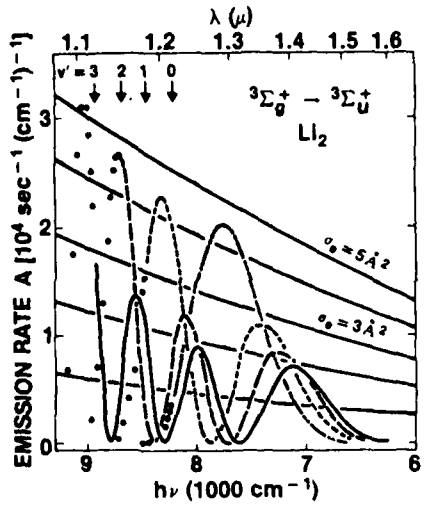

Graphical Data A-5.9. Emission rate per cm^{-1} transition energy interval and gain cross sections (σ_e) for the $1\,^3\Sigma_g^+ - 1\,^3\Sigma_u^+$ emission in Li_2. The arrows show the threshold between bound–free and bound–bound emission for each v.

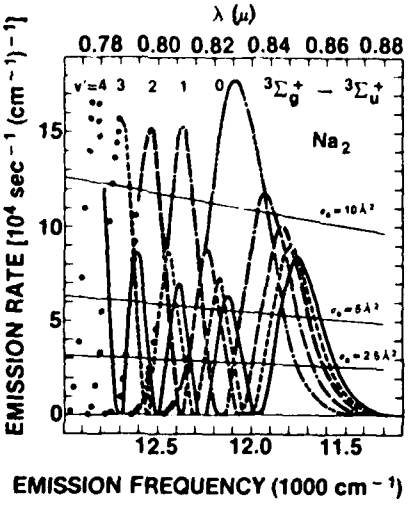

Graphical Data A-5.10. Emission rate per cm^{-1} transition energy interval and gain cross sections (σ_e) for the $1\,^3\Sigma_g^+ - 1\,^3\Sigma_u^+$ emission in Na_2.

Tabular Data A-5.11. Li_2 $^3\Sigma_g^+$ emission coefficients.[a]

	$^3\Sigma_g^+-{}^3\Sigma_u^+$				Lifetime
v'	Bound–free	Bound–bound	$^3\Sigma_g^+-{}^3\Pi_u$	Total	(ns)
0	1.56	0.04	0.023	1.62	61.9
1	1.49	0.18	0.024	1.70	58.8
2	1.33	0.43	0.025	1.79	55.8
3	1.21	0.64	0.026	1.88	53.3
4	1.26	0.68	0.027	1.97	50.8
5	1.38	0.65	0.027	2.06	48.5
6	1.44	0.68	0.028	2.15	46.4
7	1.43	0.79	0.028	2.25	44.4
8	1.47	0.85	0.029	2.34	42.7
9	1.58	0.82	0.029	2.43	41.1
10	1.68	0.82	0.029	2.53	39.5

[a]In units of 10^{7} s^{-1}.

Tabular Data A-5.12. Na_2 $^3\Sigma_g^+$ emission coefficients.[a]

	$^3\Sigma_g^+-{}^3\Sigma_u^+$				Lifetime
v'	Bound–free	Bound–bound	$^3\Sigma_g^+-{}^3\Pi_u$	Total	(ns)
0	6.74	0.02	0.009	6.77	14.8
1	6.63	0.14	0.009	6.78	14.7
2	6.29	0.48	0.010	6.78	14.7
3	5.80	1.01	0.010	6.83	14.6
4	5.40	1.52	0.010	6.92	14.4
5	5.28	1.74	0.011	7.02	14.2
6	5.42	1.68	0.010	7.11	14.1
7	5.57	1.59	0.010	7.17	13.9
8	5.53	1.67	0.009	7.20	13.9
9	5.38	1.84	0.009	7.23	13.8
10	5.40	1.92	0.009	7.33	13.6

[a]In 10^{7} s^{-1}.

Formulae A-5.13. Van der Waals formulae using Tabular Data A-5.14 and A-5.15.

The long range dispersion energy between two spherically symmetric atoms A and B at separation r is (Refs. a, b, c below).

$$u_{AB}(r) = - \sum_{\ell_1=1}^{\infty} \sum_{\ell_2=1}^{\infty} \frac{C_{AB}(\ell_1 \ell_2)}{2(\ell_1+\ell_2+1)} , \qquad (1)$$

where $C_{AB}(\ell_1 \ell_2)$ is the dispersion force coefficient corresponding to the 2^{ℓ_1}-pole-2^{ℓ_2}-pole interaction. $u_{AB}(r)$ can also be expressed as a power series of the inverse of r,

$$u_{AB}(r) = c_6/r^6 - c_8/r^8 - c_{10}/r^{10} \ \ldots , \qquad (2)$$

where the van der Waals coefficients c_6, c_8, and c_{10} may be written

$$c_6 = C_{AB}(11), \qquad (3)$$

$$c_8 = C_{AB}(12) + C_{AB}(21), \qquad (4)$$

$$c_{10} = C_{AB}(13) + C_{AB}(22) + C_{AB}(31). \qquad (5)$$

c_6 describes the dipole-dipole interaction, c_8 the quadrupole, and C_{10} the dipole-octupole interactions.

[a] J. O. Hirschfelder and W. M. Meath, Adv. Chem. Phys. 12, 1 (1967).

[b] H. Margenau and N. Kestner, Theory of Intermolecular Forces (Pergamon, London, 1967).

[c] R. Eisenshitz and F. London, Z. Phys. 60, 491 (1930).

Tabular Data A-5.14. Van der Waals coefficients for dipole–dipole, dipole–quadrupole, and quadrupole–dipole interactions and coefficients c_6 and c_8 (in atomic units).

	C_{AB} (11)	Δ%	C_{AB} (12)	C_{AB} (21)	c_8	Δ%
H–He	28.11(−1)	0.31	13.00(0)	28.66(0)	41.66(0)	0.16
–Ne	57.83(−1)	−1.28	33.98(0)	59.76(0)	93.74(0)	−1.95
–Ar	20.18(0)	−0.89	22.60(1)	20.68(1)	42.68(1)	−2.08
–Kr	28.86(0)	−1.25	35.16(1)	28.41(1)	63.57(1)	−2.35
–Xe	41.13(0)	−0.56	55.88(1)	39.65(1)	95.53(1)	−3.05
–Li	66.02(0)	0.57	26.96(2)	57.08(1)	32.67(2)	−0.01
–Na	69.90(0)	2.64	33.78(2)	60.52(1)	39.83(2)	−0.01
–K	10.53(1)	3.41	78.77(2)	90.66(1)	87.84(2)	−0.14
–Rb	12.03(1)	6.04	95.15(2)	10.37(2)	10.55(3)	−0.11
–Cs	14.20(1)	7.17	14.09(3)	12.22(2)	15.31(3)	−0.82
He–Ne	31.59(−1)	−0.93	18.24(0)	15.22(0)	33.46(0)	−2.59
–Ar	97.86(−1)	0.34	11.16(1)	46.12(0)	15.77(1)	−2.56
–Kr	13.56(0)	0.28	16.86(1)	63.56(0)	23.22(1)	−2.51
–Xe	18.18(0)	0.65	26.45(1)	84.37(0)	34.88(1)	−3.53
–Li	21.98(0)	2.72	97.06(1)	98.27(0)	10.69(2)	0.43
–Na	23.56(0)	4.27	12.18(2)	10.44(1)	13.23(2)	0.18
–K	34.72(0)	8.62	27.53(2)	15.50(1)	29.08(2)	0.36
–Rb	39.82(0)	13.42	33.14(2)	17.79(1)	34.92(2)	0.60
–Cs	46.73(0)	15.94	48.26(2)	20.86(1)	50.35(2)	0.15
Ne–Ar	20.65(0)	0.26	23.64(1)	12.01(1)	35.65(1)	−3.47
–Kr	28.40(0)	1.03	35.48(1)	16.57(1)	52.05(1)	−3.22
–Xe	37.57(0)	0.61	55.47(1)	22.03(1)	77.50(1)	−4.16
–Li	43.19(0)	1.84	19.30(2)	25.84(1)	21.89(2)	−0.85
–Na	45.91(0)	3.76	24.23(2)	27.46(1)	26.98(2)	−1.05
–K	68.11(0)	9.06	54.48(2)	40.78(1)	58.56(2)	−0.62
–Rb	78.17(0)	14.84	65.56(2)	46.79(1)	70.24(2)	−0.15
–Cs	91.64(0)	17.43	95.23(2)	54.87(1)	10.07(3)	−0.46
Ar–Kr	94.29(0)	0.00	11.63(2)	10.64(2)	22.27(2)	−2.80
–Xe	12.94(1)	0.04	18.34(2)	14.53(2)	32.86(2)	−3.49
–Li	17.27(1)	1.31	74.34(2)	18.91(2)	93.25(2)	−0.60
–Na	18.33(1)	3.02	93.25(2)	20.07(2)	11.33(3)	−0.59
–K	27.36(1)	6.30	21.29(3)	29.93(2)	24.29(3)	−0.23
–Rb	31.34(1)	10.20	25.66(3)	34.30(2)	29.09(3)	0.28
–Cs	36.85(1)	12.67	37.57(3)	40.31(2)	41.60(3)	−0.13
Kr–Xe	18.44(1)	−0.23	25.83(2)	22.52(2)	48.36(2)	−3.47
–Li	25.77(1)	0.51	10.95(3)	30.53(2)	14.01(3)	−4.64
–Na	27.33(1)	2.74	13.74(3)	32.39(2)	16.98(3)	−0.83
–K	40.88(1)	5.59	31.52(3)	48.38(2)	36.36(3)	−0.51
–Rb	46.80(1)	9.13	38.01(3)	55.41(2)	43.55(3)	−0.06
–Cs	55.08(1)	11.30	55.80(3)	65.17(2)	62.32(3)	−0.50
Xe–Li	40.30(1)	0.25	16.65(3)	49.42(2)	21.59(3)	−0.67
–Na	42.69(1)	2.54	20.87(3)	52.42(2)	26.11(3)	−0.58
–K	64.16(1)	8.21	48.43(3)	78.37(2)	56.27(3)	−0.33
–Rb	73.34(1)	6.69	58.47(3)	89.74(2)	67.44(3)	0.04
–Cs	86.52(1)	8.44	86.36(3)	10.56(3)	96.92(3)	−0.48
Li–Na	14.48(2)	0.10	52.43(3)	44.18(3)	96.61(3)	0.47
–K	23.20(2)	−0.01	13.60(4)	68.61(3)	20.46(4)	0.47
–Rb	26.00(2)	−0.38	16.62(4)	77.64(3)	24.38(4)	−0.68
–Cs	31.66(2)	−0.50	26.24(4)	93.07(3)	35.55(4)	−1.56
Na–K	24.14(2)	−0.18	14.25(4)	85.48(3)	22.80(4)	0.46
–Rb	27.07(2)	−0.63	17.41(4)	96.75(3)	27.08(4)	−0.05
–Cs	32.93(2)	−0.70	27.44(4)	11.60(4)	39.03(4)	−1.01
K–Rb	43.51(2)	−0.01	27.32(4)	25.21(4)	52.53(4)	−0.57
–Cs	53.14(2)	−0.25	43.35(4)	30.36(4)	73.71(4)	−1.25
Rb–Cs	59.40(2)	−0.00	48.79(4)	37.14(4)	85.93(4)	−1.69

Δ: Fractional percent deviations from K. T. Tang, Phys. Rev. 177, 108 (1969).

Tabular Data A-5.15. Van der Waals coefficients for the dipole–octupole, quadrupole–quadrupole, and octupole–dipole interactions and coefficient c_{10} (in atomic units).

	C_{AB} (13)	C_{AB} (22)	C_{AB} (31)	c_{10}	Δ%
H–He	99.22(0)	24.99(1)	51.09(1)	86.01(1)	0.66
–Ne	29.54(1)	65.18(1)	10.73(2)	20.20(2)	–1.35
–Ar	39.47(2)	42.22(2)	35.37(2)	11.71(3)	–1.61
–Kr	56.25(2)	65.06(2)	49.80(2)	17.11(3)	–1.79
–Xe	89.00(2)	10.29(3)	28.82(2)	26.08(3)	–2.38
–Li	15.61(4)	44.92(3)	94.57(2)	21.04(4)	0.12
–Na	21.53(4)	56.32(3)	10.03(3)	28.16(4)	–3.09
–K	55.68(4)	12.97(4)	15.00(3)	70.14(4)	–1.60
–Rb	68.97(4)	15.64(4)	17.17(3)	86.33(4)	–0.41
–Cs	12.26(5)	23.01(4)	20.20(3)	14.76(5)	–14.80
He–Ne	15.67(1)	16.34(1)	11.56(1)	43.58(1)	–1.63
–Ar	19.53(2)	98.45(1)	35.12(1)	32.88(2)	–1.19
–Kr	26.84(2)	14.81(2)	48.43(1)	46.49(2)	–1.18
–Xe	41.90(2)	23.16(2)	64.35(1)	71.50(2)	–0.97
–Li	57.75(3)	81.73(2)	75.24(1)	66.68(3)	0.54
–Na	79.86(3)	10.26(3)	79.96(1)	90.92(3)	–3.90
–K	20.03(4)	23.10(3)	11.87(2)	22.46(4)	–1.59
–Rb	24.63(4)	27.80(3)	13.62(2)	27.55(4)	0.00
–Cs	45.46(4)	40.40(3)	15.97(2)	49.66(4)	–20.96
Ne–Ar	41.39(2)	25.62(2)	10.37(2)	77.37(2)	–0.09
–Kr	56.41(2)	38.56(2)	14.34(2)	10.93(3)	–0.23
–Xe	87.79(2)	60.36(2)	19.13(2)	16.73(3)	0.59
–Li	11.54(4)	21.45(3)	22.75(2)	13.91(4)	–0.95
–Na	15.96(4)	26.93(3)	24.18(2)	18.90(4)	–5.28
–K	39.83(4)	60.67(3)	35.62(2)	46.26(4)	–2.82
–Rb	48.63(4)	73.03(3)	41.20(2)	56.64(4)	–1.13
–Cs	90.86(4)	10.62(4)	48.34(2)	10.20(5)	–22.38
Ar–Kr	18.55(3)	24.55(3)	18.60(3)	61.70(3)	0.08
–Xe	29.12(3)	38.66(3)	25.37(3)	63.14(3)	0.21
–Li	43.83(4)	15.29(4)	32.94(3)	62.42(4)	–0.74
–Na	60.56(4)	19.19(4)	34.96(3)	83.24(4)	–4.03
–K	15.35(5)	43.69(4)	52.13(3)	20.24(5)	–2.12
–Rb	18.62(5)	52.65(4)	59.74(3)	24.48(5)	–0.63
–Cs	34.47(5)	76.98(4)	70.20(3)	42.87(5)	–17.20
Kr–Xe	41.05(3)	59.33(3)	36.02(3)	13.64(4)	0.07
–Li	64.29(4)	24.43(4)	49.19(3)	93.63(4)	–1.00
–Na	88.80(4)	30.64(4)	52.18(3)	12.47(5)	–4.09
–K	22.61(5)	70.07(4)	77.97(3)	30.40(5)	–2.33
–Rb	27.91(5)	84.47(4)	89.30(3)	37.25(5)	–0.89
–Cs	50.55(5)	12.38(5)	10.50(4)	63.98(5)	–16.48
Xe–Li	96.75(4)	36.33(4)	79.27(3)	14.40(5)	–0.98
–Na	13.35(5)	49.32(4)	84.09(3)	19.12(5)	–3.71
–K	34.38(5)	11.31(5)	12.58(4)	46.94(5)	–2.05
–Rb	42.54(5)	13.63(5)	14.40(4)	57.61(5)	–0.66
–Cs	76.01(5)	20.00(5)	16.94(4)	97.70(5)	–14.44
Li–Na	30.69(5)	34.10(5)	23.57(5)	88.36(5)	–0.08
–K	87.05(5)	84.43(5)	36.34(5)	20.78(6)	–0.27
–Rb	11.04(6)	10.26(6)	41.22(5)	25.43(6)	–0.24
–Cs	17.48(6)	15.73(6)	49.24(5)	38.13(6)	–1.34
Na–K	91.42(5)	10.54(6)	49.78(5)	24.66(6)	0.58
–Rb	11.59(6)	12.81(6)	56.46(5)	30.05(6)	0.17
–Cs	18.39(6)	19.62(6)	67.43(5)	44.76(6)	–0.81
K–Rb	18.04(6)	32.27(6)	16.07(6)	66.38(6)	–0.00
–Cs	28.35(6)	49.93(6)	19.26(6)	97.54(6)	–0.34
Rb–Cs	32.15(6)	60.88(6)	24.48(6)	11.75(7)	–0.18

Δ: Fractional percent deviations from K. T. Tang, Phys. Rev. 177, 108 (1969).

B. HEAVY PARTICLE - HEAVY PARTICLE COLLISIONS

CONTENTS

		Page
B-1.	Low Energy Heavy Particle - Heavy Particle Collisions.	2673
	B-1.A. Ion-Ion Recombination.	2674
	B-1.B. Ion-Molecule Reactions	2726
	B-1.C. Energy Transfer; Quenching	2750
	B-1.D. Charge Transfer in Ion-Neutral, Ion-Ion, and Neutral-Neutral Collisions	2775
B-2.	High Energy Heavy Particle - Heavy Particle Collisions . . . . (No new entries here. See Vols. I and IV for high-energy data.)	

B-1. LOW ENERGY HEAVY PARTICLE - HEAVY PARTICLE COLLISIONS

General References

1. G. Bekefi, Principles of Laser Plasmas, Wiley, New York (1976).

2. J. B. Hasted, Physics of Atomic Collisions (Second Edition), American Elsevier Publishing Co., Inc., New York (1972).

3. H. S. W. Massey, Electronic and Ionic Impact Phenomena (Second Edition), Vol. III, Oxford University Press (1971).

4. H. S. W. Massey and H. B. Gilbody, Electronic and Ionic Impact Phenomena (Second Edition), Vol. IV, Oxford University Press (1974).

5. E. W. McDaniel, Collision Phenomena in Ionized Gases, Wiley, New York (1964).

6. Excimer Lasers, (Edited by C. K. Rhodes), Springer-Verlag, Berlin (1979).

7. M. H. Bortner and T. Baurer (Eds.), "Defense Nuclear Agency Reaction Rate Handbook" (Second Edition), DNA 1948-H (1972). Also see supplements published since 1972.

8. C. F. Barnett, E. W. McDaniel, E. W. Thomas, et al., "Bibliography of Atomic and Molecular Processes" (1950-1980), Oak Ridge National Laboratory, Oak Ridge, Tennessee. Categorized according to kind of collision, process, or property. Information concerning procurement available from D. H. Crandall, P. O. Box X, Building 6003, Oak Ridge National Laboratory, Oak Ridge, Tennessee 37830.

9. R. B. Bernstein (Ed.), Atom-Molecule Collision Theory, Plenum Press, New York (1979).

10. J. W. Gallagher, Janet Van Blerkom, E. C. Beaty, and J. R. Rumble, Jr., "Data Index for Energy Transfer Collisions of Atoms and Molecules: 1970 - 1979". NBS Special Publication 593 (1980). This is a bibliography indexed by physical processes and reactants that covers the reactant energy range 0 - 10 keV. In addition to the processes normally labelled "energy transfer", the bibliography also covers charge transfer, chemi-ionization, and other kinds of heavy particle collisional ionization. Approx. 400 pages.

Section B-1.A. ION-ION RECOMBINATION

CONTENTS

		Page
Introduction		2675
Figs. B-1.A. 1-5.	Three-body recombination coefficients for Ne^+ with the halogen negative ions in He, Ne, Ar, Kr, and Xe (graphical data)	2677
Figs. B-1.A. 6-10.	Three-body recombination coefficients for Ar^+ with the halogen negative ions in He, Ne, Ar, Kr, and Xe (graphical data)	2682
Figs. B-1.A. 11-15.	Three-body recombination coefficients for Kr^+ with the halogen negative ions in He, Ne, Ar, Kr, and Xe (graphical data)	2687
Figs. B-1.A. 16-20.	Three-body recombination coefficients for Xe^+ with the halogen negative ions in He, Ne, Ar, Kr, and Xe (graphical data)	2692
Figs. B-1.A. 21-25.	Three-body recombination coefficients for Ar_2^+ with the halogen negative ions in He, Ne, Ar, Kr, and Xe (graphical data)	2692
Figs. B-1.A. 26-30.	Three-body recombination coefficients for Kr_2^+ with the halogen negative ions in He, Ne, Ar, Kr, and Xe (graphical data)	2702
Figs. B-1.A. 31-35.	Three-body recombination coefficients for Xe_2^+ with the halogen negative ions in He, Ne, Ar, Kr, and Xe (graphical data)	2707
Figs. B-1.A. 36-37.	Three-body recombination coefficients for $NeXe^+$ with the halogen negative ions in Ne and Xe (graphical data)	2712
Figs. B-1.A. 38-39.	Three-body recombination coefficients for $ArXe^+$ with the halogen negative ions in Ar and Xe (graphical data)	2714
Figs. B-1.A. 40-41.	Three-body recombination coefficients for $KrXe^+$ with the halogen negative ions in Kr and Xe (graphical data)	2716
Figs. B-1.A. 42-43.	Three-body recombination coefficients for $ArKr^+$ with the halogen negative ions in Ar and Kr (graphical data)	2718
Figs. B-1.A. 44-45.	Three-body recombination coefficients for $NeKr^+$ with the halogen negative ions in Ne and Kr (graphical data)	2720
Figs. B-1.A. 46-47.	Three-body recombination coefficients for $XeKr^+$ with the halogen negative ions in Kr and Xe (graphical data)	2722
Figs. B-1.A. 48-49.	Recombination rate coefficient for $(Xe^+ - Cl^-)$ in Ne and $(Kr^+ - F^-)$ in Ar as a function of gas density N for various ion densities $N^{\pm}$ (graphical data)	2724

Introduction

The processes of interest here are the two- and three-body mechanisms which may respectively be written:

$$X^+ + Y^- \rightarrow [X + Y]$$

$$X^+ + Y^- + Z \rightarrow [X + Y] + Z$$

The square brackets indicate that the species may remain associated after recombination. They may also be excited. Data for the two-body case are presented as a two-body rate in units of $cm^3\ s^{-1}$. Data for the three-body case are normally presented in the form of a two-body rate for recombination ($cm^3\ s^{-1}$) as a function of the total gas density; density is often expressed as the ratio N/N_L where N is the density (cm^{-3}) and N_L is Loschmidt's number ($2.69 \times 10^{19}\ cm^{-3}$, the number density at STP).

The data presented in Figs. 1-47 of this section are the results of computations by Hoffman and Moreno (see ref. 12 below). The computations involved the theoretical work of M. R. Flannery (see ref. 5 below). We are grateful to Drs. Hoffman and Moreno for permission to use their data.

Figs. 48 and 49 present theoretical data to be published by M. R. Flannery in 1981. The references in the figure legends refer to Flannery's 1981 paper.

General References:

1. D. R. Bates, "Recombination", i "Case Studies in Atomic Physics" (Edited by E. W. McDaniel and M. R. C. McDowell), 4, 59, North-Holland, Amsterdam (1975).

2. M. R. Flannery, "Ionic Recombination", "Atomic Processes and Applications", (Edited by P. G. Burke and B. L. Moiseiwitsch), North-Holland, Amsterdam (1976).

3. M. R. Flannery, "Three-Body Recombination of Positive and Negative Ions", "Case Studies in Atomic Collision Physics", (Edited by E. W. McDaniel and M. R. C. McDowell), 2, 3, North-Holland, Amsterdam (1972).

4. M. R. Flannery, "Ion-Ion Recombination", in Applied Atomic Collisions Physics (Ed. by H. S. W. Massey, B. Bederson and E. W. McDaniel) Academic, New York (1981).

5. M. R. Flannery, "Three-Body Ion-Ion Recombination in Mercury-Halide Lasers", Chem. Phys. Letts. 56, 143 (1978). M. R. Flannery and T. P. Yang, "Ionic Recombination of Rare-Gas Atomic Ions X^+ with F^- in a Dense Gas X", Appl. Phys. Letts. 32, 327 (1978). M. R. Flannery and T. P. Yang, "Ionic Recombination of Rare-Gas Molecular Ions X_2^+ with F^- in a Dense Gas X", Appl. Phys. Letts. 32, 356 (1978). M. R. Flannery and T. P. Yang, "Ionic Recombination of Kr^+ and Kr_2^+ with F^- in Dense Buffer Rare Gases", Appl. Phys. Letts. 33, 574 (1978).

6. B. H. Mahan, "Recombination of Gaseous Ions", Advances in Chemical Physics, (Edited by I. Prigogine) 23, 1, (1973).

7. H. S. W. Massey, Negative Ions (Third Edition), Cambridge University Press, New York (1976).

8. H. S. W. Massey and H. B. Gilbody, Electronic and Ionic Impact Phenomena 4, Clarendon Press, Oxford (1974).

9. E. W. McDaniel, Collision Phenomena in Ionized Gases, Wiley, New York (1964).

10. J. T. Moseley, R. E. Olson, and J. R. Peterson, "Ion-Ion Mutual Neutralization", Case Studies in Atomic Physics (Edited by E. W. McDaniel and M. R. C. McDowell), 5, 1, North-Holland, Amsterdam (1976).

11. D. R. Bates and I. Mendaš, Proc. Roy. Soc. A 359, 275, 287 (1978).

12. J. M. Hoffman and J. B. Moreno, "Three-Body Ion-Ion Recombination Coefficients for Rare Gas-Halogen Mixtures", Sandia National Laboratories, Albuquerque, New Mexico 87185. Report No. Sand80-1486; UC-34a. August 1980.

Additional Data on Ion-Ion Recombination:

See pp. 319-322 (Vol. I) and pp. 1351-1388 (Vol. IV).

Data Needed: Experimental rate coefficients for three-body recombination in pure gases and gas mixtures at high pressures with positive identification of the recombining ionic species. "High pressure" means pressures from 1 Torr to the highest possible value.

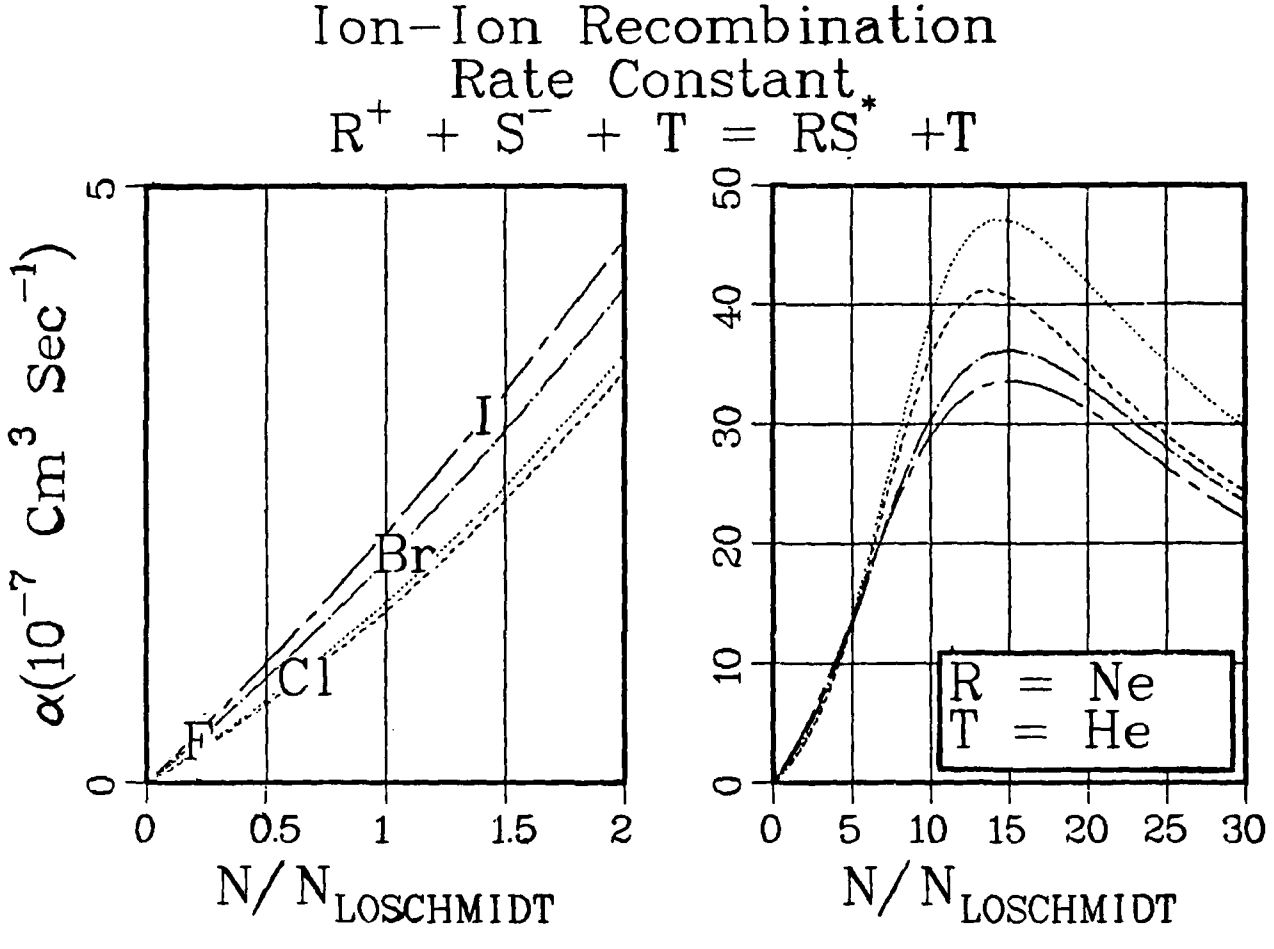

Fig. B-1.A. 1. Ion-ion recombination rate constants for the indicated processes and gases as a function of neutral gas density normalized by Loschmidt's number. The results for S = F, Cl, Br, and I are denoted respectively by dots, dashes, dots and dashes, and short and long dashes.

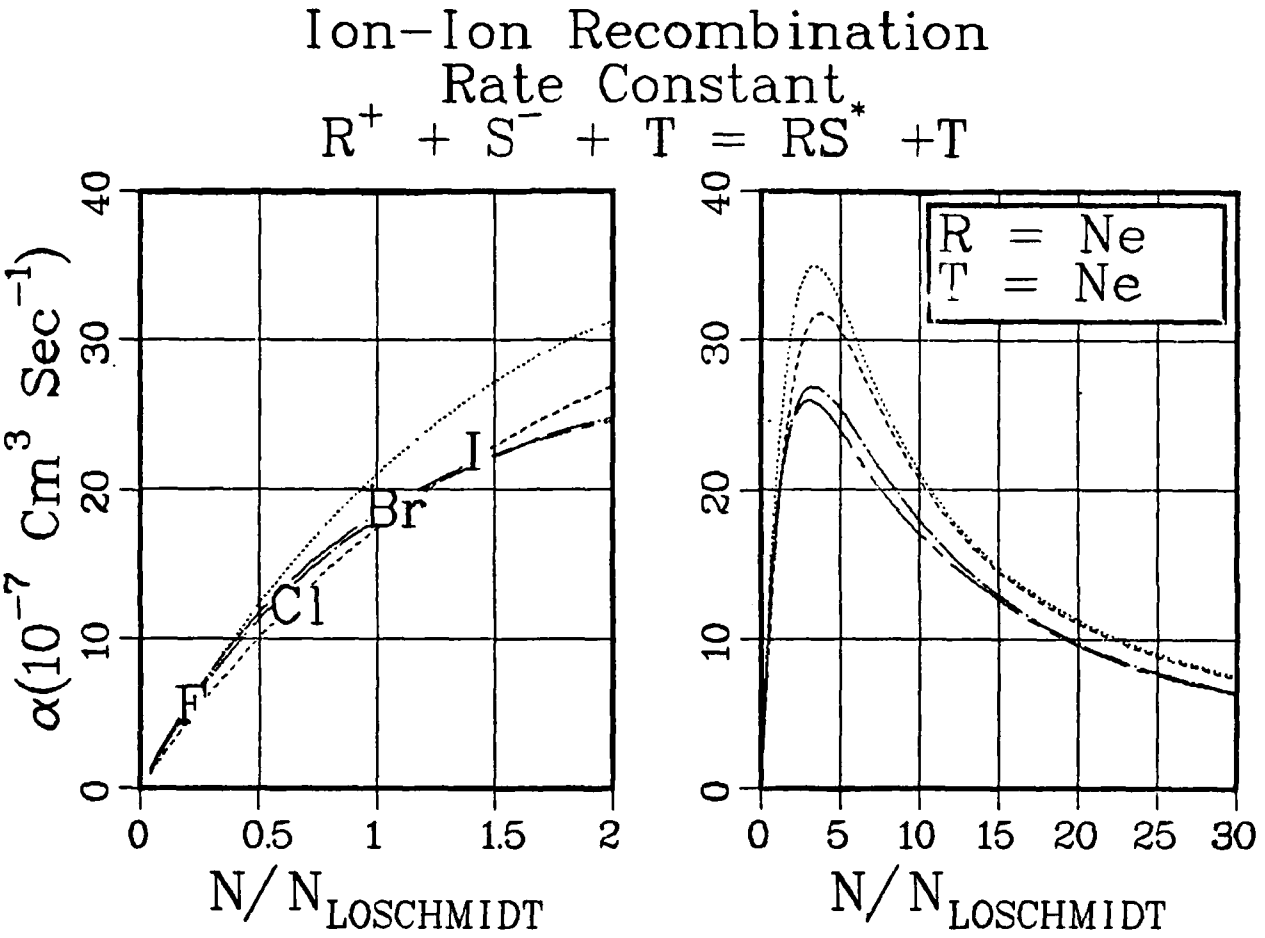

Fig. B-1.A. 2. Ion-ion recombination rate constants for the indicated processes and gases as a function of neutral gas density normalized by Loschmidt's number. The results for S = F, Cl, Br, and I are denoted respectively by dots, dashes, dots and dashes, and short and long dashes.

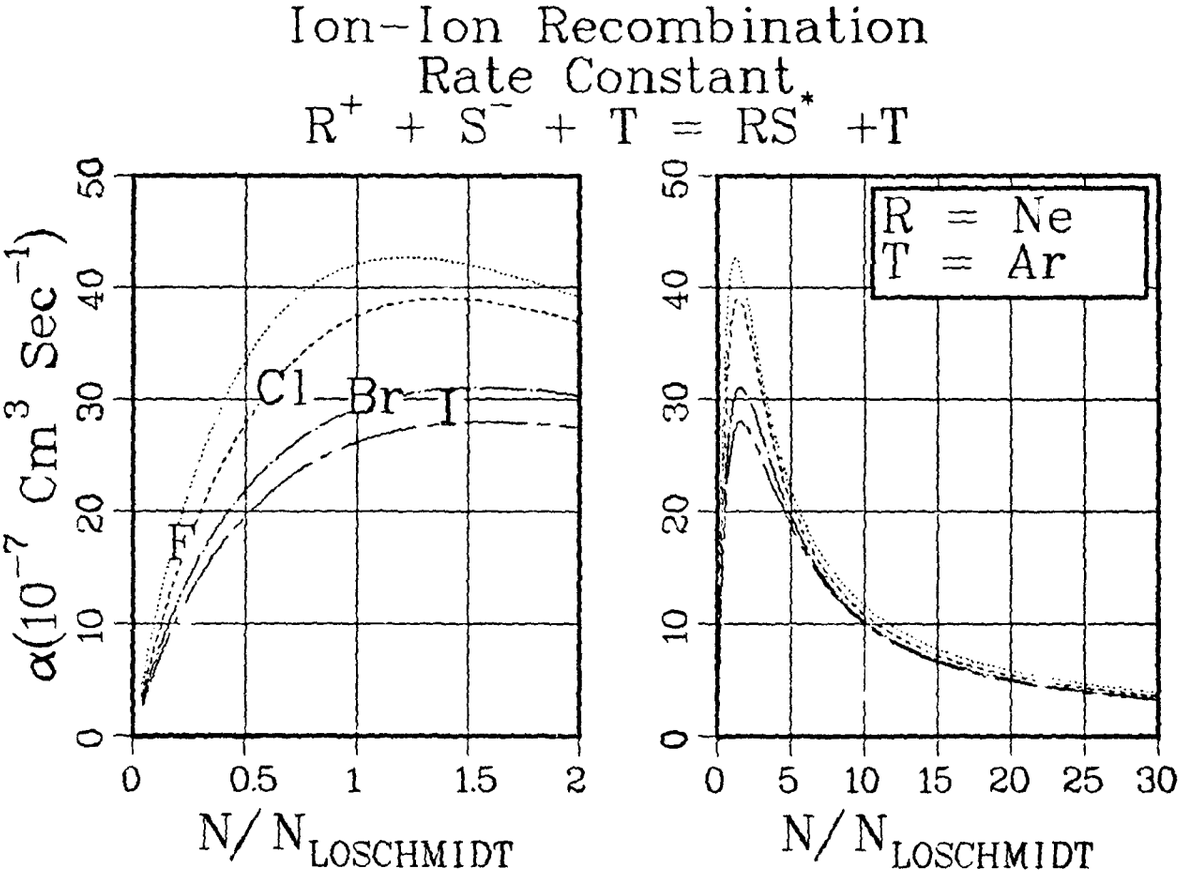

Fig. B-1.A. 3. Ion-ion recombination rate constants for the indicated processes and gases as a function of neutral gas density normalized by Loschmidt's number. The results for S = F, Cl, Br, and I are denoted respectively by dots, dashes, dots and dashes, and short and long dashes.

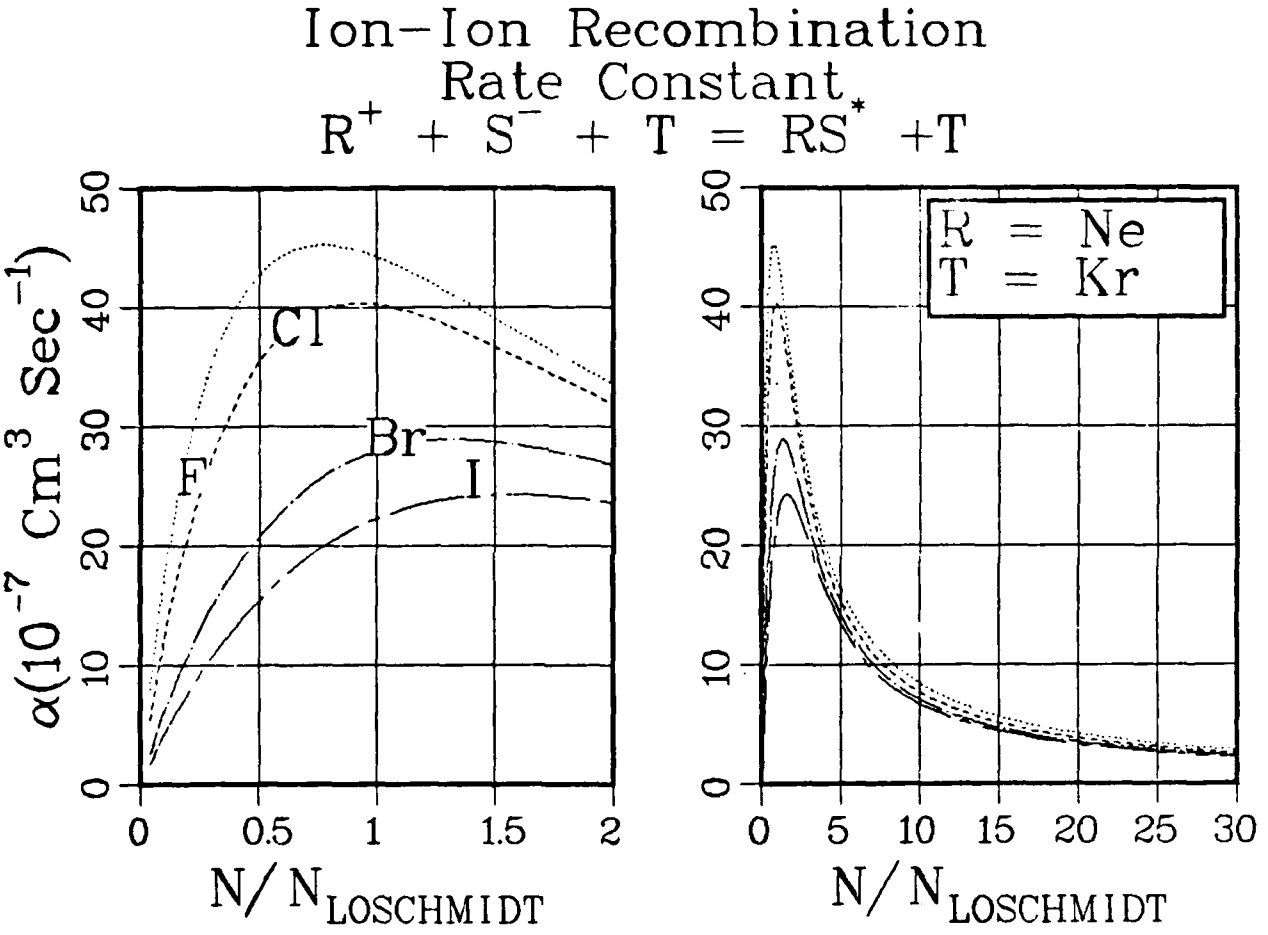

Fig. B-1.A. 4. Ion-ion recombination rate constants for the indicated processes and gases as a function of neutral gas density normalized by Loschmidt's number. The results for S = F, Cl, Br, and I are denoted respectively by dots, dashes, dots and dashes, and short and long dashes.

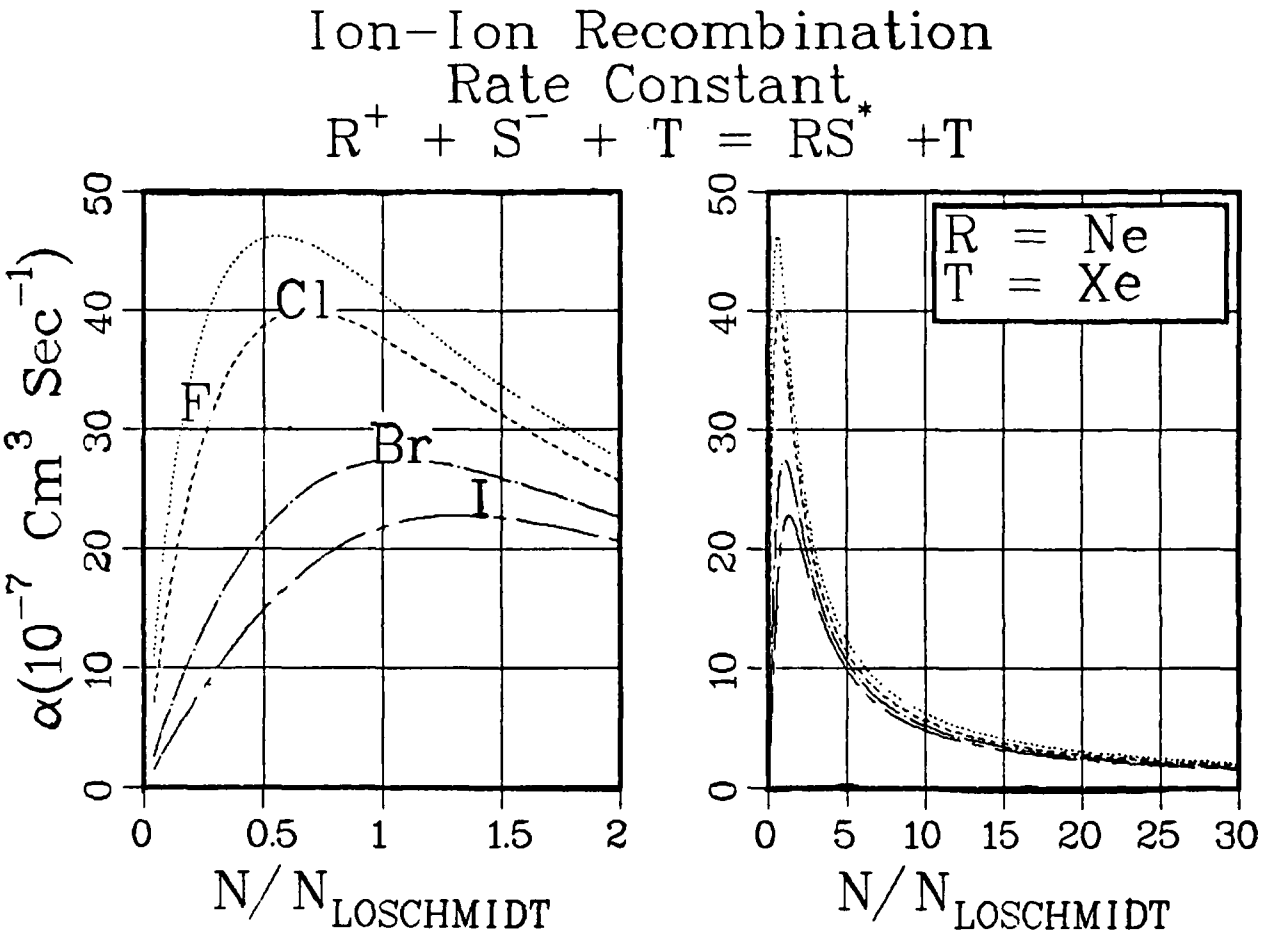

Fig. B-1.A. 5. Ion-ion recombination rate constants for the indicated processes and gases as a function of neutral gas density normalized by Loschmidt's number. The results for S = F, Cl, Br, and I are denoted respectively by dots, dashes, dots and dashes, and short and long dashes.

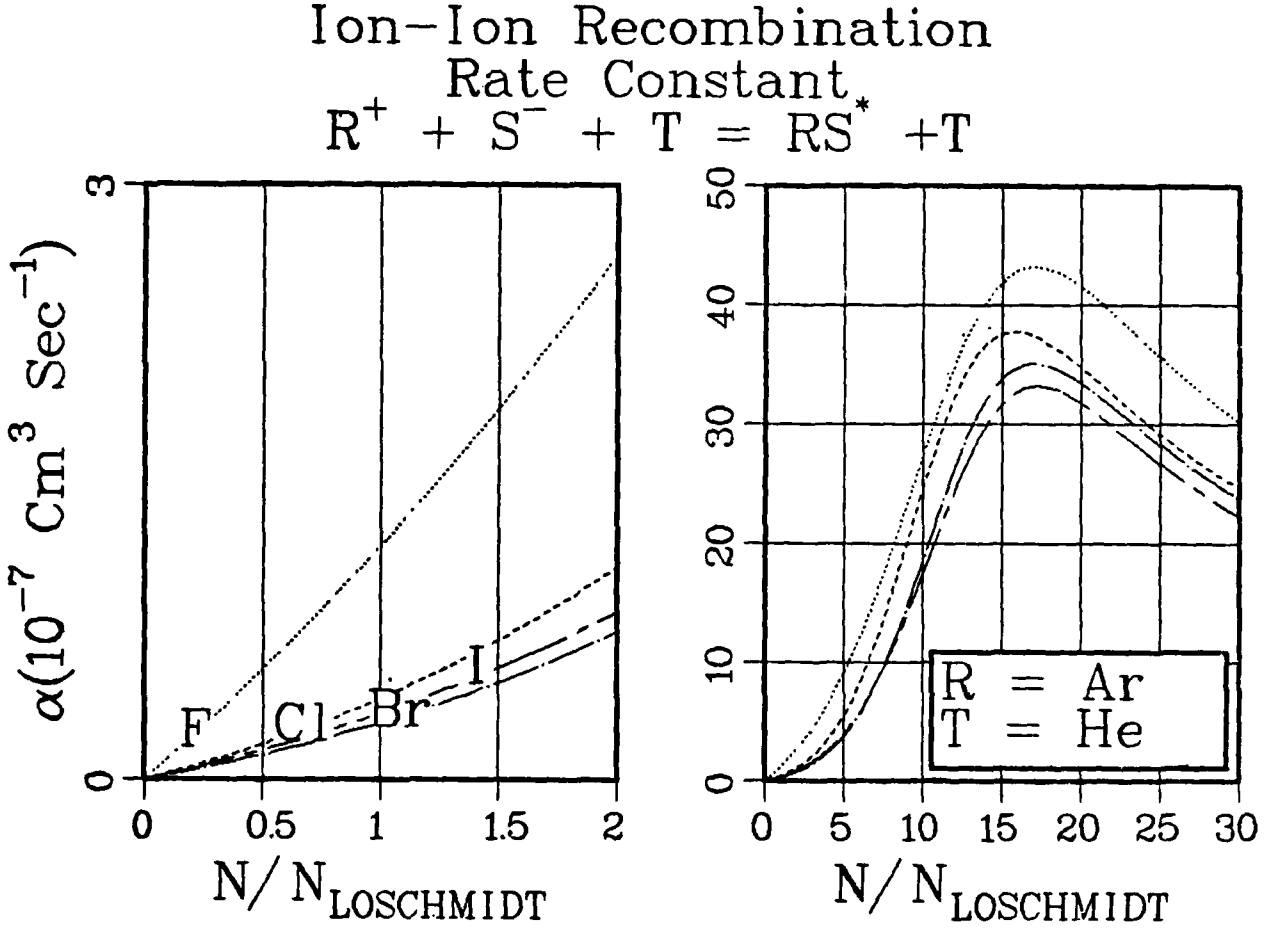

Fig. B-1.A. 6. Ion-ion recombination rate constants for the indicated processes and gases as a function of neutral gas density normalized by Loschmidt's number. The results for S = F, Cl, Br, and I are denoted respectively by dots, dashes, dots and dashes, and short and long dashes.

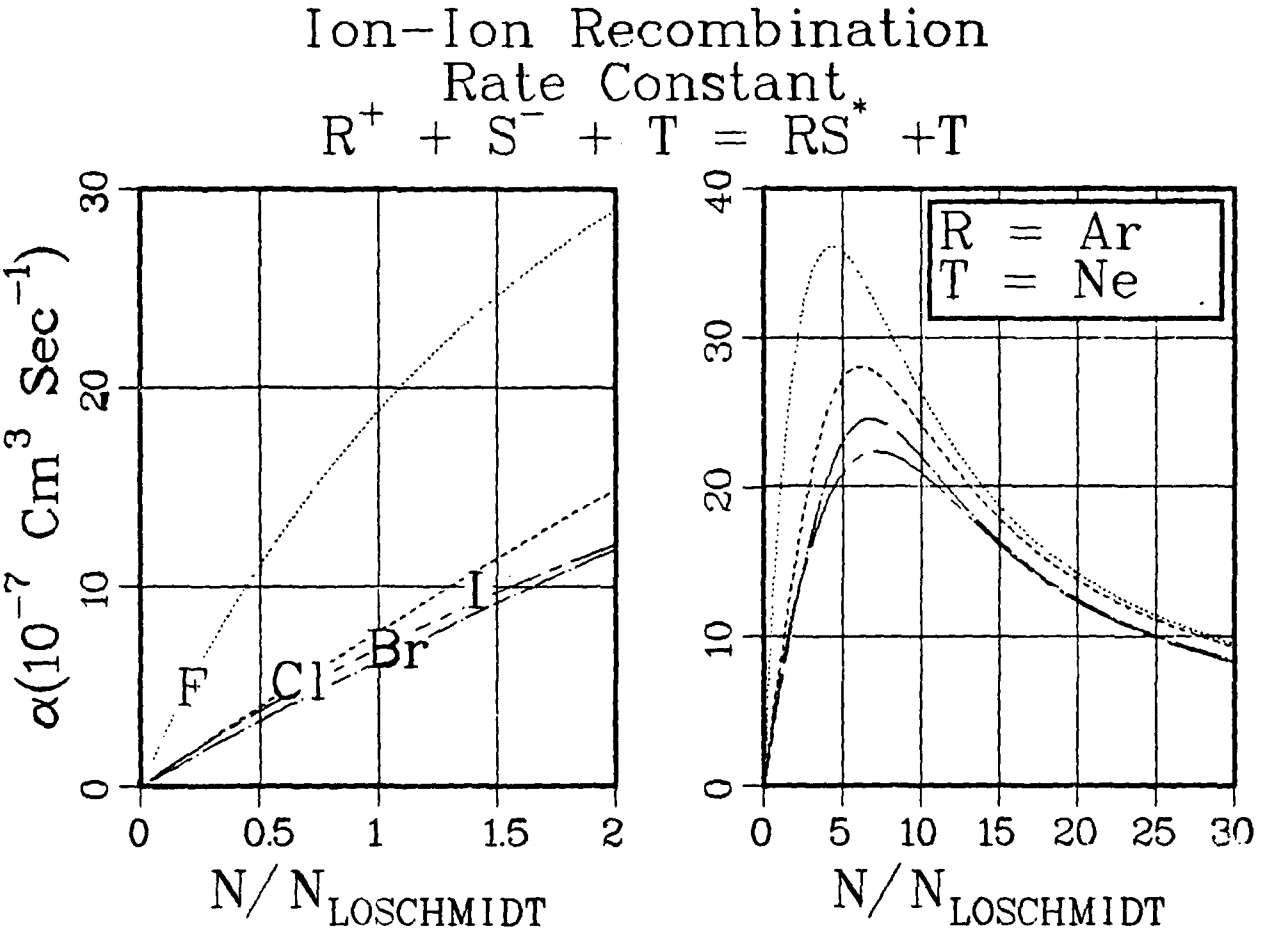

Fig. B-1.A. 7. Ion-ion recombination rate constants for the indicated processes and gases as a function of neutral gas density normalized by Loschmidt's number. The results for S = F, Cl, Br, and I are denoted respectively by dots, dashes, dots and dashes, and short and long dashes.

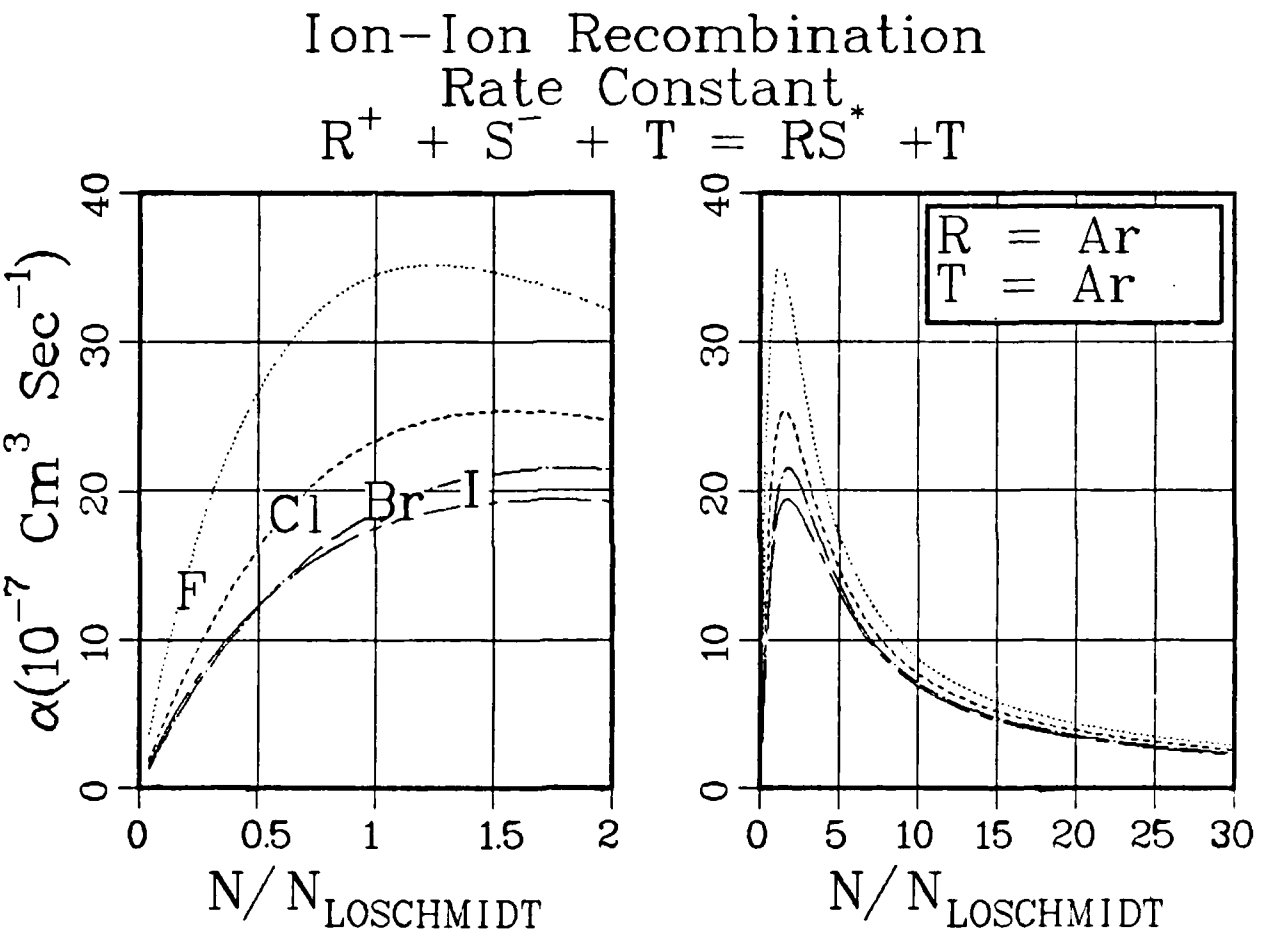

Fig. B-1.A. 8. Ion-ion recombination rate constants for the indicated processes and gases as a function of neutral gas density normalized by Loschmidt's number. The results for S = F, Cl, Br, and I are denoted respectively by dots, dashes, dots and dashes, and short and long dashes.

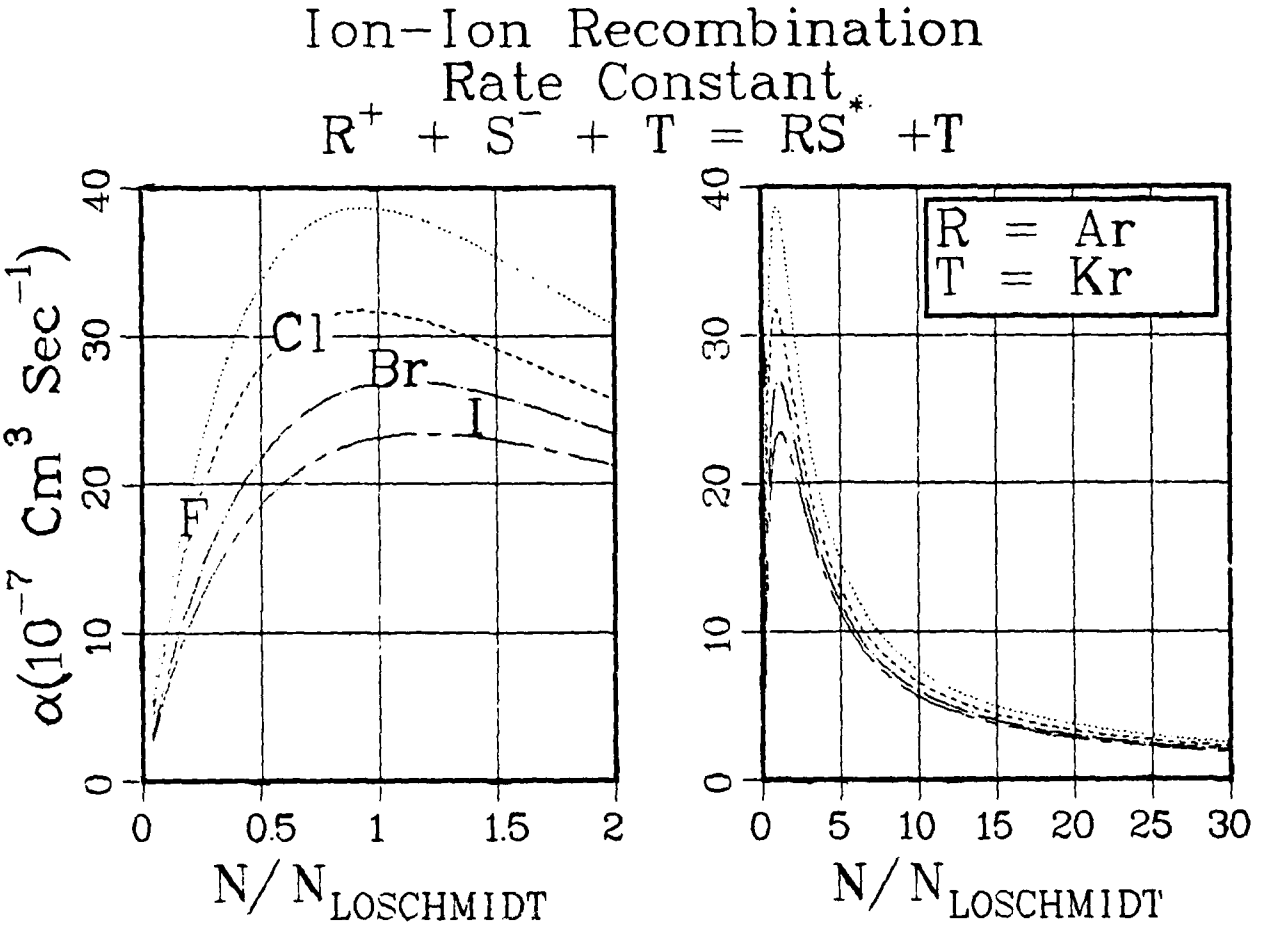

Fig. B-1.A. 9. Ion-ion recombination rate constants for the indicated processes and gases as a function of neutral gas density normalized by Loschmidt's number. The results for S = F, Cl, Br, and I are denoted respectively by dots, dashes, dots and dashes, and short and long dashes.

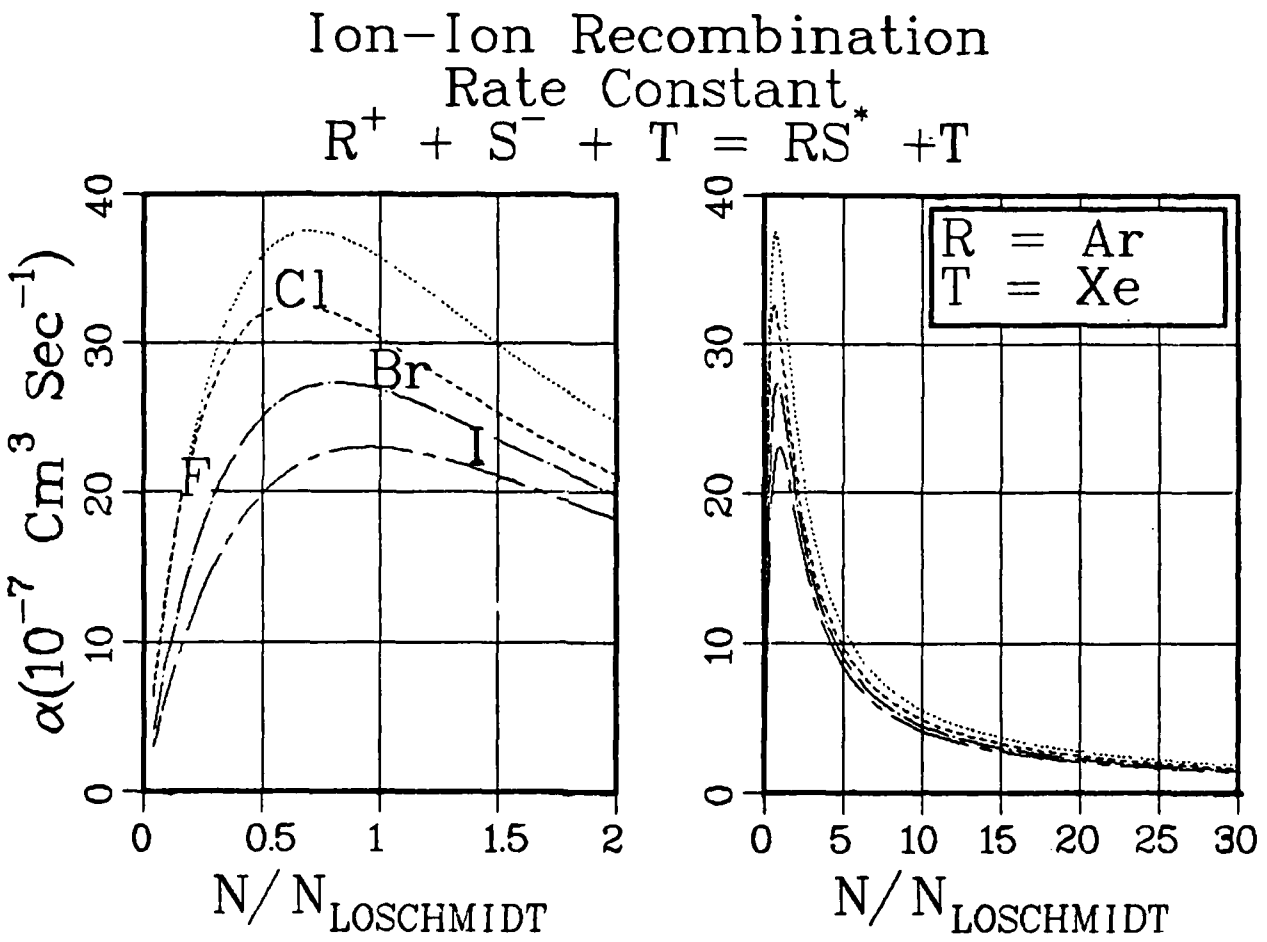

Fig. B-1.A. 10. Ion-ion recombination rate constants for the indicated processes and gases as a function of neutral gas density normalized by Loschmidt's number. The results for S = F, Cl, Br, and I are denoted respectively by dots, dashes, dots and dashes, and short and long dashes.

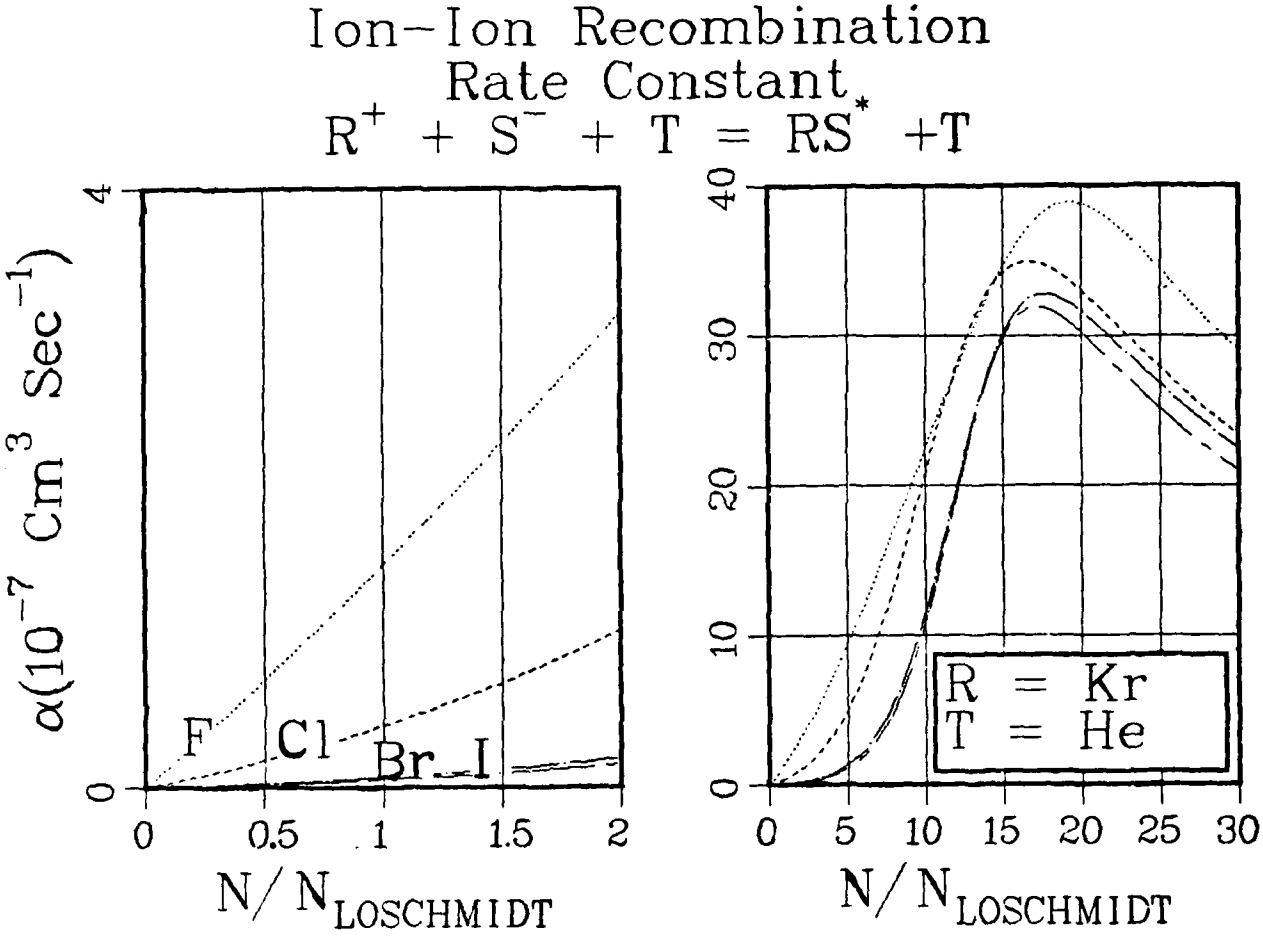

Fig. B-1.A. 11. Ion-ion recombination rate constants for the indicated processes and gases as a function of neutral gas density normalized by Loschmidt's number. The results for S = F, Cl, Br, and I are denoted respectively by dots, dashes, dots and dashes, and short and long dashes.

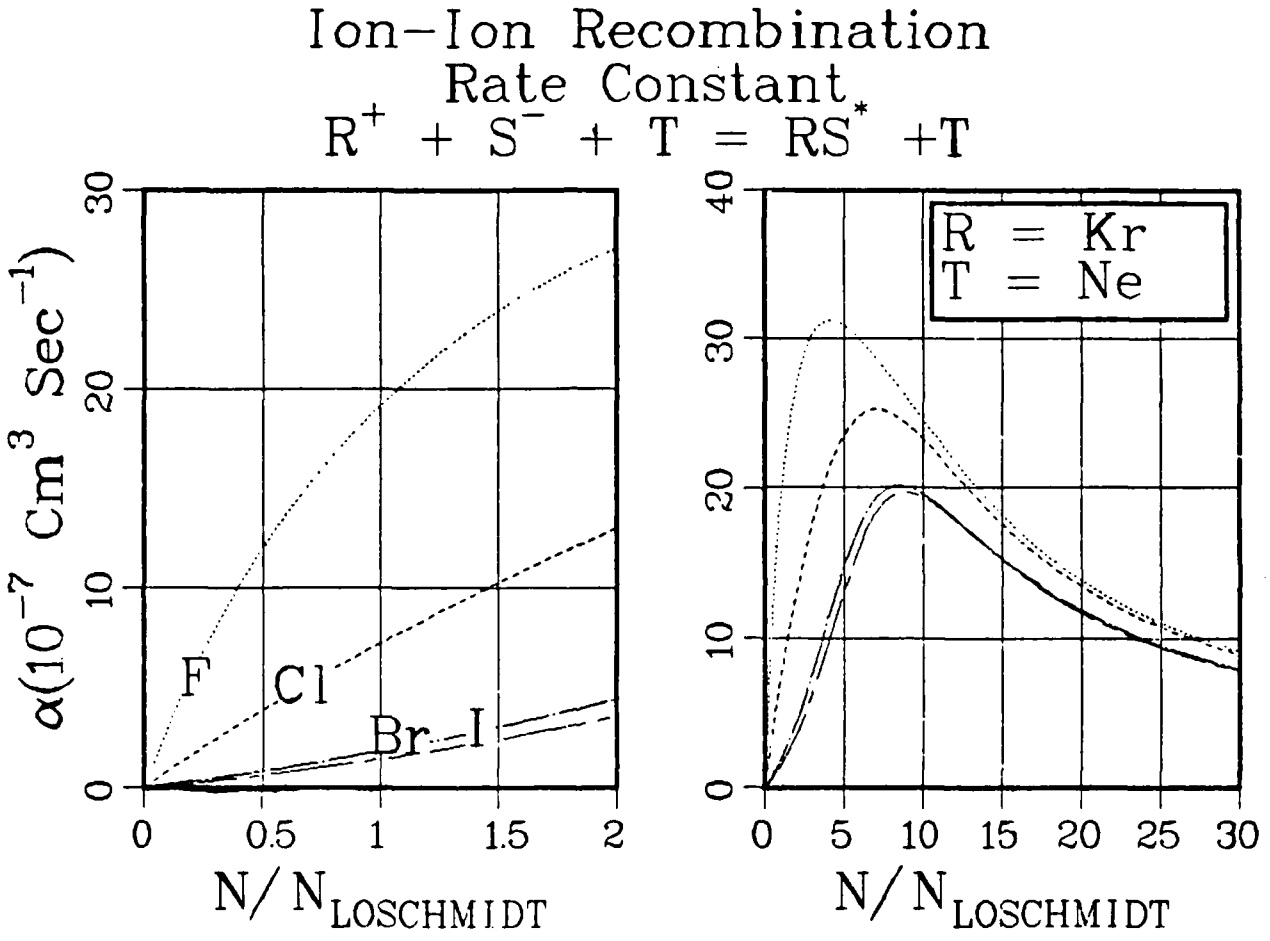

Fig. B-1.A. 12. Ion-ion recombination rate constants for the indicated processes and gases as a function of neutral gas density normalized by Loschmidt's number. The results for S = F, Cl, Br, and I are denoted respectively by dots, dashes, dots and dashes, and short and long dashes.

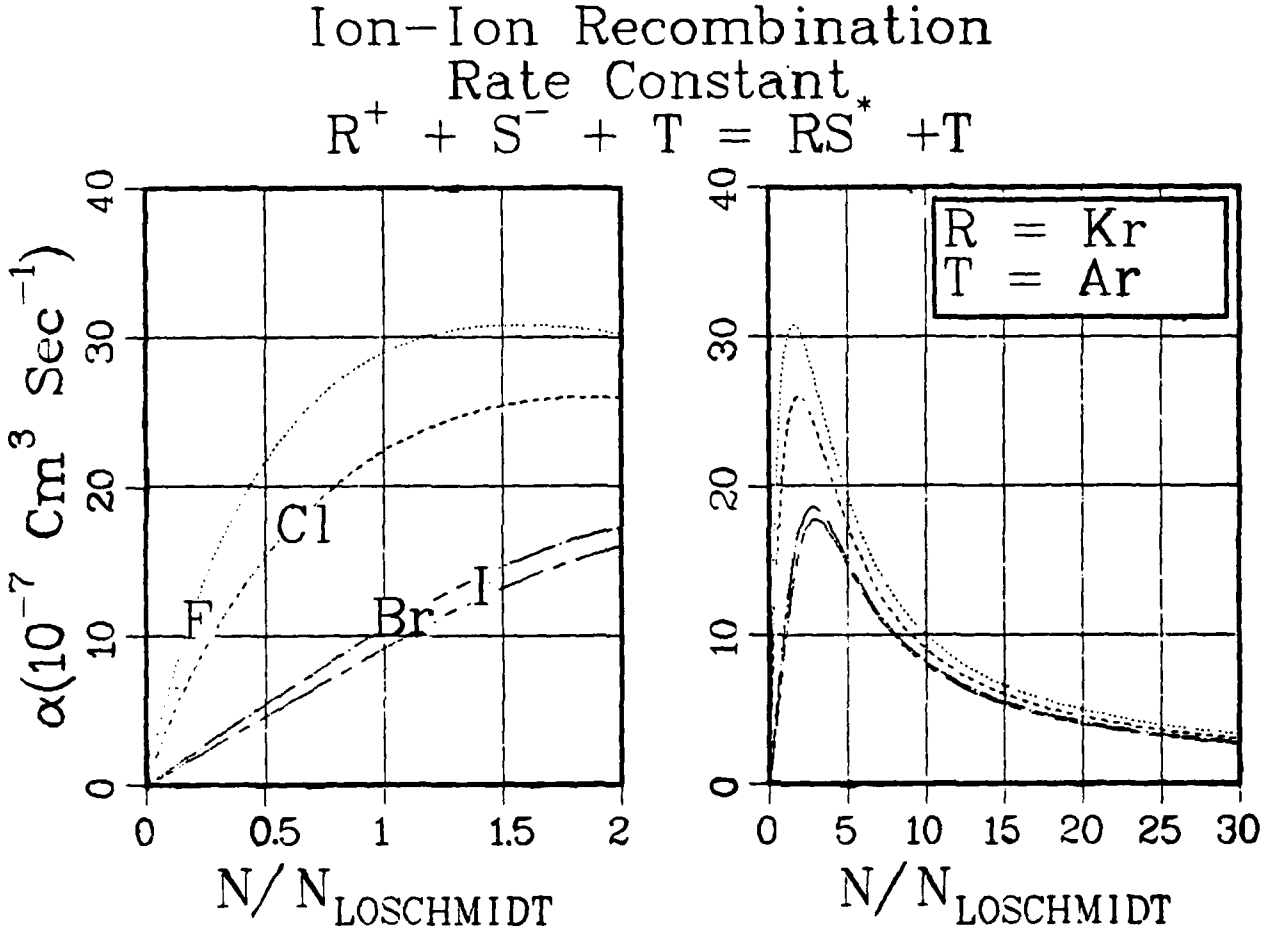

Fig. B-1.A. 13. Ion-ion recombination rate constants for the indicated processes and gases as a function of neutral gas density normalized by Loschmidt's number. The results for S = F, Cl, Br, and I are denoted respectively by dots, dashes, dots and dashes, and short and long dashes.

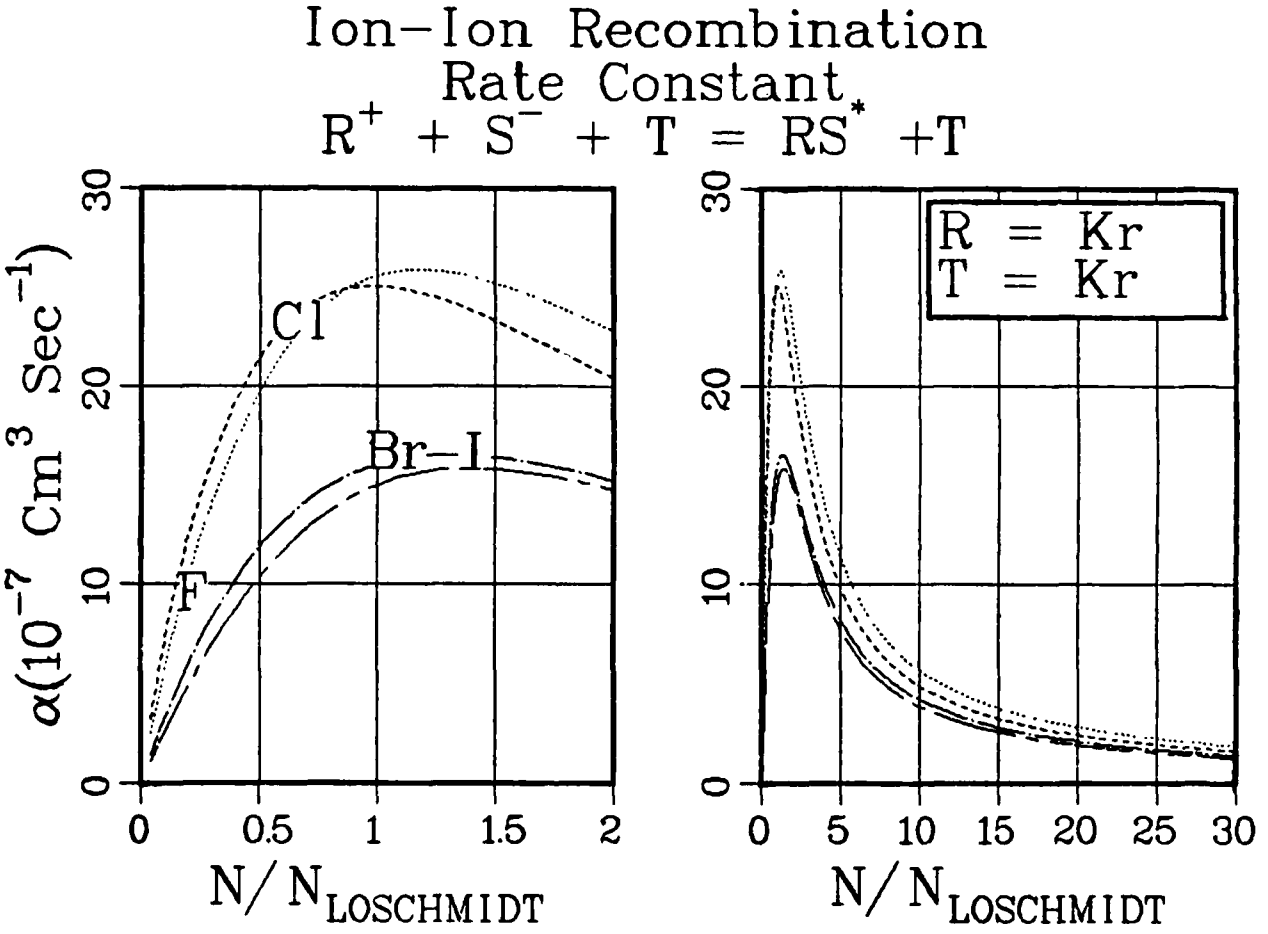

Fig. B-1.A. 14. Ion-ion recombination rate constants for the indicated processes and gases as a function of neutral gas density normalized by Loschmidt's number. The results for S = F, Cl, Br, and I are denoted respectively by dots, dashes, dots and dashes, and short and long dashes.

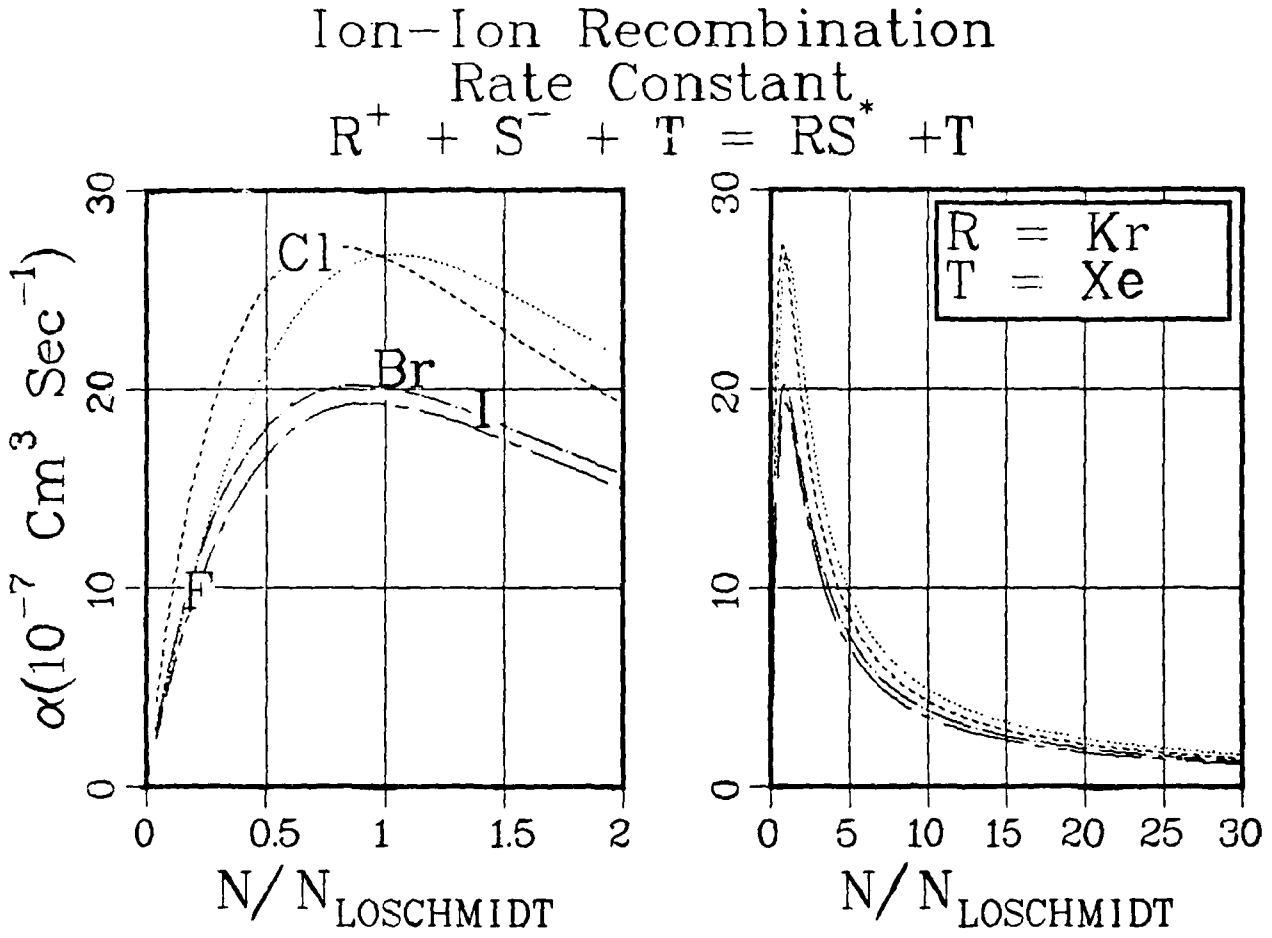

Fig. B-1.A. 15. Ion-ion recombination rate constants for the indicated processes and gases as a function of neutral gas density normalized by Loschmidt's number. The results for S = F, Cl, Br, and I are denoted respectively by dots, dashes, dots and dashes, and short and long dashes.

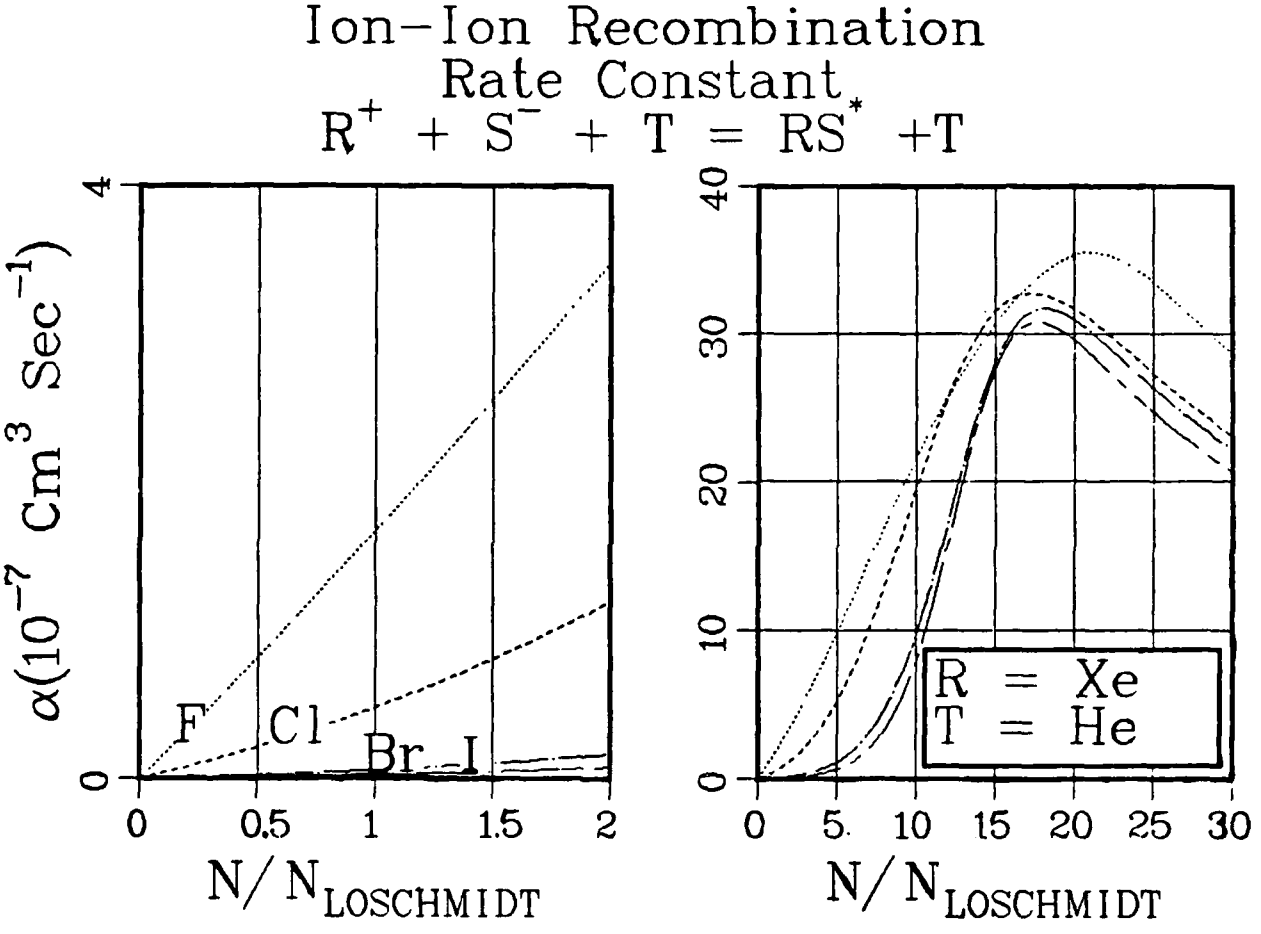

Fig. B-1.A. 16. Ion-ion recombination rate constants for the indicated processes and gases as a function of neutral gas density normalized by Loschmidt's number. The results for S = F, Cl, Br, and I are denoted respectively by dots, dashes, dots and dashes, and short and long dashes.

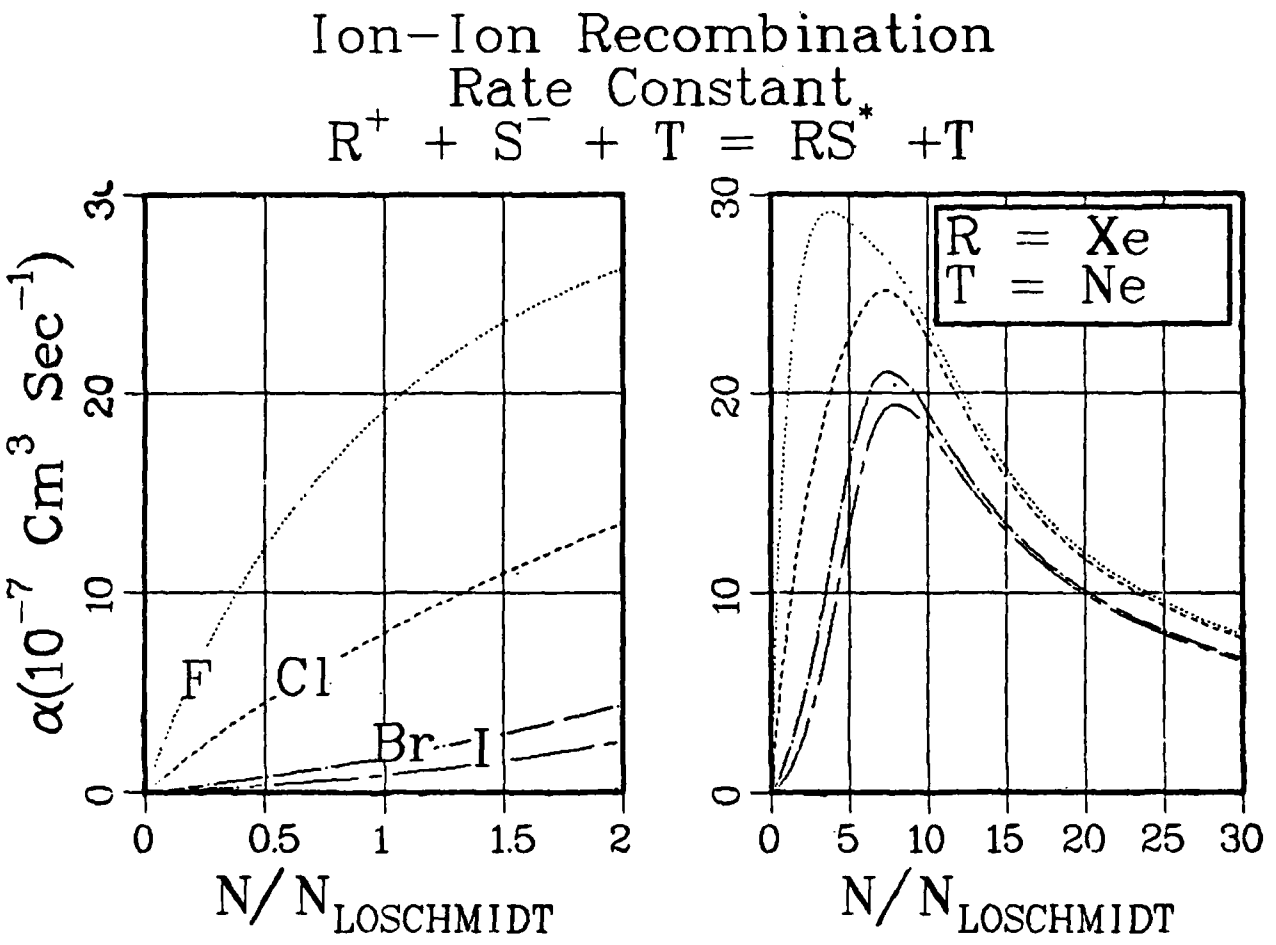

Fig. B-1.A. 17. Ion-ion recombination rate constants for the indicated processes and gases as a function of neutral gas density normalized by Loschmidt's number. The results for S = F, Cl, Br, and I are denoted respectively by dots, dashes, dots and dashes, and short and long dashes.

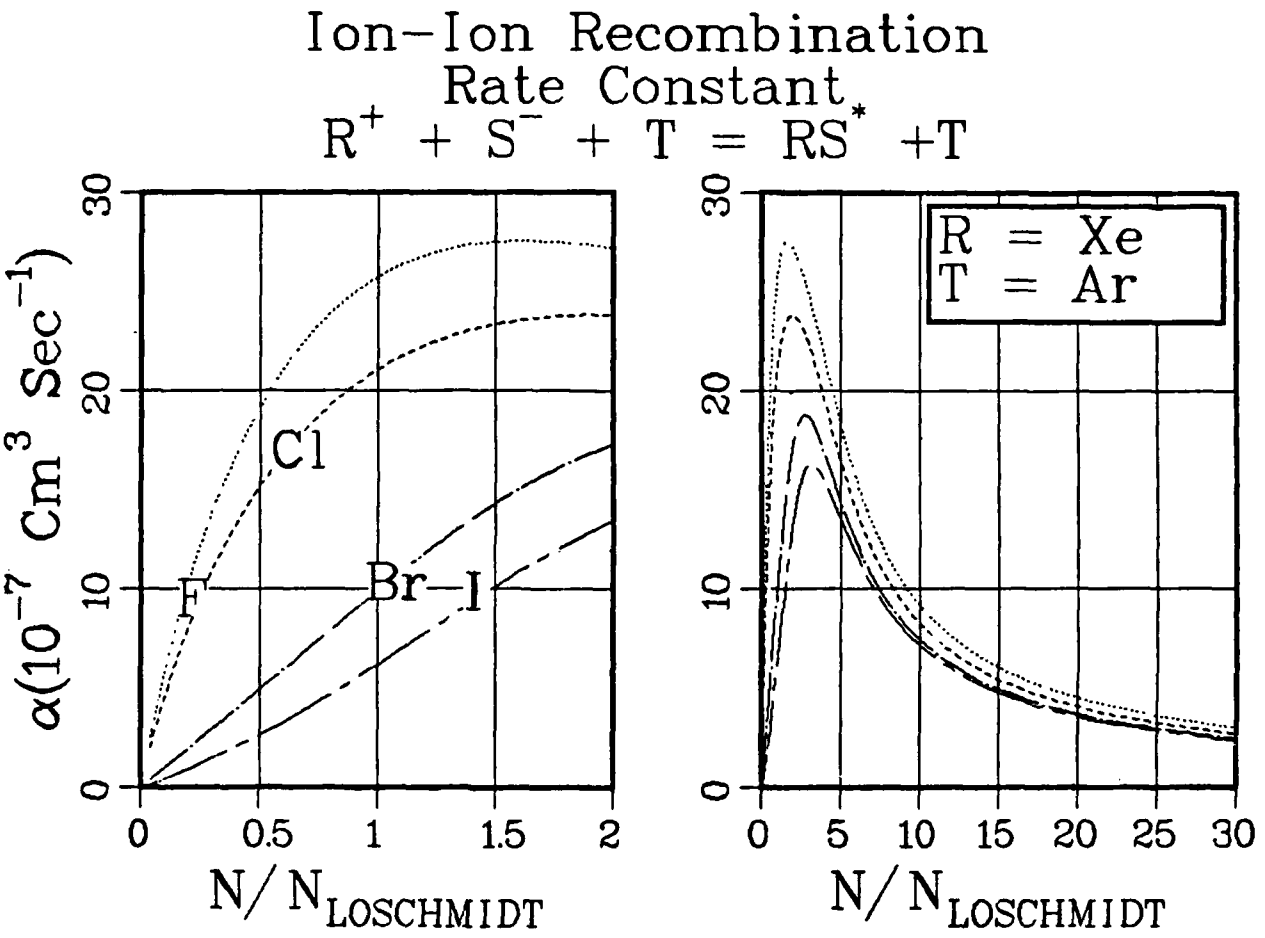

Fig. B-1.A. 18. Ion-ion recombination rate constants for the indicated processes and gases as a function of neutral gas density normalized by Loschmidt's number. The results for S = F, Cl, Br, and I are denoted respectively by dots, dashes, dots and dashes, and short and long dashes.

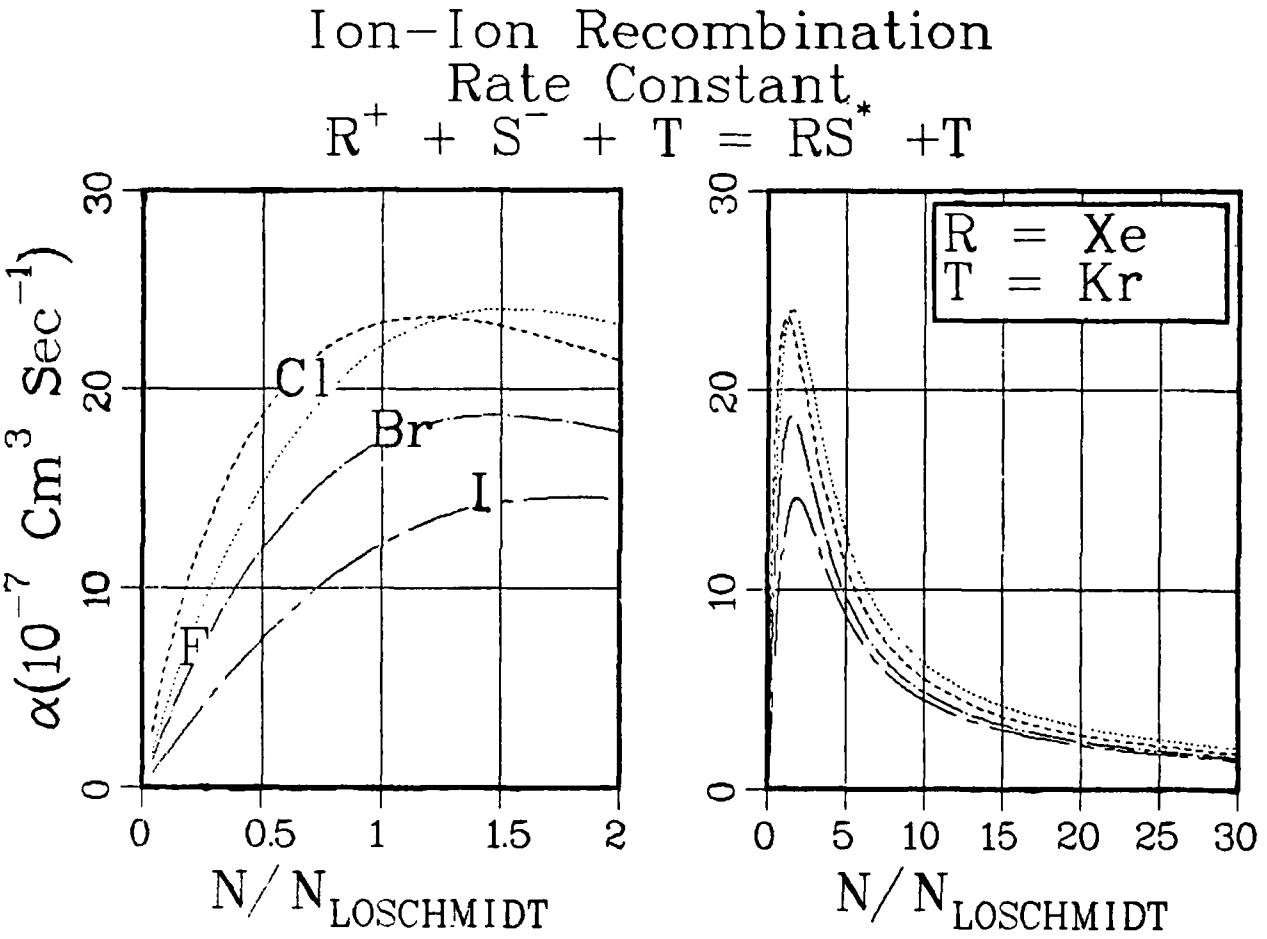

Fig. B-1.A. 19. Ion-ion recombination rate constants for the indicated processes and gases as a function of neutral gas density normalized by Loschmidt's number. The results for S = F, Cl, Br, and I are denoted respectively by dots, dashes, dots and dashes, and short and long dashes.

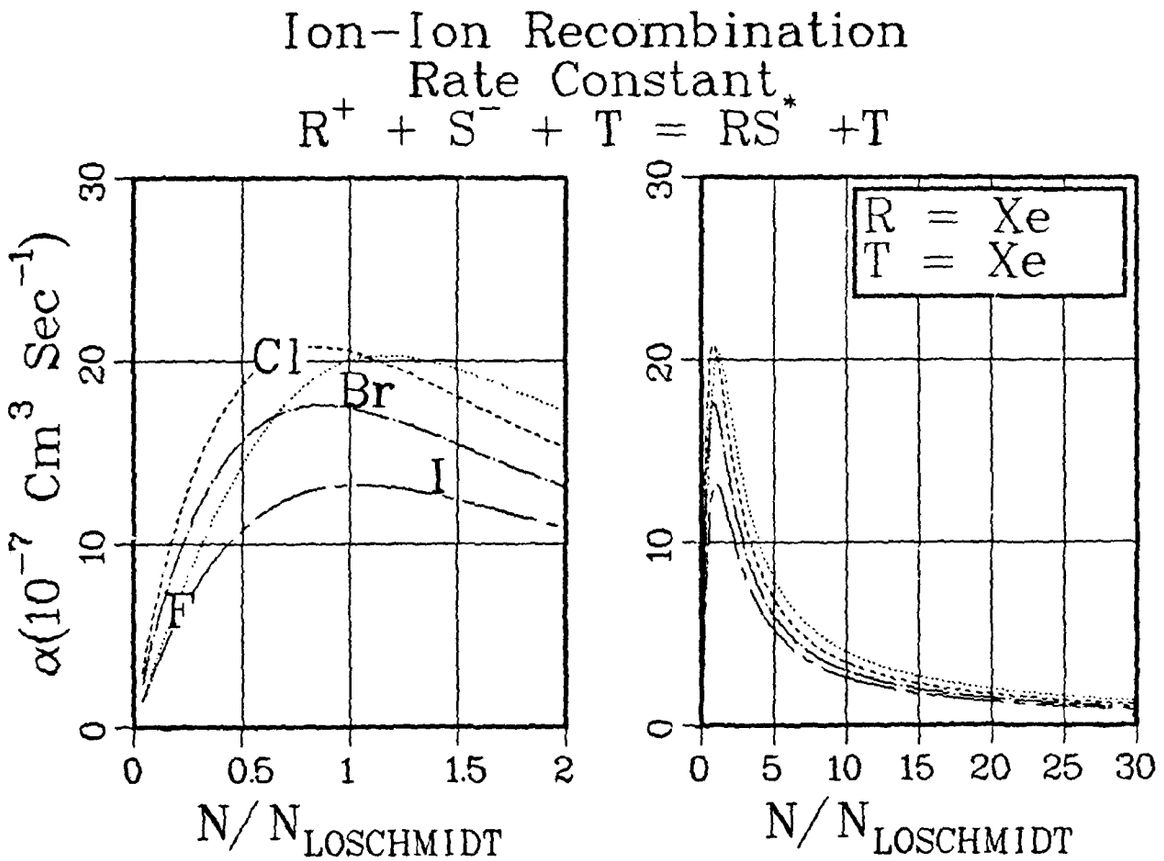

Fig. B-1.A. 20. Ion-ion recombination rate constants for the indicated processes and gases as a function of neutral gas density normalized by Loschmidt's number. The results for S = F, Cl, Br, and I are denoted respectively by dots, dashes, dots and dashes, and short and long dashes.

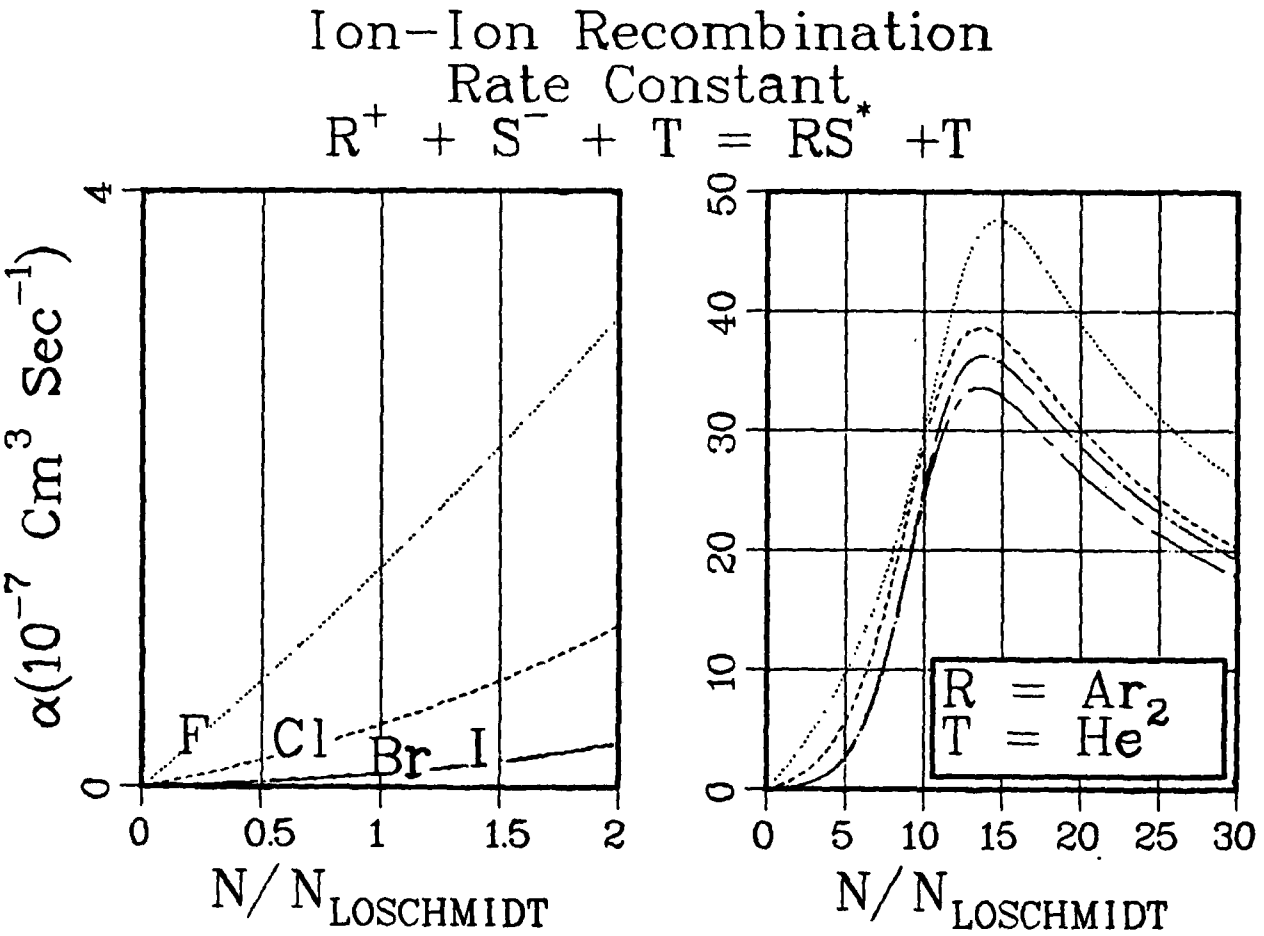

Fig. B-1.A. 21. Ion-ion recombination rate constants for the indicated processes and gases as a function of neutral gas density normalized by Loschmidt's number. The results for S = F, Cl, Br, and I are denoted respectively by dots, dashes, dots and dashes, and short and long dashes.

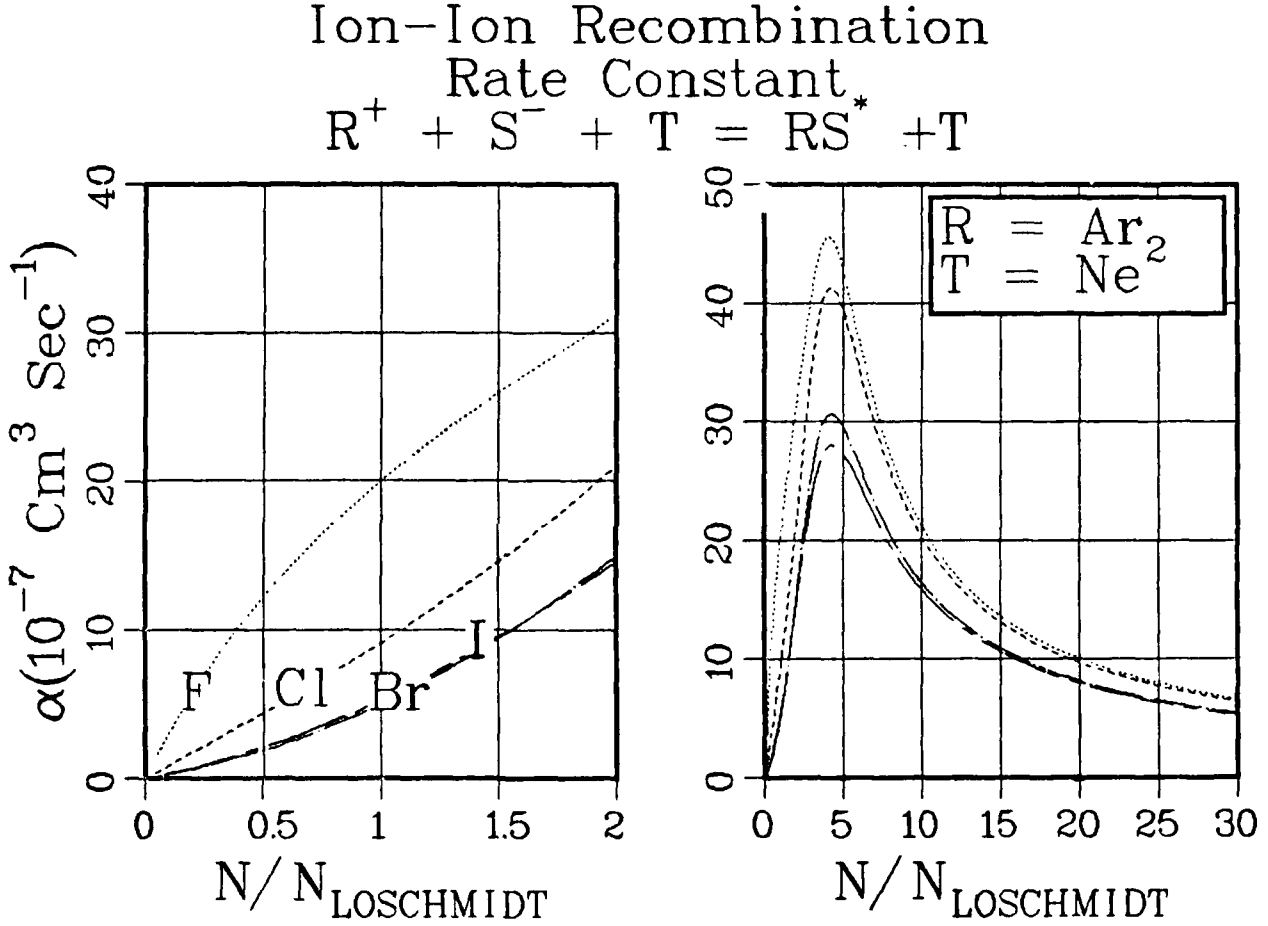

Fig. B-1.A. 22. Ion-ion recombination rate constants for the indicated processes and gases as a function of neutral gas density normalized by Loschmidt's number. The results for S = F, Cl, Br, and I are denoted respectively by dots, dashes, dots and dashes, and short and long dashes.

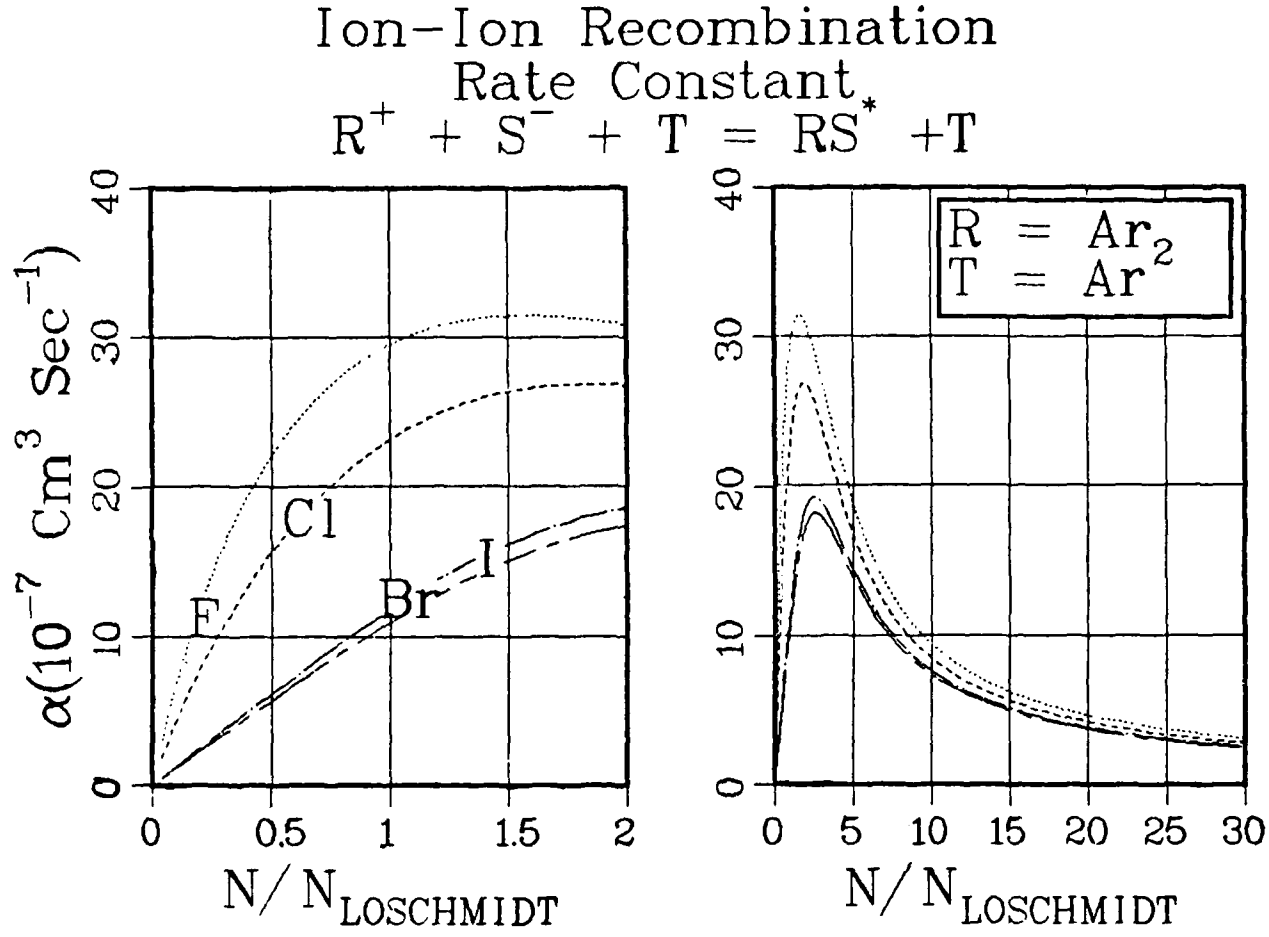

Fig. B-1.A. 23. Ion-ion recombination rate constants for the indicated processes and gases as a function of neutral gas density normalized by Loschmidt's number. The results for S = F, Cl, Br, and I are denoted respectively by dots, dashes, dots and dashes, and short and long dashes.

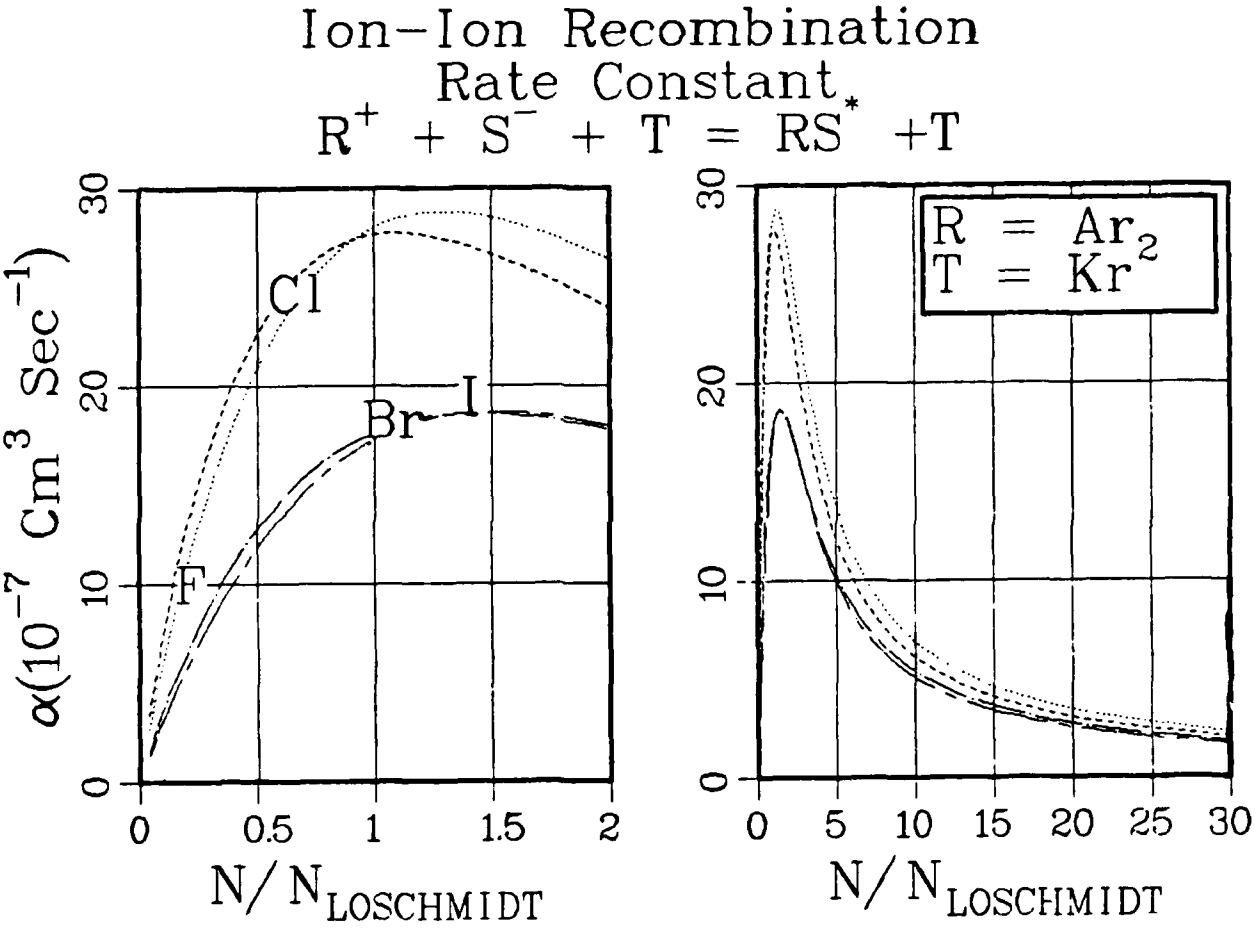

Fig. B-1.A. 24. Ion-ion recombination rate constants for the indicated processes and gases as a function of neutral gas density normalized by Loschmidt's number. The results for S = F, Cl, Br, and I are denoted respectively by dots, dashes, dots and dashes, and short and long dashes.

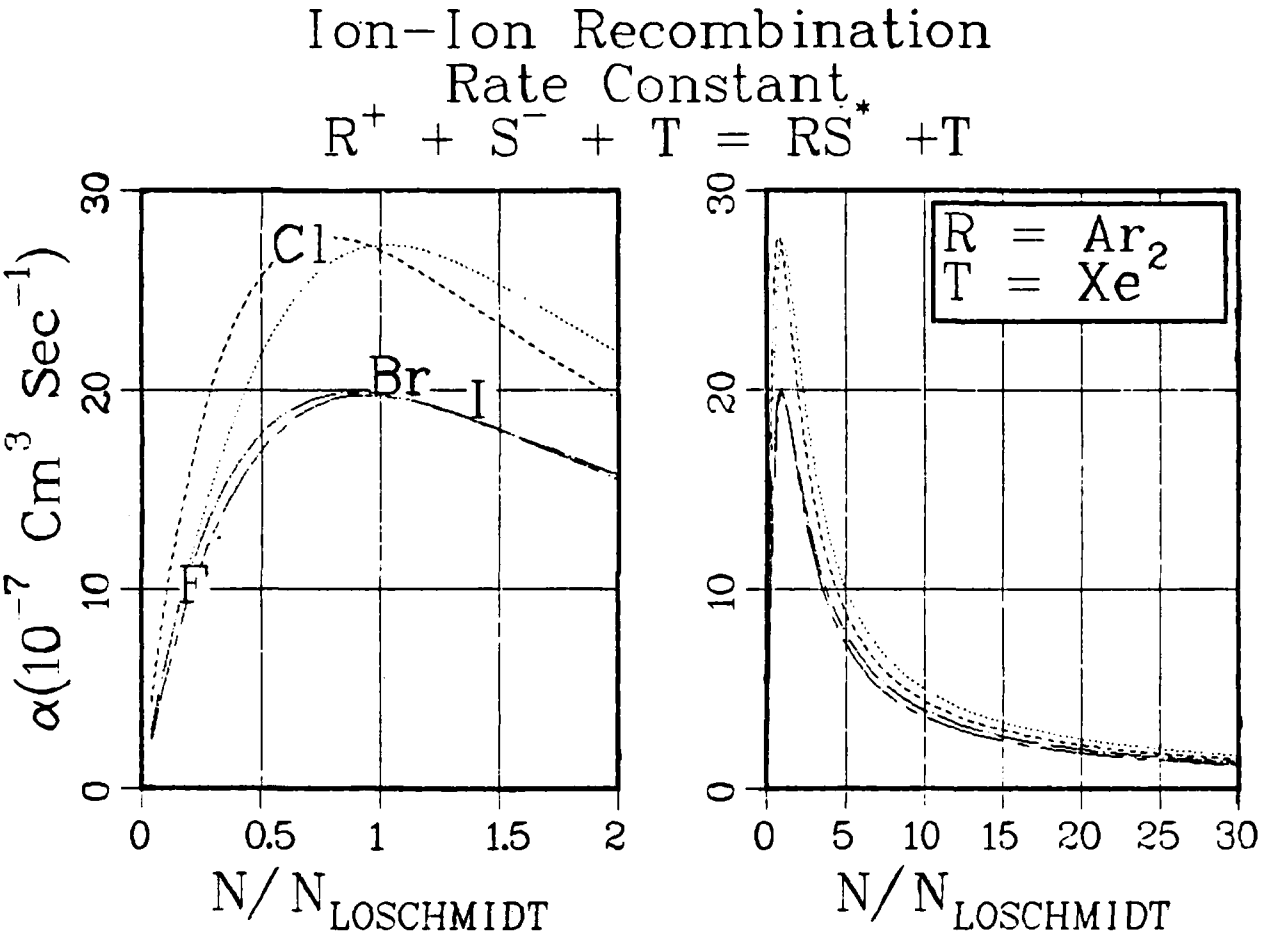

Fig. B-1.A. 25. Ion-ion recombination rate constants for the indicated processes and gases as a function of neutral gas density normalized by Loschmidt's number. The results for S = F, Cl, Br, and I are denoted respectively by dots, dashes, dots and dashes, and short and long dashes.

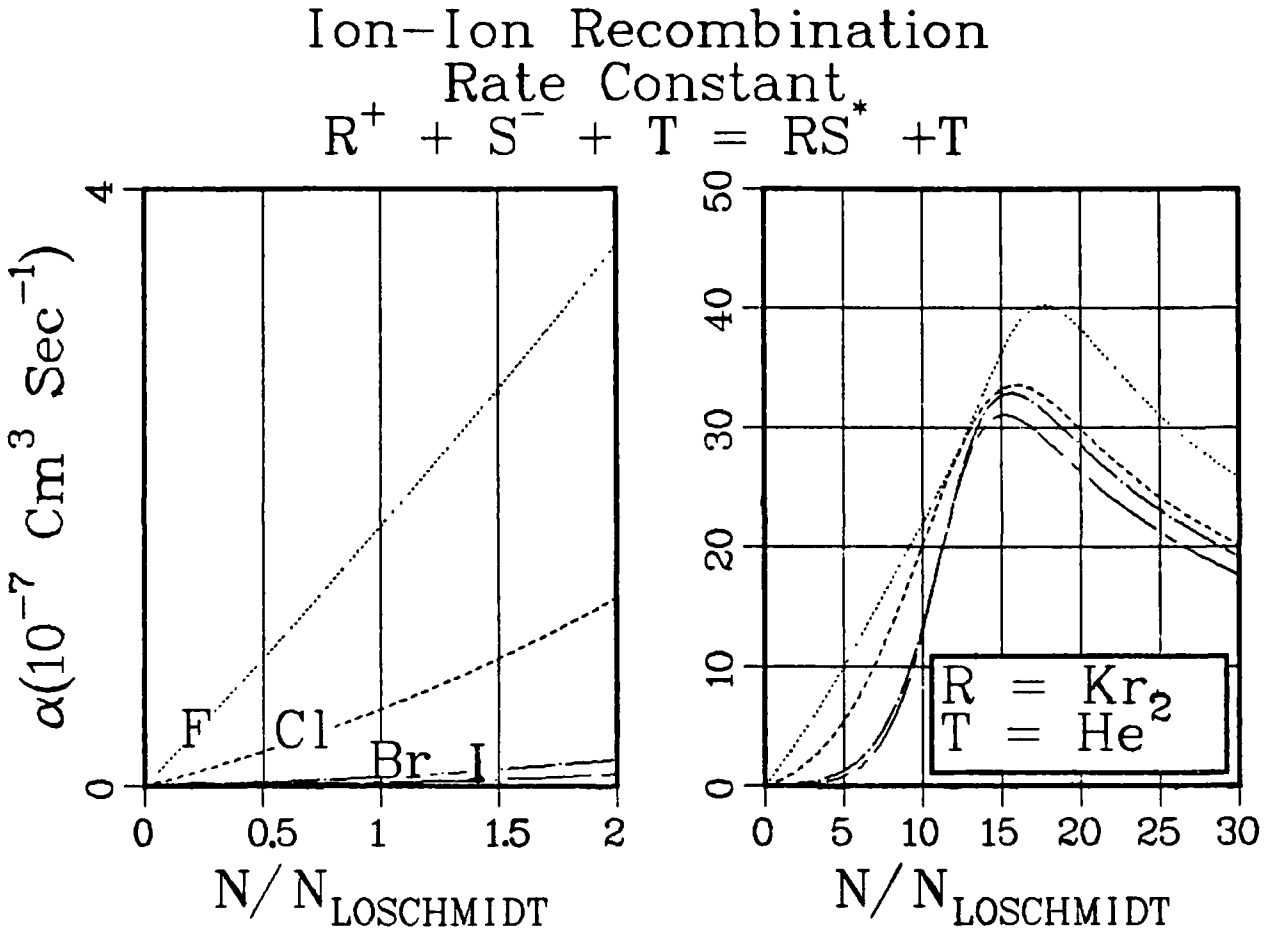

Fig. B-1.A. 26. Ion-ion recombination rate constants for the indicated processes and gases as a function of neutral gas density normalized by Loschmidt's number. The results for S = F, Cl, Br, and I are denoted respectively by dots, dashes, dots and dashes, and short and long dashes.

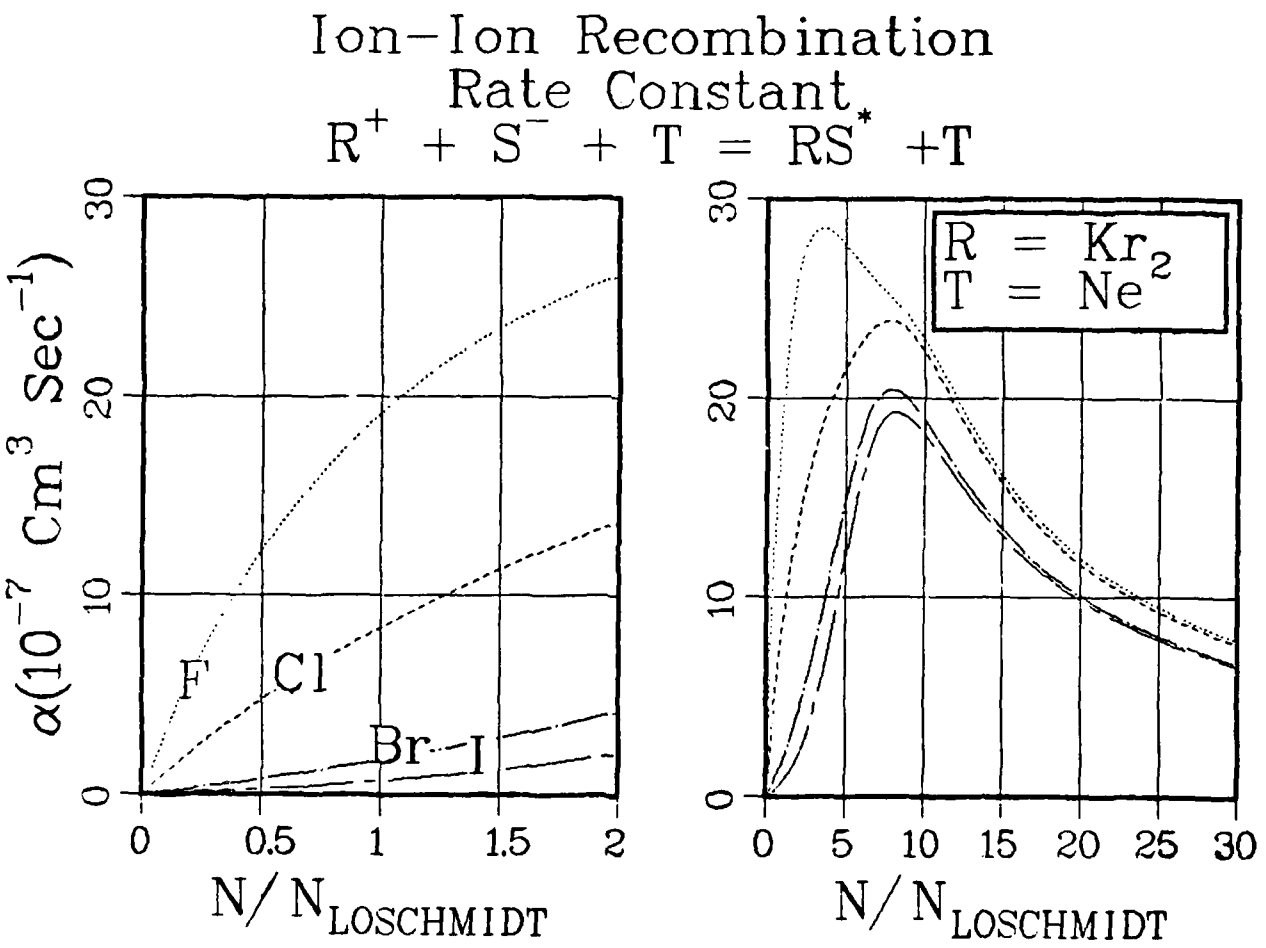

Fig. B-1.A. 27. Ion-Ion recombination rate constants for the indicated processes and gases as a function of neutral gas density normalized by Loschmidt's number. The results for S = F, Cl, Br, and I are denoted respectively by dots, dashes, dots and dashes, and short and long dashes.

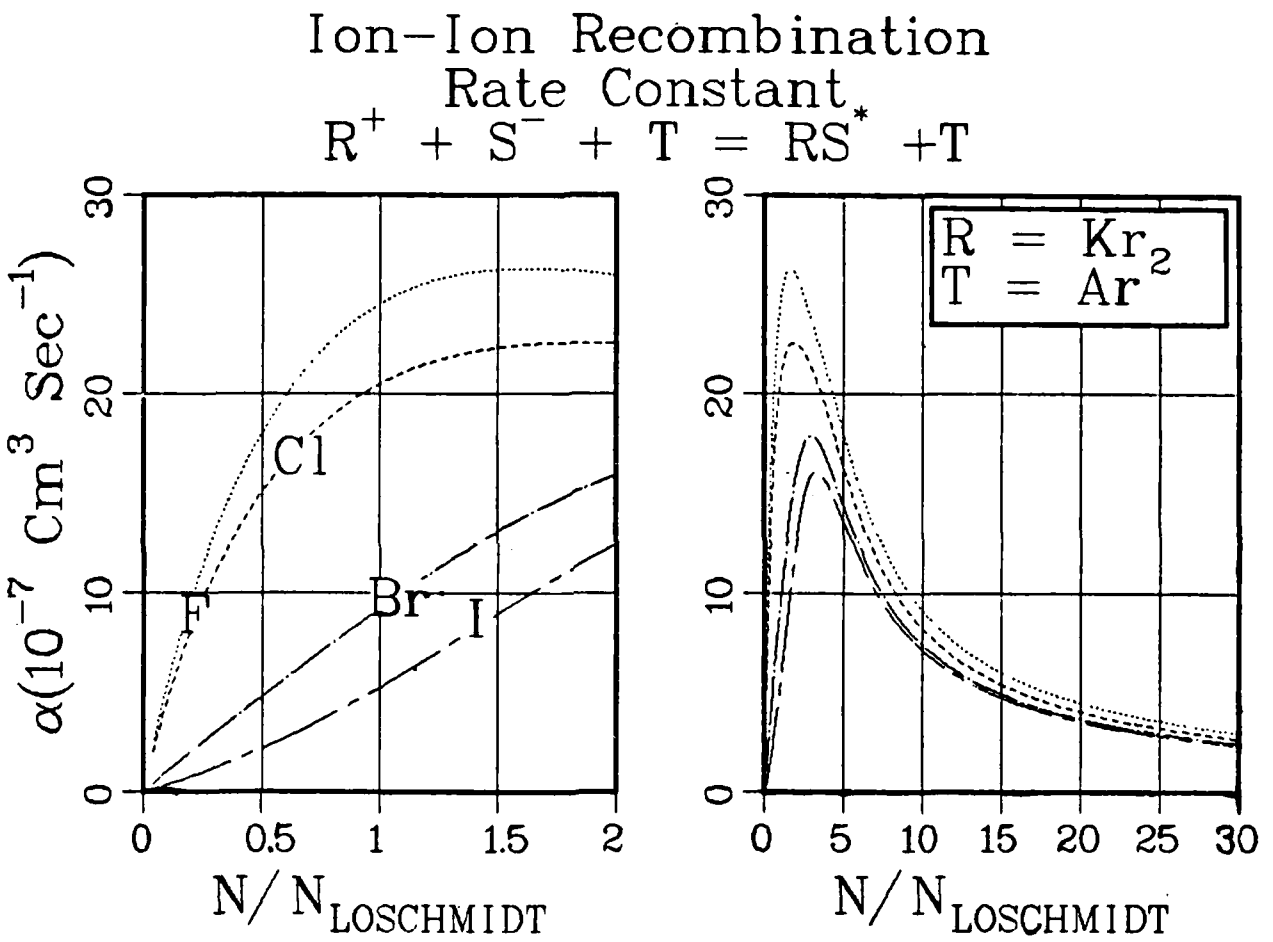

Fig. B-1.A. 28. Ion-ion recombination rate constants for the indicated processes and gases as a function of neutral gas density normalized by Loschmidt's number. The results for S = F, Cl, Br, and I are denoted respectively by dots, dashes, dots and dashes, and short and long dashes.

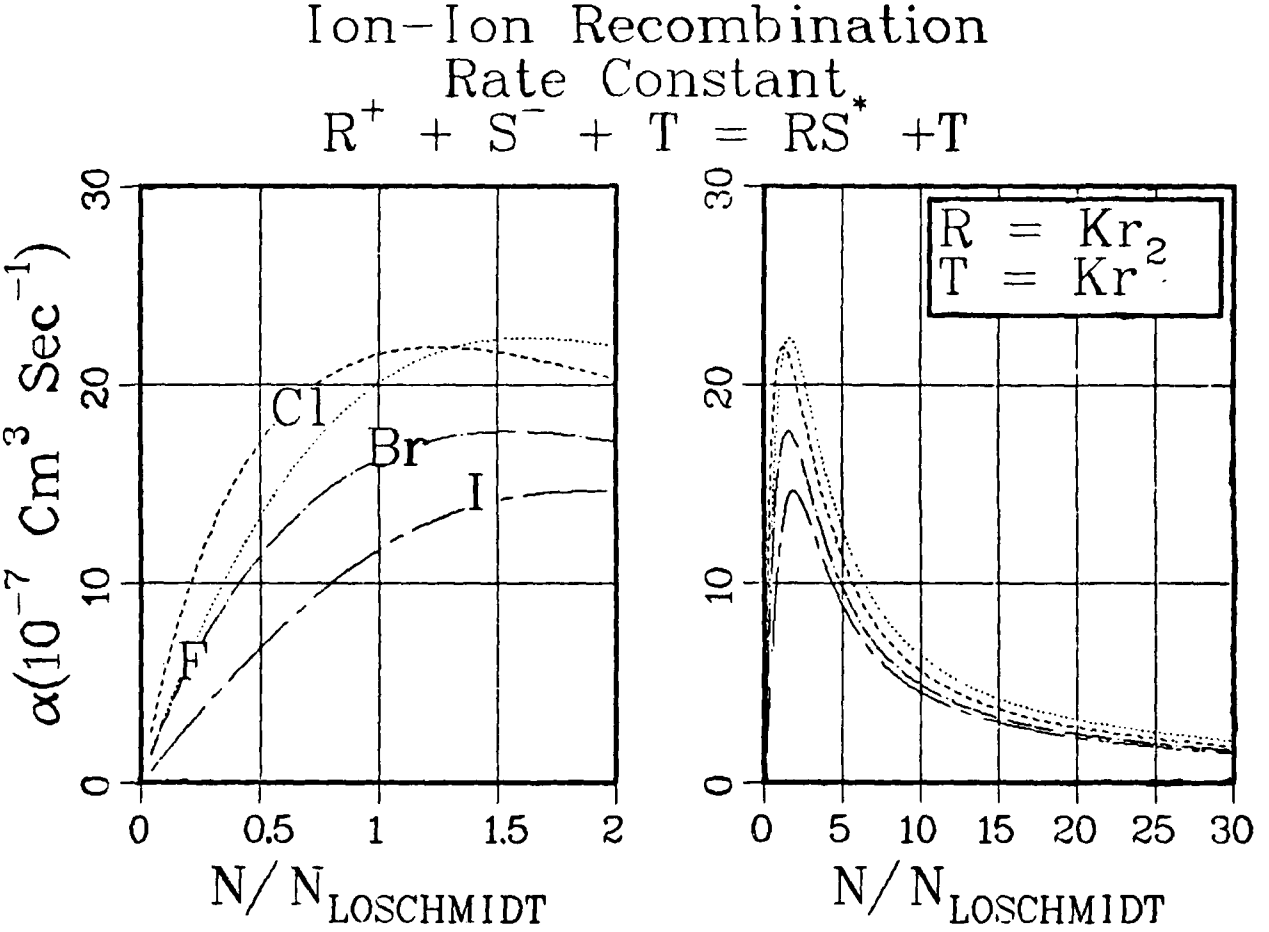

Fig. B-1.A. 29. Ion-ion recombination rate constants for the indicated processes and gases as a function of neutral gas density normalized by Loschmidt's number. The results for S = F, Cl, Br, and I are denoted respectively by dots, dashes, dots and dashes, and short and long dashes.

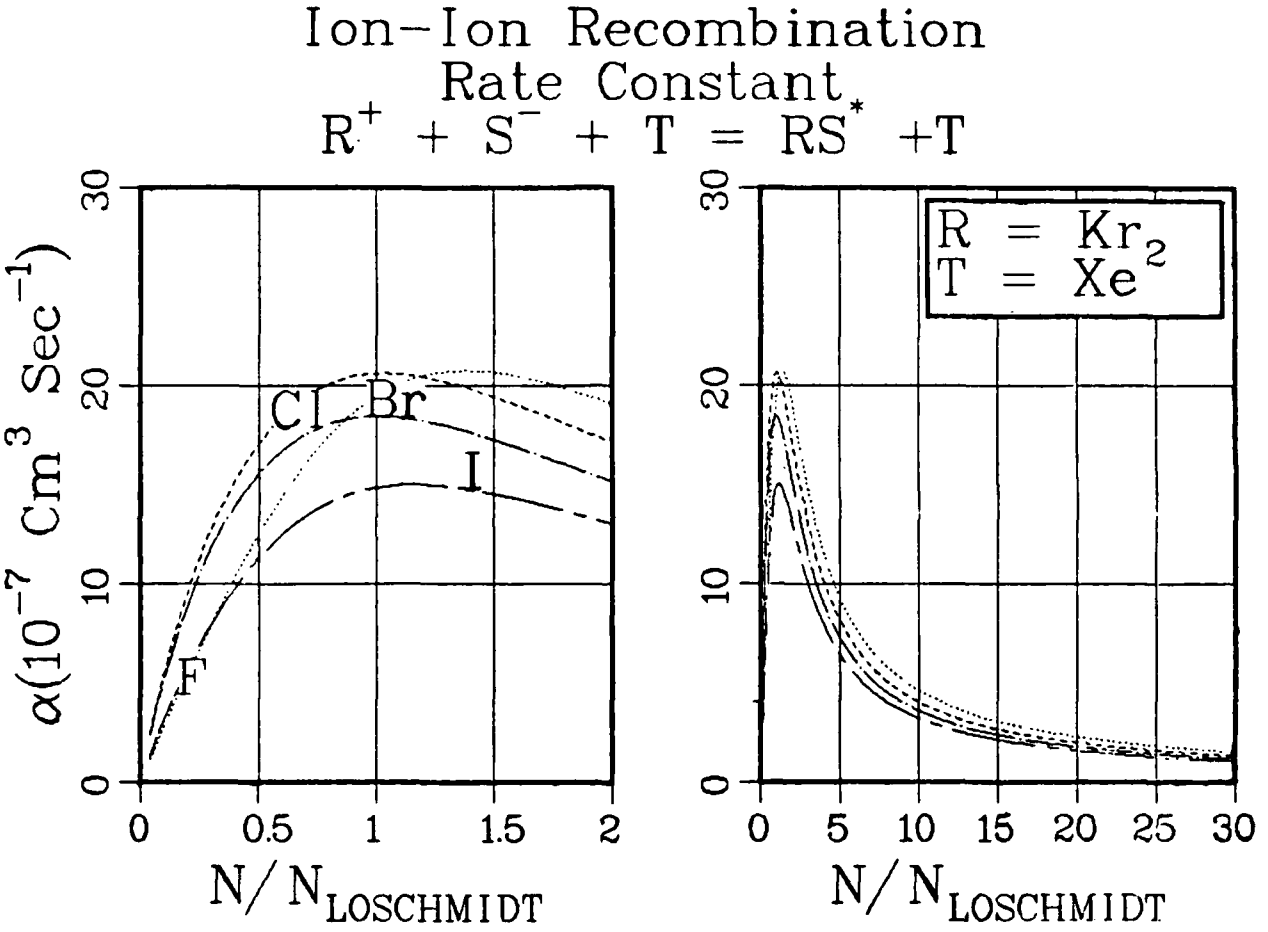

Fig. B-1.A. 30. Ion-ion recombination rate constants for the indicated processes and gases as a function of neutral gas density normalized by Loschmidt's number. The results for S = F, Cl, Br, and I are denoted respectively by dots, dashes, dots and dashes, and short and long dashes.

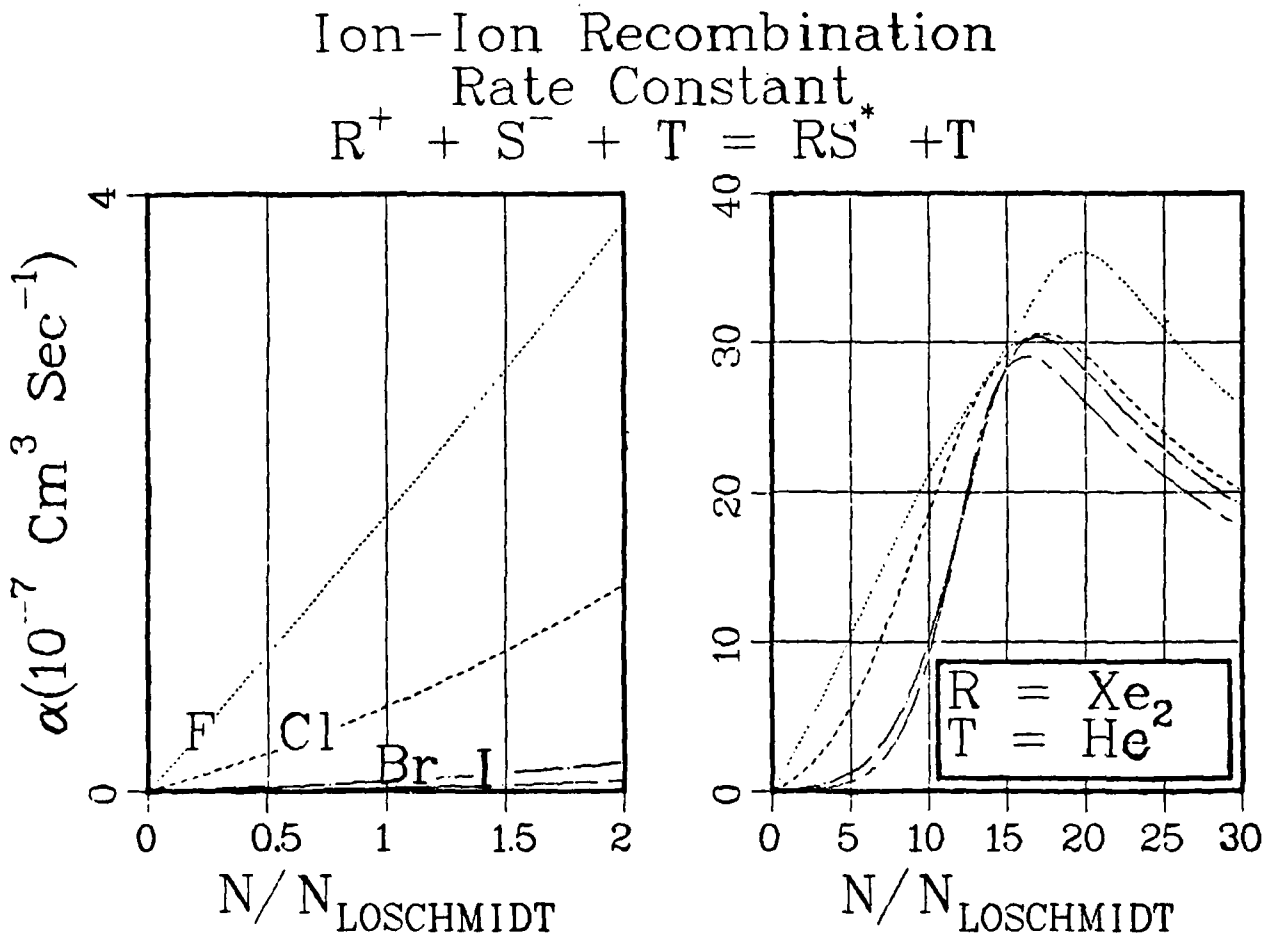

Fig. B-1.A. 31. Ion-ion recombination rate constants for the indicated processes and gases as a function of neutral gas density normalized by Loschmidt's number. The results for S = F, Cl, Br, and I are denoted respectively by dots, dashes, dots and dashes, and short and long dashes.

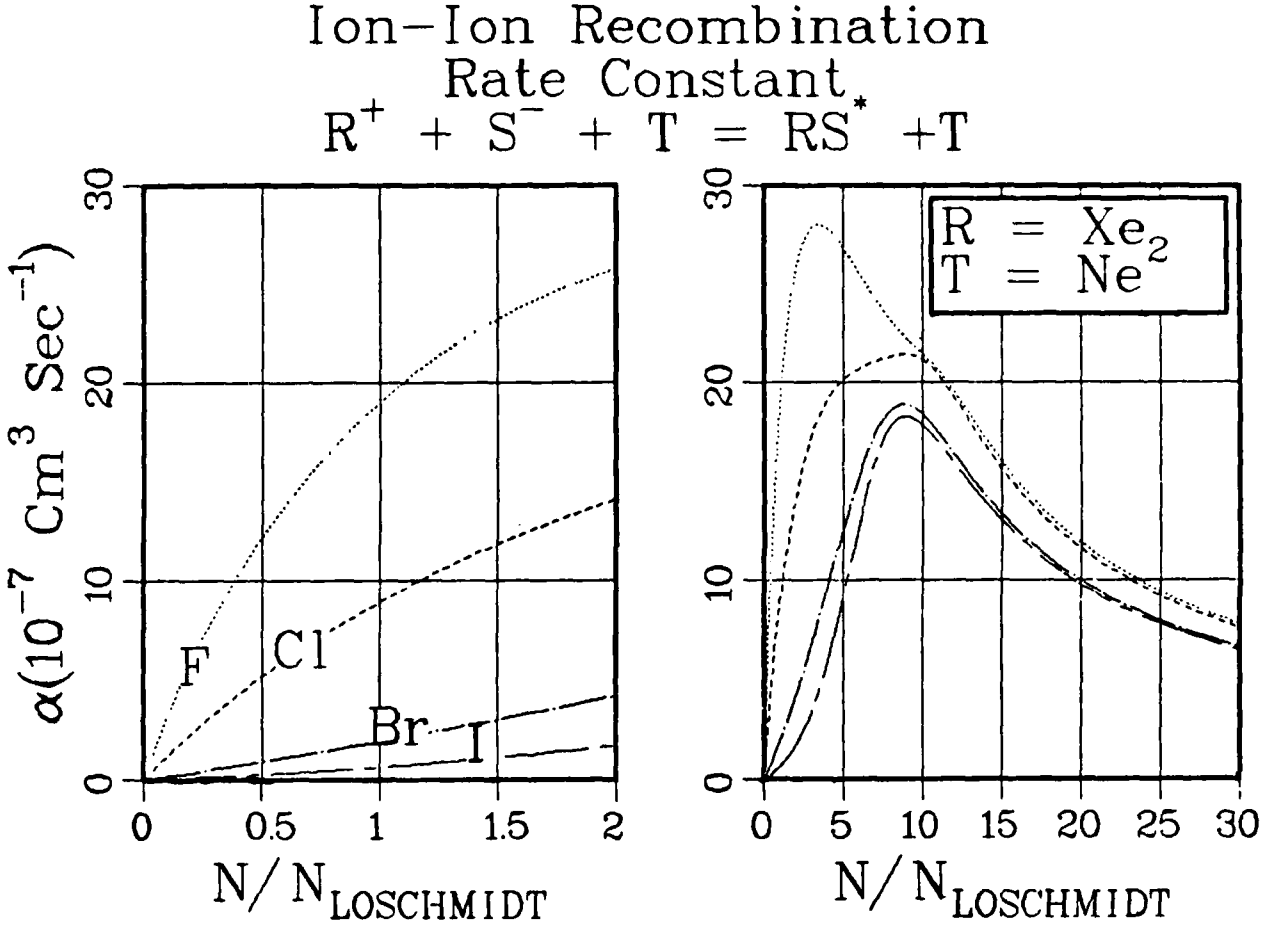

Fig. B-1.A. 32. Ion-ion recombination rate constants for the indicated processes and gases as a function of neutral gas density normalized by Loschmidt's number. The results for S = F, Cl, Br, and I are denoted respectively by dots, dashes, dots and dashes, and short and long dashes.

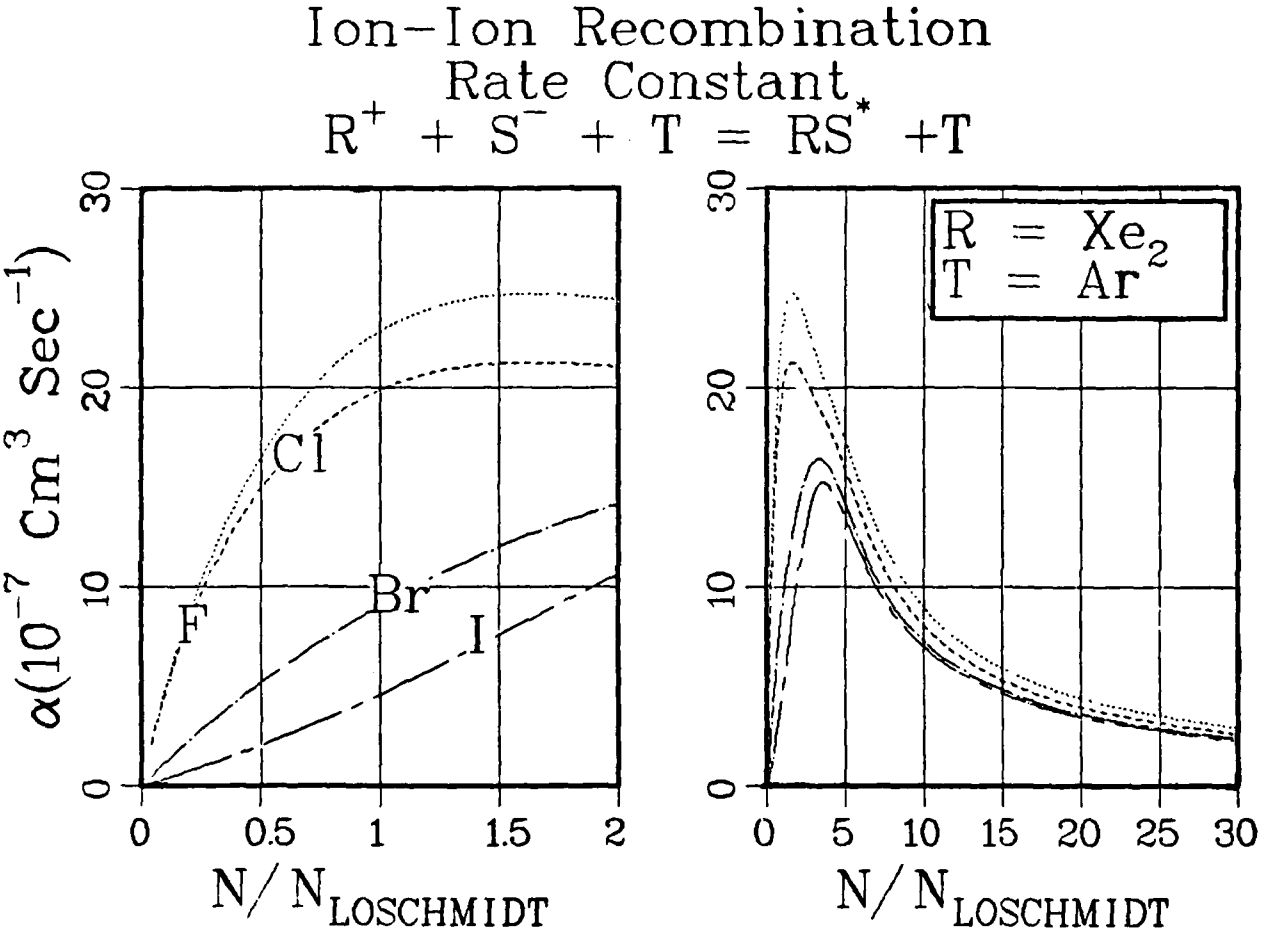

Fig. B-1.A. 33. Ion-ion recombination rate constants for the indicated processes and gases as a function of neutral gas density normalized by Loschmidt's number. The results for S = F, Cl, Br, and I are denoted respectively by dots, dashes, dots and dashes, and short and long dashes.

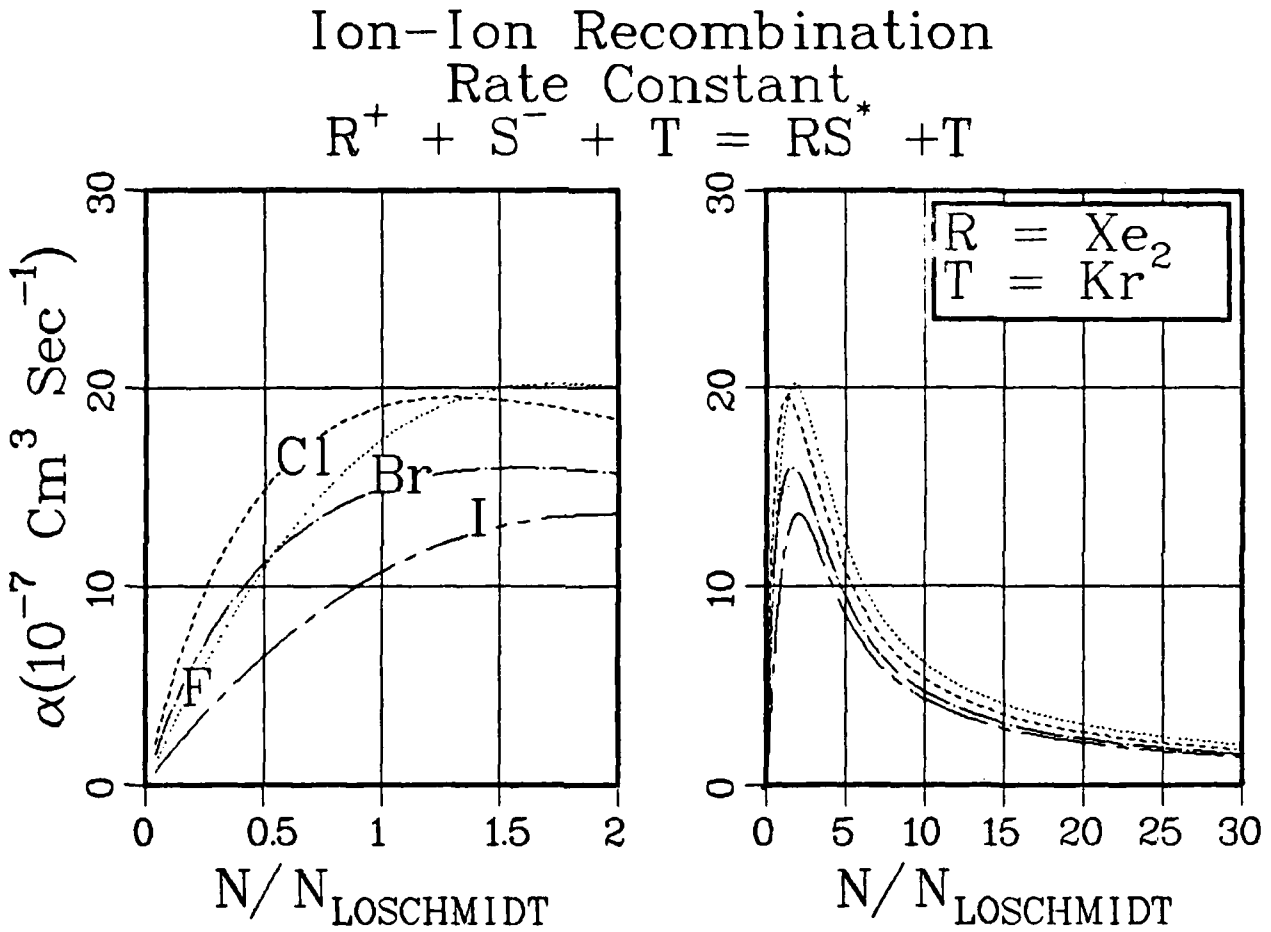

Fig. B-1.A. 34. Ion-ion recombination rate constants for the indicated processes and gases as a function of neutral gas density normalized by Loschmidt's number. The results for S = F, Cl, Br, and I are denoted respectively by dots, dashes, dots and dashes, and short and long dashes.

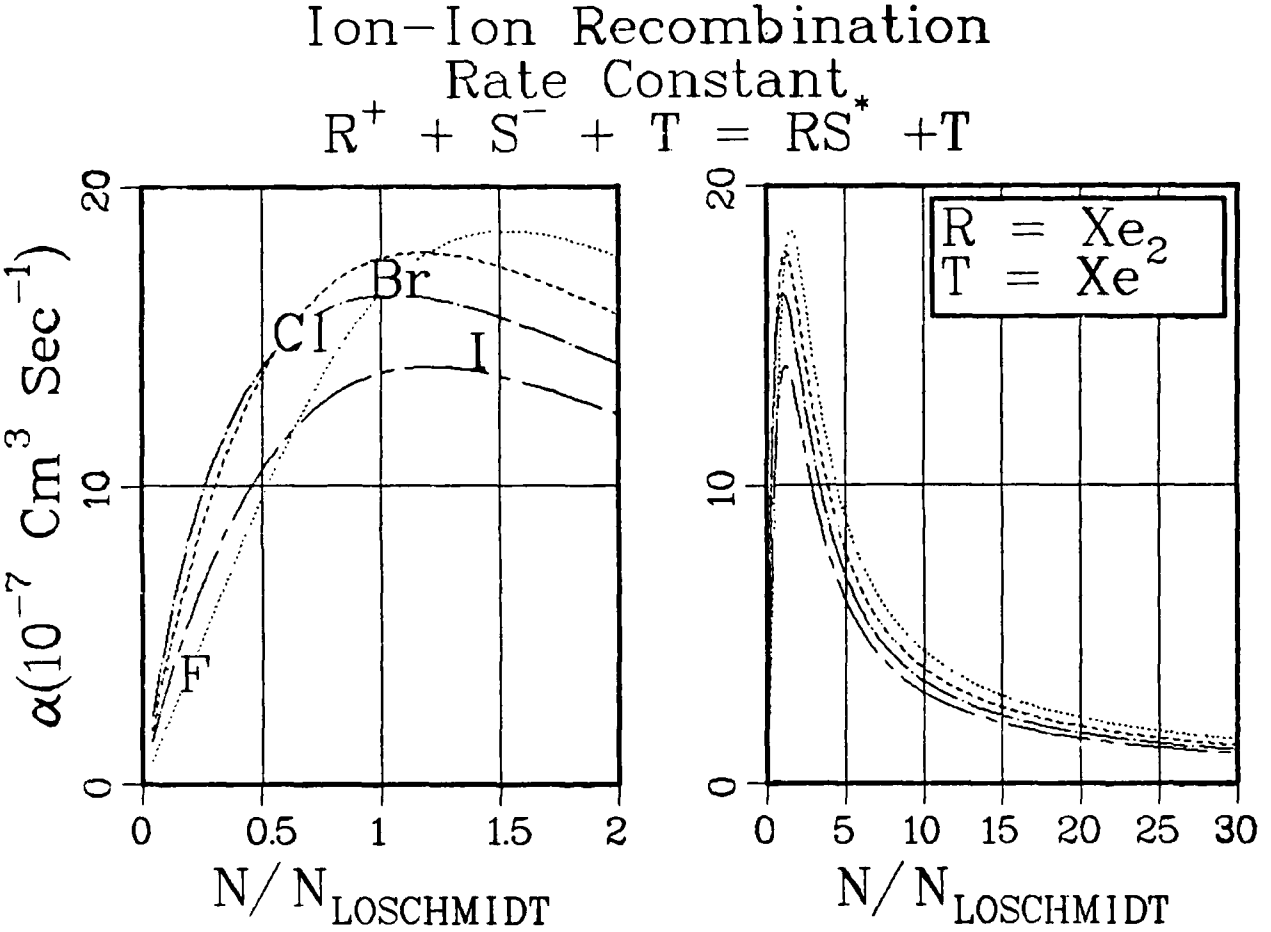

Fig. B.1.A. 35. Ion-ion recombination rate constants for the indicated processes and gases as a function of neutral gas density normalized by Loschmidt's number. The results for S = F, Cl, Br, and I are denoted respectively by dots, dashes, dots and dashes, and short and long dashes.

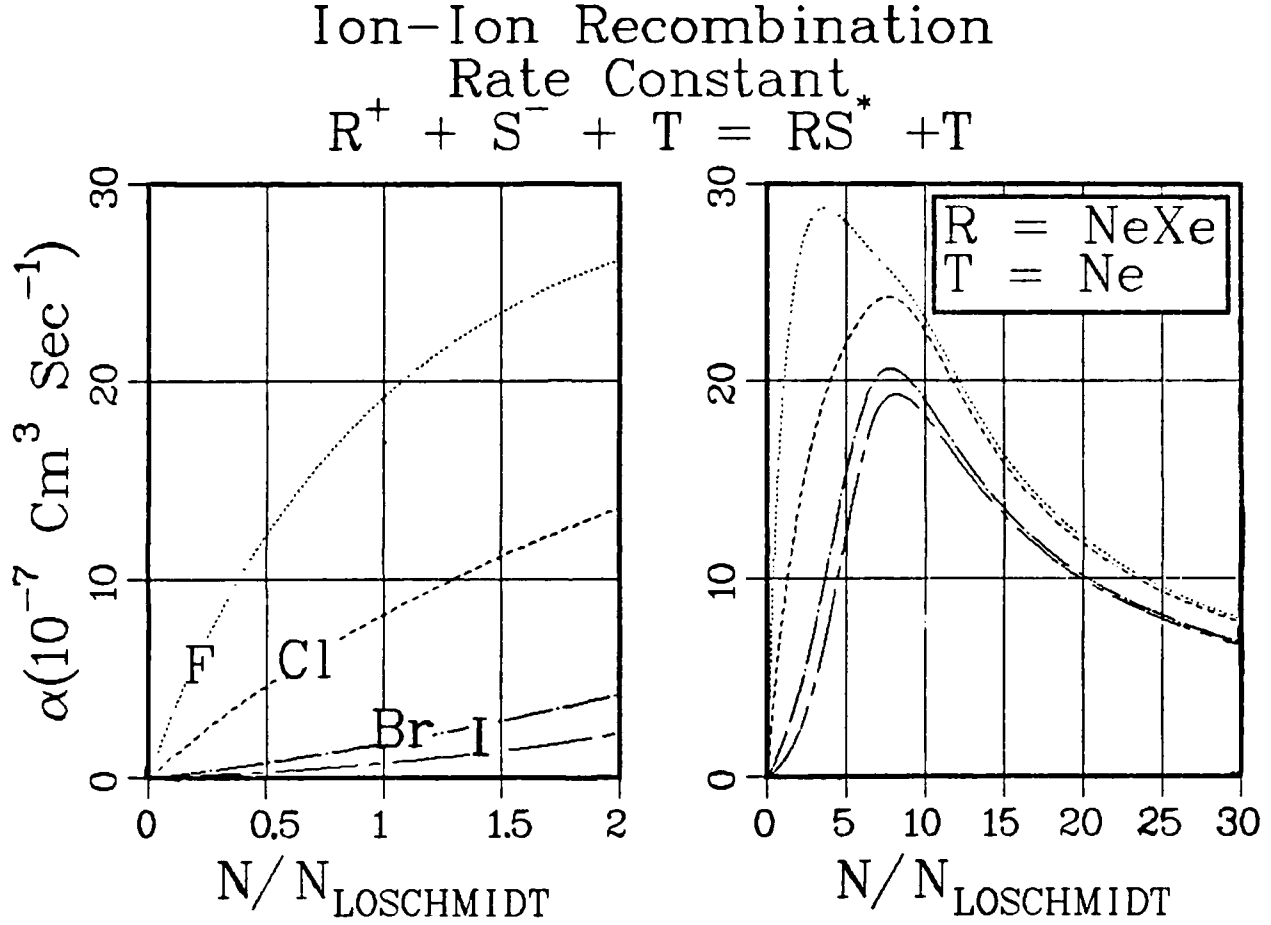

Fig. B-1.A. 36. Ion-ion recombination rate constants for the indicated processes and gases as a function of neutral gas density normalized by Loschmidt's number. The results for S = F, Cl, Br, and I are denoted respectively by dots, dashes, dots and dashes, and short and long dashes.

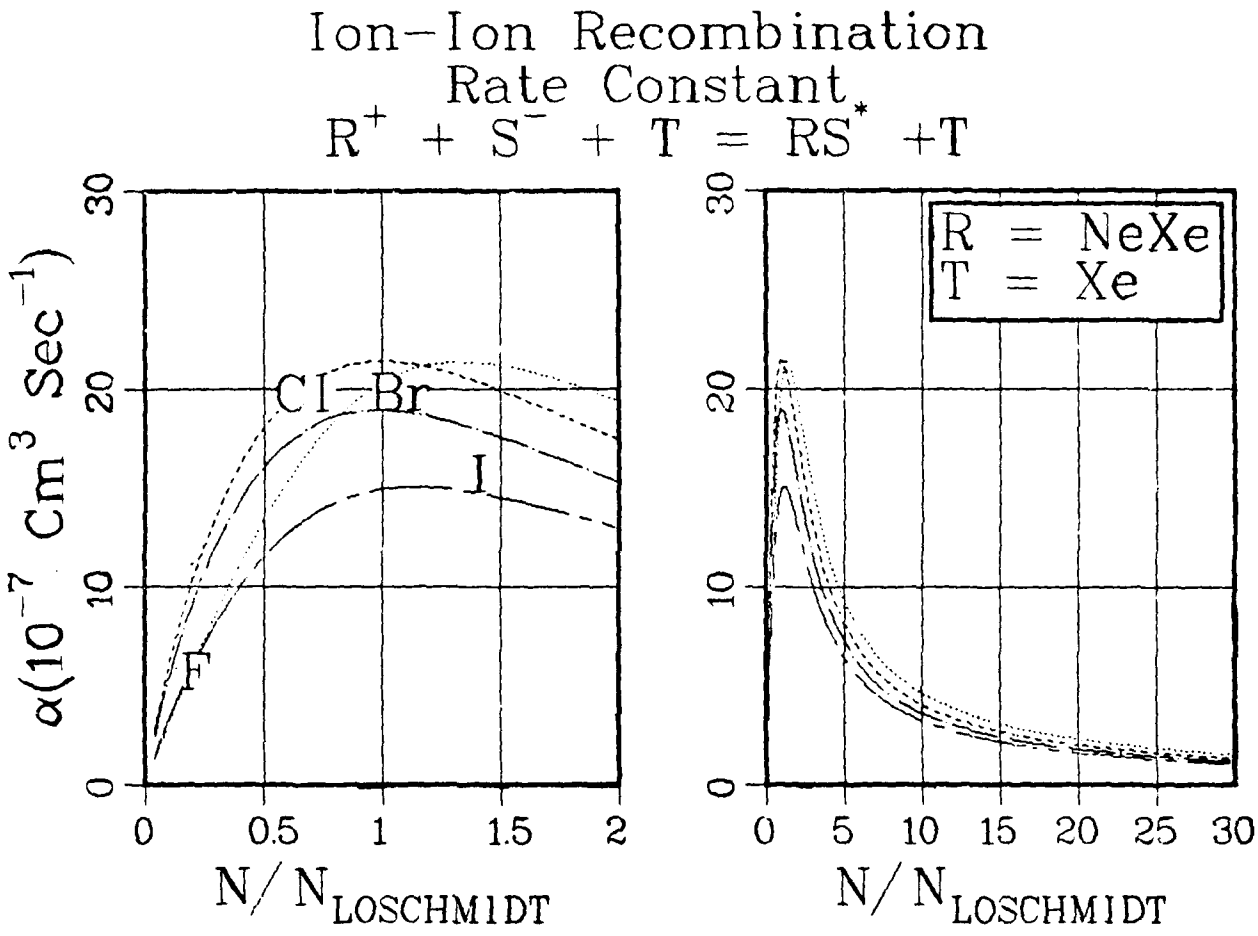

Fig. B.1.A. 37. Ion-ion recombination rate constants for the indicated processes and gases as a function of neutral gas density normalized by Loschmidt's number. The results for S = F, Cl, Br, and I are denoted respectively by dots, dashes, dots and dashes, and short and long dashes.

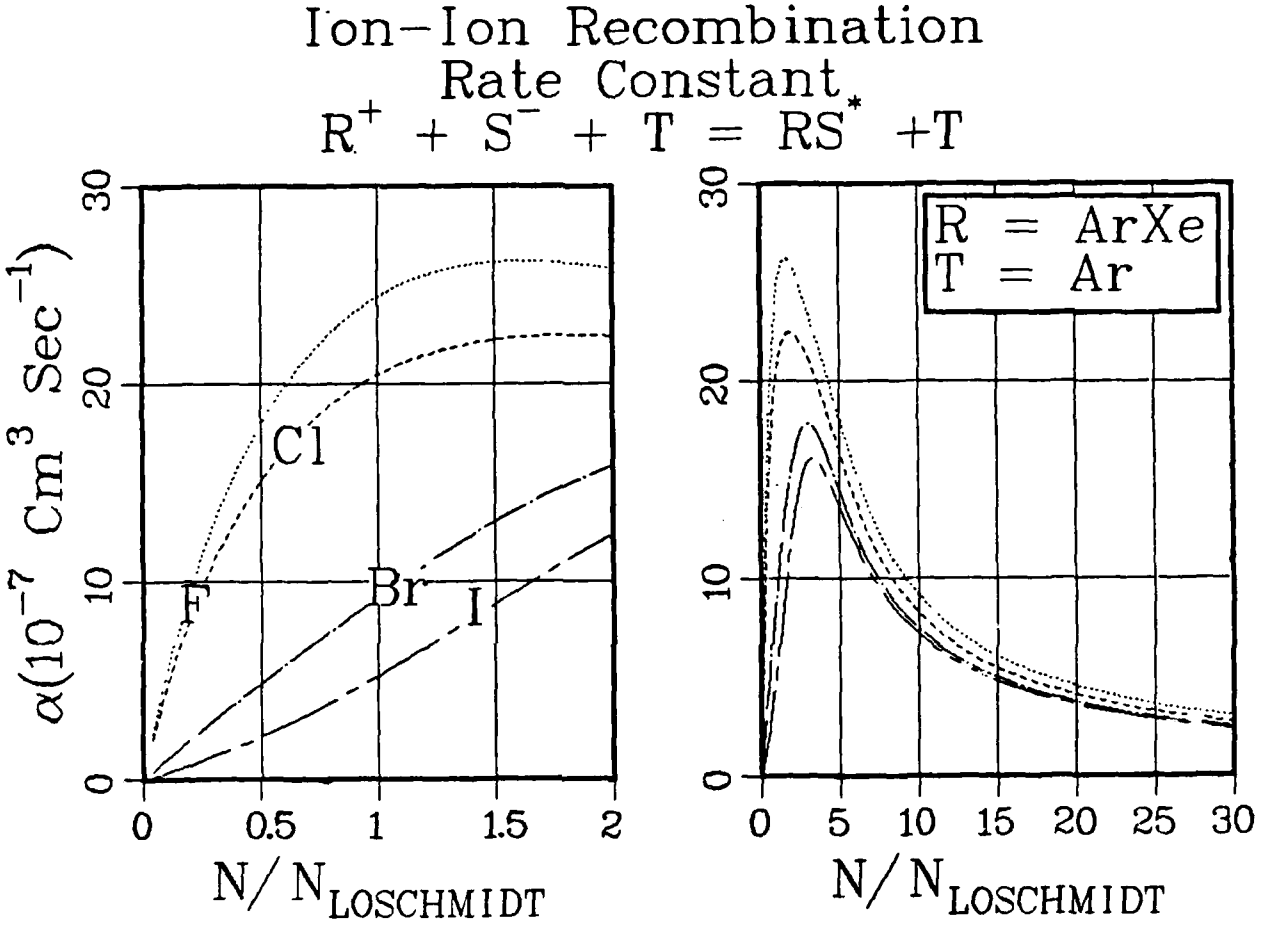

Fig. B-1.A. 38. Ion-ion recombination rate constants for the indicated processes and gases as a function of neutral gas density normalized by Loschmidt's number. The results for S = F, Cl, Br, and I are denoted respectively by dots, dashes, dots and dashes, and short and long dashes.

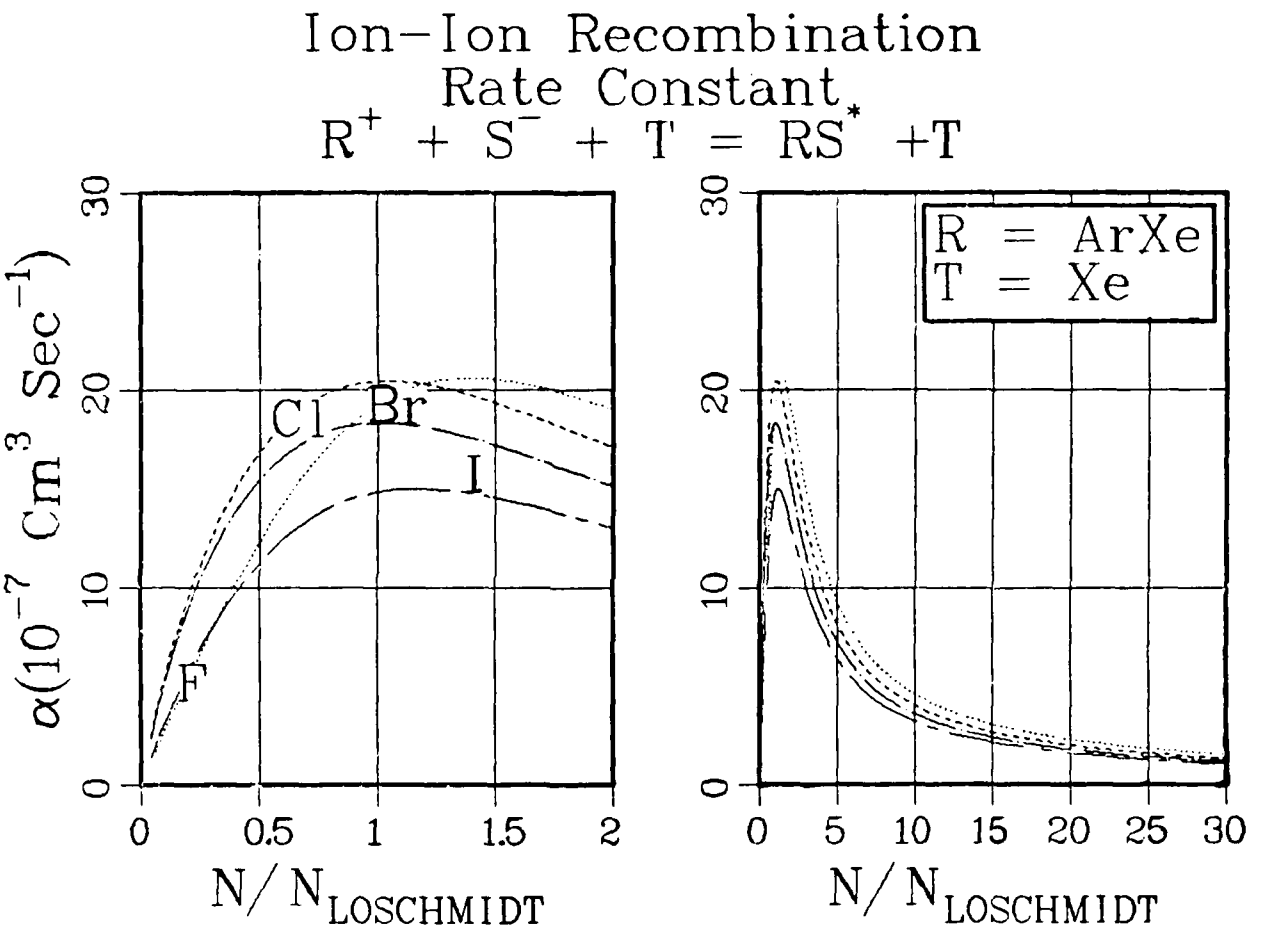

Fig. B-1.A. 39. Ion-ion recombination rate constants for the indicated processes and gases as a function of neutral gas density normalized by Loschmidt's number. The results for S = F, Cl, Br, and I are denoted respectively by dots, dashes, dots and dashes, and short and long dashes.

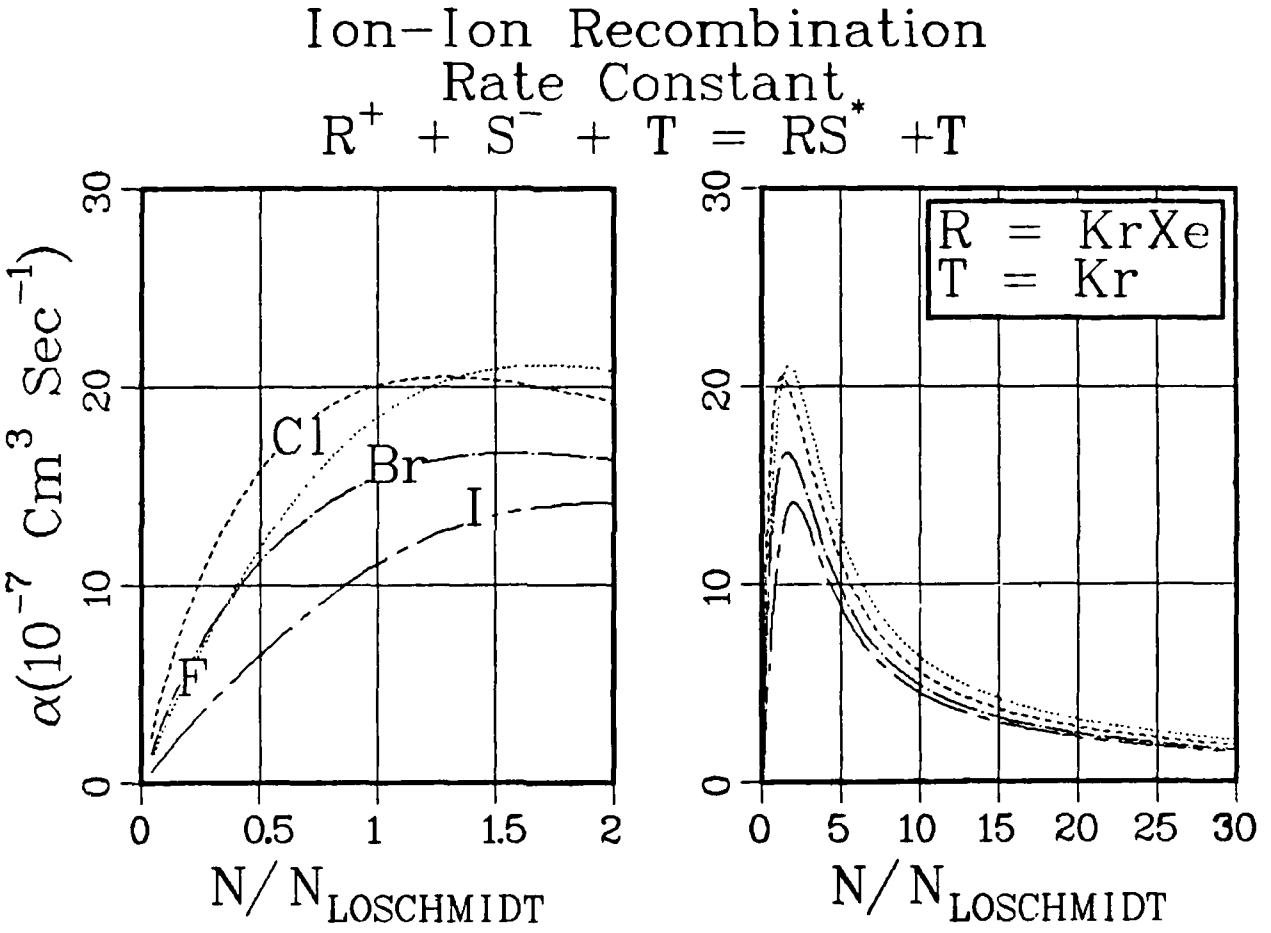

Fig. B-1.A. 40. Ion-ion recombination rate constants for the indicated processes and gases as a function of neutral gas density normalized by Loschmidt's number. The results for S = F, Cl, Br, and I are denoted respectively by dots, dashes, dots and dashes, and short and long dashes.

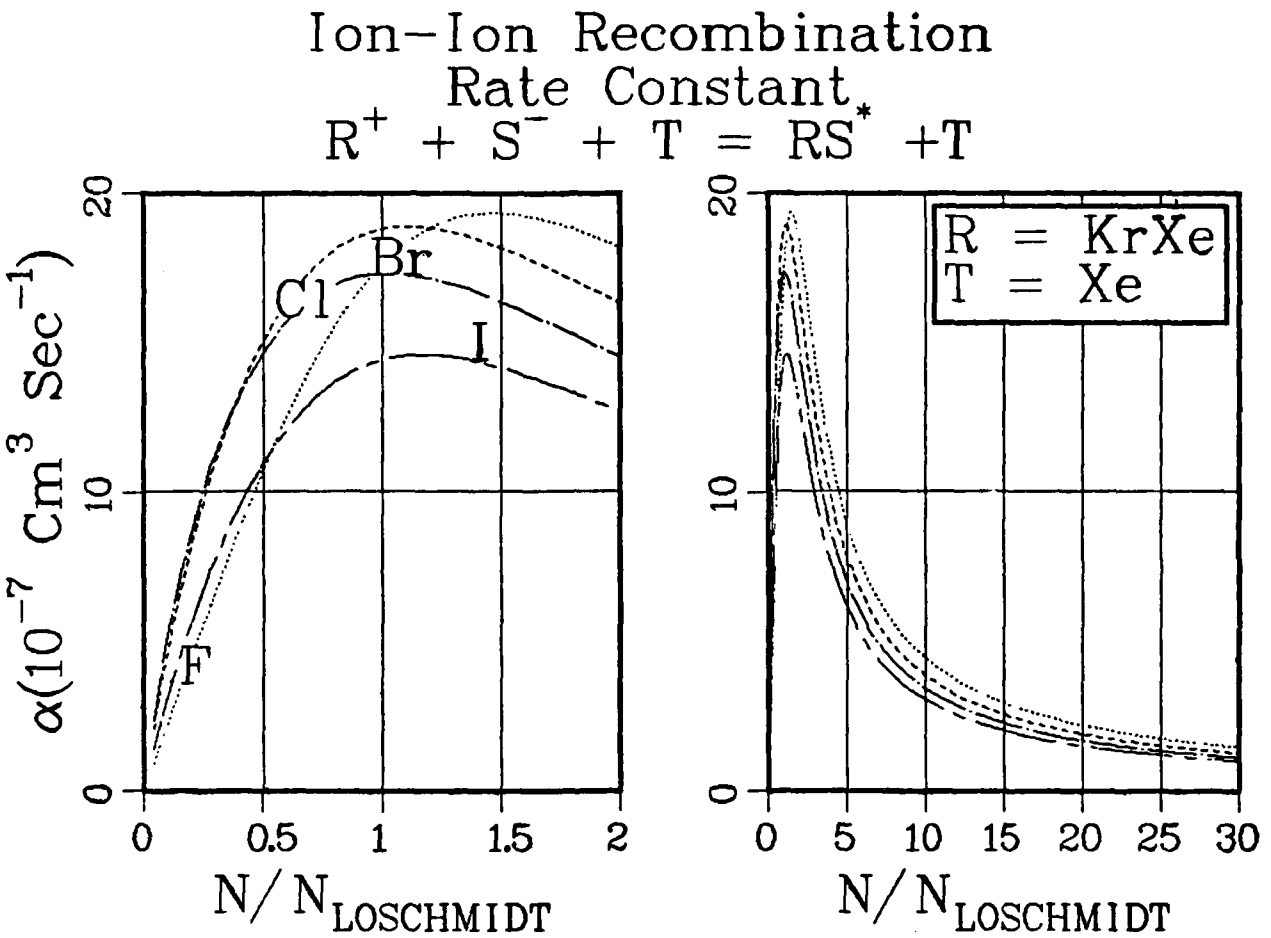

Fig. B-1.A. 41. Ion-ion recombination rate constants for the indicated processes and gases as a function of neutral gas density normalized by Loschmidt's number. The results for S = F, Cl, Br, and I are denoted respectively by dots, dashes, dots and dashes, and short and long dashes.

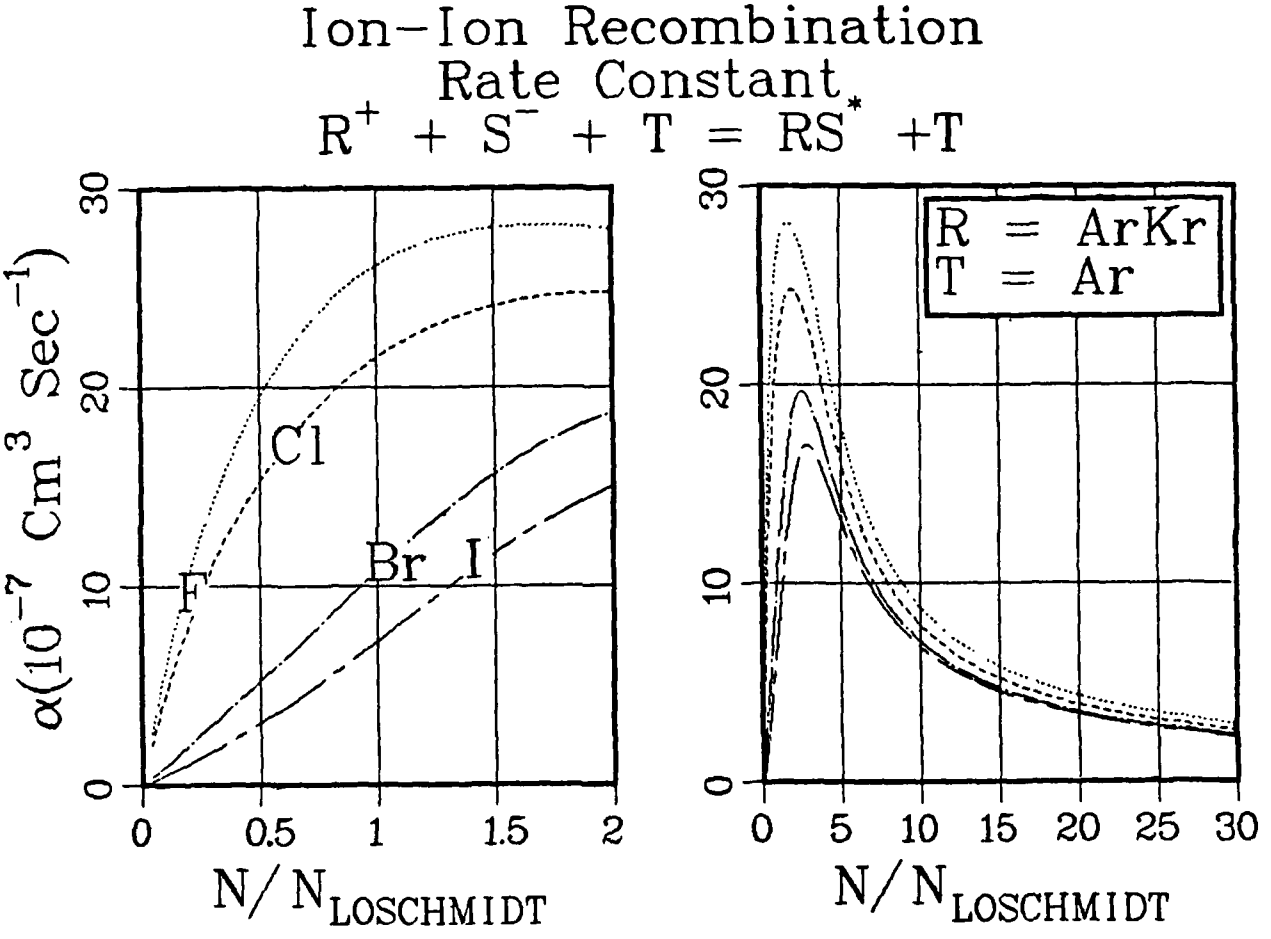

Fig. B-1.A. 42. Ion-ion recombination rate constants for the indicated processes and gases as a function of neutral gas density normalized by Loschmidt's number. The results for S = F, Cl, Br, and I are denoted respectively by dots, dashes, dots and dashes, and short and long dashes.

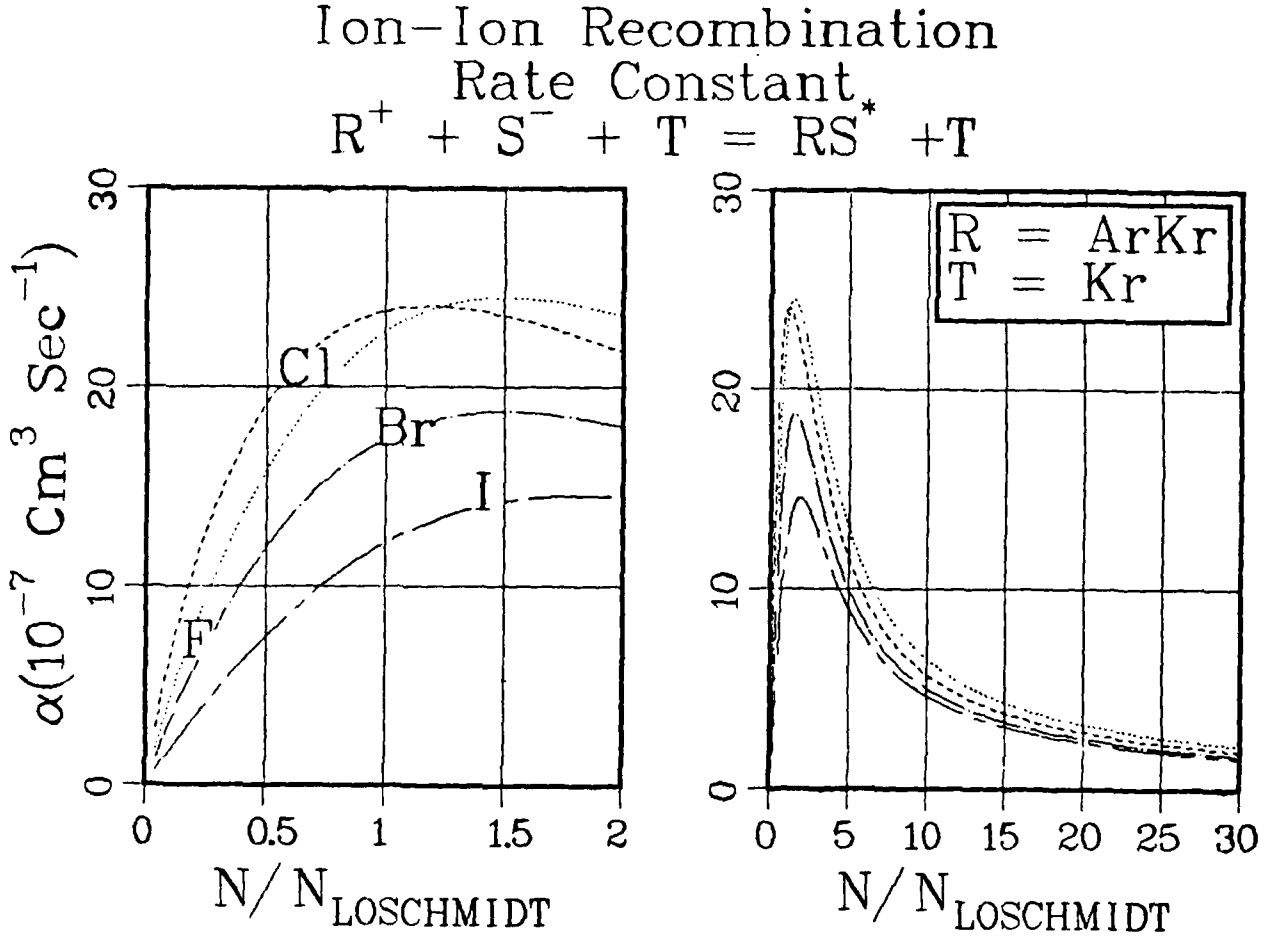

Fig. B-1.A. 43. Ion-ion recombination rate constants for the indicated processes and gases as a function of neutral gas density normalized by Loschmidt's number. The results for S = F, Cl, Br, and I are denoted respectively by dots, dashes, dots and dashes, and short and long dashes.

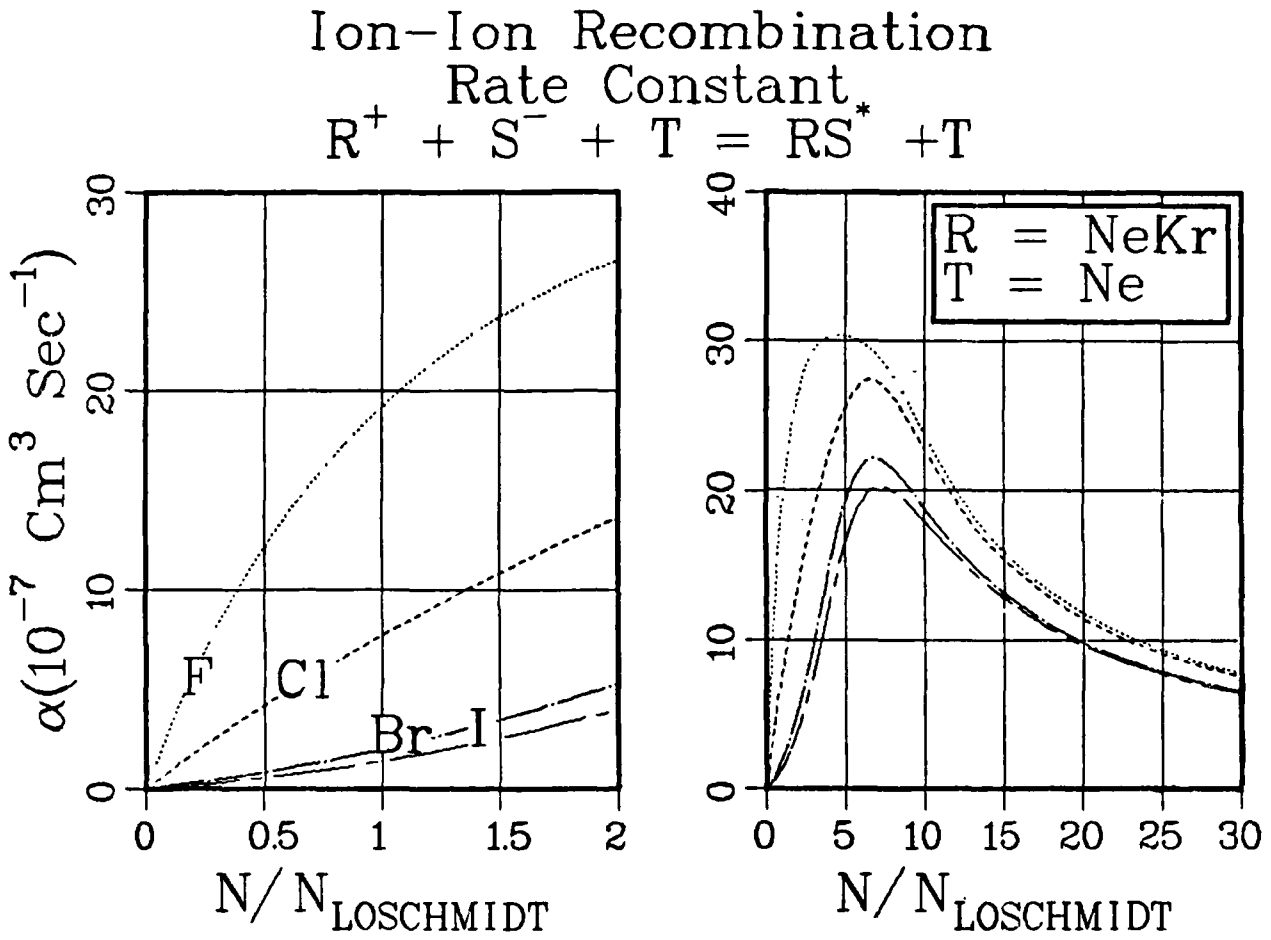

Fig. B-1.A. 44. Ion-ion recombination rate constants for the indicated processes and gases as a function of neutral gas density normalized by Loschmidt's number. The results for S = F, Cl, Br, and I are denoted respectively by dots, dashes, dots and dashes, and short and long dashes.

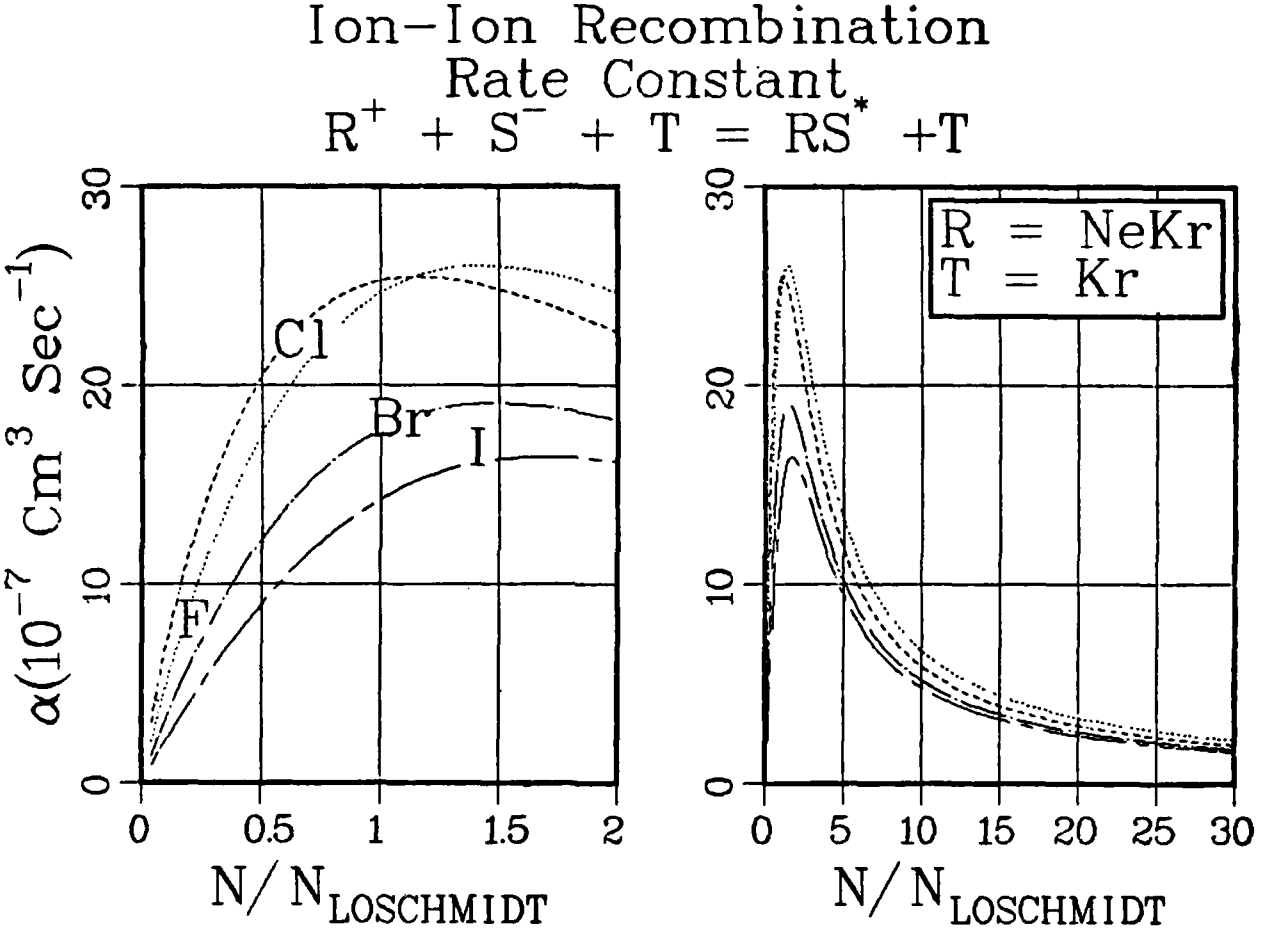

Fig. B-1.A. 45. Ion-ion recombination rate constants for the indicated processes and gases as a function of neutral gas density normalized by Loschmidt's number. The results for S = F, Cl, Br, and I are denoted respectively by dots, dashes, dots and dashes, and short and long dashes.

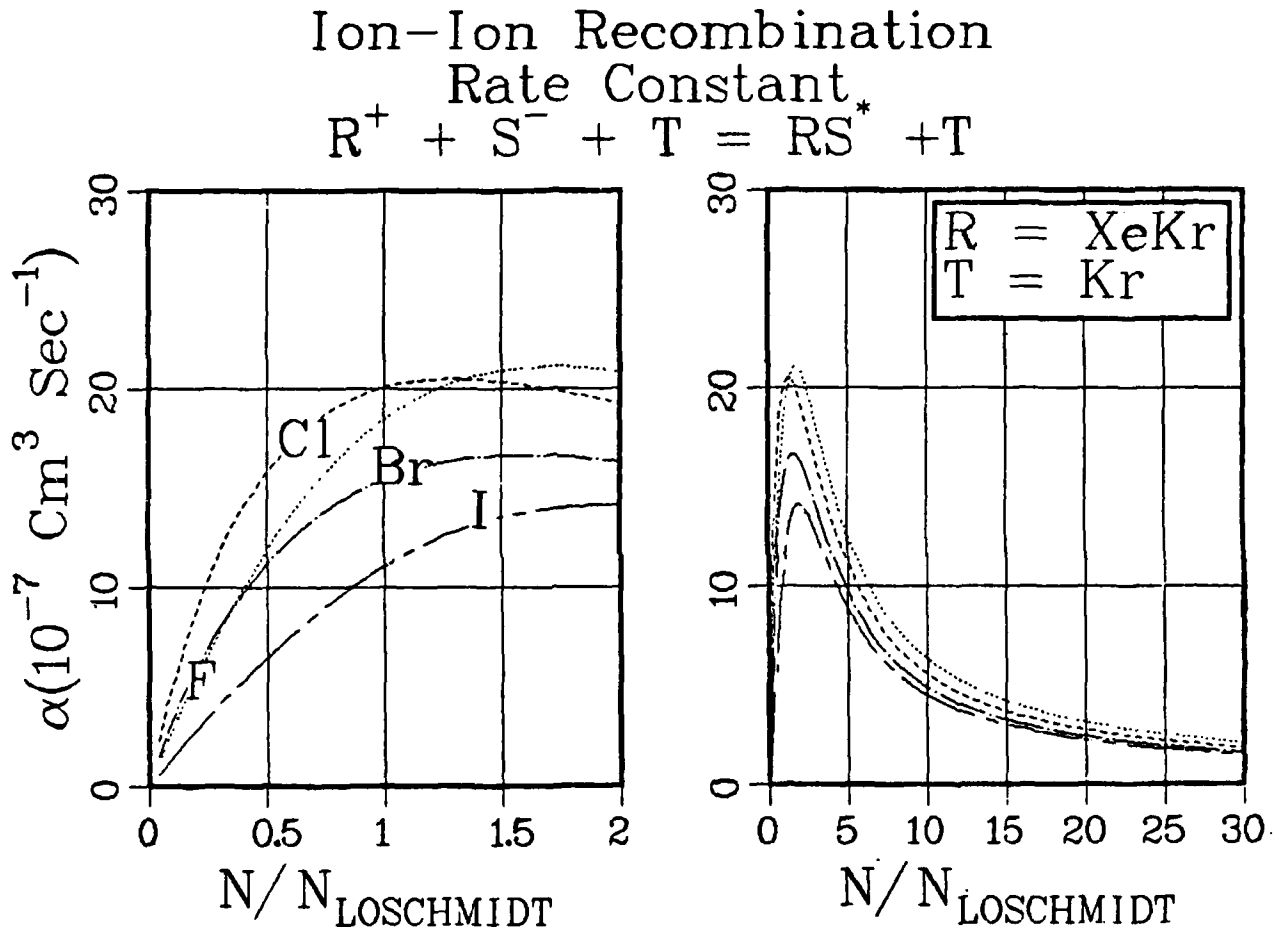

Fig. B-1.A. 46. Ion-ion recombination rate constants for the indicated processes and gases as a function of neutral gas density normalized by Loschmidt's number. The results for S = F, Cl, Br, and I are denoted respectively by dots, dashes, dots and dashes, and short and long dashes.

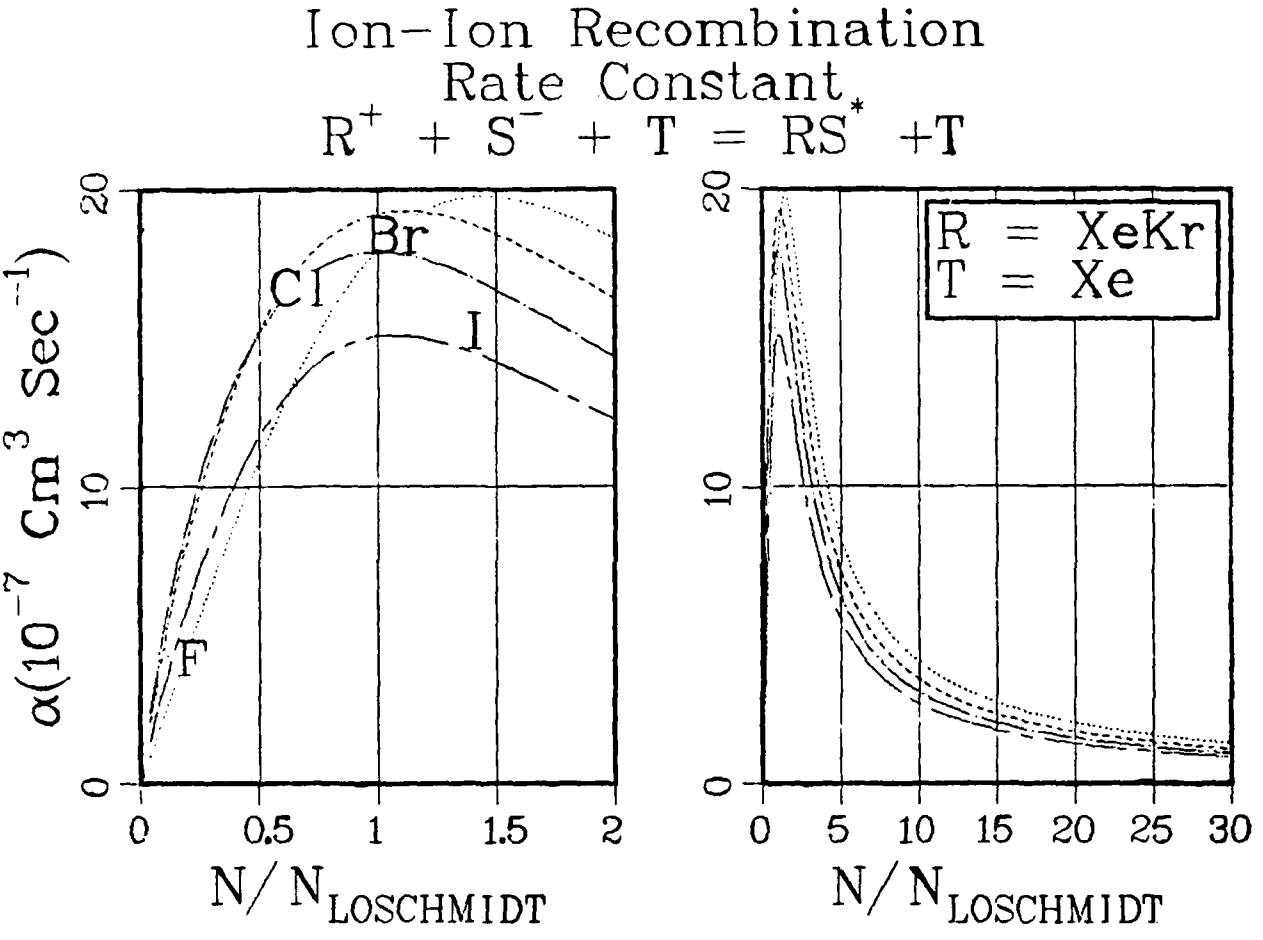

Fig. B-1.A. 47. Ion-ion recombination rate constants for the indicated processes and gases as a function of neutral gas density normalized by Loschmidt's number. The results for S = F, Cl, Br, and I are denoted respectively by dots, dashes, dots and dashes, and short and long dashes.

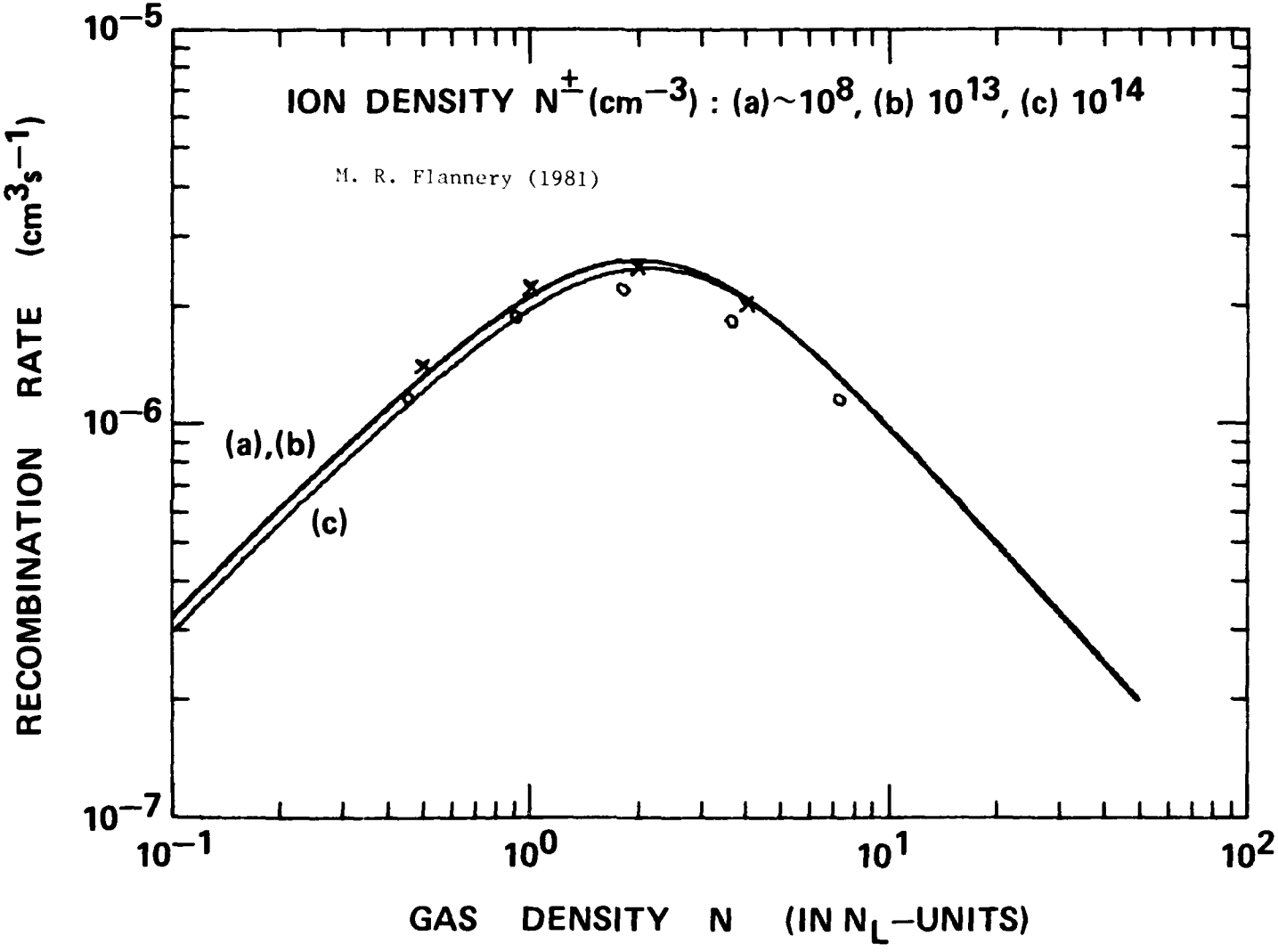

Fig. B-1.A. 48. Recombination rate coefficient $\alpha(cm^3\ s^{-1}$ at 300 K for (Kr^+-F^-) in Ar, as a function of gas density N (in units of Loschmidt's number density N_L = 2.69 10^{19} at STP). ——: Flannery (1981). X: Universal Monte-Carlo (Hard-Sphere) Plot (Bates 1980). O: Monte-Carlo (Polarization) results (Morgan et al. 1981).

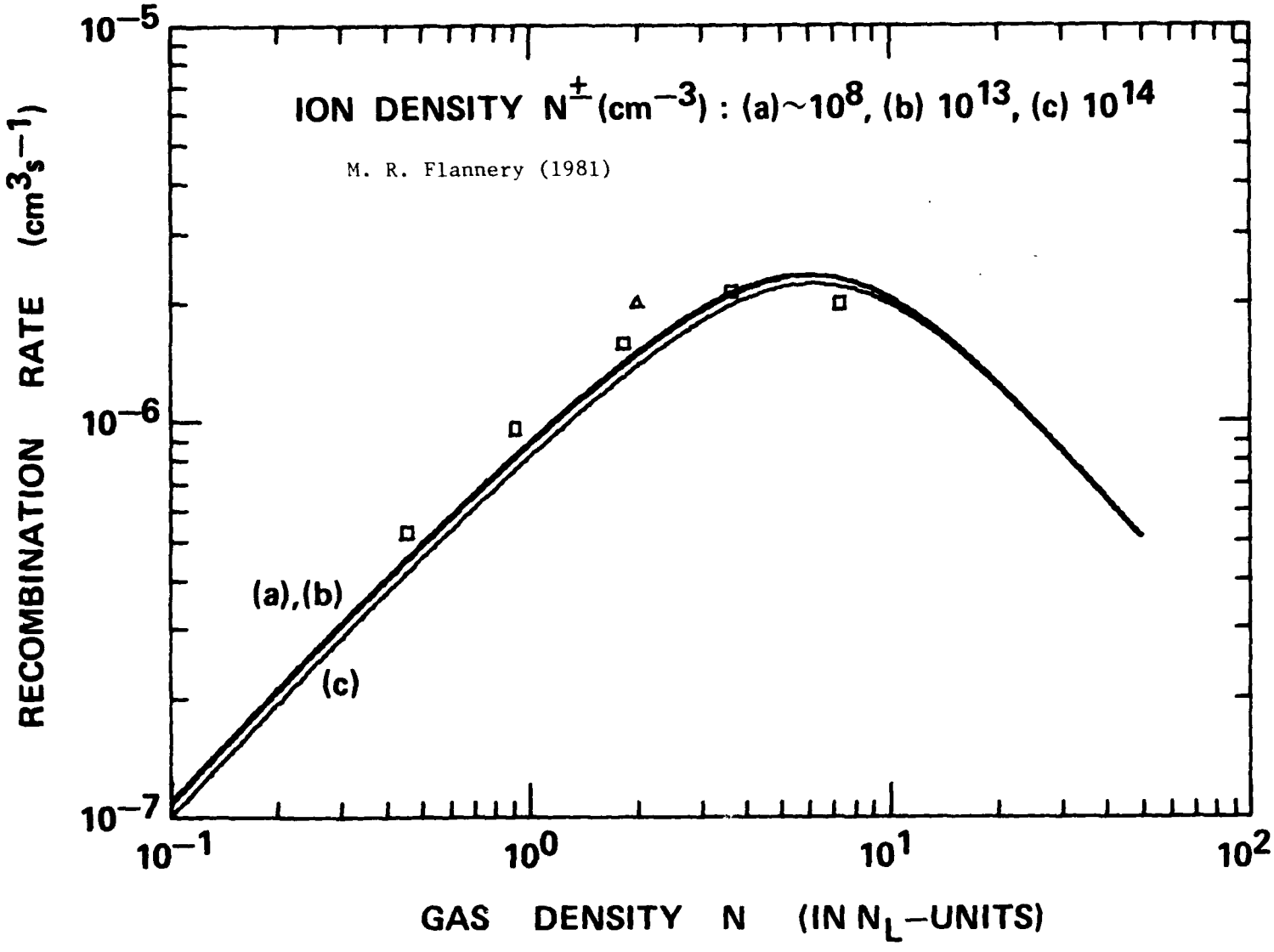

Fig. B-1.A. 49. As in Figure 48 except for (Xe^+-$C\ell^-$) in Ne. Monte-Carlo Results: ◘ (Bardsley and Wadehra 1980), Δ (Bates 1980).

Section B-1.B. ION-MOLECULE REACTIONS

CONTENTS

		Page
B-1.B-1.	Reaction Cross Sections for $Ar^+(^2P_J) + H_2(D_2)$ at 0.048 eV to 0.476 eV	2730
B-1.B-2.	A Study of the Reactions and Product Distributions of the Ground and Metastable States of C^+, N^+, S^+ and N_2^+ at 300 K.	2731
B-1.B-3.	Cross Section for State-Selected Ion-Molecule Reaction, $H_2^+(v) + H_2 \rightarrow H_3^+ + H$	2734
B-1.B-4.	Cross Section as a Function of Energy for the Ion-Molecule Reaction $H_2^+(v=0) + H_2 \rightarrow H_3^+ + H$.	2734
B-1.B-5.	Reactions of He^+ with O_2, N_2 and CH_4 as a Function of Energy	2735
B-1.B-6.	Rate Constant for the Reaction of O^+ with N_2 as a Function of Energy	2735
B-1.B-7.	Rate Constant as a Function of Energy for the Reaction of N^+ with O_2	2736
B-1.B-8.	Branching Ratios for the Reaction of N^+ with O_2	2736
B-1.B-9.	Reactions of CH_n^+(n=0 to 4) with Several Molecules	2737
B-1.B-10.	Reactions of CH_n^+(n=0 to 4) with NH_3 at 300 K.	2738
B-1.B-11.	Reactions of CH_n^+(n=0 to 4) with Molecules at 300 K.	2739
B-1.B-12.	Binary and Ternary Reactions of CH_3^+ Ions with Several Molecules at Thermal Energies	2740
B-1.B-13.	Reactions of NH_n^+(n=0 to 3) with Diatomic and Polyatomic Molecules at 300 K.	2741
B-1.B-14.	Ternary Reactions of NO^+ of the Form $NO^+ + X + Y \rightarrow NO^+ \cdot X + Y$	2743
B-1.B-15.	Reactions of N^+, N_2^+, N_3^+, N_4^+, O^+, O_2^+, and NO^+ Ions with Several Molecules at 300 K.	2744
B-1.B-16.	Reactions of O_2^+, NO^+ and O^+ Ground and Metastable States with Several Molecules at Thermal Energy	2746
B-1.B-17.	Rate Constants for the Reaction of H_2O^+ with Molecules at 300 K	2747
B-1.B-18.	Rate Constants as a Function of Energy for the Reaction of H_2O^+ with NO and NO_2	2747

Page

B-1.B-19. Rate Constants as a Function of Energy for the Reaction of H_2O^+ with CH_4 and H_2 2747

B-1.B-20. Rate Constants as a Function of Energy for the Reaction of H_2O^+ with C_2H_4 and CO 2747

B-1.B-21. Reactions of H_nCO^+(n=0 to 3) with Molecules at 300 K 2748

B-1.B-22. Reaction of $O_2^+(a^4\Pi_u)$ with CH_4 as a Function of Energy . . . 2749

General References:

1. "Collision Phenomena in Ionized Gases", E. W. McDaniel, John Wiley, New York (1964).

2. "The Mobility and Diffusion of Ions in Gases", E. W. McDaniel and E. A. Mason, John Wiley, New York (1973).

3. "Ion-Neutral Reaction Rates", D. L. Albritton, Atomic Data and Nuclear Data Tables 22, 1 (1978).

4. "Gas Phase Ion Chemistry", Edited by M. T. Bowers, Academic Press, New York (1979).

5. "Topics In Applied Physics", Vol. 30, Excimer Lasers, edited by Ch. K. Rhodes, Springer-Verlag, New York (1979).

AD-A102 279 ARMY MISSILE COMMAND REDSTONE ARSENAL AL DIRECTED E--ETC F/G 20/5
COMPILATION OF ATOMIC AND MOLECULAR DATA RELEVANT TO GAS LASERS--ETC(U)
DEC 80 E W MCDANIEL, M R FLANNERY, E W THOMAS

UNCLASSIFIED DRSMI-RH-81-4-VOL-7 NL

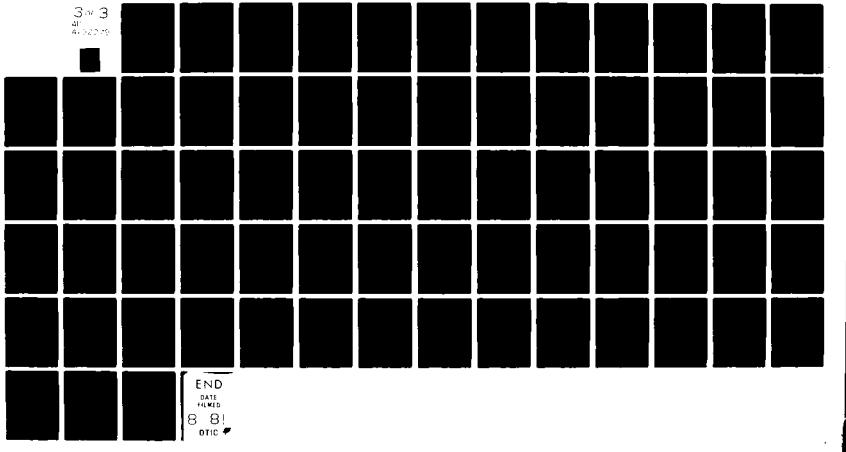

END
DATE FILMED
8 81
DTIC

Explanation of Tables

The following section contains information pertaining to ion-molecule reactions of the general form $A^+ + B \rightarrow C^+ + D$. Excluded from consideration for example are the following types of reactions:

	$A^{+*} + B \rightarrow A^+ + B^*$	Excitation transfer
	$A^* + B \rightarrow A + B + E$	Quenching
and	$A^+ + B \rightarrow A + B^+$	Single charge transfer

If a certain reaction is not located in the ion-molecule section, check the charge transfer section also. Some overlap in the two categories is unavoidable and due to space limitations there is only one listing of each reaction.

The reaction $A^+ + B \xrightarrow{k} C^+ + D$ is described as a bimolecular reaction. The concentration of A^+ obeys the first order linear differential equation $d[A^+]/_{dt} = -k[A^+][B]$.

The usual units for k are $cm^3/(molecule \cdot sec)$ abbreviated as $cm^3\ s^{-1}$. The concentrations $[A^+]$ and [B] are in units of $(molecules \cdot cm^{-3})$.

The reaction $A^+ + B + M \xrightarrow{k} C^+ + D + M$ is known as a termolecular reaction and obeys the equation $d[A^+]/_{dt} = -k[A^+][B][M]$. The units of k are $cm^6/(Molecule^2 \cdot sec)$ abbreviated as $cm^6\ s^{-1}$. Where several reaction channels are possible the probability of a certain reaction channel is described by the product ratio. If all the possible reaction channels are given by the following:

$$A^+ + B \xrightarrow{k_1} C^+ + D \qquad (1)$$

$$\xrightarrow{k_2} E^+ + F \qquad (2)$$

$$\xrightarrow{k_3} C^+ + H \qquad (3)$$

the product ratio, [i.e. probability of the reaction following channel (3)], is given by $k_3/(k_1+k_2+k_3)$.

Calculated Rate Coefficients

Langevin values for rate coefficients are calculated from the formula $k_L = 2\pi e\left(\frac{\alpha}{m_r}\right)^{1/2}$ where k_L is the Langevin rate coefficient, e is the electronic charge, α is the electric polarizability of the neutral molecule, and m_r is the reduced mass. The formula is derived assuming that the long range interaction potential is due to the ion-induced dipole force [M. McFarland, D. L. Albritton, F. C. Fehsenfeld, E. E. Ferguson, and A. L. Schmeltekopf, J. Chem. Phys. 59, 6620 (1973)]. ADO (Average Dipole Orientation) values are calculated for the case where a molecule has a dipole moment. This calculation takes into account both the dipole moment of the molecule and the ion-induced dipole moment, [see, for example, T. Su and T. Bowers, J. Chem. Phys. 58, 3027 (1973)].

Langevin and ADO values are considered accurate in the region where the ion energy approaches thermal energy. In this respect, they can be considered asymptotic values in the low energy region when the potential has certain long range features. k_L and k_{ADO} are the classical-model gas-kinetic upper limits that assume unity reaction probability for the collisions of ions with nonpolar and polar molecules, respectively. The designation k_L and k_{ADO} for Langevin and ADO values of the rate coefficient, respectively, are used throughout this section.

Tabular Data B-1. B-1. Individual reaction cross sections for the two spin orbit states Ar^+ ($^2P_{3/2}$) and Ar^+ ($^2P_{1/2}$). Ratios of the reaction cross sections are given as a function of relative collision energy.

Reactions: $Ar^+(^2P_{1/2}) + H_2 \xrightarrow{\sigma(1/2)} Ar\,H^+ + H$

and $Ar^+(^2P_{3/2}) + H_2 \xrightarrow{\sigma(3/2)} Ar\,H^+ + H$

$E_{c.m.}$ (eV)	0.048	0.095	0.238	0.476
$\sigma(1/2)/\sigma(3/2)$[a]	1.56	1.47	1.59	1.44

Ratio of the reaction cross sections as a function of relative collision energy.

Reactions: $Ar^+(^2P_{1/2}) + D_2 \xrightarrow{\sigma(1/2)} Ar\,D^+ + D$

$Ar^+(^2P_{3/2}) + D_2 \xrightarrow{\sigma(3/2)} Ar\,D^+ + D$

$E_{c.m.}$ (eV)	0.046	0.091	0.227	0.455
$\sigma(1/2)/\sigma(3/2)$[a]	1.25	1.29	1.32	1.28

[a]The accuracy is estimated to be 15%.

Reference: K. Tanaka, J. Durup, T. Kato, I. Koyano, J. Chem. Phys. 73, 586 (1980).

Tabular Data B-1.B-2. Reaction rate coefficients and product ion distribution for the ground and metastable states of C^+, N^+, S^+ and N_2^+ at 300 K.

Type of reactions studied:

$A^{+*} + B \xrightarrow{k_1}$ product, chemical reaction of metastable ion.

$A^{+*} + B \xrightarrow{k_2} A^+ + B$, quenching of metastable ion.

$A^+ + B \xrightarrow{k_4}$ product, chemical reaction of ground state ion.

Reactions of C^+

Reactant Molecule B	k_4 (cm^3 sec^{-1})	k_1+k_2 (cm^3 sec^{-1})	Reaction Channel	ΔH^a (eV)	Product Distribution	Inferred Metastable Product Distribution
H_2 [1.61(−9)][b]	endo	~1(−12)	$H_2^+ + C$	+4.2	1.0	1.0
CO [1.13(−9)]	endo	~3(−11)	$CO^+ + C$	+2.7	1.0	1.0
NO [1.06(−9)]	6.9(−10)		$NO^+ + C$	−2.1	0.86	0.0
			$N^+ + CO$	−1.4	0.14	1.0
O_2 [9.93(−10)]	7.4(−10)		$O^+ + CO$	−3.7	0.53	0.0
			$CO^+ + O$	−3.3	0.47	1.0
CO_2 [1.23(−9)]	1.1(−9)		$CO^+ + CO$	−2.9	0.90	0.0
			$CO_2^+ + C$	+2.5	0.10	1.0
H_2O [2.62(−9)]	2.4(−9)		$HCO^+ + H$	−4.4	0.90	0.0
			$H_2O^+ + C$	+1.3	0.10	1.0
NH_3 [2.43(−9)]	2.3(−9)		$H_2CN^+ + H$	−5.0	0.68	0.1
			$HCN^+ + H_2$	−2.9	0.09	0.6
			$NH_3^+ + C$	−1.1	0.23	0.3
CH_4 [1.43(−9)]	1.2(−9)		$C_2H_2^+ + H_2$	−4.2	0.50	1.0
			$C_2H_3^+ + H$	−4.1	0.50	0.0

[a] A positive sign indicates an endoergic channel.

[b] Langevin or ADO rate coefficient. Values of rate coefficients (m x 10^n) are quoted in the table as m(n).

Reference: M. Tichý, A. B. Rakshit, D. G. Listen, N. D. Twiddy, N. G. Adams, and D. Smith, Int. J. Mass. Spec. Ion Phys. 29, 231 (1979).

Tabular Data B-1.B-2.(cont.) Tichý, et al., Reactions of N^+:

Reactant Molecule B	k_4 (cm^3 sec^{-1})	k_1+k_2 (cm^3 sec^{-1})		Reaction Channel	ΔH (eV)	Product Distribution	Inferred Metastable Product Distribution
H_2 [1.59(−9)]	6.2(−10)	6.2(−10)		$NH^+ + H$	−0.7	0.68	0.0
				$H_2^+ + N$	+0.9	0.32	1.0
CO [1.08(−9)]	4.3(−10)	1.1(−9)		$NO^+ + C$	−0.7	0.10	0.1
				$CO^+ + N$	−0.5	0.90	0.9
NO [1.00(−9)]	5.3(−10)	1.1(−9)		$NO^+ + N$	−5.3	0.79	0.5
				$N_2^+ + O$	−2.3	0.21	0.5
O_2 [9.49(−10)]	6.0(−10)	6.0(−10)		$NO^+ + O$	−6.6	0.32	0.1
				$O_2^+ + N$	−2.1	0.50	0.5
				$O^+ + NO$	−2.3	0.18	0.4
CO_2 [7.59(−10)]	1.1(−9)	1.1(−9)		$CO^+ + NO$	−1.5	0.27	0.3
				$CO_2^+ + N$	−0.7	0.73	0.7
H_2O [2.50(−9)]	2.8(−9)	2.8(−9)		$NO^+ + H_2$	−6.7	0.15	0.5
				$H_2O^+ + N$	−1.9	0.85	0.5
NH_3 [2.32(−9)]	2.3(−9)	2.5(−9)		$N_2H^+ + H_2$	−6.2	0.10	0.1
				$NH_3^+ + N$	−4.4	0.60	0.1
				$NH_2^+ + NH$	−2.4	0.30	0.8
CH_4 [1.38(−9)]	1.1(−9)	1.1(−9)		$CH_3^+ + NH$	−3.9	0.42	0.2
				$H_2CN^+ + H + H$	−3.2	0.38	0.4
				$CH_4^+ + N$	−1.8	0.06	0.1
				$HCN^+ + H_2 + H$	−1.1	0.14	0.3
Reactions of N_2^+ :							
H_2 [1.54(−9)]	1.8(−9)	1.8(−9)*	0.2	$N_2H^+ + H$	−0.56	0.75	0.3
				$H_2^+ + N_2$	−0.06	0.25	0.7
NO [8.12(−10)]	4.4(−10)	9.4(−10)	0.5	$NO^+ + N_2$	−6.30	1.00	1.0
O_2 [7.66(−10)]	4.7(−11)	6.8(−10)* 1.1(−10)	0.5	$O_2^+ + N_2$	−3.36	1.00	1.0
CO_2 [9.11(−10)]	8.4(−10)	~1(−9)* 7.8(−10)	<0.1	$CO_2^+ + N_2$	−1.70	1.00	1.0
H_2O [2.12(−9)]	3.0(−9)	3.0(−9)*	≲0.5	$H_2O^+ + N_2$	−2.90	0.81	0.8
				$N_2H^+ + OH$	−0.14	0.19	0.2
NH_3 [1.98(−9)]	1.9(−9)	1.8(−9)*	<0.1	$NH_3^+ + N_2$	−5.36	1.00	1.0
CH_4 [1.18(−9)]	1.3(−9)	2(−9)* ~1(−9)	<0.4	$CH_3^+ + N_2 + H$	−1.16	0.89	0.8
				$CH_2^+ + N_2 + H_2$	−0.26	0.11	0.2

Tabular Data B-1.B-2.(cont.) Tichý *et al.*

Reactions of S^+:

Reactant Molecule B	k_4 ($cm^3\ sec^{-1}$)	k_1+k_2 ($cm^3\ s^{-1}$)	$\frac{k_2}{k_1+k_2}$	Reaction Channel	ΔH (eV)	Product Distribution	Inferred Metastable Product Distribution
H_2 [1.53(−9)]	endo	5.0(−10)	0.5	$SH^+ + H$	+0.9	1.00	1.0
NO [7.85(−10)]	2.7(−10)	8.3(−10)	0.1	$NO^+ + S$	−1.1	1.00	1.0
O_2 [7.30(−10)]	2.1(−11)	8.0(−10)		$SO^+ + O$	−0.01	0.62	0.0
		1.0(−10)	<0.1	$O_2^+ + S$	+1.8	0.38	1.0
CO_2 [5.80(−10)]	endo	6.6(−10)	0.5	$SO^+ + CO$	+0.3	1.00	1.0
H_2O [2.10(−9)]	endo	2.0(−9)	0.5	$SH^+ + OH$	+1.6	0.43	0.4
				$H_2O^+ + S$	+2.4	0.57	0.6
NH_3 [1.93(−9)]	1.7(−9)	1.7(−9)	0.3	$NH_3^+ + S$	−0.2	0.77	0.0
				$NH_2S^+ + H$		0.23	1.0
CH_4 [1.15(−9)]	3.5(−10)	1.3(−9)	<0.1	$CH_3S^+ + H$	−0.4	0.71	0.2
		4.8(−10)		$CH_3^+ + SH$	+0.3	0.08	0.2
				$CH_2S^+ + H + H$	+2.3	0.21	0.6

Tabular Data B-1.B-3. State-selected ion-molecule reactions of H_2^+.

Cross sections for the reaction $H_2^+(v) + H_2 \xrightarrow{\sigma} H_3^+ + H$

v*	σ [1.] (10^{-16} cm^2)	relative[1.] to v = 0	relative[2.] to v = 0
0	51 ± 2	1.00	1.00
1	45 ± 3	0.89 ± 0.06	0.94
2	46 ± 3	0.90 ± 0.07	0.86
3	42 ± 3	0.83 ± 0.07	0.83

1. $\overline{E}_{cm}$ = 0.11 eV average collision energy.
2. $\overline{E}_{cm} \leq$ 0.32 eV average collision energy

Reference: 1. I. Koyano, K. Tanaka, J. Chem. Phys. 72, 4858 (1980).
2. W. A. Chupka, M. E. Russell, K. Refay, J. Chem. Phys. 48, 1518 (1968).

Graphical Data B-1.B-4. Reaction cross section as a function of average collision energy, $\overline{E}_{cm}$, for the reaction $H_2^+(v=0) + H_2 \rightarrow H_3^+ + H$.

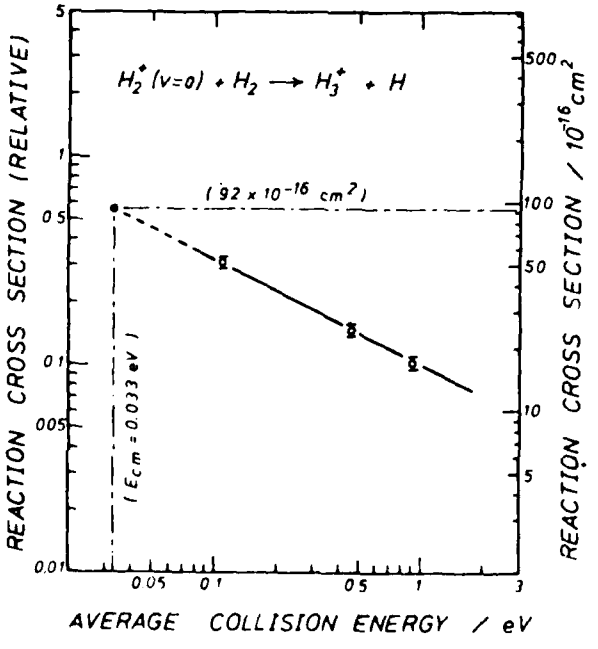

Reference: I. Koyano, K. Tanaka, J. Chem. Phys. 72, 4858 (1980).

*v - vibrational quantum number.

Tabular Data B-1.B-5. Ion-molecule reactions of He^+ with O_2, N_2 and CH_4. Energy dependence of the rate constants for the loss of He^+ in the reactions:

$He^+ + O_2 \xrightarrow{k}$ He + products, $He^+ + CH_4 \xrightarrow{k}$ He + products

and $He^+ + N_2 \xrightarrow{k}$ He + products.

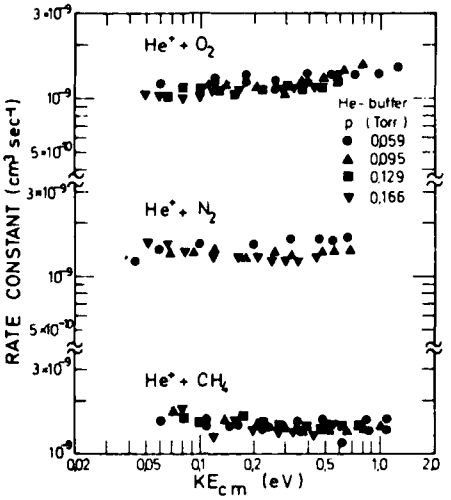

Tabular Data B-1.B-6. Ion-molecule reactions of O^+ with N_2. Energy dependence of the rate constant for the loss of O^+ in the reaction:

$O^+ + N_2 \xrightarrow{k} O + \text{products}$.

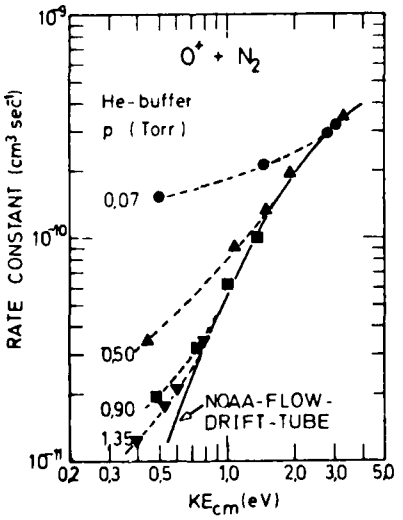

Reference: W. Lindinger, E. Alge, H. Stori, R. N. Varney, H. Helm, P. Holzmann and M. Pahl, Int. J. Mass. Spect. Ion Phys. 30, 251 (1979).

Tabular Data B-1.B-7. Rate constants as a function of center-of-mass energy for the reaction, $N^+ + O_2 \rightarrow$ products.

CB - crossed beams
SIFT - selected ion flow tube
ICR - ion cyclotron resonance
SA - static afterglow
FA - flowing afterglow
MS - mass spectrometer
SDT - static drift tube
FDT - flow drift tube

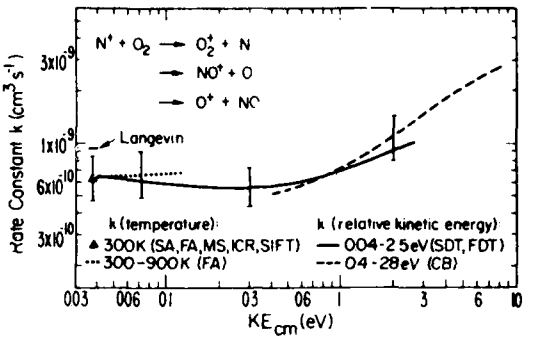

Reference: F. Howorka, I. Dotan, F. C. Fehsenfeld and D. L. Albritton, J. Chem. Phys. 73, 758 (1980).

Tabular Data B-1.B-8. Branching ratios of the reaction $N^+ + O_2 \rightarrow$ products as a function of relative energy.

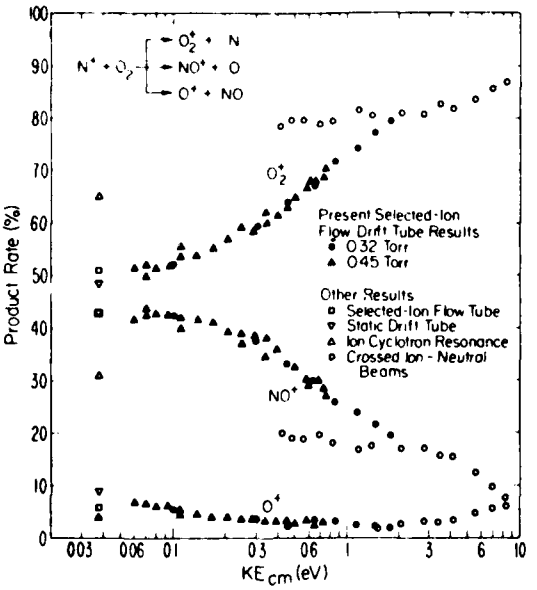

Reference: F. Howorka, I. Dotan, F. C. Fehsenfeld and D. L. Albritton, J. Chem. Phys. 73, 758 (1980).

Tabular Data B-1.B-9. Reaction of simple hydrocarbon ions with molecules at thermal energies.

Reaction rate coefficients and ionized product for the reactions $CH_n^+ + M \rightarrow$ products at 300 K for n = 0 to 4 and M as shown.

M	C^+	CH^+	CH_2^+	CH_3^+	CH_4^+
H_2	No reaction observed [1.59(−9)]	1.2 (−9) $CH_2^+ + H$ [1.58(−9)]	1.6 (−9) $CH_3^+ + H$ [1.57(−9)]	1.3 (−28) $CH_3^+ \cdot H_2 + He$ [1.57(−9)]	3.3 (−11) $CH_5^+ + H$ [1.56(−9)]
N_2	No reaction observed [1.07 (−9)]	5.3 (−29)[b] $CH^+ \cdot N_2 + He$ [1.04 (−9)]	1.4 (−28)[b] $CH_2^+ \cdot N_2 + He$ [1.02 (−9)]	5.3 (−29)[b] $CH_3^+ \cdot N_2 + He$ [9.94(−10)]	No reaction observed [9.73(−10)]
O_2	9.9 (−10) $O^+ + CO$ 62% $CO^+ + O$ 38% [1.00 (−9)]	9.7 (−10) $HCO^+ + O$ $O^+ + HCO$ $CO^+ + OH$ [9.74 (−10)]	9.1 (−10) $HCO^+ + OH$ $H_2CO^+ + O$ [9.48 (−10)]	~1 (−29)[b] $CH_3^+ \cdot O_2 + He$ [9.26 (−10)]	4.4 (−10) $O_2^+ + CH_4$ [9.06(−10)]
CO	No reaction observed [1.13 (−9)]	~7 (−12) $HCO^+ + C$ [1.10 (−9)]	≤5 (−12) $HCO^+ + CH$ ~2 (−27)[b] $CH_2^+ \cdot CO + He$ [1.07 (−9)]	2.2 (−27)[b] $CH_3^+ \cdot CO + He$ [1.05 (−9)]	1.4 (−9) $HCO^+ + CH_3$ [1.02 (−9)]
CO_2	1.1 (−9) $CO^+ + CO$ [1.24 (−9)]	1.6 (−9) $HCO^+ + CO$ [1.20 (−9)]	1.6 (−9) $H_2CO^+ + CO$ [1.17 (−9)]	7.1 (−28)[b] $CH_3^+ \cdot CO_2 + He$ [1.14 (−9)]	1.2 (−9) $HCO_2^+ + CH_3$ [1.11 (−9)]
H_2O	2.5 (−9) $HCO^+ + H$ [2.62 (−9)]	2.9 (−9) $HCO^+ + H_2$ $H_2CO^+ + H$ $H_3O^+ + C$ [2.56 (−9)]	2.9 (−9) $H_3CO^+ + H$ $H_3O^+ + CH$ [2.50 (−9)]	~1 (−26)[b] $CH_3^+ \cdot H_2O + He$ [2.46 (−9)]	2.6 (−9) $H_3O^+ + CH_3$ [2.42 (−9)]
CH_4	1.2 (−9) $C_2H_3^+ + H$ $C_2H_2^+ + H_2$ [1.43 (−9)]	1.3 (−9) $C_2H_3^+ + H_2$ $C_2H_2^+ + H_2 + H$ $C_2H_4^+ + H$ [1.40 (−9)]	1.2 (−9) $C_2H_4^+ + H_2$ $C_2H_5^+ + H$ [1.37 (−9)]	1.2 (−9) $C_2H_5^+ + H_2$ [1.35 (−9)]	1.5 (−9) $CH_5^+ + CH_3$ [1.32 (−9)]

[a]Three-body reactions (in units of $cm^6\ s^{-1}$) are distinguished from 2-body reactions (in units of $cm^3\ s^{-1}$) by the association of the He atom with the 3-body product ion. The major products are underlined where there is more than one product channel. The square brackets contain the appropriate Langevin rate coefficient except in the case of H_2O where there is a significant additional contribution arising from its permanent dipole moment. Rate coefficients are as indicated, e.g. for $CH^+ + H_2$, k = 1.2 (-9) is equivalent to $1.2 \times 10^{-9}\ cm^3\ s^{-1}$. The "approximate" sign ~ indicates that the rate coefficient is accurate to within a factor of two. "No reaction observed" implies an equivalent 2-body rate coefficient of less than 5 (-13) $cm^3\ s^{-1}$.

[b]Three-body reaction, unit of rate coefficient is $cm^6\ sec^{-1}$.

Reference: D. Smith and N. G. Adams, Int. J. Mass Spect. Ion Phys. 23, 123 (1977).

Tabular Data B-1.B-10. Reactions of CH_n^+ (where n = 0 to 4) with ammonia at 300 K.

Rate coefficients and percentage product ion distribution obtained at 300 K in reactions of C^+, CH^+, CH_2^+, CH_3^+ and CH_4^+ with NH_3.

Reactant ion	Percentage ionized product distribution			Rate coefficients × 10^9 cm^3 s^{-1}		
		present[f]	previous	experimental: present[f]	experimental: previous	ADO
C^+	H_2CN^+	75	47 [a] 5 [b]			
	NH_3^+	22	50 [a] 95 [b]	2.3	2.3 [a,b]	2.44
	HCN^+	3	3 [a]			
CH^+	H_2CN^+	68				
	NH_3^+	17	–	2.7	–	2.39
	NH_4^+	15				
CH_2^+	H_3CN^+	55	80 [c]	2.8	1.5 [c], 2.0 [d]	2.34
	NH_4^+	45	20 [c]			
CH_3^+	H_3CN^+	70(88) [e]	80 [c]	2.2	0.83 [c], 1.3 [d]	2.29
	$CH_3NH_3^+$	20				
	NH_4^+	10(12) [e]	20 [c]	(1.8) [e]		
CH_4^+	NH_3^+	59	51 [c]	2.8	1.35 [c], 2.2 [d]	2.25
	NH_4^+	41	49 [c]			

References;

[a] V. G. Anicich, W. T. Huntress Jr. and J. H. Futrell, Chem. Phys. Letters 40, 233 (1976).

[b] H. I. Schiff, R. S. Hemsworth, J. D. Payzant, and D. K. Bohme, Astrophys. J. 191, L49 (1974).

[c] W. T. Huntress Jr., R. F. Pinizzotto Jr., and J. P. Landenslager, J. Am. Chem. Soc. 95, 4107 (1973).

[d] M. S. B. Munson and F. H. Field, J. Am. Chem. Soc. 87, 4242 (1965).

[e] The bracketed values relate to the product distribution and rate coefficient for the H_4CN^+ and NH_3^+ channels only.

[f] D. Smith and N. G. Adams, Chem. Phys. Letts. 47, 145 (1977).

Tabular Data B-1.B-11. Binary reactions of CH_n^+ ions in the reaction $CH_n^+ + M \rightarrow$ products where M is the following: COS, H_2, H_2S, H_2CO, CH_3OH, CH_3NH_2, CO_2, H_2O.

Rate coefficients and percentage product ion distributions (bracketed) for the reactions of CH_n^+ (n = 0 to 4) with several molecules at 300 K. Rate coefficients are expressed as, for example, 2.0(-9) to represent 2.0×10^{-9} cm^3 sec^{-1}.

M	C^+	CH^+	CH_2^+	CH_3^+	CH_4^+
COS	$CS^+ + CO$(80) $COS^+ + C$(20) 2.0(-9)	$HCS^+ + CO$(55) $HCOS^+ + C$(45) 1.9(-9)	$HCS^+ + HCO$(60) $H_2CS^+ + CO$(40) 1.8(-9)	$H_3CS^+ + CO$(100) 1.2(-9)	$HCOS^+ + CH_3$(70) $COS^+ + CH_4$(30) 1.4(-9)
H_2S	$HCS^+ + H$(75) $H_2S^+ + C$(25) 1.7(-9)	$HCS^+ + H_2$(70) $H_3S^+ + C$(30) 2.1(-9)	$H_3CS^+ + H$(80) $HCS^+ + H_2 + H$(10) $H_3S^+ + CH$(10) 2.3(-9)	$H_3CS^+ + H_2$(100) 1.4(-9)	$H_3S^+ + CH_3$(55) $H_2S^+ + CH_4$(45) 2.1(-9)
H_2CO	$CH_2^+ + CO$(60) $H_2CO^+ + C$(20) $HCO^+ + CH$(20) 3.9(-9)	$CH_3^+ + CO$(30) $H_3CO^+ + C$(30) $HCO^+ + CH_2$(30) $H_2C_2O^+ + H$(10) 3.2(-9)	$HCO^+ + CH_3$(85) $H_3C_2O^+ + H$(10) $H_2C_2O^+ + H_2$(5) 3.3(-9)	$HCO^+ + CH_4$(100) $CH_3^+ \cdot H_2CO + He$ [a] 1.6(-9)	$H_3CO^+ + CH_3$(55) $H_2CO^+ + CH_4$(45) 3.6(-9)
CH_3OH	$CH_3^+ + HCO$(80) $H_3CO^+ + CH$(20) 2.6(-9)	$CH_3^+ + H_2CO$(50) $CH_3OH_2^+ + C$(40) $H_3CO^+ + CH_2$(10) 2.9(-9)	$CH_3OH_2^+ + CH$(50) $H_3CO^+ + CH_3$(50) 2.6(-9)	$H_3CO^+ + CH_4$(100) $CH_3^+ \cdot CH_3OH + He$ [a] 2.3(-9)	$CH_3OH^+ + CH_4$(60) $CH_3OH_2^+ + CH_3$(40) 3.0(-9)
CH_3NH_2	$CH_3NH_2^+ + C$(65) $CH_2NH_2^+ + CH$(35) 2.2(-9)	$CH_2NH_2^+ + CH_2$(50) $CH_3NH_3^+ + C$(40) $CH_3NH_2^+ + CH$(10) 2.2(-9)	$CH_2NH_2^+ + CH_3$(55) $CH_3NH_2^+ + CH_2$(35) $CH_3NH_3^+ + CH$(10) 2.1(-9)	$CH_3NH_2^+ + CH_3$(55) $CH_2NH_2^+ + CH_4$(45) $CH_3^+ \cdot CH_3NH_2 + He$ [a] 2.2(-9)	$CH_3NH_2^+ + CH_4$(60) $CH_2NH_2^+ + CH_4 + H$(40) 2.2(-9)
CO_2	$CO^+ + CO$(100) 1.1(-9)	$HCO^+ + CO$(100) 1.6(-9)	$H_2CO^+ + CO$(100) 1.6(-9)	$CH_3^+ \cdot CO_2 + He$ [a] ternary	$HCO_3^+ + CH_3$(100) 1.2(-9)
H_2O	$HCO^+ + H$(100) 2.5(-9)	$HCO^+ + H_2$ $H_2CO^+ + H$ $H_3O^+ + C$ 2.9(-9)	$H_3CO^+ + H$ $H_3O^+ + CH$ 2.9(-9)	$CH_3^+ \cdot H_2O + He$ [a] ternary	$H_3O^+ + CH_3$(100) 2.6(-9)

[a] Ternary association products observed. The rate coefficient quoted is that for the binary channel only.

Tabular Data B-1.B-12. Rate coefficients and product ion distributions for the reactions of CH_3^+ with molecules at 300 K and 225 K. Rate coefficients for both binary ($cm^3\ sec^{-1}$) and ternary ($cm^6\ sec^{-1}$) channels are given. The reactions studied are the following:

$$A^+ + B + M \xrightarrow{k_c} AB^+ + M.$$

M is a stabilizing gas (He). The reaction can be further broken down as

$$A^+ + B \underset{\tau_d}{\overset{k_1}{\rightleftharpoons}} (AB^+)^* \text{ followed by } (AB^+)^* + M \xrightarrow{fk_2} AB^+ + M$$
$$\xrightarrow{(1-f)k_2} A^+ + B + M.$$

where f is the fraction that result in forming the complex AB^+. A^+ is CH_3^+ and B is the reactant molecule.

Reactant molecule	Rate coefficients and products			$f\tau_d$(s)	
	binary	ternary			
B	300 K	300 K	225 K	300 K	225 K
H_2	–	$CH_3^+ \cdot H_2$			
		1.3(−28)	4.3(−28)	1.4(−10)	4.6(−10)
N_2	–	$CH_3^+ \cdot N_2$			
		5.3(−29)	2.0(−28)	9.1(−11)	3.6(−10)
O_2	–	$CH_3^+ \cdot O_2$			
		≈1(−29)	2.7(−29)	≈2(−11)	5.3(−11)
CO	–	$CH_3^+ \cdot CO$			
		2.2(−27)	5.3(−27)	3.8(−9)	9.1(−9)
CO_2	–	$CH_3^+ \cdot CO_2$			
		7.1(−28)	3.1(−27)	1.2(−9)	5.2(−9)
H_2O	–	$CH_3^+ \cdot H_2O$			
		>3(−26)	–	>2(−8)	–
NH_3	H_4CN^+(88)	$CH_3^+ \cdot NH_3$			
	NH_4^+(12)	>7(−26)	–	>6(−8)	–
	1.8(−9)				
H_2CO	HCO^+(100)	$CH_3^+ \cdot H_2CO$			
	1.6(−9)	3.5(−26)	–	2.2(−8)	–
CH_3OH	H_3CO^+(100)	$CH_3^+ \cdot CH_3OH$			
	2.3(−9)	>4(−26)	–	>3(−8)	–
CH_3NH_2	$CH_3NH_3^+$(55)	$CH_3^+ \cdot CH_3NH_2$			
	$CH_2NH_2^+$(45)	>3(−27)	–	>3(−9)	–
	2.2(−9)				
COS	H_3CS^+(100)	–	–	–	–
	1.4(−9)				
H_2S	H_3CS^+(100)	–	–	–	–
	1.2(−9)				
C_2H_2	$C_3H_3^+$(100)	–	–	–	–
	1.2(−9)				
CH_4	$C_2H_5^+$(100)	–	–	–	–
	1.2(−9)				

Reference: D. Smith and N. G. Adams, Chem. Phys. Letts. 54, 535 (1978).

Tabular Data B-1.B-13. Rate coefficients and product ion distributions for the reactions of N^+, NH^+, NH_2^+, and NH_3^+ with a series of molecules at 300 K. The reactant ions and molecules are arranged in order of their recombination energies and ionization potentials, respectively, the magnitudes of which are indicated in eV below each reactant species. The proton detachment energies for the ions and proton affinities for the neutral molecules are indicated in eV above each reactant species. The binary rate coefficients are indicated as, for example, 1.0(-9) representing 1.0×10^{-9} cm^3 s^{-1}. The percentage of each ion product is given in round brackets after the product ion and the Langevin or ADO theoretical rate coefficient for each reaction is given in square brackets below the experimentally determined value. The ternary rate coefficient (cm^6 s^{-1}) is quoted for the $N^+ + N_2$ reaction.

	N^+ 14.55 eV	4.2 eV NH^+ 13.10 eV	6.1 eV NH_2^+ 11.4 eV	8.0 eV NH_3^+ 10.17 eV
9.4 eV CH_3NH_2 8.97 eV	H_4CN^+(70), H_2CN^+(10) $CH_3NH_2^+$(7), H_3CN^+(7) CH_3^+(6) 2.0(−9) [2.21(−9)]	H_4CN^+(45), $CH_3NH_2^+$(20) $CH_3NH_3^+$(20), H_2CN^+(20) H_3CN^+(5) 2.1(−9) [2.15(−9)]	$CH_3NH_2^+$(50), $CH_3NH_3^+$(20) H_4CN^+(20), NH_4^+(10) 1.8(−9) [2.11(−9)]	$CH_3NH_2^+$(50) $CH_3NH_3^+$(35) NH_4^+(15) 1.8(−9) [2.06(−9)]
5.0 eV NO 9.25	NO^+(85) N_2^+(15) 5.3(−10) [9.99(−10)]	NO^+(80) N_2H^+(20) 8.9(−10) [9.76(−10)]	NO^+(100) 7.0(−10) [9.55(−10)]	NO^+(100) 7.2(−10) [9.37(−10)]
9.0 eV NH_3 10.17 eV	NH_3^+(82) N_2H^+(9) NH_2^+(9) 2.4(−9) [2.32(−9)]	NH_3^+(75) NH_4^+(25) 2.4(−9) [2.28(−9)]	NH_4^+(70) NH_3^+(30) 2.3(−9) [2.24(−9)]	NH_4^+(100) 2.2(−9) [2.21(−9)]
7.4 eV H_2S 10.42 eV	H_2S^+(56), SH^+(29) S^+(12), NH^+(3) 1.9(−9) [1.86(−9)]	H_2S^+(55), H_2NS^+(15) SH^+(15), HNS^+(15) 1.7(−9) [1.82(−9)]	H_2S^+(40), NH_3^+(25) H_3S^+(15), NH_4^+(10) SH^+(10) 1.8(−9) [1.78(−9)]	NH_4^+(100) 1.3(−9) [1.74(−9)]
7.9 eV CH_3OH 10.85 eV	CH_3OH^+(40), H_2CO^+(~30) H_3CO^+(16), NO^+(~10) CH_3^+(4) 3.1(−9) [2.42(−9)]	H_3CO^+(70), HCO^+(15) $CH_3OH_2^+$(10), H_2CO^+(15) 3.0(−9) [2.36(−9)]	$CH_3OH_2^+$(85) NH_3^+(15) 3.1(−9) [2.31(−9)]	NH_4^+(100) 2.2(−9) [2.26(−9)]
7.2 eV H_2CO 10.9 eV	H_2CO^+(~65) HCO^+(25) NO^+(~10) 2.9(−9) [2.92(−9)]	HCO^+(55) H_2CO^+(30) H_3CO^+(15) 3.3(−9) [2.85(−9)]	H_3CO^+(80) NH_3^+(20) 2.8(−9) [2.79(−9)]	NH_4^+(100) 1.1(−9) [2.74(−9)]

*The reactions of NH_4^+ were also studied but because of the low reactivity of this ion, these data are not included in the table.

Reference: N. G. Adams, D. Smith, J. F. Paulson, J. Chem. Phys. 72, 288 (1980).

Tabular Data B-1.B-13. (cont.) Adams, et al.

	N^+ 14.55 eV	4.2 eV NH^+ 13.10 eV	6.1 eV NH_2^+ 11.4 eV	8.0 eV NH_3^+ 10.17 eV
6.2–7.4 eV	COS^+(73)	COS^+(85), NS^+(5)	H_2NS^+(80)	
COS	S^+(22)	SH^+(5), $HCOS^+$(5)	H_2NCO^+(15)	
11.17 eV	CS^+(5)		$HCOS^+$(5)	
	1.4(−9)	1.8(−9)	1.5(−9)	~2(−12)
	[1.89(−9)]	[1.84(−9)]	[1.79(−9)]	[1.74(−9)]
4.3 eV	O_2^+(51)	O_2^+(55)	H_2NO^+(85)	
O_2	NO^+(43)	NO^+(25)	HNO^+(15)	
12.06 eV	O^+(6)	HO_2^+(20)		
	6.1(−10)	8.2(−10)	1.4(−10)	<5(−13)
	[9.49(−10)]	[9.27(−10)]	[9.07(−10)]	[8.87(−10)]
7.2 eV	H_2O^+(100)	H_3O^+(30), H_2O^+(30)	H_3O^+(95)	
H_2O		NH_2^+(25), HNO^+(10)	NH_4^+(5)	(NH_4^+)
12.61 eV		NH_2^+(5)		
	2.8(−9)	3.5(−9)	2.9(−9)	≤3(−11)
	[2.50(−9)]	[2.46(−9)]	[2.42(−9)]	[2.38(−9)]
5.4 eV	CH_3^+(51), H_2CN^+(10)	H_2CN^+(70)	NH_3^+(100)	NH_4^+(100)
CH_4	HCN^+(6), CH_4^+(3)	NH_2^+(20)		
12.70 eV		CH_3^+(10)		
	9.1(−10)	9.6(−10)	9.2(−10)	4.8(−10)
	[1.38(−9)]	[1.36(−9)]	[1.33(−9)]	[1.31(−9)]
5.4 eV	CO_2^+(75)	HCO_2^+(35)		
CO_2	CO^+(25)	HNO^+(35)		
13.77 eV		NO^+(30)		
	1.0(−9)	1.1(−9)	<1(−12)	<1(−13)
	[1.16(−9)]	[1.13(−9)]	[1.10(−9)]	[1.08(−9)]
6.1 eV	CO^+(88)	NCO^+(55)	$NH_2^+ \cdot CO$ + He(100)	
CO	NO^+(12)	HCO^+(45)	pressure independent	
14.01			0.22–0.52 Torr	
	4.5(−10)	9.8(−10)	2.4(−11)	<5(−13)
	[1.08(−9)]	[1.05(−9)]	[1.03(−9)]	[1.01(−9)]
4.3 eV	NH^+(100)	NH_2^+(85)	NH_3^+(100)	
H_2		H_3^+(15)		(NH_4^+)
15.43 eV	4.8(−10)	1.5(−9)	2.7(−10)	<5(−13)
	[1.59(−9)]	[1.58(−9)]	[1.58(−9)]	[1.57(−9)]
5.0 eV	N_3^+ + He(100)	N_2H^+(100)		
N_2	5.2(−30)	6.5(−10)	<5(−13)	<5(−14)
15.58 eV		[9.94(−10)]	[9.73(−10)]	[9.55(−10)]

Tabular Data B-1.B-14. Rate coefficients for the reactions $NO^+ + X + Y \rightarrow NO^+ \cdot X + Y$ at the temperatures shown. The error figure on the data is ± 30%. A rate of e.g., 5×10^{-30} cm^6 sec^{-1} is shown as 5(-30) for convenience.

Reactant gas X	Third body Y	Temperature (K)	Rate coefficient ($cm^6 s^{-1}$)	reference
N_2	He	200	<5.0(-33)	2
		80	~5.0(-30)	4
	N_2	300	≤1.0(-30)	5
		300	2.0(-31)	3
		225	1.5(-30)	5
		220	≥1.0(-30)	1
		130	8.0(-30)	1
O_2	He	200	<6.0(-34)	2
	Ar	200	<2.0(-32)	2
	N_2	300	3±2(-31)	5
		225	5±2(-31)	5
	O_2	300	9.0(-32)	3
CO_2	He	300	4.5(-30)	5
		290	4.0(-30)	2
		235	7.2(-30)	2
		197	1.0(-29)	2
	Ar	300	5.0(-30)	5
		214	2.4(-29)	2
		196	3.1(-29)	2
	N_2	300	9.5(-30)	5
		225	2.5(-28)	5
		200	2.5(-29)	2
	CO_2	300	2.4(-29)	3

References: (1) R. Johnsen, C. M. Huang, and M. A. Biondi, J. Chem. Phys. 63, 3374 (1975).

(2) D. B. Dunkin, F. C. Fehsenfeld, A. L. Schmeltekopf, and E. E. Ferguson, J. Chem. Phys. 54, 3817 (1971).

(3) J. M. Heimerl and J. M. Vanderhoff, J. Chem. Phys. 60, 4362 (1974).

(4) E. E. Ferguson, A. L. Schmeltekofp, F. C. Fehsenfeld, D. L. Albritton, Investigations of Atmospheric Ion-Neutral Processes, Final Report DNA 3211F, July 1973, Defense Nuclear Agency Washington, D. C. 20305.

(5) D. Smith, N. G. Adams, D. Grief, J. Atmos. Terr. Phys. 39, 513 (1977).

Tabular Data B-1.B-15. Rate coefficients and product ion distributions for the reactions of N^+, N_2^+, N_3^+, N_4^+, O^+, O_2^+, and NO^+ with a series of molecules. The binary rate coefficients are indicated as, for example, 1.0(-9), meaning 1.0×10^{-9} cm^3 s^{-1}. The percentage of each ion product is indicated in brackets after each ion. The ternary association reactions are indicated by the inclusion of either He, N_2, or He/N_2 after the product ion and have units of cm^6 s^{-1}. The reactant ions and molecules are arranged in order of their recombination energies and ionization potentials (indicated in eV). The Langevin or ADO theoretical rate coefficient for each reaction is given in square brackets. ∿ implies a factor of 2 accuracy.

	N_2^+ 15.578 eV	N^+ 14.549 eV	N_4^+ 14.51 eV	O^+ 13.616 eV	O_2^+ 12.063 eV	N_3^+ 11.50 eV	NO^+ 9.25 eV
CH_3NH_2	$CH_2NH_2^+$(73) CH_3^+(21) $CH_3NH_3^+$(6)	$CH_2NH_2^+$(70), H_2CN^+(10) $CH_3NH_2^+$(7), H_3CN^+(7) CH_3^+(6)	$CH_2NH_2^+$(82) H_2CN^+(10) $CH_3NH_2^+$(8)	$CH_2NH_2^+$(79) H_2CN^+(15) $CH_3NH_2^+$(6)	$CH_3NH_2^+$(65) $CH_2NH_2^+$(35)	CH_2NH^+(79) $CH_3NH_2^+$(21)	$CH_3NH_2^+$(100)
8.97 eV	1.2(-9) [1.79(-9)]	2.0(-9) [2.21(-9)]	1.2(-9) [1.53(-9)]	2.1(-9) [2.11(-9)]	~1(-9) [1.73(-9)]	1.1(-9) [1.62(-9)]	8.2(-10) [1.75(-9)]
NH_3	NH_3^+(100)	NH_3^+(82) N_2H^+(9) NH_2^+(9)	NH_3^+(100)	NH_3^+(100)	NH_3^+(100)	NH_3^+(100)	$NO^+ \cdots NH_3 + He/N_2$
10.17 eV	1.9(-9) [1.98(-9)]	2.4(-9) [2.32(-9)]	1.8(-9) [1.78(-9)]	1.2(-9) [2.24(-9)]	2.0(-9) [1.93(-9)]	2.1(-9) [1.85(-9)]	~3(-28)
H_2S	SH^+(75) S^+(15) H_2S^+(10)	H_2S^+(56), SH^+(29) S^+(12), NH^+(3)	H_2S^+(97) S^+(3)	H_2S^+(68) HS^+(21) S^+(11)	H_2S^+(100)	H_2S^+(82) HNS^+(15) H_2NS^+(3)	$NO^+ \cdots H_2S + He/N_2$
10.42 eV	1.5(-9) [1.49(-9)]	1.9(-9) [1.86(-9)]	1.2(-9) [1.27(-9)]	2.0(-9) [1.78(-9)]	1.4(-9) [1.44(-9)]	1.0(-9) [1.35(-9)]	~1(-28)
CH_3OH	CH_3^+(79) H_3CO^+(12) CH_3OH^+(9)	CH_3OH^+(40) H_2CO^+(~30), H_3CO^+(16) NO^+(~10), CH_3^+(4)	CH_3OH^+(65) H_3CO^+(35)	H_2CO^+(70) CH_3OH^+(25) H_2CO^+(5)	CH_3OH^+(~50) H_3CO^+(~50)	CH_3OH^+(50) H_3CO^+(28) NO^+(22)	$NO^+ \cdots CH_3OH + He/N_2$
10.85 eV	1.4(-9) [1.95(-9)]	4.9(-9) [2.42(-9)]	2.2(-9) [1.67(-9)]	1.9(-9) [2.31(-9)]	~1(-9) [1.89(-9)]	1.0(-9) [1.77(-9)]	~1(-28)
H_2CO	HCO^+(87) H_2CO^+(13)	H_2CO^+(~65) HCO^+(25) NO^+(~10)	H_2CO^+(72) HCO^+(28)	H_2CO^+(60) HCO^+(40)	H_2CO^+(90) HCO^+(10)	N_2H^+(52), H_2CO^+(26) HCO^+(16), NH_2^+(6)	$NO^+ \cdots H_2CO + He/N_2$
10.9 eV	2.9(-9) [2.37(-9)]	2.9(-9) [2.92(-9)]	1.8(-9) [2.04(-9)]	3.5(-9) [2.79(-9)]	2.3(-9) [2.29(-9)]	1.9(-9) [2.16(-9)]	~5(-28)

Reference: D. Smith, N. G. Adams, and T. M. Miller, J. Chem. Phys. 69, 308 (1978).

Tabular Data B-1.B-15. (cont.) Ref.: Smith, Adams and Miller.

	N_2^+ 15.578 eV	N^+ 14.549 eV	N_4^+ 14.51 eV	O^+ 13.616 eV	O_2^+ 12.063 eV	N_3^+ ≤ 11.50 eV	NO^+ 9.25 eV
COS	S^+(80) COS^+(20)	COS^+(73) S^+(22) CS^+(5)	COS^+(100)	COS^+(97) S^+(3)	COS^+(100)	NS^+(90) COS^+(8) NO^+(2)	$NO^+ \cdots COS + He/N_2$
11.17 eV	1.3(−9) [1.45(−9)]	1.4(−9) [1.89(−9)]	4.6(−10) [1.18(−9)]	6.7(−10) [1.79(−9)]	1.0(−9) [1.39(−9)]	4.3(−10) [1.28(−9)]	<2(−29)
O_2	O_2^+(100)	O_2^+(51) NO^+(43) O^+(6)	O_2^+(100)	O_2^+(100)	$O_2^+ \cdots O_2 + He$	NO^+(70) NO_2^+(30)	$NO^+ \cdots O_2 + N_2$
12.063 eV	5.1(−11) [7.66(−10)]	6.1(−10) [9.49(−10)]	2.5(−10) [6.56(−10)]	1.9(−11) [9.07(−10)]	5.0(−31)	5.1(−11) [6.95(−10)]	(3 ± 2)(−31)
H_2O	H_2O^+(82) N_2H^+(18)	H_2O^+(100)	H_2O^+(100)	H_2O^+(100)	$O_2^+ \cdots H_2O + He$	H_2NO^+(100)	$NO^+ \cdots H_2O + He$
12.614 eV	2.8(−9) [2.12(−9)]	2.8(−9) [2.50(−9)]	3.0(−9) [1.90(−9)]	3.2(−9) [2.42(−9)]	8.7(−29)	3.3(−10) [2.36(−9)]	3.6(−29)
CH_4	CH_3^+(93) CH_2^+(7)	CH_3^+(51), H_2CN^+(40), HCN^+(6), CH_4^+(3)	CH_4^+(90) $H_4CN_2^+$(10)	CH_4^+(89) CH_3^+(11)	H_2COOH^+(70) H_2CO^+(15) H_2O^+(15)	H_2CN^+(95) $CH_2NH_2^+$(5)	$NO^+ \cdots CH_4 + He/N_2$
12.704 eV	1.0(−9) [1.18(−9)]	9.4(−10) [1.38(−9)]	1.0(−9) [1.07(−9)]	1.0(−9) [1.33(−9)]	6.3(−12) [1.16(−9)]	4.8(−11) [1.11(−9)]	<2 (−29)
CO_2	CO_2^+(100)	CO_2^+(75) CO^+(25)	CO_2^+(100)	O_2^+(100)	$O_2^+ \cdots CO_2 + He \cdots$		$NO^+ \cdots CO_2 + He$
13.769 eV	7.7(−10) [9.11(−10)]	1.0(−9) [1.16(−9)]	7.0(−10) [7.59(−10)]	9.4(−10) [1.10(−9)]	2.3(−29) T = 200 K	<5(−14) [8.13(−10)]	4.5(−30)
CO	CO^+(100)	CO^+(88) NO^+(12)	CO^+(100)	...	...	$N_3^+ \cdots CO + He/N_2$	$NO^+ \cdots CO + CO$
14.013 eV	7.4(−11) [8.78(−10)]	4.5(−10) [1.08(−9)]	~5(−10) [7.60(−10)]	<5(−13) [1.03(−9)]		~7(−29)	1.9(−30)
H_2	N_2H^+(100)	NH^+(100)	N_2H^+(87) N_4H^+(13)	OH^+(100)	$O_2^+ \cdots H_2 + He$	N_2H^+(100)	...
15.427 eV	2.1(−9) [1.54(−9)]	4.8(−10) [1.59(−9)]	5.8(−12) [1.51(−9)]	1.7(−9) [1.58(−9)]	7.4(−31) T = 80 K	~2(−13) [1.52(−9)]	<1(−13) [1.54(−9)]
N_2	$N_2^+ \cdots N_2$ $+ He/N_2$	$N^+ \cdots N_2 + He/N_2$	...	NO^+(100)	$O_2^+ \cdots N_2 + N_2$	...	$NO^+ \cdots N_2 + N_2$
15.578 eV	1.1(−29)	5.2(−30)		1.2(−12) [9.73(−10)]	8(−31)		≲1(−30)

Tabular Data B-1.B-16. Reaction rate coefficients of the ground and metastable excited states of O_2^+, NO^+ and O^+ with atmospheric gases at thermal energy. The type of reactions studied are the following:

$$A^{+*} + B \xrightarrow{k_1} C^+ + D \text{ ion-molecule reaction}$$

$$A^{+*} + B \xrightarrow{k_2} A^+ + B \text{ collisional quenching}$$

$$A^+ + B \xrightarrow{k_3} E^+ + F \text{ ground-state ion-molecule reaction}$$

where $k^* = k_1 + k_2$.

Reactions with $O_2^{+*}(a^4\Pi_u)$ and $O_2^+(x^2\Pi_g)$

Reactant	Reaction	$k_3[x]$	k^* [a]
CO_2	$O_2^{+*} + CO_2 \rightarrow CO_2^+ + O_2 + 2.1$ eV	endo	7.2(−10)
			8.0(−10)†
N_2	$O_2^{+*} + N_2 \rightarrow N_2^+ + O_2 + 0.48$ eV	endo	6.0(−10)
CO	$O_2^{+*} + CO \rightarrow CO^+ + O_2 + 2.07$ eV (83%)	endo	1.8(−10)
	$\rightarrow CO_2^+ + O + 2.68$ eV (17%)		
H_2	$O_2^{+*} + H_2 \rightarrow O_2H^+ + H + 2.33$ eV (85%)	endo	1.0(−9)
	$\rightarrow H_2^+ + O_2 + 0.65$ eV (15%)		0.9(−9)†
Ar	$O_2^{+*} + Ar \rightarrow Ar^+ + O_2 + 0.33$ eV	endo	4(−10)
NO	$O_2^+(x) + NO \rightarrow NO^+ + O_2 + 2.81$ eV	4.8(−10)	
	$O_2^{+*} + NO \rightarrow NO^+ + O_2 + 6.84$ eV		1.0(−9)
O_2	$O_2^{+*} + O_2 \rightarrow O_2^+ + O_2 + 4.03$ eV	endo	4.6(−10)†

Reactions with $NO^{+*}[a\,^3\Sigma]$ and $NO^+[x\,^1\Sigma]$

Reactant	Reaction	$k^* = k_1 + k_2$	k_2
Ar	$NO^{+*} + Ar \rightarrow Ar^+ + NO - 0.1$ eV	3.5(−11)	
CO	$NO^{+*} + CO \rightarrow CO^+ + NO + 1.63$ eV	7.2(−10)	
		6.4(−10)†	
CO_2	$NO^{+*} + CO_2 \rightarrow CO_2^+ + NO + 1.88$ eV	1.06(−9)	
N_2	$NO^{+*} + N_2 \rightarrow N_2^+ + NO + 0.09$ eV (55%)	7.7(−10)	3.5(−10)
	$\rightarrow NO^+(x) + N_2 + 6.4$ eV (45%)	7.7(−10)†	
O_2	$NO^{+*} + O_2 \rightarrow O_2^+ + NO + 3.6$ eV (30%)	3.3(−10)†	2.3(−10)
	$\rightarrow NO^+(x) + O_2 + 6.4$ eV (70%)		
H_2	$NO^{+*} + H_2 \rightarrow H_2^+ + NO + 0.22$ eV (12%)	1.4(−9)†	1.2(−9)
	$\rightarrow NO^+(x) + H_2 + 6.4$ eV (88%)		

Reactions with $O^+(^4S)$, $O^+(^2D,^2P)$ and O_2^{+*}

Reactant	Reaction	$k_3(^4S)$	$k^*(^2D,^2P)$
O_2	$O^+ + O_2 \rightarrow O_2^+ + O + 1.56$ eV	2.3(−11)	
	$O^{+*} + O_2 \rightarrow O_2^+ + O + 4.85, 6.54$ eV		1.3(−10)
N_2	$O^+ + N_2 \rightarrow NO^+ + N + 1.13$ eV	1.4(−12)	
	$O^{+*} + N_2 \rightarrow N_2^+ + O + 1.34, 3.03$ eV (90%)	1.4(−12)	1.5(−10)
	$\rightarrow NO^+ + N + 4.42, 6.11$ eV (10%)		
	$O_2^{+*} + N_2 \rightarrow O_2^+ + N_2^+$		
NO	$O^+ + NO \rightarrow NO^+ + O + 4.37$ eV	<8(−12)	
	$O^{+*} + NO \rightarrow NO^+ + O + 7.66, 9.35$ eV		1.2(−9)
CO	$O^{+*} + CO \rightarrow CO^+ + O + 2.89, 4.58$ eV		1.3(−9)
	$O_2^{+*} + CO \rightarrow O_2^+ + CO^+$		

Rate coefficients listed as a(-b) represent a x 10^{-b}. The accuracy is ± 30%. † rate *constant obtained using monitor-ion method.*

Reference: J. Glosik, A. B. Rakshit, N. D. Twiddy, N. G. Adams, and D. Smith, J. Phys. B Atom. Molec. Phys. 11, 3365 (1978).

Tabular Data B-1.B-17. Rate constants for the reactions of H_2O^+ with molecules at 300 K.

Reaction		Exothermicity, eV.	Rate Constant (10^{-10} cm^3 sec^{-1})
$H_2O^+ + NO_2$	$\rightarrow NO_2^+ + H_2O$	2.9	12±3.6
$H_2O^+ + O_2$	$\rightarrow O_2^+ + H_2O$	0.6	3.3±1.0
$H_2O^+ + NO$	$\rightarrow NO^+ + H_2O$	3.4	4.5±1.3
$H_2O^+ + C_2H_4$	$\rightarrow C_2H_4^+ + H_2O$	2.1	16±4.8
	$\rightarrow C_2H_5^+ + OH$	0.8	
$H_2O^+ + CO$	$\rightarrow HCO^+ + OH$	0.1	4.2±1.3
$H_2O^+ + CH_4$	$\rightarrow CH_4^+ + H_2O$	−0.1	12±3.6
	$\rightarrow H_3O^+ + CH_3$	1.7	
$H_2O^+ + H_2$	$\rightarrow H_3O^+ + H$	1.7	8.3±2.5

Graphical Data B-1.B-18. Rate constants for the reactions of H_2O^+ with NO and NO_2 at relative energies of 0.04 - 2 eV.

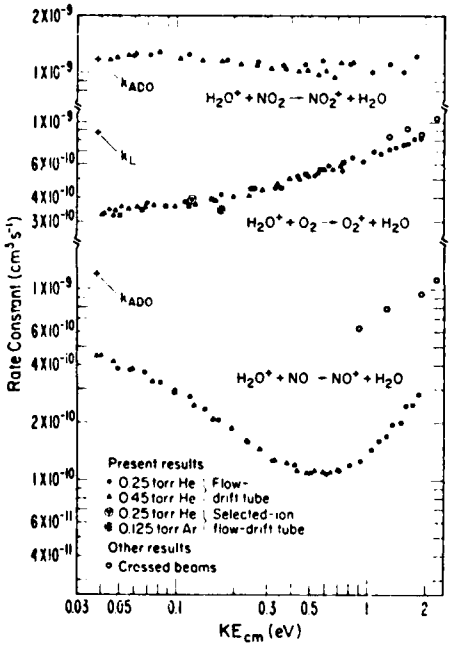

Open circles represent crossed beam data (B. R. Turner and J. A. Rutherford, J. Geophys. Res. 73, 6751 (1968)).

Graphical Data B-1.B-19. Rate constants for the reactions of H_2O^+ with CH_4 and H_2 at relative energies of 0.04 - 2 eV.

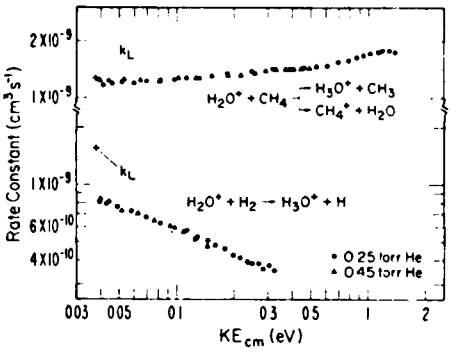

Graphical Data B-1.B-20. Rate constants for the reactions of H_2O^+ with C_2H_4 and CO at relative energies of 0.04 - 2 eV.

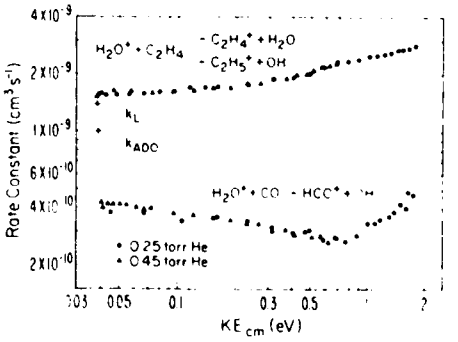

Reference: I. Dotan, W. Lindinger, B. Rowe, D. W. Fahey, F. C. Fehsenfield, and D. L. Albritton, Chem. Phys. Letts. 72, 67 (1980).

Tabular Data B-1.B-21. Reactions of H_nCO^+ with molecules at 300 K.

Reaction: $H_nCO^+ + M \rightarrow$ products.

Reaction rate coefficients and percentage product ion distributions for the reactions of H_nCO^+ (n = 0 - 3) with various neutrals at 300 K. A rate constant of a x 10^{-b} is represented by a(-b).[1,2]

M	CO^+	HCO^+	H_2CO^+	H_3CO^+
H_2	$HCO^+ + H$	—	—	—
	1.8 (−9)	< 4 (−14)	< 4 (−14)	< 4 (−14)
O_2	$O_2^+ + CO$		$HCO^+ + HO_2$ (70)	
		—	$H_2O_2^+ + CO$ (30)	—
	1.2 (−10)	< 2 (−13)	1.1 (−10)	< 4 (−14)
CO_2	$CO_2^+ + CO$	—	—	—
	1.0 (−9)	< 2 (−13)	< 4 (−14)	< 4 (−14)
COS	$COS^+ + CO$ (90)	$HCOS^+ + CO$	$H_2S^+ + 2\,CO$ (56)	
	$S^+ + 2\,CO$ (10)		$HCOS^+ + HCO$ (41)	—
			$H_2COS^+ + CO$ (3)	
	1.2 (−9)	1.1 (−9)	1.0 (−9)	< 4 (−13)
H_2O	$H_2O^+ + CO$	$H_3O^+ + CO$	$H_3O^+ + HCO$	$H_3O^+ + H_2CO$
	2.2 (−9)	2.5 (−9)	2.6 (−9)	~3 (−11)
NH_3	$NH_3^+ + CO$	$NH_4^+ + CO$	$NH_4^+ + HCO$ (75)	$NH_4^+ + H_2CO$
			$NH_3^+ + H_2CO$ (25)	
	1.8 (−9)	1.9 (−9)	1.7 (−9)	2.0 (−9)
H_2CO	$HCO^+ + HCO$ (55)	$H_3CO^+ + CO$	$H_3CO^+ + HCO$	$H_3CO^+ \cdot H_2CO + He$
	$H_2CO^+ + CO$ (45)			
	3.0 (−9)	3.2 (−9)	3.2 (−9)	~2 (−27)
CH_3OH	$H_3CO^+ + H + CO$	$CH_3OH_2^+ + CO$	$CH_3OH_2^+ + HCO$ (90)	$CH_3OH_2^+ + H_2CO$
			$H_3CO^+ + H_3CO$ (10)	
	2.4 (−9)	2.4 (−9)	2.4 (−9)	1.9 (−9)
CH_4	$CH_5^+ + CO$ (61)		$H_3CO^+ + CH_3$ (85)	
	$HCO^+ + CH_3$ (35)	—	$C_2H_5O^+ + H$ (15)	—
	$CH_3CO^+ + H$ (4)			
	1.3 (−9)	< 1 (−13)	1.1 (−10)	< 4 (−14)

(1) Rate coefficients have units of $cm^3\ s^{-1}$ except in the case of the 3-body association reaction (asterisked). Rate coefficients are as indicated: e.g., for $CO^+ + H_2$, k = 2.0(-9) is equivalent to 2.0 x 10^{-9} $cm^3\ s^{-1}$. The numbers in parentheses after each product channel represent the percentage product ion distribution. Where no significant reaction was observed an upper limit to the rate coefficient is quoted. In the reactions of H_nCO^+ with N_2, the replacement of CO by N_2 to yield $H_nN_2^+$ could not be detected and thus is not subject to the upper limit quoted.

(2) For reactions of H_nCO^+ ions with N_2 and CO, k < 4(-14).

Reference: N. G. Adams, D. Smith, and D. Grief, Int. J. Mass Spect. Ion Phys. 26, 405 (1978).

Tabular Data B-1.B-22. Rate constants for the reaction of $O_2^+(a^4\Pi_u)$ ions with CH_4 at relative kinetic energies 0.04 - 1.2 eV. Experiment was performed in a flow-drift tube with He buffer gas. The reactions studied are the following:

$$O_2^+(a^4\Pi_u) + CH_4 \xrightarrow{K_1} CH_3^+ + HO_2 + 3.8 \text{ eV}$$

$$\xrightarrow{K_2} CH_4^+ + O_2 + 3.4 \text{ eV}$$

$$\xrightarrow{K_3} O_2^+(X^2\Pi_g) + CH_4 + 4.0 \text{ eV}$$

The rate constant k applies to the total loss of O_2 metastables where $k^* = k_1 + k_2 + k_3$.

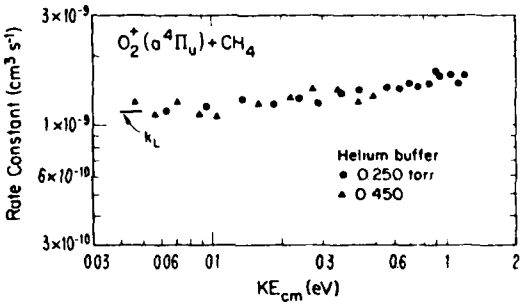

The experimental uncertainty of the data is believed to be less than 40%. The relative magnitude for the first two processes was determined to be approximately $k_1/k_2 \approx 2$.

Reference: W. Lindinger, D. L. Albritton, and F. C. Fehsenfeld, J. Chem. Phys. 70, 2038 (1979).

SECTION B-1.C. COLLISIONAL QUENCHING AND ENERGY TRANSFER.

CONTENTS

		Page
Introduction		
General References.		
B-1. C-1	Rate Coefficients for Quenching of He (2^3S)	2753
B-1. C-2	Rate Coefficients and Cross Sections for Quenching Metastable States of Ar, Kr, Xe	2754
B-1. C-3	Rate Coefficients for Population Transfer Between Levels of Argon	2756
B-1. C-4	Rate Coefficients for Quenching $O(^1D)$	2757
B-1. C-5	Branching Ratios for Reaction of $O(^1D_2)$ with N_2O	2758
B-1. C-6	Rate Coefficients for Collision Induced Emission from $S(^1S)$	2759
B-1. C-7	Cross Section for De - Excitation of Ca and of Sr	2759
B-1. C-8	Quenching and Energy Transfer for Hydrides	2760
B-1. C-9	Rate Coefficient for Isotopic Vibrational Energy Transfer in HCℓ + HCℓ	2766
B-1. C-10	Rate Coefficients for Quenching Rare Gas Halides	2767
B-1. C-11	Collision Induced Energy Transfer from Rotational and Vibrational States of S_2	2769
B-1. C-12	Rate Coefficients for Vibrational Quenching of GeF and SiF	2770
B-1. C-13	Rate Coefficients for Vibrational Quenching of NH_3	2770
B-1. C-14	Cross Sections for Quenching Rotational States of CsF	2771
B-1. C-15	Rate Coefficients for Quenching Mercury Halides	2772
B-1. C-16	Rate Coefficient for Vibrational Quenching of O_3 by HCℓ	2773
B-1. C-17	Rate Coefficients for Vibrational Quenching of CO_2 and N_2O	2774

INTRODUCTION

This section represents an update of Section B-1.C of Technical Report H-78-1 "Compilation of Data Relevant to Nuclear Pumped Lasers" Volume IV, U.S. Army Missile Research and Development Command, Redstone Arsenal, December 1978. It includes the results of a literature search for the period August 1978 to August 1980. In order to limit transcription errors published data tables have been reproduced in their original form although this does result in the data presentation having a lack of logical order. Where possible the full reaction equation has been presented. Where the post collision states are not specified then it was not clear from the original publication what final states were involved.

To aid in location of reactions of interest we list below the excited species being quenched with the table or figure number where the data are located. Excited species are separated into mono-,di-and tri-atomic molecules and ordered by increasing molecular weight.

Reaction Locator

Excited State	Table or Figure Number.
Monoatomic Species	
He	B-1. C-1
O	B-1. C-4 & C-5
S	B-1. C-6
Ar	B-1. C-2 & C-3
Ca	B-1. C-7
Kr	B-1. C-2
Sr	B-1. C-7
Xe	B-1. C-2
Diatomic Species	
LiH	B-1. C-8
HF	B-1. C-8
HCℓ	B-1. C-8 & C-9
DCℓ	B-1. C-8
SiF	B-1. C-12
S_2	B-1. C-11
HBr	B-1. C-8
DBr	B-1. C-8
GeF	B-1. C-12
KrF	B-1. C-10
XeF	B-1. C-10
CsF	B-1. C-14
HgCℓ	B-1. C-15
HgBr	B-1. C-15
HgI	B-1. C-15

Reaction Locator

Excited State	Table or Figure Number.
Triatomic Species	
O_3	B-1. C-16
CO_2	B-1. C-17
N_2O	B-1. C-17

General References

1. J. W. Gallagher, Janet Van Blerkom, E. C. Beaty, and J. R. Rumble, Jr., "Data Index for Energy Transfer Collisions of Atoms and Molecules: 1970-1979". NBS Special Publication 593 (1980). This is a bibliography indexed by physical processes and reactants that covers the reactant energy range 0-10 keV.

2. "Rate Constants and Quenching Mechanisms from the Metastable States of Argon, Krypton, and Xenon". I. E. Velazco, J. H. Kolts, and Setser, J. Chem. Phys. 69, 4357 (1978).

3. "Gas Phase Ion Chemistry", Vol. 1, edited by M. T. Bowers (Academic Press Inc. N.Y. (1979)).

4. "Excimer Lasers". Topics in Applied Physics, Vol. 30, edited by Ch. K. Rhodes. (Springer-Verlag New York (1979)).

5. "Atomic and Molecular Collision Processes in Rare-Gas-Halide Lasers and Rare-Gas Excimer Lasers". M. R. Flannery, International Journal of Quantum Chemistry: Quantum Chemistry Symposium, 13, 501 (1979).

6. "Electronic Transition Lasers II", edited by L. F. Wilson, S. N. Suchard and J. J. Steinfield (MIT Press, Cambridge, Mass, 1979).

Tabular Date B-1. C-1. Rate Coefficients for Quenching of $He(2^3S)$.

A) Three body rates for $He(2^3S)+X+X \rightarrow He(?)+X+X$ (units of 10^{-30} cm^6 sec^{-1}) at 300^oK.

Reactant	Rate coefficient
Kr	0.86(+0.3, −0.86)
Xe	2.2(±0.6)
H_2	1.2(±0.3)
O_2	3.1(±1.2)
NO	4.3(±2.0)
HBr	2.4(+4.8, −2.4)
HCl	2.9(±2.9)
H_2O	19(±15)
N_2O	8.8(±3.0)
NO_2	6.6(±2.6)
CO_2	
NH_3	8.4(±4.0)
CH_4	
C_2H_6	6.3(±2.0)
C_3H_8	8.1(±2.0)
CCl_2F_2(F-12)	6.5(±4.0)
CCl_3F(F-11)	15.4(±7.0)

B) Two body rates for $He(2^3S)+X \rightarrow He(?)+X$ (units of 10^{-11} cm^3 sec^{-1}) at 300^oK.

Reactant														
Kr	Xe	H_2	O_2	NO	HBr	HCl	H_2O	N_2O	NO_2	NH_3	C_2H_6	C_3H_8	CCl_2F_2	CCl_3F
10	12.5	3.8	19	23	78	58	78	44	63	88	30	31	47	80

Reference. C. B. Collins and F. W. Lee, J. Chem. Phys. 70, 1275 (1979).

Tabular Data B-1. C-2. Rate Coefficients and Cross Sections for Quenching Metastable States of Ar, Kr and Xe.

$$Ar^m(\text{or } Kr^m \text{ or } Xe^m)+X \rightarrow Ar(\text{or Kr or Xe})+X$$

Cross sections: σ ($\mathring{A}^2$)

Reaction rates: $K_Q(cm^3\ sec^{-1})$

Temperature: 300^oK

	$Ar(^3P_2)$		$Ar(^3P_0)$		$Kr(^3P_2)$		$Xe(^3P_2)$	
Reagent	k_Q	σ	k_Q	σ	k_Q	σ	k_Q	σ
Xe	18[a]	40	30	58	16[f]	46		
Kr	0.6[f]	1.3	0.2[d]	0.5				
Hg		30[h]			20 ± 10	60 ± 30	< 0.001	< 0.004
H_2	6.6[f]	3.6	7.8[d]	4.3	3.0	1.7	1.6[c]	0.9
D_2	4.7[d]	3.6	7.8[d]	5.9	2.5	1.9		
CO	1.4[d]	2.3	13[d]	21	5.8	10.5	3.6[c]	7.0
N_2	3.6[g]	5.8	1.6[d]	2.5	0.39	0.7	1.9[c]	3.7
NO	22[d]	36	25[d]	41	19	35	27[f]	54
N_2O	44[d]	81	48[d]	87	31	66	44[c]	100
O_2	21[d]	35	24[d]	41	16	31	22[c]	44
SO_2	64	126			58	139		
CO_2	53[d]	97	59[d]	106	40	85	45[c]	103
COS	79[d]	155						
HCl	37[e]	65					56[e]	119
HBr	52[f]	106					61[e]	173
HI	75[e,k]	155[k]						
F_2	75[e]	132	90	160	72[f]	146	75[f]	161
Cl_2	71[e]	142	72	138	73[f]	179	72[f]	193
Br_2	65[e]	147			61	179	60[e]	202
ICl	61[e]	138			49	143	50[e]	171
IBr					71	216		
ClF	74[b]	141			68	156	60[f]	148
OF_2	57[e]	107			53	121	57[e]	139
NOCl	48[e]	95					51[e]	135
NOF	36[e]	68			47[e]	102	45	106
NF_3	14[e]	28	7	13	12	29	9[e]	23
N_2F_4	31[e]	65			33[e]	90		
BF_3					23	56		
CF_3OF	43[e]	91			42[e]	114	47[e]	143
SF_4	33	71	41	88				
SF_6	16	36	17[d]	38	18	51	23	75
SeF_6	71[e]	166					65[e]	246
TeF_6	58[e]	135					63[e]	230
SO_2F_2	42	89						
S_2Cl_2	54	115			48	129	49	150
$SOCl_2$	67	145			58	163	58	182
CS_2	106[d]	218			80	210		
CF_3I	47	108			49	148	52[e]	184
CF_3Br	31	69	34	77	50	145	42	140
PCl_3	53[e]	116						
$COCl_2$	47	100	42	89	52	140		

Tabular Data B-1. C-2 (continued)

Reagent	$Ar(^3P_2)$		$Ar(^3P_0)$		$Kr(^3P_2)$		$Xe(^3P_2)$	
	k_Q	σ	k_Q	σ	k_Q	σ	k_Q	σ
SiF_4					22	59		
$SiCl_4$					69	206		
CF_3Cl	22[f]	47	27	57	14	38		
CF_2Cl_2	37	81	57	116				
CCl_3F	55	121	43	95				
CCl_4	100[j]	220			69	201		
CF_4	4[d]	8	4[d]	8	0.07	0.2	0.03	0.1
CF_3H	31[d]	64			15	37	0.2	0.6
CF_2H_2					35	79	41	99
CFH_3	34	58			46	90	44	91
CH_4	33[d]	45	55	74	37	54	33[c]	49
H_2O	48[i]	67						
CH_3OH	60[i]	100						
H_2S	86	146					70	145
NH_3	54[i]	74			90	135		
PH_3					59	115		
HCN	58[d]	94						
BrCN	46[e]	91						
C_2N_2					51	114		
C_2H_6	66[d]	109			50	93	64[c]	125
C_3H_8	73[d]	134					0.54	123
$n\text{-}C_4H_{10}$	76[d]	149			72	166	68	170
C_5H_{12}	100[i]	200					72	192
C_2H_2	56[d]	89					70	130
C_2H_4	54	99					58	110
C_6H_6	79[i]	161						
$C_6H_5CH_3$	88[i]	154						

Reference: J. Velazco, J. H. Kolts and D. W. Setser. J. Chem. Phys. 69, 4357 (1969).

Note: This reference contains many comparisons with data from other sources.

Tabular Data B-1. C-3 Rate Coefficients for Population Transfer Between Levels of Argon

$$Ar(3p^5\ 4p)_i + Ar(^1S_o) \underset{k_{ji}}{\overset{k_{ij}}{\rightleftarrows}} Ar(3p^5\ 4p)_j + Ar(^1S_o)$$

Temperature: 300^oK

Coefficients in units of $10^{12}\ cm^3\ s^{-1}$

i \ j	1	2	3	4	5	6	7	8	9	10
1										
2			0.5							
3				27.5	0.3	44	1.4	1.9	0.8	
4			23		0.7	4.8	3.2	1.4	3.3	
5				1.7		11.3		9.5		
6							4.1	6	1	
7						2.5		14.3	23.3	
8						0.3	0.8		18.2	1
9								6.8		5.1
10										

Reference: T. D. Nguyen and N. Sodeghi, Phys. Rev. A 18, 1388 (1978).

Tabular Data B-1. C-4 Rate Coefficients for Quenching $O(^1D)$.

$$O(^1D) + X \rightarrow O(?) + X$$

Reaction rates k in units of 10^{-10} cm^3 s^{-1}.

Temperature $T(^oK)$

N_2O		H_2		HCl		NH_3		CH_4	
T(K)	k	T(K)	k	T(K)	k	T(K)	k	T(K)	k
359	1.3	352	1.1	379	1.5	354	2.3	357	1.6
359	1.2	333	0.95	355	1.4	354	2.4	352	1.5
352	1.0	313	0.95	354	1.4	333	2.5	324	1.4
352	1.0	295	0.93	337	1.4	313	2.5	314	1.2
352	1.0	273	0.98	328	1.5	297	2.7	290	1.4
351	1.2	243	1.1	314	1.4	293	2.4	258	1.2
343	1.1	233	0.96	300	1.4	273	2.4	253	1.3
334	1.1	223	1.0	293	1.3	253	2.5	228	1.5
316	1.1	213	0.94	293	1.4	253	2.4	222	1.4
294	1.2	204	1.0	292	1.4	233	2.5	203	1.4
289	1.3			291	1.5	223	2.4	198	1.4
253	1.2			273	1.4	214	2.8		
244	1.2			262	1.3	213	2.3		
234	1.1			253	1.4	204	2.7		
223	1.2			253	1.4				
212	1.2			233	1.4				
208	1.1			230	1.3				
207	1.1			223	1.5				
204	1.1			213	1.5				
				199	1.4				

Also at 298^oK only: -

O_3	O_2	N_2	CO_2	H_2O
2.4 ± 0.5	0.37 ± 0.07	0.28 ± 0.6	1.0 ± 0.2	2.3 ± 0.4

Reference: J. A. Davison, H. I. Schiff, G. E. Streit, J. R. McAfee, A. L. Schmeltekopt and C. J. Howard, J. Chem. Phys. 67, 5021 (1977).

Graphical Data B-1. C-5. Branching Ratios for reaction of $O(^1D_2)$ with N_2O.

Data represent the ratio of reaction rates k_a/k_b for reaction 1a and 1b of the following set, measured with an He buffer gas.

reaction channels

$$O(^1D_2) + N_2O \rightarrow \begin{cases} N_2 + O_2 & (1a) \\ 2NO & (1b) \\ N + NO_2 & (1c) \\ O(^3P) + N_2O & (1d) \\ 2O(^3P) + N_2 & (1e) \end{cases}$$

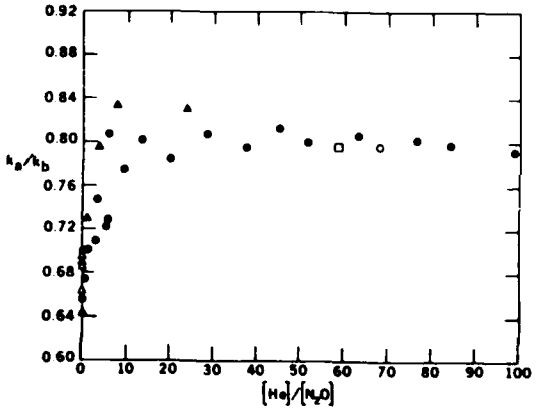

Ratio as a function of He to N_2O molecular number density at 300°K

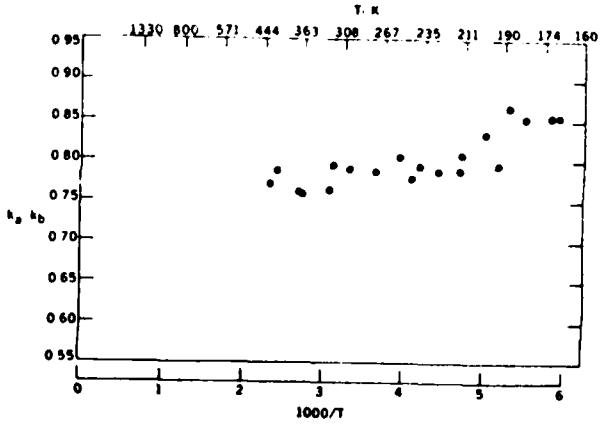

Ratio as a function of temperature at a molecular number density ratio (He to N_2O) of 56.

Reference: J. A. Davison, C. J. Howard, H. I. Schiff and F. C. Fehsenfeld, J. Chem. Phys. 70, 1697 (1979).

Tabular Data B-1. C-6 Rate Coefficients for Collision Induced Emission from $S(^1S)$.

$$S(^1S) + X \rightarrow S(^1D) + X + h\nu$$

$$X = He, Ar, N_2, H_2, Kr, Xe$$

Temperature: 232, 296 and 425°K

Gas	Rate coefficient k (cm^3 $molecule^{-1}$ sec^{-1}) 232 °K	296 °K[a]	425 °K
He	$(4.3 \pm 0.7) \times 10^{-20}$	$(5.6 \pm 0.9) \times 10^{-20}$	$(5.4 \pm 0.6) \times 10^{-20}$
Ar	$(4.8 \pm 0.3) \times 10^{-18}$	$(4.2 \pm 0.3) \times 10^{-18}$	$(4.9 \pm 0.3) \times 10^{-18}$
N_2	$(4.0 \pm 0.2) \times 10^{-18}$	$(3.3 \pm 0.2) \times 10^{-18}$	$(4.4 \pm 0.2) \times 10^{-18}$
H_2	$(1.86 \pm 0.19) \times 10^{-18}$	$(1.73 \pm 0.15) \times 10^{-18}$	$(2.4 \pm 0.2) \times 10^{-18}$
Kr	$(1.96 \pm 0.15) \times 10^{-17}$	$(1.5 \pm 0.1) \times 10^{-17}$	$(1.5 \pm 0.1) \times 10^{-17}$
Xe	$(1.65 \pm 0.15) \times 10^{-16}$	$(1.1 \pm 0.05) \times 10^{-16}$	$(8.6 \pm 0.4) \times 10^{-17}$

[a]G. Black, R. L. Sharpless, and T. G. Slanger, J. Chem. Phys. 63, 4551 (1975).

Reference: G. Black and R. L. Sharpless, J.Chem. Phys. 70, 5571 (1979).

Tabular Data B-1. C-7 Cross Section for De-Excitation of Ca and of Sr.

$$Ca(^1P_1) + X \rightarrow Ca(^3P_J) + X$$

$$Sr(^1P_1) + X \rightarrow Sr(^3P_J) + X$$

$$X = He, Ne, Ar, Kr, Xe.$$

Date are reaction cross sections ($Å^2$) measured at 900°K for Ca and 800°K for Sr.

	Calcium	Strontium
He	0.025	0.38
Ne	0.028	0.61
Ar	0.046	1.6
Kr	0.064	1.4
Xe	1.15	0.25

Reference: J. J. Wright and L. C. Balling, J. Chem. Phys. 73, 1617 (1980).

Tabular Data B-1. C-8

Quenching and Energy Transfer for Hydrides

Reaction			Temperature or Energy	Reaction Rate or Cross Section†	Reference
LiH(j=1) + HCℓ	→	LiH(j=0) + HCℓ	0.74eV	64 $Å^2$	4
	→	LiH(j=2) + HCℓ	0.74eV	157 $Å^2$	4
	→	LiH(j=3) + HCℓ	0.74eV	67 $Å^2$	4
	→	LiH(j=4) + HCℓ	0.74eV	33 $Å^2$	4
	→	LiH(j=5) + HCℓ	0.74eV	23 $Å^2$	4
	→	LiH(j=6) + HCℓ	0.74eV	11 $Å^2$	4
LiH(j=1) + DCℓ	→	LiH(j=0) + DCℓ	0.74eV	88 $Å^2$	4
	→	LiH(j=2) + DCℓ	0.74eV	203 $Å^2$	4
	→	LiH(j=3) + DCℓ	0.74eV	93 $Å^2$	4
	→	LiH(j=4) + DCℓ	0.74eV	53 $Å^2$	4
	→	LiH(j=5) + DCℓ	0.74eV	29 $Å^2$	4
	→	LiH(j=6) + DCℓ	0.74eV	21 $Å^2$	4
HF(v=3) + HCℓ	→	HF + HCℓ	298°K	$1.18\pm0.14\times10^{-11}$ cm^3 s^{-1}	2
HF(v=3) + CO_2	→	HF + CO_2	298°K	$10.4\pm1.3\times10^{-12}$ cm^3 s^{-1}	2
HF(v=3) + N_2O	→	HF + N_2O	298°K	$1.41\pm0.13\times10^{-11}$ cm^3 s^{-1}	2
HF(v=3) + CO	→	HF + CO	298°K	$2.9\pm0.3\times10^{-12}$ cm^3 s^{-1}	2
HF(v=3) + N_2	→	HF + N_2	298°K	$7.1\pm0.6\times10^{-14}$ cm^3 s^{-1}	2
HF(v=3) + O_2	→	HF + O_2	298°K	$1.9\pm0.6\times10^{-14}$ cm^3 s^{-1}	2

Tabular Data B-1. C-8 (continued)

Quenching and Energy Transfer for Hydrides.

Reaction	Temperature or Energy	Reaction rate or Cross Section†	Reference
$HCl(v=2) + H \rightarrow HCl(v=1) + H$	$296^{o}K$	$9\pm5\times10^{-12}$ cm^3 s^{-1}	5
$HCl(v=2) + H \rightarrow Cl + H_2(v=1,0)$	$296^{o}K$	$17\pm8\times10^{-12}$ cm^3 s^{-1}	5
$HCl(v=2) + Cl \rightarrow HCl(v=1) + Cl$	$294^{o}K$	$32\pm8\times10^{-12}$ cm^3 s^{-1}	5
	$381^{o}K$	$34\pm7\times10^{-12}$ cm^3 s^{-1}	5
	$439^{o}K$	$37\pm10\times10^{-12}$ cm^3 s^{-1}	5
$HCl(v=2) + Cl \rightarrow HCl(v=0) + Cl$	$294^{o}K$	$1\pm3\times10^{-12}$ cm^3 s^{-1}	5
	$381^{o}K$	$4\pm4\times10^{-12}$ cm^3 s^{-1}	5
	$439^{o}K$	$0\pm3\times10^{-12}$ cm^3 s^{-1}	5
$HCl(v=1) + Cl \rightarrow HCl(v=0) + Cl$	$294^{o}K$	7.4×10^{-12} cm^3 s^{-1}	5
	$350^{o}K$	7.6×10^{-12} cm^3 s^{-1}	5
	$381^{o}K$	9.9×10^{-12} cm^3 s^{-1}	5
	$411^{o}K$	7.6×10^{-12} cm^3 s^{-1}	5
	$439^{o}K$	8.1×10^{-12} cm^3 s^{-1}	5
$HCl(v=2) + HCl(v=1) \rightarrow 2HCl(v=1)$	$294^{o}K$	3.1 ± 0.5 cm^3 s^{-1}	5
	$350^{o}K$	3.2 ± 0.5 cm^3 s^{-1}	5
	$381^{o}K$	3.2 ± 0.5 cm^3 s^{-1}	5
	$411^{o}K$	2.7 ± 0.4 cm^3 s^{-1}	5
	$439^{o}K$	2.3 ± 0.4 cm^3 s^{-1}	5
$H\ ^{35}Cl(v=1) + H\ ^{37}Cl(v=0) \rightleftarrows H\ ^{35}Cl(v=0) + H\ ^{37}Cl(v=1)$	$298^{o}K$	$1.91\pm0.04\times10^{-11}$ cm^3 s^{-1} (see also Fig. B-1. C-9 for dependence on temperature).	1

Tabular Date B-1. C-8 (continued)

Quenching and Energy Transfer for Hydrides.

Reaction	Temperature or Energy	Reaction rate or Cross Section†	Reference
$D\ ^{35}Cl(v=1)+D\ ^{37}Cl(v=0) \rightleftarrows D\ ^{35}Cl(v=0)+D\ ^{37}Cl(v=1)$	298°K	$1.18\pm0.08\times10^{-11}$ cm^3 s^{-1}	1
$HCl(v=1) + N_2O \rightarrow HCl(v=0) + N_2O$	300°K	10×10^{-3} s^{-1} torr^{-1}	3
	400°K	5×10^{-3} s^{-1} torr^{-1}	3
	500°K	5.6×10^{-3} s^{-1} torr^{-1}	3
	600°K	5.5×10^{-3} s^{-1} torr^{-1}	3
	700°K	5.0×10^{-3} s^{-1} torr^{-1}	3
$HCl(v=1) + CO_2 \rightarrow HCl(v=0) + CO_2$	300°K	9.3×10^{-3} s^{-1} torr^{-1}	3
	400°K	8.2×10^{-3} s^{-1} torr^{-1}	3
	500°K	5.1×10^{-3} s^{-1} torr^{-1}	3
	600°K	2.6×10^{-3} s^{-1} torr^{-1}	3
	700°K	2.4×10^{-3} s^{-1} torr^{-1}	3
	800°K	3.1×10^{-3} s^{-1} torr^{-1}	3
	900°K	3.7×10^{-3} s^{-1} torr^{-1}	3
$HCl(v=1) + N_2O(m,n^{\ell},0) \rightarrow HCl(v=0) + N_2O(m,n^{\ell},1)$	300°K	36×10^{-3} s^{-1} torr^{-1}	3
	400°K	25×10^{-3} s^{-1} torr^{-1}	3
	500°K	22×10^{-3} s^{-1} torr^{-1}	3
	600°K	24×10^{-3} s^{-1} torr^{-1}	3
	700°K	27×10^{-3} s^{-1} torr^{-1}	3

Tabular Data B-1. C-8 (continued)

Quenching and Energy Transfer for Hydrides.

Reaction	Temperature or Energy	Reaction rate or Cross Section†	Reference
$HCl(v=1) + CO_2(m,n^l,0) \rightarrow HCl(v=0) + CO_2(m,n^l,1)$	300°K	83×10^{-3} s^{-1} torr^{-1}	3
	400°K	58×10^{-3} s^{-1} torr^{-1}	3
	500°K	47×10^{-3} s^{-1} torr^{-1}	3
	600°K	43×10^{-3} s^{-1} torr^{-1}	3
	700°K	43×10^{-3} s^{-1} torr^{-1}	3
	800°K	45×10^{-3} s^{-1} torr^{-1}	3
	900°K	48×10^{-3} s^{-1} torr^{-1}	3
$HCl(v=0) + N_2O(m,n^l,1) \rightarrow HCl(v=1) + M(m,n^l,0)$	300°K	1.5×10^{-3} s^{-1} torr^{-1}	3
	400°K	2.4×10^{-3} s^{-1} torr^{-1}	3
	500°K	3.3×10^{-3} s^{-1} torr^{-1}	3
	600°K	4.9×10^{-3} s^{-1} torr^{-1}	3
	700°K	6.9×10^{-3} s^{-1} torr^{-1}	3
$HCl(v=0) + CO_2(m,n^l,1) \rightarrow HCl(v=1) + M(n,m^l,0)$	300°K	6.3×10^{-3} s^{-1} torr^{-1}	3
	400°K	8.4×10^{-3} s^{-1} torr^{-1}	3
	500°K	10.0×10^{-3} s^{-1} torr^{-1}	3
	600°K	11.9×10^{-3} s^{-1} torr^{-1}	3
	700°K	14.3×10^{-3} s^{-1} torr^{-1}	3
	800°K	17.1×10^{-3} s^{-1} torr^{-1}	3
	900°K	20.2×10^{-3} s^{-1} torr^{-1}	3

Tabular Data B-1. C-8 (continued)

Quenching and Energy Transfer for Hydrides.

Reaction	Temperature or Energy	Reaction rate or Cross Section†	Reference
$HCl(v=2) + Br \rightarrow HCl(v=1) + Br$	295°K	$1.4\pm0.4\times10^{-12}$ cm^3 s^{-1}	5
	355°K	$2.0\pm0.6\times10^{-12}$ cm^3 s^{-1}	5
	390°K	$2.2\pm0.6\times10^{-12}$ cm^3 s^{-1}	5
$HCl(v=2) + Br \rightarrow HCl(v=0) + Br$	295°K	$0.3\pm0.3\times10^{-12}$ cm^3 s^{-1}	5
	355°K	$0.4\pm0.35\times10^{-12}$ cm^3 s^{-1}	5
	390°K	$1.1\pm0.6\times10^{-12}$ cm^3 s^{-1}	5
$HCl(v=1) + Br \rightarrow HCl(v=0) + Br$	295°K	$0.33\pm0.18\times10^{-12}$ cm^3 s^{-1}	5
	355°K	$0.25\pm0.07\times10^{-13}$ cm^3 s^{-1}	5
	390°K	$0.38\pm0.6\times10^{-12}$ cm^3 s^{-1}	5
$H\ ^{79}Br(v=1)+H\ ^{81}Br(v=0) \rightleftarrows H\ ^{79}Br(v=0)+H\ ^{81}Br(v=1)$	298°K	$1.50\pm0.06\times10^{-11}$ cm^3 s^{-1}	1
$D\ ^{79}Br(v=0)+D\ ^{81}Br(v=0) \rightleftarrows D\ ^{79}Br(v=0)+D\ ^{81}Br(v=1)$	298°K	$8.34\pm0.17\times10^{-12}$ cm^3 s^{-1}	1

Notes:

†Reaction rates at a specified temperature are given in units of cm^3 s^{-1} per molecule or in units of s^{-1} torr^{-1}. Reactions measured at a specified energy are shown as a cross section measured in Å^2.

References:

(1) A. B. Horwitz and S. R. Leone, J. Chem. Phys. 69, 5319 (1978).

(2) I. W. M. Smith and D. J. Wrigley, Chem. Phys. Letts. 70, 481 (1980).

(3) L. Doyennette, F. A. Adel, A. Chakroun, M. Margotin-Maciou and L. Henry, J. Chem. Phys. 69, 5334 (1978).

(4) P. J. Dagdigian, B. E. Wilcomb and M. H. Alexander, J. Chem. Phys. 71, 1670 (1979).

(5) R. G. Macdonald and C. Bradley Moore, J. Chem. Phys. 73, 1681 (1980).

Graphical Data B-1. C-9 Rate Coefficient for Isotopic Vibrational Energy Transfer in H ^{35}Cℓ - H ^{37}Cℓ.

$$H\ ^{35}Cℓ(v=1) + H\ ^{37}Cℓ(v=0) \rightleftarrows H\ ^{35}Cℓ(v=0) + H\ ^{37}Cℓ(v=1)$$

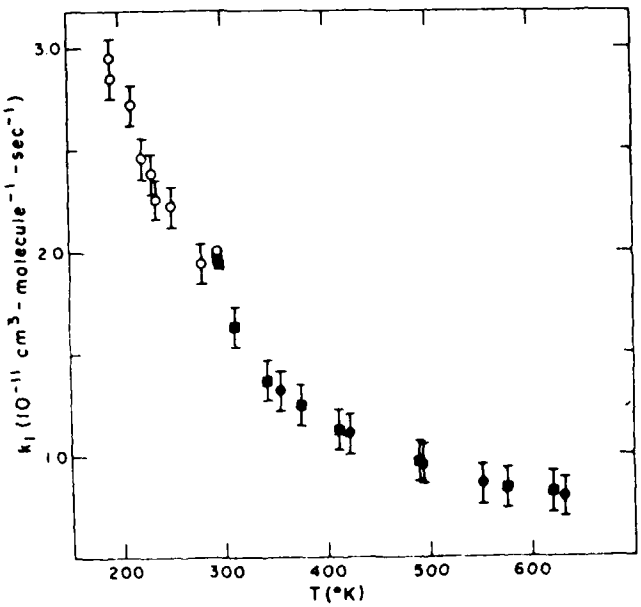

Reference: A. B. Horvitz and S. R. Leone, J. Chem. Phys. 70, 4916 (1970).

Tabular Data B-1. C-10. Rate Coefficients for Quenching Rare Gase Halides.

Reaction	Temp. °K	Rate Coefficient	Reference
$KrF(B) + He \rightarrow$ Quenching	300	3.3×10^{-13} cm^3 s^{-1}	1
$KrF(B) + 2He \rightarrow$ Quenching	300	$< 10^{-33}$ cm^6 s^{-1}	1
$KrF(B) + Ne \rightarrow$ Quenching	300	1.6×10^{-12} cm^3 s^{-1}	1
$KrF(B) + 2Ne \rightarrow$ Quenching	300	$< 10^{-32}$ cm^6 s^{-1}	1
$KrF(B) + Ar \rightarrow$ Quenching	300	1.8×10^{-12} cm^3 s^{-1}	2
$KrF(B) + 2Ar \rightarrow$ Quenching	300	1.1×10^{-31} cm^6 s^{-1}	2
$KrF(B) + Kr \rightarrow$ Quenching	300	$< 1.6\times10^{-12}$ cm^3 s^{-1}	3
$KrF(B) + Ar + Kr \rightarrow$ Quenching	300	6.2×10^{-31} cm^6 s^{-1}	3
$KrF(B) + 2Kr \rightarrow$ Quenching	300	9.7×10^{-31} cm^6 s^{-1}	2
$KrF(B) + Xe \rightarrow$ Quenching	300	$> 10^{-9}$ cm^3 s^{-1}	1
$KrF(B) + F_2 \rightarrow$ Quenching	300	4.8×10^{-10} cm^3 s^{-1}	2
$KrF(B) + NF_3 \rightarrow$ Quenching	300	5.2×10^{-11} cm^3 s^{-1}	1
$XeF(B) + He \rightarrow$ Quenching	300	4.07×10^{-13} cm^3 s^{-1}	4
$XeF(C) + He \rightarrow$ Quenching	300	1.2×10^{-13} cm^3 s^{-1}	5
$XeF(B) + Ne \rightarrow$ Quenching	300	7.68×10^{-13} cm^3 s^{-1}	4
$XeF(B) + 2Ne \rightarrow$ Quenching	300	2.5×10^{-33} cm^3 s^{-1}	6
$XeF(C) + Ne \rightarrow$ Quenching	300	3×10^{-13} cm^3 s^{-1}	5
$XeF(B) + Ar \rightarrow$ Quenching	300	4.92×10^{-12} cm^3 s^{-1}	4
$XeF(C) + Ar \rightarrow$ Quenching	300	9×10^{-14} cm^3 s^{-1}	5
$XeF(B) + Kr \rightarrow$ Quenching	300	2.1×10^{-11} cm^3 s^{-1}	7
$XeF(B) + Xe \rightarrow$ Quenching	300	3.27×10^{-11} cm^3 s^{-1}	4
$XeF(C) + Xe \rightarrow$ Quenching	300	1.0×10^{-12} cm^3 s^{-1}	5
$XeF(B) + F_2 \rightarrow$ Quenching	300	3.8×10^{-10} cm^3 s^{-1}	4
$XeF(C) + F_2 \rightarrow$ Quenching	300	8×10^{-11} cm^3 s^{-1}	5
$XeF(B) + NF_3 \rightarrow$ Quenching	300	2.8×10^{-11} cm^3 s^{-1}	4
$XeF(C) + NF_3 \rightarrow$ Quenching	300	1.6×10^{-11} cm^3 s^{-1}	5
$XeF(B) + XeF_2 \rightarrow$ Quenching	300	2.56×10^{-10} cm^3 s^{-1}	4
$XeF(C) + XeF_2 \rightarrow$ Quenching	300	1.7×10^{-10} cm^3 s^{-1}	5
$XeF(B) + N_2 \rightarrow$ Quenching	300	2.3×10^{-11} cm^3 s^{-1}	6
$XeF(C) + N_2 \rightarrow$ Quenching	300	4×10^{-13} cm^3 s^{-1}	5

Note: For information on different quenching paths for XeF^* see Refc. 7.

References:

(1) J. G. Eden, R. W. Wynant, S. K. Searles and R. Burnham, J. Appl. Phys. 49, 5368 (1978).

(2) J. G. Eden, R. W. Wynant, S. K. Searles and R. Burnham, Appl. Phys. Letts. 32, 733 (1978).

(3) J. H. Jacob, M. Rokni, J. A. Mangano and R. Brochu, Appl. Phys. Lett. 32, 109 (1978).

(4) J. G. Eden, and R. W. Wynant, Opt. Lett. 2, 13 (1978) and J. Chem. Phys. 68, 2850 (1978).

(5) R. W. Wynant, Appl. Phys. Lett. 36, 493 (1980).

(6) M. Rokni, J. H. Jacob, J. A. Mangano and R. Brochu, Appl. Phys. Lett. 32, 223 (1978).

(7) H. C. Brashears and D. W. Setser, Appl. Phys. Lett. 33, 821 (1978).

Tabular Data B-1. C-11. Collision Induced Energy Transfer From Vibrational and Rotational States of S_2.

$S_2(v' = 4, N' = 40, J' = 4) + X$

$\rightarrow S_2(v' =$ all other values$) + X$	rate V
$\rightarrow S_2(v' = 3) + X$	rate $V_{4,3}$
$\rightarrow S_2(v' = 5) + X$	rate $V_{4,5}$
$\rightarrow S_2(v' = 4, N'', J'' = N'' + 1) + X$	rate R_{F_1}
$\rightarrow S_2(v' = 4, N'', J'' = N'' - 1) + X$	rate R_{F_3}
$\rightarrow S_2(v' = 4, N'', J'' = N'') + X$	rate R_{F_2}

Temperature: $300^{\circ}K$

Vibrational Transfer
10^{-10} cm^3 s^{-1}

Gas	V	$V_{4,3}$	$V_{4,5}$
He	2.0 ± 0.2	1.09 ± 0.12	0.54 ± 0.04
Ne	1.55 ± 0.10	0.70 ± 0.07	0.33 ± 0.03
Ar	1.22 ± 0.13	0.61 ± 0.06	0.29 ± 0.03
Kr	2.08 ± 0.15	0.97 ± 0.10	0.38 ± 0.04
Xe	2.6 ± 0.2	1.06 ± 0.11	0.52 ± 0.05
H_2	5.3 ± 0.6	2.4 ± 0.2	1.08 ± 0.18
N_2	2.5 ± 0.2	1.15 ± 0.10	0.49 ± 0.05

Rotational Transfer
10^{-10} cm^3 s^{-1}

		He	Ar	Xe
	F_1 levels			
R_{F_1}	50	0.24 ± 0.07	0.17 ± 0.08	0.13 ± 0.03
	46	0.45 ± 0.09	0.26 ± 0.09	0.16 ± 0.03
	44	0.58 ± 0.15	0.32 ± 0.11	0.18 ± 0.05
	42	1.21 ± 0.18	0.80 ± 0.14	0.39 ± 0.07
	38	1.05 ± 0.12	0.71 ± 0.15	0.42 ± 0.08
	36	0.57 ± 0.09	0.33 ± 0.08	0.19 ± 0.05
	34	0.43 ± 0.07	0.24 ± 0.06	0.18 ± 0.03
	F_3 levels			
R_{F_3}	48	0.36 ± 0.11	0.14 ± 0.07	0.10 ± 0.03
	44	0.54 ± 0.09	0.29 ± 0.08	0.09 ± 0.03
	42	0.40 ± 0.08	0.27 ± 0.09	0.07 ± 0.03
	40	0.27 ± 0.15	0.18 ± 0.09	0.07 ± 0.03
	F_2 levels			
R_{F_2}	42	0.07 ± 0.06	0.06 ± 0.06	0.08 ± 0.08
	40	...	...	0.04 ± 0.04

References: T. A. Caugher, and D. R. Crosley, J. Chem. Phys. 69, 3379. (1978). Ibid. 71, 736 (1979).

Tabular Data B-1. C-12 Rate Coefficients for Vibrational Quenching of GeF and SiF.

$GeF(A^2\Sigma, v'=0,1,2)$ + Gas → Quenching

Temperature 300°K

State pumped (GeF)	Quenching gas	Quenching rate (sec^{-1} $Torr^{-1}$)
$A^2\Sigma(v'=0)$	$GeH_4 + F_2 + He$	1.0×10^5
$A^2\Sigma(v'=1)$	He	1.6×10^5
	SF_6	1.0×10^6
	N_2	5.8×10^6
	$GeH_4 + F_2 + He$	9.0×10^4
$A^2\Sigma(v'=2)$	He	1.6×10^5
	SF_6	5.9×10^5
	N_2	6.9×10^6
	$GeH_4 + F_2 + He$	6.0×10^4

$SiF(A^2\Sigma, v'=0)$ + Gas → Quenching

Temperature 300°K

State pumped (SiF)	Quenching gas	Quenching rate (sec^{-1} $Torr^{-1}$)
$A^2\Sigma(v'=0)$	$SiH_4 + F_2 + He$	1.4×10^5
$A^2\Sigma(v'=0)$	He	6.5×10^4

Reference: R. A. Anderson, L. Hanko and S. J. Davis, J. Chem. Phys. 68, 3286, (1978).

Tabular Data B-1. C-13 Rate Coefficients for Vibrational Quenching of NH_3.

$NH_3(v=1)$ + M → Quenching.

M	k (μsec^{-1} $Torr^{-1}$)	k (cm^3 $molecule^{-1}$ sec^{-1})
NH_3[b]	1.3	3.9×10^{-11}
NH_3[c]	1.2	3.6×10^{-11}
He	9.3×10^{-3}	2.8×10^{-13}
Ar	5.9×10^{-3}	1.8×10^{-13}
N_2	1.2×10^{-2}	3.6×10^{-13}
O_2	1.4×10^{-2}	4.2×10^{-13}

Reference: F. E. Hovis, C. B. Moore, J. Chem. Phys. 69, 4947, (1978).

Tabular Data B-1. C-14 Cross Sections for Quenching of Rotational States of CsF.

$$CsF(j_i, m_i) + X \rightarrow CsF(j_f, m_f) + X.$$

Collision velocity: Configuration A $480 m\ s^{-1}$

Configuration B $550 m\ s^{-1}$

Data are cross sections in $Å^2$.

Transition type		$\Delta j = 1$, $\Delta m = 0$			$\Delta j = 2$ $\Delta m = 0$		$\Delta j = 1$, $\Delta m = 1$		$\Delta j = 0$, $\Delta m = 1$	
Gas	Configuration	(1, 0) → (2, 0)	(2, 0) → (1, 0)	(2, 0) → (3, 0)	(3, 0) → (2, 0)	(3, 0) → (1, 0)	(1, 1) → (2, 0)	(2, 0) → (3, 1)	(1, 1) → (1, 0)	(3, 0) → (3, 1)
He	A	···	3.9 ± 0.5	7.2 ± 2.5	3 ± 1	0.9 ± 0.3	···	···	···	···
	B	17 ± 4	3 ± 1	···	···	···	2.9 ± 2	7 ± 2	···	···
Ne	A	···	4 ± 1.5	5.6 ± 1	1.6 ± 0.5	0.8 ± 0.3	···	···	···	···
	B	13 ± 3	3.5 ± 1	3 ± 1	2.2 ± 0.5	···	3.1 ± 1	2.5 ± 1	4.1 ± 3	5.5 ± 2
Ar	A	···	4.4 ± 1.5	5.7 ± 1	2.4 ± 1	0.6 ± 0.3	···	···	···	···
	B	14 ± 3	···	3.2 ± 1	2.2 ± 1	···	5.1 ± 2	2.3 ± 1	5 ± 4	4.5 ± 2
Kr	A	···	1.9 ± 1	4 ± 1	2.3 ± 0.5	0.5 ± 0.3	···	···	···	···
	B	13 ± 3	···	2.5 ± 1	1.9 ± 0.5	···	5.4 ± 2	2 ± 1	7 ± 4	4.5 ± 2
Xe	A	···	3 ± 1	5 ± 1	3.5 ± 1	0.7 ± 0.3	···	···	···	···
CH_4	A	···	2.7	6.3	4.0	0.8	···	···	···	···
CF_4	A	···	2.3	6.5	4.7	1.2	···	···	···	···
SF_6	A	···	2.2	4.7	2.4	0.5	···	···	···	···
C_2H_6	A	···	4.3 ± 1.2	13.8 ± 3.3	7.8 ± 2.1	0.25 ± 0.1	···	···	···	···
N_2	A	···	10 ± 3.5	47 ± 12	29 ± 8	0.65 ± 0.2	···	···	···	···
CO	A	···	12.2 ± 3.6	54 ± 12	43 ± 10	0.8 ± 0.2	···	···	···	···
CO_2	A	···	19.2 ± 5.6	96 ± 25	74 ± 28	1.8 ± 0.5	···	···	···	···
N_2O	A	···	14	94	91	2.3	···	···	···	···
CH_3Cl	A	···	28	165	194	8.2	···	···	···	···
CH_3Br	A	···	23	151	127	5.6	···	···	···	···
CF_3H	A	···	135 ± 50	620 ± 170	420 ± 115	17 ± 5	···	···	···	···
CF_3Cl	A	···	29	207	196	6.5	···	···	···	···
CF_3Br	A	···	33	225	217	7.5	···	···	···	···

Reference: U. Borkenhagen, H. Malthan and J. P. Toennies, J. Chem. Phys. 71, 1722 (1979).

Tabular Data B-1. C-15. Rate Coefficients for Quenching Mercury Halides.

$$HgX(B^2\Sigma_{1/2}) + Y \rightarrow \text{Quenching.}$$

$$HgI(C^2\pi_{1/2}) + Y \rightarrow \text{Quenching.}$$

where X = Cℓ, Br, I

Y = see below.

Temperature: $300^{o}K$

Note: The data are the product of the reaction rate k ($cm^3\ s^{-1}$) and the lifetime of the excited state τ (s).

	$k\tau(cm^3)$			
Y	$HgCℓ^*$ (B)	$HgBr^*$ (B)	$Hgℓ^*$ (B)	$Hgℓ^*$ (C)
He	9.0×10^{-22}	$< 8.0\times10^{-22}$	$< 8.0\times10^{-22}$	4.2×10^{-19}
Ne	7.3×10^{-22}	$< 8.0\times10^{-22}$	$< 8.0\times10^{-22}$	5.6×10^{-19}
Ar	1.1×10^{-21}	1.7×10^{-21}	2.9×10^{-21}	1.8×10^{-18}
Kr	1.6×10^{-21}	-	-	-
Xe	6.9×10^{-21}	8.9×10^{-21}	6.1×10^{-21}	4.5×10^{-18}
Xe (3 body)	2.7×10^{-40} cm^6	$< 3.0\times10^{-41}$ cm^6	$< 3.0\times10^{-41}$ cm^6	-
N_2	1.4×10^{-21}	$< 8.0\times10^{-22}$	$< 8.0\times10^{-22}$	2.6×10^{-18}
$Cℓ_2$	3.8×10^{-8}	-	-	-
HCℓ	2.5×10^{-18}	-	-	-
$CCℓ_4$	3.5×10^{-18}	-	-	-
Br_2	-	6.9×10^{-18}	-	-
HBr	-	3.0×10^{-18}	-	-
CF_3Br	-	2.1×10^{-18}	-	-
$CCℓ_3Br$	-	4.4×10^{-18}	-	-
I_2	-	-	-	$< 3.0\times10^{-17}$
$CF_3^{\pm}$	-	-	-	7.9×10^{-18}

Reference: A. Mandl, J. H. Parks and C. Roxlo, Proceedings of the International Conference on Lasers '79. p. 828.

Graphical Data B-1. C-16. Rate Coefficient for Vibrational Quenching of O_3 by HCℓ.

$$HC\ell + O_3(001) \rightarrow HC\ell + O_3(000)$$

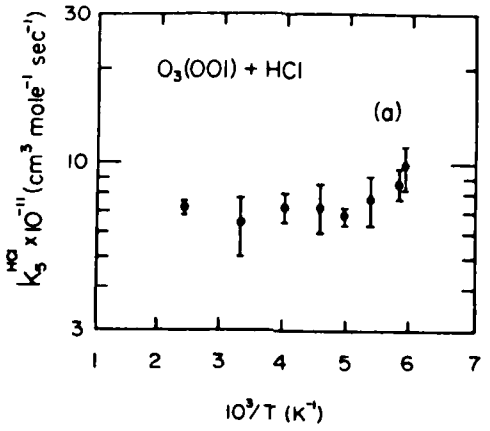

Reference: R. J. Gordon, P. Brutto, and J. Moore, J. Chem. Phys. 69, 3439 (1978).

Tabular Data B-1. C-17. Rate Coefficients for Vibrational Quenching of CO_2 and N_2O.

Note: Reaction rates are given in units of sec^{-1} $torr^{-1}$.

Reaction	Temperature ^oK	Rate Sec^{-1} $torr^{-1}$
$N_2O(m,n^{\ell},1) + HC\ell \rightarrow N_2O(m,n^{\ell},0) + HC\ell$	300	12.5×10^{-3}
	400	10.2×10^{-3}
	500	9.7×10^{-3}
	600	9.4×10^{-3}
	700	8.9×10^{-3}
$N_2O(0,0,1) + CH_4 \rightarrow$ Quenching	300	5.4×10^{-3}
$+ CH_3D \rightarrow$ Quenching	300	40×10^{-3}
$+ CH_2D_2 \rightarrow$ Quenching	300	86×10^{-3}
$+ CHD_3 \rightarrow$ Quenching	300	145×10^{-3}
$+ CD_4 \rightarrow$ Quenching	300	199×10^{-3}
$CO_2(m,n^{\ell},1) + HC\ell \rightarrow CO_2(m,n^{\ell},0) + HC\ell$	300	3.7×10^{-3}
	400	2.8×10^{-3}
	500	2.7×10^{-3}
	600	3.3×10^{-3}
	700	3.8×10^{-3}
	800	4.5×10^{-3}
	900	5.3×10^{-3}
$CO_2(0,0,1) + CH_4 \rightarrow$ Quenching	300	4.7×10^{-3}
$CH_3D \rightarrow$ Quenching	300	43.6×10^{-3}
$CH_2D_2 \rightarrow$ Quenching	300	99.0×10^{-3}
$CHD_3 \rightarrow$ Quenching	300	153.0×10^{-3}
$CD_4 \rightarrow$ Quenching	300	181.0×10^{-3}

References: R. Mehl, S. A. McNeil, L. Napolitano, L. M. Portal, W. S. Drozdoski and R. D. Bates, J. Chem. Phys. 69, 5349 (1978).

L. Doyennette, F. A. Adel, A. Chakroun, M. Margottin-Maciou and L. Henry, J. Chem. Phys. 69, 5334 (1978).

Section B-1.D. CHARGE TRANSFER IN ION-NEUTRAL, ION-ION AND NEUTRAL-NEUTRAL COLLISIONS.

CONTENTS

	Page
Explanation of Coverage	2776
Tabular Data: Positive Ion-Neutral Atom Collisions	2777
Tabular Data: Negative Ion-Neutral Atom Collisions	2784
Tabular Data: Neutral-Neutral Collisions	2785
Tabular Data: Positive Ion-Negative Ion Collisions	2786
Figures	2787
References	2795

Explanation of Coverage

The data presented here are for processes involving electron exchange between two colliding systems as represented by the following equations:

$$A^+ + B \rightarrow A + B^+ \quad (1)$$

$$A^- + B \rightarrow B + A^- \quad (2)$$

$$A + B \rightarrow A^+ + B^- \quad (3)$$

$$A^+ + B^- \rightarrow A + B \quad (4)$$

Reactions 1,2 and 3 are conventionally known as charge transfer or electron capture while reaction 4 is known as mutual neutralization. In some cases where molecular species are involved the post-collision system may dissociate; such reactions are included. We do not, however, consider here ion-molecule reactions where transfer of atoms between projectile and target molecules occurs; such reactions are considered in Section B-1.B. The energy range covered here is from thermal to approximately 100 eV, with a few exceptions where graphical data were available both below and above 100 eV and there was no reason not to present the entire graph. The reactions are listed in tabular form and where only a single datum point is available this is given in the table. Where the reaction has been studied over a range of energies the table refers to a figure which can be found immediately following the table. Data are presented in the form of cross sections (in cm^2 or $\AA^2$) or reaction rates (in cm^3/sec). In one case there is a 3-body reaction ($A^+ + B + C \rightarrow A + B^+ + C$) where the reaction rate is in cm^6/sec. In all cases the datum is a cross section or reaction rate per projectile (atom or molecule) incident.

This table represents an update and continuation of Section B-1 (Vol. I) of Technical Report H-78-1 ("Compilation of Data Relevant to Rare Gas - Rare Gas and Rare Gas - Monohalide Excimer Lasers") and Sections B-1 and B-2 (Volume IV) of Technical Report H-78-1 ("Compilation of Data Relevant to Nuclear Pumped Lasers") both volumes being published by the U.S. Army Missile Command, Redstone Arsenal, Alabama (in December 1977 and December 1978 respectively). The data are gleaned from a search of publications in the years 1978 through August 1980. In view of the continuing evolution of laser mechanisms we have not restricted the search to rare gas and rare gas-halide mechanisms but include also metallic and molecular species. A rather complete listing of thermal energy reaction rates published through 1977 can be found in the compendium by Albritton (Atomic and Nuclear Data Tables 22, 2 (1978)). The present listing should be regarded only as updating the work of Albritton for the limited area of charge transfer.

The table separates reactions of the types 1,2,3 and 4 defined above. Within each section the reactants are ordered first by increasing projectile mass and secondly by increasing target mass. In many cases the designation of a particle as projectile or target is arbitrary and irrelevant.

Reaction	Temperature, Velocity, or Energy	Cross Section or Reaction Rate	Reference
Positive Ion - Atom Collisions.			
$H_3^+ + Mg \rightarrow H_2 + H + Mg^+$	1eV	24×10^{-10} cm^3/sec	1
	2eV	19.2×10^{-10} cm^3/sec	1
	3eV	18.8×10^{-10} cm^3/sec	1
	4eV	19.2×10^{-10} cm^3/sec	1
	5eV	20.6×10^{-10} cm^3/sec	1
	6eV	23.0×10^{-10} cm^3/sec	1
	10eV	27.5×10^{-10} cm^3/sec	1
	15eV	32.5×10^{-10} cm^3/sec	1
	20eV	35.9×10^{-10} cm^3/sec	1
$He^+ + H_2 \rightarrow He + H^+ + H$	78-700°K	Fig. 1.	2,3
	330°K	1.1×10^{-13} cm^3/s	2
	78°K	1.5×10^{-13} cm^3/s	2
$He^{2+} + H_2 \rightarrow He(3d\ ^1D) + 2H^+$	10eV	2 Å^2	4
	20eV	1 Å^2	4
	50eV	0.7 Å^2	4
	100eV	0.3 Å^2	4
	250eV	0.2 Å^2	4
	500eV	0.05 Å^2	4
$He^+ + D_2 \rightarrow He + D^+ + D$	310°K	1.1×10^{-14} cm^3/s	2
	78°K	2.4×10^{-14} cm^3/s	2
$He^{2+} + H_2 \rightarrow He(3d\ ^3D) + 2H^+$	10eV	0.2 Å^2	4
	20eV	0.1 Å^2	4
	50eV	6×10^{-2} Å^2	4
	100eV	4×10^{-2} Å^2	4
	250eV	2×10^{-2} Å^2	4
	500eV	1×10^{-2} Å^2	4
$He^+ + 2H_2 \rightarrow He + products.$	330°K	4.4×10^{-31} cm^6/s	2
	78°K	1.8×10^{-30} cm^6/s	2
$He^+ + 2D_2 \rightarrow He + products.$	310°K	2.7×10^{-31} cm^6/s	2
	78°K	2.1×10^{-30} cm^6/s	2
$He^+ + He \rightarrow He + He^+$	2-100eV	Fig. 2	5
$^4He^+ + {}^3He^{2+} \rightarrow {}^4He^{2+} + {}^3He^+$	10-10,000eV	Fig. 3	6

Tabular Data B-1.D (Continued)

Reaction			Temperature, Velocity, or Energy	Cross Section or Reaction Rate	Reference
$He^2 + He$	→	$He(3d\ ^1D) + He^{2+}$	200eV	$0.5x10^{-3}$ $Å^2$	4
			500eV	$1x.1^{-3}$ $Å^2$	4
$He^{2+} + He$	→	$He(3d\ ^3D) + He^{2+}$	200eV	$1x10^{-3}$ $Å^2$	4
			500eV	$2x10^{-3}$ $Å^2$	4
$He^+(1s) + Ne$	→	$He^* + Ne^+$	0.1→500eV	Fig. 4	7
$He^{2+} + Ne$	→	$He(3d\ ^1D) + Ne^{2+}$	50eV	$2x10^{-2}$ $Å^2$	4
			100eV	$1x10^{-2}$ $Å^2$	4
			250eV	$5x10^{-3}$ $Å^2$	4
			500eV	$4x10^{-3}$ $Å^2$	4
$He^{2+} + Ne$	→	$He(3d\ ^3D) + Ne^{2+}$	50eV	$5x10^{-2}$ $Å^2$	4
			100eV	$4x10^{-2}$ $Å^2$	4
			250eV	$2x10^{-2}$ $Å^2$	4
			500eV	$2x10^{-2}$ $Å^2$	4
$He^{2+} + Ne$	→	$He^+ + Ne^+$	0-32eV	Fig. 5	8
$He^{2+} + Ne$	→	$He^+ + Ne^+$	300°K	$8.4x10^{-10}cm^3/sec$	9
$He^+ + Mg$	→	$He + Mg^{2+} + e$	300°K	$1.6x10^{-15}cm^2$	10
$He^{2+} + O_2$	→	$He(3d\ ^1D) + 2O^+$	10eV	2 $Å^2$	4
			20eV	1 $Å^2$	4
			50eV	0.2 $Å^2$	4
			100eV	0.1 $Å^2$	4
			250eV	$7x10^{-2}$ $Å^2$	4
			500eV	$5x10^{-2}$ $Å^2$	4
$He^{2+} + O_2$	→	$He(3d\ ^3D) + 2O^+$	10eV	7 $Å^2$	4
			20eV	5 $Å^2$	4
			50eV	0.6 $Å^2$	4
			100eV	0.4 $Å^2$	4
			250eV	0.2 $Å^2$	4
			500eV	0.2 $Å^2$	4
$He^{2+} + Ar$	→	$He^+ + Ar^+(?)$	300°K	$2.6x10^{-9}$	9

Tabular Data B-1.D (Continued)

Reaction			Temperature, Velocity, or Energy	Cross Section or Reaction Rate	Reference
$He^+ + Ca$	→	$He + Ca^{2+} + e$	300°K	$1.8 \times 10^{-15} cm^2$	10
$He^{2+} + Kr$	→	$He^+ + Kr^{2+} + e$	300°K	$3.9 \times 10^{-9} cm^3/sec$	9
$He^+ + Sr$	→	$He + Sr^{2+} + e$	300°K	$2.7 \times 10^{-15} cm^2$	10
$He^{2+} + Xe$	→	$He^+ + Xe^{2+} + e$	300°K	$4.7 \times 10^{-9} cm^3/sec$	9
$He^+ + Ba$	→	$He + Ba^{2+} + e$	300°K	$3.0 \times 10^{-15} cm^2$	10
$N^{2+} + He$	→	$N^+ + He^+$	1-13eV	Fig. 6	8
$N^+ + H_2O$	→	$N + H_2O^+$	300°K	$2.8 \times 10^{-9} cm^3/sec$	11
$N^+ + Th$	→	$N + Th^+$	2-500eV	Fig. 7	12
$N^+ + U$	→	$N + U^+$	2-500eV	Fig. 8	12
$O^{2+} + He$	→	$O^+ + He^+$	1-13eV	Fig. 6	8
$O^+ + H_2O$	→	$O + H_2O^+$	300°K	$3.2 \times 10^{-9} cm^3/sec$	11
$O^+ + NH_3$	→	$O + NH_3^+$	300°K	$1.2 \times 10^{-9} cm^3/sec$	11
$O^+ + O_2$	→	$O + O_2^+$	300°K	$1.9 \times 10^{-11} cm^3/sec$	11
$O^+ + O_2$	→	$O + O_2^+$	300°K	$2.3 \times 10^{-11} cm^3/sec$	13
$O^+ + Th$	→	$O + Th^+$	2-500eV	Fig. 7	12
$O^+ + U$	→	$O + U^+$	2-500eV	Fig. 8	12
$NH_3^+ + Mg$	→	$NH_3 + Mg^+$	1eV	$6.7 \times 10^{-10} cm^3/sec$	1
			2eV	$3.9 \times 10^{-10} cm^3/sec$	1
			3eV	$3.7 \times 10^{-10} cm^3/sec$	1
			4eV	$3.7 \times 10^{-10} cm^3/sec$	1
			5eV	$3.8 \times 10^{-10} cm^3/sec$	1
			6eV	$3.8 \times 10^{-10} cm^3/sec$	1
			10eV	$4.5 \times 10^{-10} cm^3/sec$	1
			15eV	$5.2 \times 10^{-10} cm^3/sec$	1
			20eV	$5.9 \times 10^{-10} cm^3/sec$	1

Tabular Data B-1.D (Continued)

Reaction	Temperature, Velocity, or Energy	Cross Section or Reaction Rate	Reference
$H_2O^+ + Mg \rightarrow H_2O + Mg^+$	2eV	18.4×10^{-10} cm^3/sec	1
	3eV	14.2×10^{-10} cm^3/sec	1
	4eV	13.3×10^{-10} cm^3/sec	1
	5eV	12.5×10^{-10} cm^3/sec	1
	6eV	12.8×10^{-10} cm^3/sec	1
	10eV	14.4×10^{-10} cm^3/sec	1
	15eV	17.1×10^{-10} cm^3/sec	1
	20eV	19.0×10^{-10} cm^3/sec	1
$Ne^{2+} + He \rightarrow Ne^+ + He^+$	3-10eV	Fig. 9	8
$Ne^+ + Ne \rightarrow Ne + Ne^+$	300°K	0.3×10^{-9} cm^3/sec	14
$Ne^{2+} + Ne \rightarrow Ne^+ + Ne^+$	8-18eV	Fig. 5	8
$Ne^{2+} + Ar \rightarrow Ne^+ + Ar^+$	0-24eV	Fig. 10	8
$Ne^{2+}(1s) + Ar \rightarrow Ne^+ + Ar^+$(or Ar^{2+}+e?)	300°K	1.0×10^{-9} cm^3/sec	9
$Ne^{2+}(^1D) + Ar \rightarrow Ne^+ + Ar^+$(or Ar^{2+}+e?)	300°K	7.0×10^{-10} cm^3/sec	9
$Ne^{2+}(^3P) + Ar \rightarrow Ne^+ + Ar^+$	300°K	5.3×10^{-10} cm^3/sec	9
$Ne^+ + Ca \rightarrow Ne + Ca^{2+} + e$	300°K	1.9×10^{-15} cm^2	10
$Ne^{2+}(^1S) + Kr \rightarrow Ne^+ + Kr^+$(or Kr^{2+}+e?)	300°K	1.7×10^{-9} cm^3/sec	9
$Ne^{2+}(^1D) + Kr \rightarrow Ne^+ + Kr^+$(or Kr^{2+}+e?)	300°K	8.0×10^{-10} cm^3/sec	9
$Ne^{2+}(^3P) + Kr \rightarrow Ne^+ + Kr^+$(or Kr^{2+}+e?)	300°K	1.7×10^{-9} cm^3/sec	9
$Ne^+ + Sr \rightarrow Ne + Sr^{2+} + e$	300°K	4.9×10^{-15} cm^2	10
$Ne^{2+}(^1S) + Xe \rightarrow Ne^+ + Xe^{2+} + e$	300°K	2.0×10^{-9} cm^3/sec	9
$Ne^{2+}(^1D) + Xe \rightarrow Ne^+ + Xe^{2+} + e$	300°K	1.6×10^{-9} cm^3/sec	9
$Ne^{2+}(^3P) + Xe \rightarrow Ne^+ + Xe^+$(or Xe^{2} +e?)	300°K	1.9×10^{-9} cm^3/sec	9
$Ne^+ + Ba \rightarrow Ne + Ba^{2+} + e$	300°K	8.0×10^{-15} cm^2	10

Tabular Data B-1.D (Continued)

Reaction	Temperature, Velocity or Energy	Cross Section or Reaction Rate	Reference
$N_2^+ + CH_4 \rightarrow N_2 + CH_4^+$	50-1000eV	Fig. 11	15
$N_2^+ + CD_4 \rightarrow N_2 + \text{products}$	300^oK	$10.6\times10^{-10}cm^3/sec$	16
$N_2^+ + NH_3 \rightarrow N_2 + NH_3^+$	300^oK	$1.9\times10^{-19}cm^3/sec$	11
$N_2^+ + N_2 \rightarrow N_2 + N_2^+$	50-1000eV	Fig. 12	15
$N_2^+ + CO \rightarrow N_2 + CO^+$	300^oK	$7.4\times10^{-11}cm^3/sec$	11
$N_2^+ + O_2 \rightarrow N_2 + O_2^+$	300^oK	$5.1\times10^{-11}cm^3/sec$	11
$N_2^+ + CO_2 \rightarrow N_2 + CO_2^+$	300^oK	$7.7\times10^{-10}cm^3/sec$	11
$N_2^+ + Th \rightarrow N_2 + Th^+$	2-500eV	Fig. 16	12
$N_2^+ + U \rightarrow N_2 + U^+$	2-500eV	Fig. 13	12
$CO^+ + CH_4 \rightarrow CO + CH_4^+$	50-1000eV	Fig. 11	15
$CO^+ + CO \rightarrow CO + CO^+$	50-1000eV	Fig. 12	15
$O_2^+ + NH_3 \rightarrow O_2 + NH_3^+$	300^oK	$2.0\times10^{-9}cm^3/sec$	11
$O_2^+(v=0 \text{ to } 7) + O_2 \rightarrow O_2 + O_2^+$	1-40eV	Fig. 14	17
$O_2^+ + H_2S \rightarrow O_2 + H_2S^+$	300^oK	$1.4\times10^{-9}cm^3/sec$	11
$O_2^+ + COS \rightarrow O_2 + COS^+$	300^oK	$1.0\times10^{-9}cm^3/sec$	11
$Ar^{2+} + He \rightarrow Ar^+ + He^+$	0-9eV	Fig. 9	8
$Ar^{2+}(^1S) + He \rightarrow Ar^+ + He^+$	300^oK	$\leq 2\times10^{-14}cm^3/sec$	9
$Ar^{2+}(^1D) + He \rightarrow Ar^+ + He^+$	300^oK	$\geq 1.4\times10^{-10}cm^3/sec$	9
$Ar^{2+}(^3P) + He \rightarrow Ar^+ + He^+$	300^oK	$7\times10^{-11}cm^3/sec$	9
$Ar^{3+} + He \rightarrow Ar^{2+} + He^+$	0-6eV	Fig. 9	8

Tabular Data B-1.D (Continued)

Reaction			Temperature, Velocity, or Energy	Cross Section or Reaction Rate	Reference
$Ar^+ + CH_4$	→	Ar + products	300°K	11.0×10^{-10} cm^3/sec	16
$Ar^{2+}(^1S) + Ne$	→	$Ar^+ + Ne^+$	300°K	1×10^{-13} cm^3/sec	9
$Ar^{2+}(^1D) + Ne$	→	$Ar^+ + Ne^+$	300°K	$< 3.7\times10^{-12}$ cm^3/sec	9
$Ar^{2+}(^3P) + Ne$	→	$Ar^+ + Ne^+$	300°K	3.7×10^{-12} cm^3/sec	9
$Ar^{2+} + Ne$	→	$Ar^+ + Ne^+$	0-22eV	Fig. 5	8
$Ar^+ + N_2$	→	$Ar + N_2^+$	300°K	4.9×10^{-12} cm^3/sec	18
$Ar^+ + N_2$	→	$Ar + N_2^+$	300°K	$\sim 0.85\times10^{-11}$ cm^3/sec	19
$Ar^{2+} + N_2$	→	$Ar^+ + N_2^+$	300°K	20×10^{-11} cm^3/sec	19
$Ar^{2+} + N_2$	→	$Ar^+ + N^+ + N$	300°K	10×10^{-11} cm^3/sec	19
$Ar^+ + CO$	→	$Ar + CO^+$	300°K	0.35×10^{-10} cm^3/sec	18
$Ar^+ + O_2$	→	$Ar + O_2^+$	300°K	0.43×10^{-10} cm^3/sec	18
$Ar^+ + O_2$	→	$Ar + O_2^+$	300°K	5.8×10^{-11} cm^3/sec	19
$Ar^{2+} + O_2$	→	$Ar^+ + O_2^+$	300°K	170×10^{-11} cm^3/sec	19
$Ar^+ + Ar$	→	$Ar + Ar^+$	300°K	0.46×10^{-9} cm^3/sec	14
$Ar^{2+} + Ar$	→	$2Ar^+$	300°K	0.04×10^{-11} cm^3/sec	19
$Ar^{2+} + Ar$	→	$Ar^+ + Ar^+$	0-34eV	Fig. 10	8
$Ar^+ + CO_2$	→	$Ar + CO_2^+$	300°K	5.6×10^{-10} cm^3/sec	18
$Ar^{2+}(^1S) + Kr$	→	$Ar^+ + Kr^+$	300°K	1.4×10^{-9} cm^3/sec	9
$Ar^{2+}(^1D) + Kr$	→	$Ar^+ + Kr^+$	300°K	$\leq 2\times10^{-13}$ cm^3/sec	9
$Ar^{2+}(^3P) + Kr$	→	$Ar^+ + Kr^+$	300°K	$\leq 2\times10^{-13}$ cm^3/sec	9

Tabular Data B-1.D (Continued)

Reaction	Temperature Velocity or Energy	Cross Section or Reaction Rate	Reference
$Ar^{2+} + Kr \rightarrow Ar^{+} + Kr^{+}$	0-3keV	Fig. 15	8
$Ar^{2+}(^1S) + Xe \rightarrow Ar^{+} + Xe^{+}$	300°K	$1\times10^{-9}cm^3/sec$	9
$Ar^{2+}(^1D) + Xe \rightarrow Ar^{+} + Xe^{+}$	300°K	$\sim 1.5\times10^{-9}cm^3/sec$	9
$Ar^{2+}(^3P) + Xe \rightarrow Ar^{+} + Xe^{+}$	300°K	$1.5\times10^{-9}cm^3/sec$	9
$N_3^{+} + NH_3 \rightarrow$ products + NH_3^{+}	300°K	$2.1\times10^{-9}cm^3/sec$	11
$CO_2^{+} + Th \rightarrow CO_2 + Th^{+}$	2-500eV	Fig. 16	12
$CO_2^{+} + U \rightarrow CO_2 + U^{+}$	2-500eV	Fig. 13	12
$N_4^{+} + NH_3 \rightarrow$ products + NH_3^{+}	300°K	$1.8\times10^{-9}cm^3/sec$	11
$N_4^{+} + H_2O \rightarrow$ products + H_2O^{+}	300°K	$3.0\times10^{-9}cm^3/sec$	11
$N_4^{+} + O_2 \rightarrow$ products + O_2^{+}	300°K	$2.5\times10^{-10}cm^3/sec$	11
$N_4^{+} + CO_2 \rightarrow$ products + CO_2^{+}	300°K	$7.0\times10^{-10}cm^3/sec$	11
$N_4^{+} + COS \rightarrow$ products + COS^{+}	300°K	$4.6\times10^{-10}cm^3/sec$	11
$Kr^{2+} + He \rightarrow Kr^{+} + He^{+}$	300°K	$<1\times10^{-14}cm^3/sec$	9
$Kr^{+} + CH_4 \rightarrow Kr$ + products	300°K	$12.0\times10^{-10}cm^3/sec$	16
$Kr^{2+}(^1S) + Ne \rightarrow Kr^{+} + Ne^{+}$	300°K	$1.3\times10^{-10}cm^3/sec$	9
$Kr^{2+}(^1D) + Ne \rightarrow Kr^{+} + Ne^{+}$	300°K	$9\times10^{-10}cm^3/sec$	9
$Kr^{2+}(^3P) + Ne \rightarrow Kr^{+} + Ne^{+}$	300°K	$1\times10^{-10}cm^3/sec$	9
$Kr^{2+} + Ar \rightarrow Kr^{+} + Ar^{+}$	300°K	$<1\times10^{-13}cm^3/sec$	9
$Kr^{+} + Kr \rightarrow Kr + Kr^{+}$	300°K	$0.34\times10^{-9}cm^3/sec$	14
$Kr^{+} + Kr \rightarrow Kr + Kr^{+}$	0.04-10eV	Fig. 17	20
$Kr^{2+}(^1D, ^1S) + Kr \rightarrow Kr^{+} + Kr$	300°K	$4.6\times10^{-14}cm^3/sec$	9
$Kr^{2+} + Kr \rightarrow Kr + Kr^{2+}$	0.04-20eV	Fig. 17	20

Tabular Data B-1.D (Continued)

Reaction			Temperature, Velocity, or Energy	Cross Section or Reaction Rate	Reference
$Kr^{2+}(^3P) + Kr$	→	$Kr^+ + Kr^+$	300°K	5.0×10^{-14} cm^3/sec	9
$Kr^{2+} + Xe$	→	$Kr^+ + Xe^+$	300°K	1.2×10^{-11} cm^3/sec	9
$Xe^{2+} + Ne$	→	$Xe^+ + Ne^+$	300°K	$< 1\times10^{-14}$ cm^3/sec	9
$Xe^{2+}(^3P) + N_2$	→	$Xe^+ + N_2^+$	300°K	1.0×10^{-9} cm^3/sec	21
$Xe^{2+}(^1D_2) + N_2$	→	$Xe^+ + N_2^+$	300°K	7.8×10^{-10} cm^3/sec	21
$Xe^{2+}(^1S_o) + N_2$	→	$Xe^+ + N_2^+$	300°K	3.8×10^{-12} cm^3/sec	21
$Xe^{2+}(^3P) + O_2$	→	$Xe^+ + O_2^+$	300°K	1.2×10^{-9} cm^3/sec	21
$Xe^{2+}(^3P_2) + Ar$	→	$Xe^+ + Ar^+$	300°K	3.9×10^{-10} cm^3/sec	9
$Xe^{2+}(^3P) + Ar$	→	$Xe^+ + Ar^+$	300°K	2.9×10^{-10} cm^3/sec	21
$Xe^{2+}(^3P_{0,1}, {}^1S, {}^1D) + Ar$	→	$Xe^+ + Ar^+$	300°K	$< 2\times10^{-14}$ cm^3/sec	9
$Xe^{2+}(^3P) + CO_2$	→	$Xe^+ + CO_2^+$	300°K	1.1×10^{-9} cm^3/sec	21
$Xe^{2+} + Kr$	→	$Xe^+ + Kr^+$	300°K	$< 8\times10^{-14}$ cm^3/sec	9
$Xe^+ + Xe$	→	$Xe + Xe^+$	0.04→10eV	Fig. 17.	20
$Xe^+ + Xe$	→	$Xe + Xe^+$	300°K	0.36×10^{-9} cm^3/sec	2
$Xe^{2+} + Xe$	→	$Xe + Xe^{2+}$	0.04→20eV	Fig. 17.	20
$Xe^{2+}(^1D_2) + Xe$	→	$Xe^+ + Xe^+$	300°K	1.0×10^{-12} cm^3/sec	21
$Xe^{2+}(^1S_0) + Xe$	→	$Xe^+ + Xe^+$	300°K	3.1×10^{-12} cm^3/sec	21
$Cs^+ + Cs$	→	$Cs + Cs^+$	300°K	7.10×10^{-14} cm^2	22
		Negative Ion - Atom Collisions			
$O^- + NO_2$	→	$O + NO_2^-$	0.01-1eV	Fig. 18.	23
$O^- + O_3$	→	$O + O_3^-$	0.3eV	2.0×10^{-10} cm^3/sec	24

Tabular Data B-1.D (Continued)

Reaction			Temperature, Velocity, or Energy	Cross Section or Reaction Rate	Reference
$OH^- + O_3$	→	$OH + O_3^-$	0.3eV	$5.0 \times 10^{-10} cm^3/sec$	24
$F^- + O_3$	→	$F + O_3^-$	0.3eV	$2 \times 10^{-14} cm^3/sec$	24
$F^- + O_3$	→	$F + O_3^-$	0.5-6.5eV	Fig. 19	24
$S^- + O_3$	→	$S + O_3^-$	0.3eV	$0.9 \times 10^{-10} cm^3/sec$	24
$C_2H^- + O_3$	→	$C_2H + O_3^-$	0.3eV	$0.02 \times 10^{-10} cm^3/sec$	24
$SH^- + O_3$	→	$SH + O_3^-$	0.3eV	$0.6 \times 10^{-10} cm^3/sec$	24
$SH^- + O_3$	→	$SH + O_3^-$	0.5-6.5eV	Fig. 20	24
$NO_2^- + O_3$	→	$NO_2 + O_3^-$	0.3eV	$0.9 \times 10^{-10} cm^3/sec$	24
$NO_2^- + O_3$	→	$NO_2 + O_3^-$	0-8.0eV	Fig. 21.	24
$SO^- + SO_2$	→	$SO + SO_2^-$	0.01-1eV	Fig. 22	23
$O_3^- + NO_2$	→	$O_3 + NO_2^-$	0.4.5eV	Fig. 23	24
$O_3^- + NO_2$	→	$O_3 + NO_2^-$	0-9.5eV	Fig. 21	24
$Cl_2^- + O_3$	→	$Cl_2 + O_3^-$	0.3eV	$0.02 \times 10^{-10} cm^3/sec$	24
$Br^- + NO_2$	→	$Br + NO_2^-$	1.5-6.5eV	Fig. 24	24
$Br^- + O_3$	→	$Br + O_3^-$	1.5-6.5eV	Fig. 24	24
$I^- + O_3$	→	$I + O_3^-$	1.5-6.5eV	Fig. 25	24
		Neutral-Neutral Collisions			
Li + Cl_2	→	$Li^+ + Cl_2^-$	1820-2590°K	Fig. 26	25
Li + Br	→	$Li^+ + Br^-$	1820-2590°K	Fig. 26	25
Li + I	→	$Li^+ + I^-$	1820-2590°K	Fig. 26	25
Na + Cl_2	→	$Na^+ + Cl_2^-$	1820-2590°K	Fig. 26	25

Tabular Data B-1.D (Continued)

Reaction			Temperature, Velocity, or Energy	Cross Section or Reaction Rate	Reference
$Na + Br$	→	$Na^+ + Br^-$	1820-2590°K	Fig. 26	25
$Na + I$	→	$Na^+ + I^-$	1820-2590°K	Fig. 26	25
$K + O_2$	→	$K^+ + O_2^-$	3.5-2000eV	Fig. 27	26
$K + Cl$	→	$K^+ + Cl^-$	1820-2590°K	Fig. 26	25
$K + Br$	→	$K^+ + Br^-$	1820-2590°K	Fig. 26	25
$K + I$	→	$K^+ + I^-$	1820-2590°K	Fig. 26	25
$Cs + O_2$	→	$Cs^+ + O_2^-$	2.5-1000eV	Fig. 28	26
$Cs + Se F_6$	→	$Cs^+ + Se F_6^-$	0.75-12eV	Fig. 29	27
		Positive-Ion Negative-Ion Collisions			
$Li^+ + Cl^-$	→	$Li + Cl$	1820-2590°K	Fig. 30	25
$Li^+ + Br^-$	→	$Li + Br$	1820-2590°K	Fig. 30	25
$Li^+ + I^-$	→	$Li + I$	1820-2590°K	Fig. 30	25
$Na^+ + Cl^-$	→	$Na + Cl$	1820-2590°K	Fig. 30	25
$Na^+ + Br^-$	→	$Na + Br$	1820-2590°K	Fig. 30	25
$Na^+ + I^-$	→	$Na + I$	1820-2590	Fig. 30	25
$NO^+ + Cl^-$	→	$NO + Cl$	2200-2630°K	Fig. 31	28
$NO^+ + Br^-$	→	$NO + Br$	2200-2630°K	Fig. 31	28
$NO^+ + I^-$	→	$NO + I$	2200-2630	Fig. 31	28
$K^+ + Cl^-$	→	$K + Cl$	1820-2590°K	Fig. 30	25
$K^+ + Br^-$	→	$K + Br$	1820-2590°K	Fig. 30	25
$K^+ + I^-$	→	$K + I$	1820-2590°K	Fig. 30	25

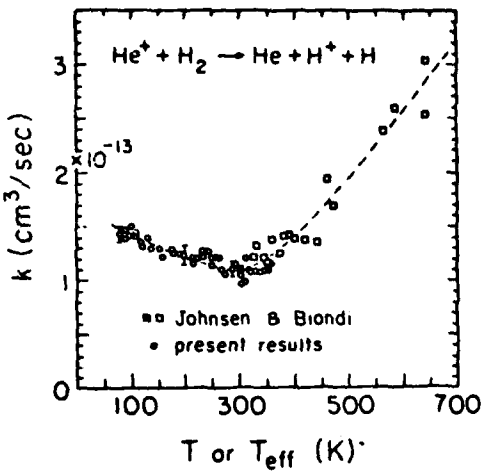

Fig. 1

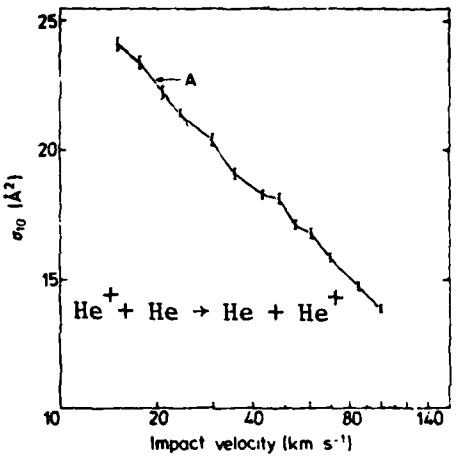

Fig. 2

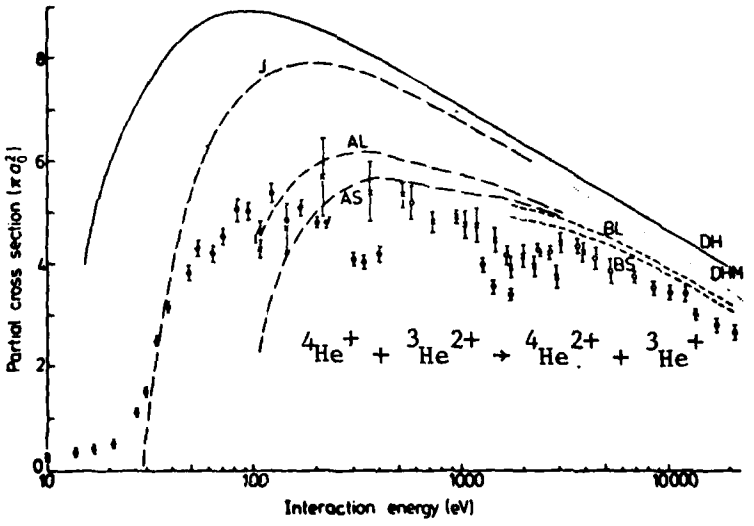

Fig. 3

Data points are measurements. Energy is defined for center of mass frame. Lines are various theories - see original reference (6) for details.

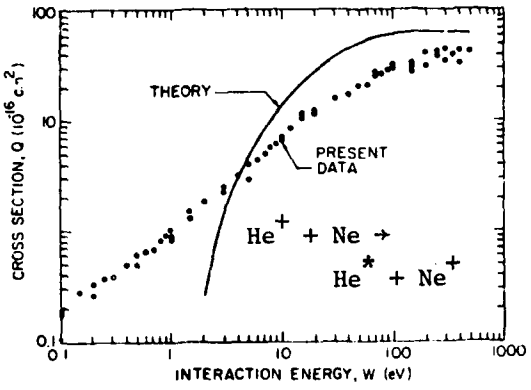

Fig. 4

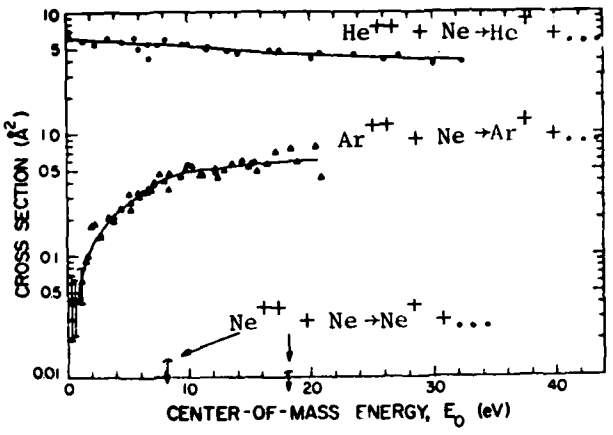

Fig. 5

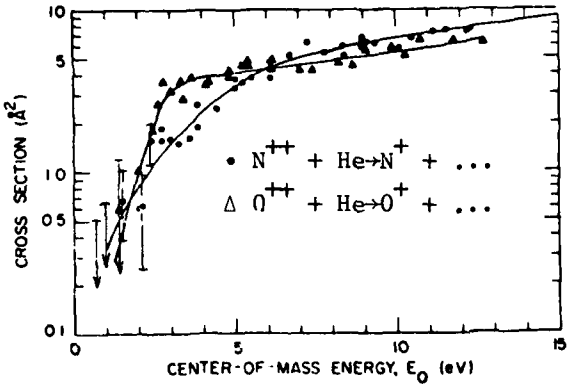

Fig. 6

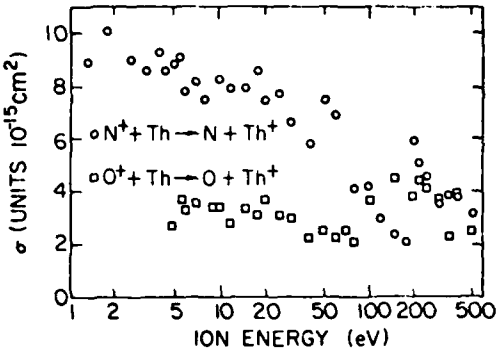

Fig. 7

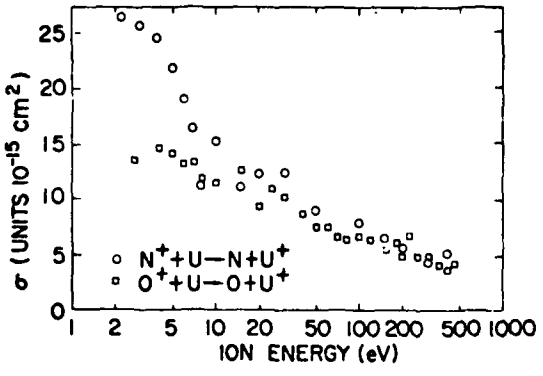

Fig. 8

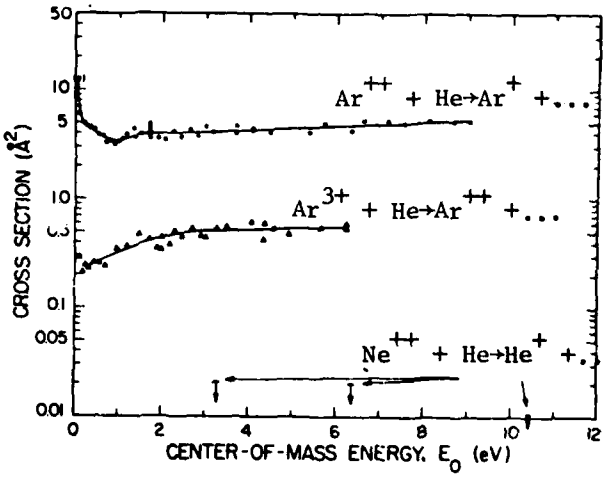

Fig. 9

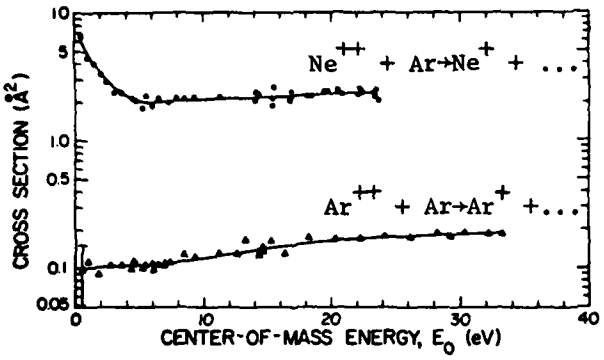

Fig. 10

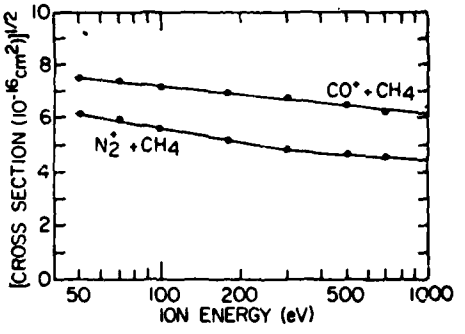

Fig. 11

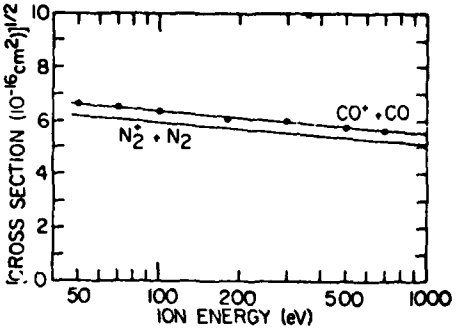

Fig. 12

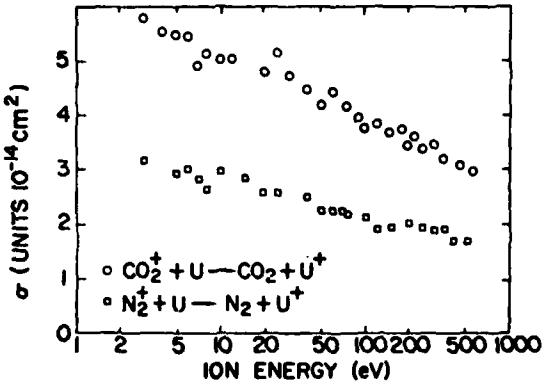

Fig. 13

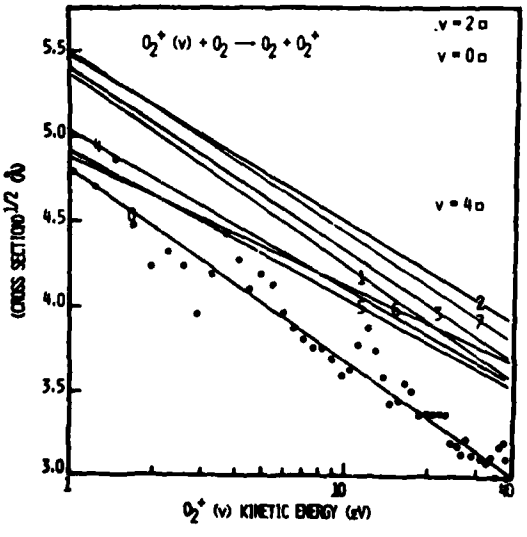

Fig. 14 Data points shown only for transfer from the v=0 level; data for remaining levels (v=1 thru 7) shown by least squares fit straight line.

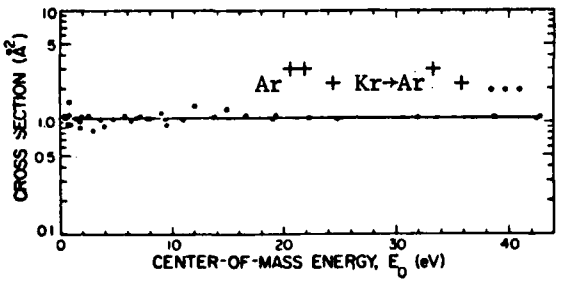

Fig. 15

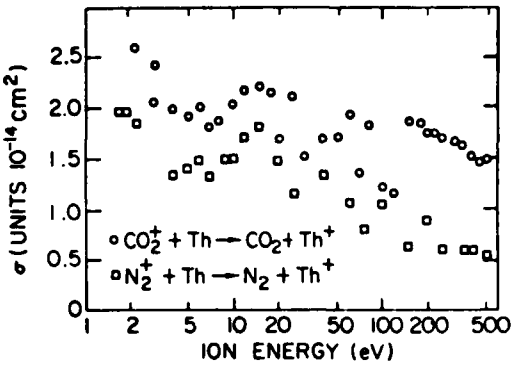

Fig. 16

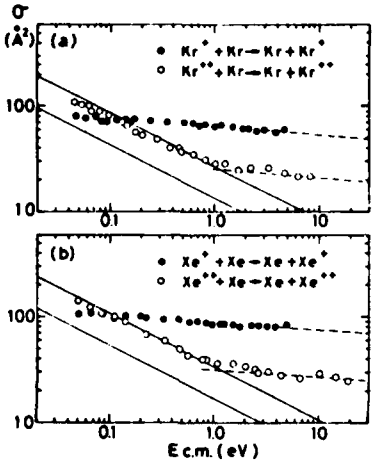

Fig. 17

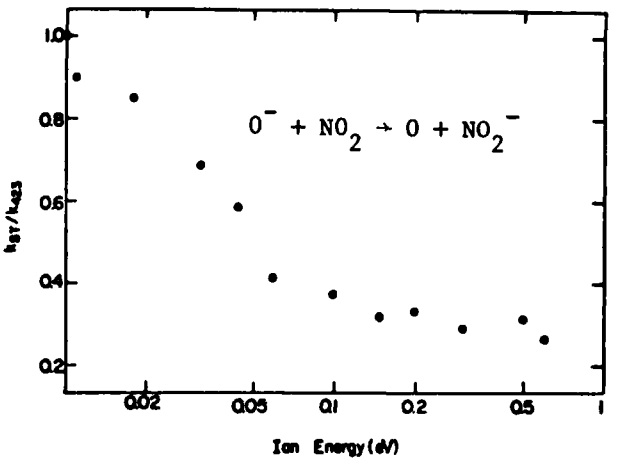

Fig. 18

Relative variation of reaction rate (arbitrary units).

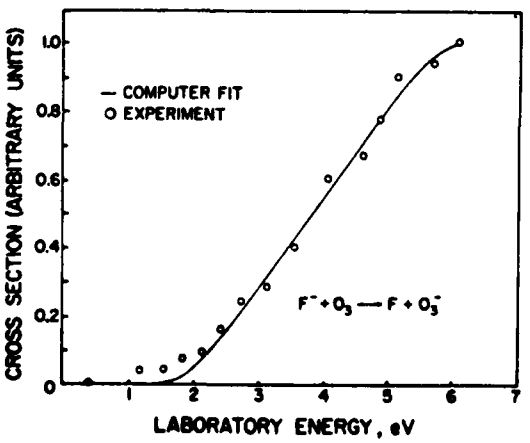

Fig. 19

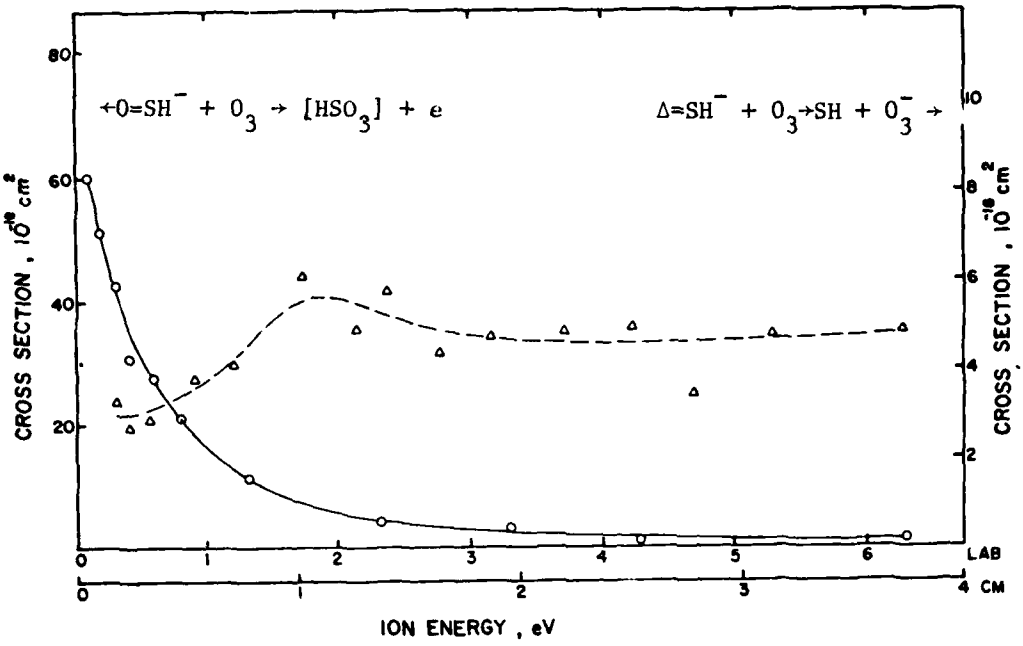
○=SH⁻ + O3 → [HSO3] + e
Δ=SH⁻ + O3→SH + O3⁻ →
CROSS SECTION , 10⁻¹⁸ cm²
CROSS SECTION , 10⁻¹⁸ cm²
ION ENERGY , eV
LAB
CM

Fig. 20

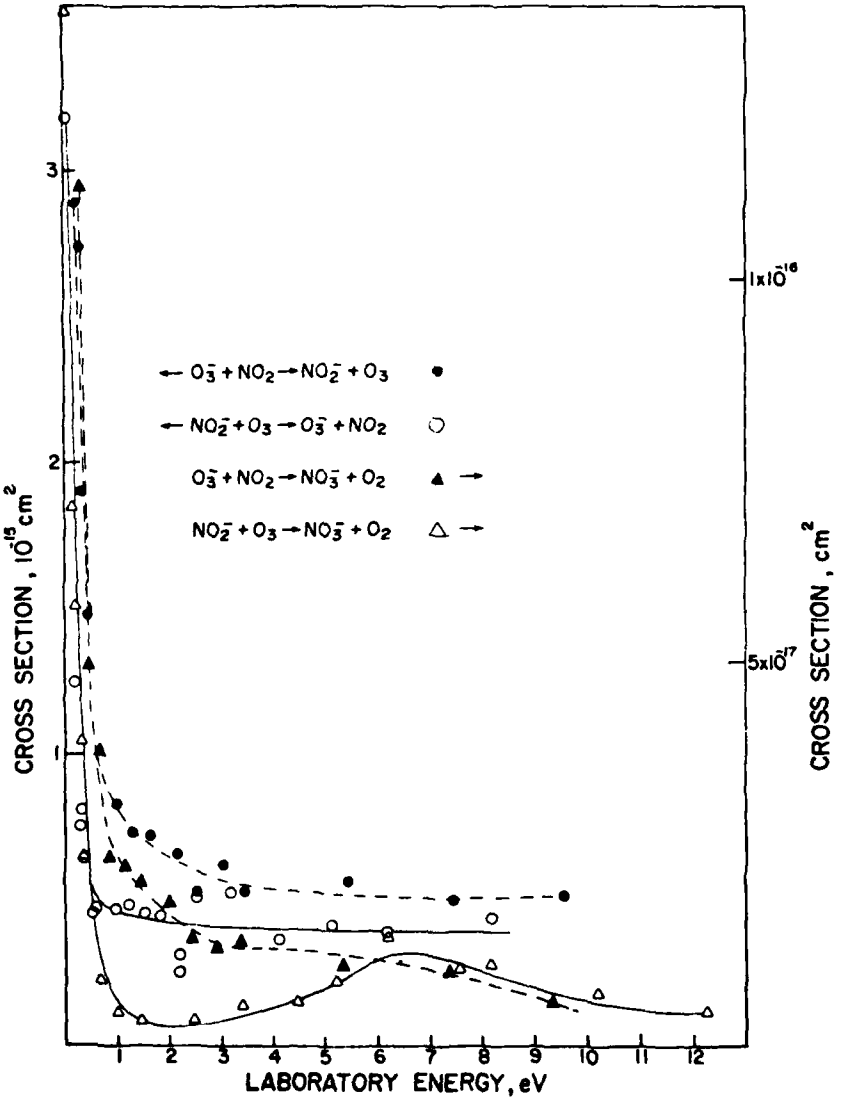
O3⁻ + NO2 → NO2⁻ + O3
NO2⁻ + O3 → O3⁻ + NO2
O3⁻ + NO2 → NO3⁻ + O2
NO2⁻ + O3 → NO3⁻ + O2
CROSS SECTION , 10⁻¹⁵ cm²
CROSS SECTION , cm²
1x10⁻¹⁶
5x10⁻¹⁷
LABORATORY ENERGY, eV

Fig. 21

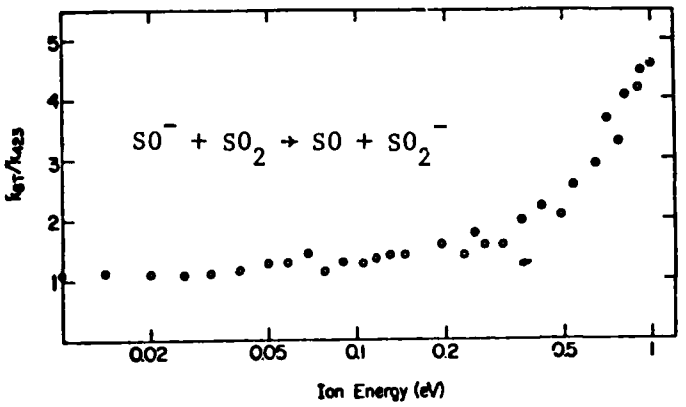

Fig. 22 Relative variation of reaction rate (arbitrary units).

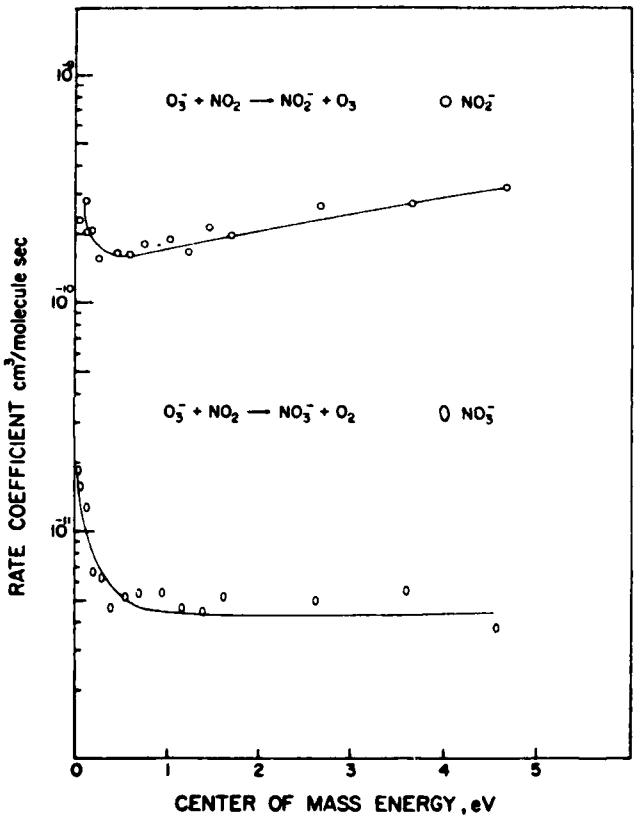

Fig. 23

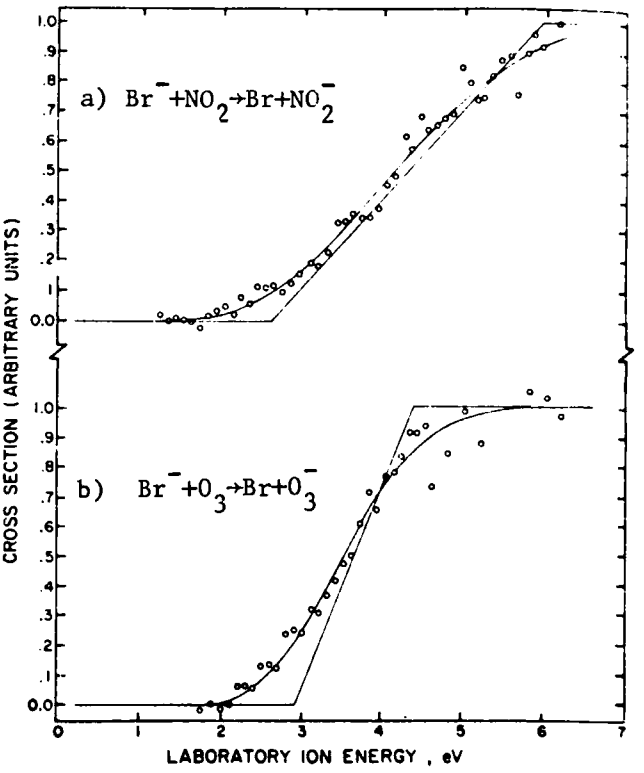

Fig. 24

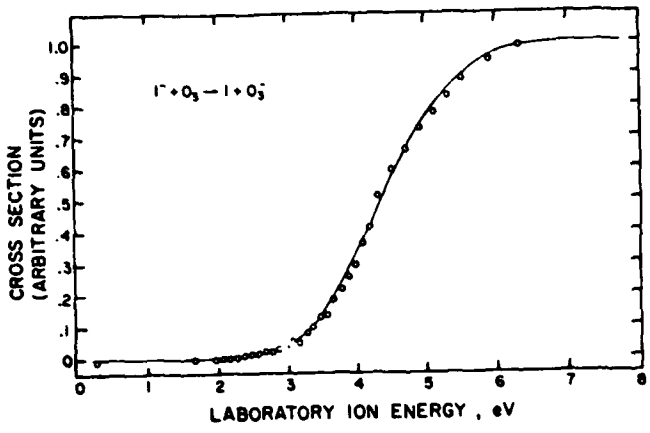

Fig. 25

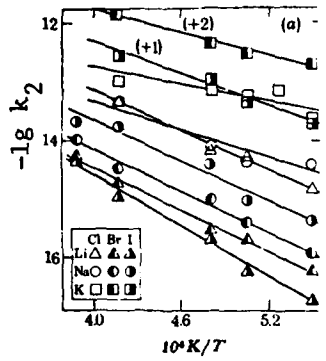

Fig. 26 Reaction rates k_2 (cm^3/sec) for $A + X \rightarrow A^+ + X^-$ where A is Li, Na, K and X is Cℓ, Br, I. In two cases graphs are shifted vertically (by +1 and +2) for clarity .

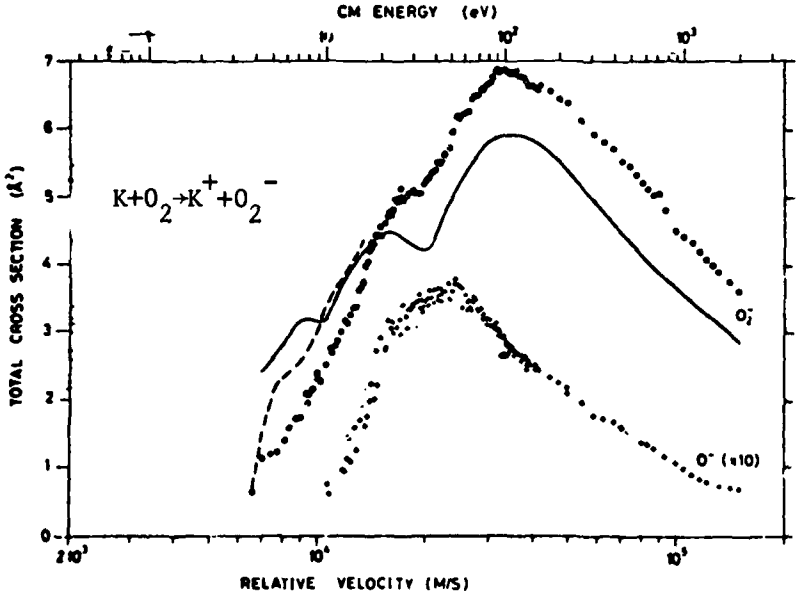

Fig. 27 Graph shows also data for O^- formation. Line is theory.

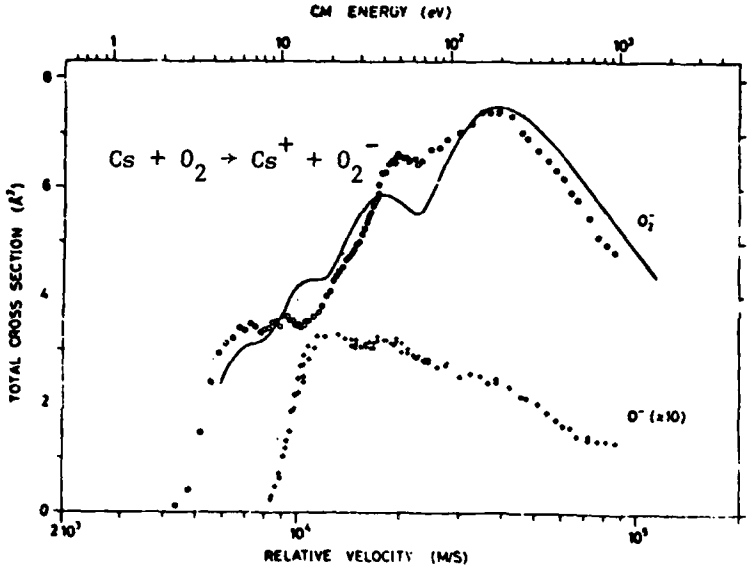

Fig. 28. Graph shows data also for O^- formation. Line is theory.

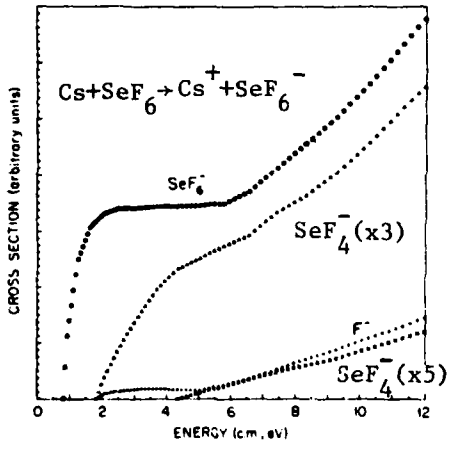

Fig. 29. Graph shows data also for formation of other negative ions.

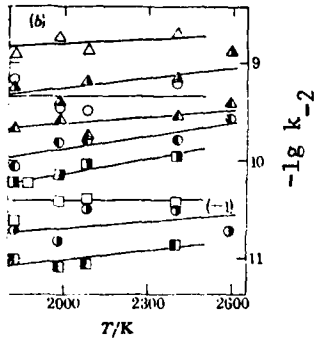

Fig. 30. Reaction rate k_{-2} (cm^3/sec) for $A^+ + X^- \rightarrow A + X$. Where A is Li (triangle), Na (circle) or K (square) and X is Cℓ (open), Br (shaded left) or I (shaded right). In one case graph is shown shifted vertically by -1 for clarity.

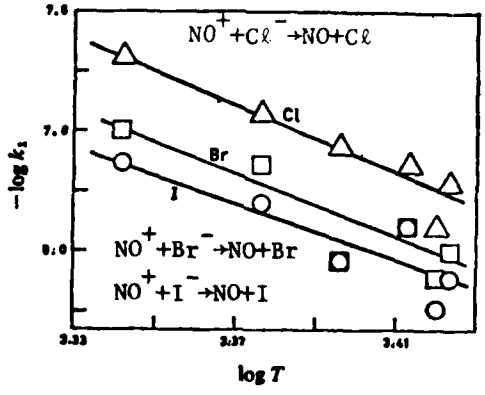

Fig. 31. Reaction rate in units of cm^3/sec.

REFERENCES

1. T. P. Radus and R. F. Porter, J. Phys. Chem 82, 513 (1978).
2. R. Johnsen, A. Chen and M. B. Biondi, J. Chem. Phys. 72, 3085 (1980).
3. R. Johnsen and M. A. Biondi, J. Chem. Phys. 61, 2112 (1974).
4. G. D. Myers, J. G. Ambrose, P. B. James, and J. J. Leventhal, Phys. Rev. A 18, 85 (1978).
5. E. A. Hinds and R. Novick, J. Phys. B. 11, 2201 (1978).
6. B. Peart and K. Dolder, J. Phys. B, 12, 4155 (1979).
7. S. Y. Tang and R. H. Neynaber, Phys. Rev. A 18, 1925 (1978).
8. W. B. Maier and B. Stewart, J. Chem. Phys. 68, 4228 (1978).
9. R. Johnsen and M. A. Biondi, Phys. Rev. A 20, 87 (1979).
10. V. V. Zhukov, E. L. Latush, M. F. Sem, Sov. Phys. J. 20, 957 (1977).
11. D. Smith, N. G. Adams and T. M. Miller, J. Chem. Phys. 69, 308 (1978).
12. J. A. Rutherford, and D. A. Vroom, J. Chem. Phys. 69, 332 (1978).
13. J. Glosik, A. B. Rakshit, N. D. Twiddy, N. G. Adams and D. Smith, J. Phys.B 11, 3365 (1978).
14. J. D. C. Jones, D. G. Lister, K. Birkinshaw and N. D. Twiddy, J. Phys. B 13, 799 (1980).
15. N. G. Utterback, B. Van Zyl, J. Chem. Phys. 68, 2742 (1978).
16. Yip-Hoi Li and A. G. Harrison, Int. J. Mass Spectron. and Ion Phys. 28, 289 (1978).
17. T. Baer, P. T. Murray, and L. Squires, J. Chem. Phys., 68, 4901 (1978).
18. A. B. Rakshit, H. M. P. Stock, D. P. Wareing and N. D. Twiddy, J. Phys. B 11, 4237 (1978)
19. F. Howorka, J. Chem. Phys. 68, 804 (1978).
20. K. Okuno, T. Koizumi and Y. Kaneko, Phys. Rev. Letts 40, 1708 (1978).
21. N. G. Adams, D. Smith and D. Grief, J. Phys. B 12, 791 (1979).
22. H. Nienstäd, D. Gawlik, G. zu Pulitz and H. G. Weber, Z. Physik A 288, 109 (1978).
23. I. Dotan and F. S. Klein, Int. J. Mass Spectrom, and Ion Phys. 29, 137 (1979).

24. C. Lifshitz, R. L. C. Wu, T. O. Tiernan and D. T. Terwilliger, J. Chem . Phys 68, 247 (1978).

25. N. A. Burdett and A. N. Hayhurst, Philos. Trans. R. Soc. London Ser. A 290, 299 (1979).

26. A. W. Kleyn, M. M. Hubers, and J. Los, Chem. Phys. 34, 55 (1978).

27. R. N. Compton, P. W. Reinhardt and C. D. Cooper, J. Chem. Phys. 68, 2023 (1978).

28. N. A. Burdett and A. N. Hayhurst, J. Chem. Soc. Faraday Trans. 1 74, 63 (1978).

DISTRIBUTION

	No. of Copies
School of Physics Georgia Institute of Technology ATTN: Dr. E. W. McDaniel	50
K. J. McCann	10
Dr. F. L. Eisele	10
E. W. Thomas	10
Dr. W. M. Pope	10
Dr. M. R. Flannery	10
Atlanta, Georgia 30332	
Joint Institute for Laboratory Astrophysics University of Colorado ATTN: J. W. Gallagher	10
J. R. Rumble	10
E. C. Beaty	10
Boulder, Colorado 80302	
Eckerd College ATTN: Dr. H. W. Ellis	10
St. Petersburg, Florida 33733	
Physics Department Georgia State University ATTN: S. T. Manson	10
Atlanta, Georgia 30303	
Defense Technical Information Center Cameron Station	2
Alexandria, Virginia 22314	
Director Ballistic Missile Defense Advanced Technology Center ATTN: ATC, Mr. J. D. Carlson	1
ATC-O, Mr. W. Davies	1
Mr. G. Sanmann	1
Mr. J. Hagefstration	1
-T, Dr. E. Wilkinson	1
-R, Mr. Don Schenk	1
P. O. Box 1500 Huntsville, Alabama 35807	
Defense Advanced Research Project 1400 Wilson Boulevard ATTN: Director, Laser Division	1
Arlington, Virginia 22209	

	No. of Copies
Lawrence Livermore Laboratory P. O. Box 808 ATTN: Dr. Joe Fleck Dr. John Emmet Livermore, California 94550	 1 1
Los Alamos Scientific Laboratory P. O. Box 1663 ATTN: Dr. Keith Boyer (MS 550) Los Alamos, New Mexico 87544	 1
Central Intelligence Agency ATTN: Mr. Julian C. Nall (OSI/PSTD) Washington, D.C. 20505	 1
US Army Research Office ATTN: Dr. Robert Lontz P. O. Box 12211 Research Triangle Park, North Carolina 27709	 2
DRSMI-LP, Mr. Voigt	1
-R, Dr. McCorkle	1
-RR, Dr. Hartman	1
-RH, Dr. Honeycutt	1
Mr. Cason	1
Dr. Roberts (Additional Distribution)	485
-RPR	3
-RPT, (Record Set)	1
-RPT, (Reference Copy)	1